UNIVERSITAT DE BARCELONA

Departament de Geodinàmica i Geofísica

Hydrogeophysics as a Multidisciplinary Tool on Aquifer Appraisal: Focus on AMT Capabilities

Memòria presentada per Ester Falgàs Parra per optar al Títol de Doctora per la Universitat de Barcelona.

Aquesta Tesis ha estat realitzada dins el Programa de Doctorat Ciències de la Terra, bienni 2002-2004, de la Universitat de Barcelona sota la direcció del Dr. Juanjo Ledo.

Dr. J. Ledo

Ester Falgàs Parra

Barcelona, Setembre de 2007

Agraïments

Hi ha tantes coses que m'agradaria comentar d'aquests quatre anys que no hi hauria espai, però primer de tot s'ha de ser humil i agraït en tot el que ens a donat la vida.

Primerament vull agrair al Dr. Juanjo Ledo per haver acceptat ser el meu tutor i haver-me guiat tots aquest anys, per la seva comprensió, dedicació, energia i il·lusió per tirar endavant moltíssimes coses a la vegada.

Així mateix voldria expressar el meu agraïment al Dr. Alex Marcuello per ser l'investigador principal del Projecte Geoelec on s'inscriu la beca de la meva tesis, i als investigadors T. Teixidó, J. Plata, F. Rubio i F. Rivera que hi varen participar . També com a part del equip vull mostrar el meu agraïment a la Dr. Pilar Queralt pels seus consells, consideracions i rigorositat en el llenguatge.

Voldria agrair a tot l'equip del grup de recerca GGAC, dirigit pel Dr. Muñoz, així com al grup EXES del departament per l'important suport logístic i de coneixement rebut.

De la meva estada a Strasbourg voldria agrair l'oportunitat que se'm va oferir per participar en el projecte de la Soutte amb el Dr. Pascal Shailac i Dr. Guy Marquis, leaders del dream-team. D'altra banda, de l'estada a California voldria agrair l'acolliment i la dedicació de la Dr Louise Pellerin, i la Dr. Darcy McPhee com a "jefas" del Projecte de Nevada. D'aquell cantó del mon segurament el que recordaré més és com d'americans són els americans!

Així com a conjunt, voldria donar el meu més profund agraïment al equip de recerca dels 'geofísics' per haver-me obert les portes a un món totalment nou per mi, la MT, i que com ja saben el vaig trobar màgic des del primer dia, (isn't it Alan?). Per donar-me la oportunitat de conèixer els mètodes geofísics tant de prop, de poder assistir a congressos per veure que es movia, i poder fer un parell de estades a l'estranger. Voldria agrair als jefes Juanjo, Pim, i Alex, i a la inclassificable Bea, que no està en aquest grup però si que hi és, pel seu increïble bagatge i visió de com fer les coses,i per haver tirat endavant l'organització del 18th EMIW, el que va ser un gran tinglado. També voldria agrair tot el temps compartit amb les Annes i la Claudia per ser els meus referents indiscutibles, per les estones passades, consells, i les mil aplicacions i compilacions. I als que venen darrere meu, els nearsurface Mireia i Miquel, el superfieldman

Oriol i el nou fitxatge Fabian amb un munt de cosetes divertides per recordar. Entre tots hem estat un bon equip!.

També voldria recordar el companys del departament d'aquí Barcelona i dels departaments on he anat a espetegar, per moments i cotilleos memorables, per les paelletes, calçotades, hores de dinar i i i.... I voldria donar-vos les gràcies a tots els que m'heu acompanyat al camp i que segurament amb més d'una ocasió heu tastat com pesen els aparells geofísics! Jordi, Claudia, Antonio, Joanna, Hector, Miquel, Mireia, Oriol, Sara,i el meu pare....a tot us en dec una!

Aquesta tesis ha estat escrita en l'idioma anglosaxó aquest que ens costa tant!. Val a dir, que això ha estat possible gràcies a l'assessorament lingüístic i la inestimable ajuda rebuda del Marc, la Darcy, en Grant i l'Anna, l'Arne i en Kasturi. Gràcies a tots per llegir-vos el meu trogloenglish!

Pel que fa al terreny personal voldria agrair al meus amics, els de sanfe, els de barcelona i als que esteu escampats pel món per haver-me descobert tantes coses de la vida, per les escalades, festetes, aventurilles, i xerrades infinites sense les que segurament no hagués trobat la sal de la vida. I a tots aquells que m'heu fet obrir els ulls i donar-me força per fer passos valents.

I especialment quatre paraules pel Miquel, el que haig d'agrair el suport incondicional, els ànims, les carícies, els somnis, els nous amics, i la descoberta de la bici i l'esquí de muntanya. Per coneixem tant, tot i preguntar-me tot sovint pel llibre de instruccions, i animar-me constantment per seguir endavant sobretot ara al final.

Evidentment a la meva família haig d'agrair-los tot, tot i tot. Per confiar en mi en les meves grans decisions i per tants sopars tots junts intentant no parlar de política. Als meus pares Isabel i Jaume per estar tant il·lusionats en aquesta empresa, i per intentar treure'm sempre alguna paraula tot i entendre poca cosa de la MT. I a l'Oriol, la Norma, l' Agnès, i la Joaneta, pel seu ritme de vida, i que sense ells la casa estaria molt buida. Als meus avis i sobretot a la meva àvia a la que segurament li dec moltes reflexions indirectes.

Si hagués de resumir el que més recordaré de tot plegat segurament són totes les persones que m'he anat creuat durant tots aquests anys i dels punts de vista tant personals de cadascú, el que m'han fet créixer. Segurament sense tots vosaltres no hauria estat possible aquesta tesi, moltes gràcies doncs a tots.

INDEX

Resum

Introducció, objectius i estructura

L'aigua és un element essencial per a la vida. Actualment és, i en el futur continuarà sent, un tema candent tant en el panorama polític com en el científic.

La zona més superficial de la escorça terrestre té una importància vital des del punt de vista antròpic i socioeconòmic. Aquesta zona conté la major part dels recursos i reserves hídriques, és d'on s'extreuen els recursos geològics, on s'implementa l'agricultura, on se sustenten els ecosistemes que influencien el nostre clima i on s'emmagatzemen bona part dels residus que generem. Alguns autors han qualificat aquesta àrea com la zona crítica on s'estableixen complexes relacions entre processos antròpics induïts, processos hidrogeològics, geoquímics i geobiològics.

Per tal de no contaminar i no exhaurir ni els recursos ni les reserves hídriques, és necessària una planificació i una gestió efectiva, sent aquest un dels grans reptes d'aquest segle. El creixement econòmic i demogràfic en determinades zones requereix majors volums d'aigua disponible, la qual cosa remarca la necessitat de mantenir i protegir les fonts d'abastament conegudes així com d'investigar sobre nous recursos. Durant el darrer segle, el creixement econòmic s'ha produït moltes vegades a expenses del medi natural, malmetent parcial o totalment les reserves i els recursos. L'actual conscienciació mediambiental però, aposta per a minimitzar aquest impacte ja que la disponibilitat d'aigua de qualitat és crucial per l'actual ritme de desenvolupament de la societat moderna.

Per tal de poder identificar i caracteritzar en detall les masses d'aigua subterrània, és necessària una caracterització precisa de l'aigua emmagatzemada (tant biològicament com química), i si és possible, determinar els límits per on flueix i les propietats hidràuliques del sistema. La informació que aporten els pous d'abastament i els piezòmetres (registres litològics,

lectures piezomètriques, anàlisis hidroquímiques i tests de bombament) moltes vegades no són suficients per tal d'assolir una caracterització detallada dels medis subterranis. En general els pous i peizòmetres no es troben distribuïts homogèniament, sinó que aporten informació puntual, i són tècniques invasives, que mal gestionades poden modificar el sistema de flux. Els mètodes geofísics són no invasius, cost efectius i poden aportar dades contínues tant espacial com temporalment, és a dir els mètodes geofísics tenen un enorme potencial per complementar les dades hidrogeològiques. Val a dir, però, que les dades hidrogeològiques són estrictament necessàries per a calibrar i validar els models geofísics i, posteriorment, utilitzar-les en les aproximacions petrofísiques que relacionen els models geofísics amb els paràmetres i les propietats hidrogeològiques.

La disciplina científica de la hidrogeofísica ha sorgit en el darrers anys com a resposta a la demanda de caracterització del medi subsuperficial de manera detallada i no invasiva. El desenvolupament de la hidrogeofísica vol superar la cartografia d'anomalies geofísiques per poder extreure així informació quantitativa de les propietats i dels processos hidrogeològics. Actualment s'investiga el potencial de mètodes geofísics diversos per aproximar-se als sistemes aqüífers des de molt diverses perspectives i escales de treball (Rubin and Hubbard, 2005; Buttler, 2006).

La hidrogeofísica com tantes altres geociències, es basa en l'experiència prèvia i tecnològica que la industria minera i petrolera han desenvolupat. L'escala de treball, però, ha de ser modificada per tal que la tecnologia pugui ser aplicable al medi subsuperficial, ja que les condicions de pressió, temperatura i profunditat són diferents i els contrastos de propietats són molt més subtils. A més a més, la caracterització geofísica del medi subterrani des d'un punt de vista hidrogeològic, a part d'aportar informació de l'estructura i propietats estàtiques del sistemes aqüífers està interessada en la dinàmica del flux subterrani i per tant, obre la perspectiva de les investigacions 4D. La caracterització de l'estructura hidrogeològica, l'emmagatzematge, el moviment i transport, i el quimisme de l'aigua són les claus per entendre globalment els processos i paràmetres hidrogeològics que defineixen cada sistema aqüífer.

Diversos problemes hidrogeològics es poden caracteritzar amb mètodes geofísics, com per exemple, la geometria de l'aqüífer, la posició del basament i dels contorns, les propietats hidràuliques del sistema (sigui un aqüífer porós o fracturat), les heterogeneïtats i zones d'alta permeabilitat, les zones d'alt contingut d'argiles, la qualitat de l'aigua, o el monitoratge de processos dinàmics. A més a més, els mètodes geofísics poden treballar a diferents escales, oferint diferents tipus de resolució i de profunditat d'investigació. Es poden estudiar des d'aqüífers regionals i les seves grans unitats hidrològiques (a través de mètodes aerotransportats

o superficials), fins a zones de recàrrega o propietats puntuals (a través de diagrafies i mètodes superficials d'alta resolució) (Fig.2.1, Taula 2.1). La tria del tipus d'instrumentació per a cada investigació depèn sobretot dels objectius de l'estudi, la resolució i la precisió desitjades, les condicions del medi, el temps, el pressupost, els recursos computacionals i la informació prèvia de que es disposa.

La present memòria de tesi doctoral '*Hydrogeophysics as a multidisciplinary tool on aquifer appraisal: Focus on AMT capabilities',* es centra en l'ús i el desenvolupament de la hidrogeofísica com a eina multidisciplinària per a la millora del coneixement dels sistemes aqüífers. Concretament, s'avalua el mètode audiomagnetotel·lúric per a aquest tipus d'investigacions que, conjuntament amb d'altres informacions geofísiques i hidrogeològiques, poden aportar un millor coneixement dels sistemes aqüífers. Bàsicament, la memòria ha estat dividida en dues parts. La primera part (Part I), té un caràcter més teòric on, primerament, s'ha introduït la disciplina de la hidrogefísica en sentit ampli: s'ha revisat la metodologia de l'aplicació dels mètodes geofísics per resoldre problemes hidrogeològics, els seus fonaments, els tipus d'aplicacions, les limitacions i les expectatives. Seguidament, s'ha revisat el mètode audiomagnetotel·lúric en detall per la seva idoneïtat en l'aproximació als sistemes aqüífers. Seguint el fil conductor de la hidrogeofísica i el mètode audiomagnetotel·lúric (AMT), la segona part de la memòria (Part II) està composada per tres capítols. Aquests desenvolupen tres estudis hidrogeofísics multidisciplinaris, on el mètode audiomagnetotel·lúric ha tingut un paper clau en l'estimació de propietats i de processos dels diferents sistemes a tres escales de treball diferents. Finalment, per concloure, s'han presentat les principals consideracions i conclusions derivades de tots els capítols, així com les perspectives futures per a millorar i completar la feina presentada en aquesta memòria.

Part I

Capítol primer, Introducció. Aquest capítol té caràcter de presentació, on s'introdueix la motivació i objectius generals de la tesi. Es mostra la importància i els reptes a assolir per a estudiar els sistemes aqüífers des d'una perspectiva multidisciplinar, combinant la informació hidrogeològica i geofísica. Per altra banda, es detalla l'estructura de la tesi i es presenta un breu resum de cada capítol.

Capítol segon, La Hidrogeofísica. Aquest capítol té com a objectiu revisar l'estat del desenvolupament i de les línies de recerca actuals de la hidrogeofísica. La hidrogeofísica es pot definir com la disciplina que utilitza les mesures geofísiques per a cartografiar, i estimar les propietats i els processos que són importants en els estudis hidrogeològics com serien l'estimació dels recursos hídrics, el transport de contaminants, el monitoratge de processos de recàrrega i infiltració, i les investigacions ecològiques i climàtiques. En aquest sumari s'ha intentat mostrar les grans perspectives i el gran interès que s'ha mostrat, tant des del món científic com sociopolític, per a desenvolupar certs mètodes geofísics d'una manera efectiva per amb l'objectiu de reconèixer en detall els sistemes hidrològics. Així, s'ha evidenciat la creixent importància de la hidrogeofísica en el camp mediambiental i d'enginyeria civil en els principals congressos geofísics, geològics i hidrogeològics internacionals dels darrers anys.

Un dels principals reptes i alhora virtuts d'aquesta disciplina és la seva multidisciplinarietat, és a dir, la integració de les dades hidrogeològiques i geofísiques per a crear models globals més restringits i fiables. Des d'un punt de vista hidrogeològic els mètodes geofísics poden ser utilitzats per a:

- Cartografia de la geometria de l'aqüífer, posició del nivell piezomètric, posició i morfologia del basament, abast de plomall de contaminació, caracterització de zones de falles i fractures i zones d'aigües termals.
- Estimació quantitativa de paràmetres hidrològics (ja sigui de quantitat o qualitat d'aigua) i dels paràmetres de porositat i permeabilitat hidràulica que controlen el flux.
- Caracterització i monitoratge de processos dinàmics per tal de visualitzar el canvi de propietats en un sistema natural o forçat (ja sigui monitoritzant un procés de infiltració en la zona vadosa, intrusió salina, o transport de contaminants, entre d'altres.

En aquest capítiol també s'exposa una visió general de la metodologia estàndard en l'ús de mètodes geofísics, des dels diferents tipus d'instruments i de la seva implementació al camp fins als processos de modelat que resolen el problema directe o invers. Les principals propietats del subsòl que poden ser inferides a través dels mètodes geofísics (conductivitat elèctrica, densitat, velocitat de les ones P i S, constat dielèctrica, susceptibilitat magnètica) (Fig. 2.3, Taula 2.1) han estat presentades. En particular, la resistivitat elèctrica, ha estat considerada una propietat física ideal per a l'estudi dels dominis hidrogeològics ja que la resistivitat elèctrica obtinguda depèn de les propietats hidrogeològiques del medi: tipus de material, estructura

porosa, qualitat i quantitat d'aigua. Tanmateix, la contribució de cada factor a la senyal geofísica és complex, i per tant la transformació de paràmetres geofísics a paràmetres hidrogeològics encara no té una solució única, sinó que cada cas particular intenta trobar una solució raonable.

Els mètodes geofísics aplicats a la hidrogeologia que presenten unes perspectives de futur més prometedores han estat revisats, presentats i documentats detalladament. Els mètodes que s'han presentat són els següents: mètodes elèctrics (ERT tomografia elèctrica de resistivitat, IP polarització induïda, SP potencial espontani), mètodes electromagnètics (TDEM electromagnètic en el domini del temps, FDEM electromagnètic en el domini de les freqüències, AMT audiomagnetotel·lúric, GPR georadar de subsòl, NMR ressonància magnètica nuclear), mètodes sísmics, mètodes gravimètrics i magnètic. S'ha desenvolupat la seva base teòrica i els seus trets més característics i s'han presentat els objectius que es poden assolir, tant en resolució com en profunditat d'investigació. S'han mostrat exemples rellevants d'aplicacions, així com les seves limitacions tant en la instrumentació, com en els tipus de dades i models.

L'últim apartat d'aquest capítol es centra en revisar i enumerar els principals reptes que la hidrogeofísica ha de superar per oferir una aplicabilitat eficaç, i per tant, on s'està desenvolupant la recerca actual. Així doncs, els temes que tenen actualment una importància clau són: 1) el desenvolupament de les relacions petrofísiques, 2) el desenvolupament de mètodes d'integració de les dades geofísiques i hidrogeològiques i finalment, 3) la millora de les metodologies instrumentals i de modelització numèriques dels mètodes geofísics.

1) L'aproximació a les relacions petrofísiques que es presenta a la memòria, està basada en els exemples de models de resistivitat i models de permitivitat. No existeix una llei universal que lligui els models geofísics de resistivitat i permitivitat amb paràmetres hidrogeològics i per tant, s'utilitzen relacions petrofísiques estàndard amb patrons ideals per a cada medi. Les variables de les lleis estàndard s'obtenen calibrant una gran quantitat de dades geofísiques i hidrogeològiques en els mateixos punts. En el cas dels models de resistivitat aquestes lleis o relacions més usades (modificades per cada medi) són, per exemple, les equacions de Koseny-Carman per obtenir la permeabilitat hidràulica, o la llei d'Archie (Archie, 1942) per obtenir la porositat, la resistivitat del medi o la resistivitat del fluid. Similarment, en els models de permeabilitat elèctrica les equacions que més s'utilitzen són les equacions de Topp (Topp *et al.,*1980) i CRIM (Wharton *et al.*, 1980) per obtenir la quantitat d'aigua o inferir indirectament la porositat.

2) La integració de dades geofísiques i hidrogeològiques segueix dues línies d'actuació: i) el model determinista via cartografia directa i/o aplicant una relació petrofísica o ii) seguint un model probabilístic que engloba els mètodes geoestadístics i de simulació. Actualment s'estan fent grans avenços en el desenvolupament dels mètodes d'inversió conjunta on tant dades geofísiques de diversa procedència com dades hidrogeològiques s'usen simultàniament per a produir estimacions i models que satisfacin tots els conjunts de dades.

3) La millora en la metodologia d'aplicació dels mètodes geofísics es dirigeix a temes tant diversos com són la millora instrumental, el processat de les dades o la millora dels mètodes de modelització. En la instrumentació s'intenta que els equips siguin més portables, millorar la resolució sense perdre profunditat d'investigació, millorar el tractament del soroll de les dades i implementar noves tecnologies de comunicacions entre els sensors i les bases de d'emgatzematge i de processat. D'altra banda, el modelat multidimensional de les dades geofísiques ha d'experimentar encara una millora substancial, ja que no totes les tècniques geofísiques es poden modelar en 2D o 3D. Per tant es treballa en el desenvolupament matemàtic d'algorismes 2D i 3D, per obtenir millors resultats amb un menor temps de computació.

Capítol tercer, El mètode Audiomagnetotel·lúric (AMT). En aquest capítol s'ha aprofundit en els fonaments del mètode audiomagnetotel·lúric, ja que aquesta tesi doctoral es centra en l'avaluació d'aquest mètode per a les investigacions hidrogeològiques. El mètode audiomagnetotel·lúric és un mètode electromagnètic en el domini de les freqüències. D'aquest es pot obtenir la distribució de resistivitat d'un volum de l'espai, és per tant, un mètode de mesura 3D real. Es fonamenta en la mesura simultània de les fluctuacions temporals del camp elèctric i magnètic a través d'un dispositiu de dos parells d'elèctrodes i dues bobines d'inducció disposades perpendicularment (Vozoff, 1991)(Fig.3.1). La relació entre les components horitzontals dels camps magnètics i elèctrics es relacionen a través del tensor d'impedàncies, Z_{ij}, per cada freqüència de registre (ω), sent ij les direccions perpendiculars xy.

$$\begin{pmatrix} E_i(\omega) \\ E_j(\omega) \end{pmatrix} = \begin{pmatrix} Z_{ii}(\omega) & Z_{ij}(\omega) \\ Z_{ji}(\omega) & Z_{jj}(\omega) \end{pmatrix} \begin{pmatrix} H_i(\omega) \\ H_j(\omega) \end{pmatrix}$$

Les components del tensor poder ser escalades per obtenir una resistivitat aparent,

$$\rho_{a,ij}(\omega) = \frac{1}{\omega\mu}\left|Z_{ij}(\omega)\right|^2 \qquad \text{i una fase} \qquad \varphi_{ij}(\omega) = arctg\left(Z_{ij}(\omega)\right)$$

La profunditat d'investigació d'aquet mètode ve determinada per la resistivitat elèctrica del medi i per la freqüència dels camps electromagnètics mesurats. Una aproximació raonable a la profunditat d'investigació és l'anomenada "skin depth", δ, que correspon a la distància en la que l'amplitud del camp electromagnètic incident s'ha atenuat un factor 1/e. En un espai uniforme, aquest valor podria aproximar-se com a $\delta \approx 501\sqrt{2\pi\rho/\omega}$ en metres. Per tant, per un mateix medi, les altes freqüències recuperen informació de la zona més superficial, mentre que les baixes freqüències obtenen informació més regional i profunda. Val a dir, que canvis en els valors de resistivitat del medi exerceixen un control crític en la profunditat de investigació (en el mateix rang de freqüències) i conseqüentment, en la resolució de la informació obtinguda. La profunditat d'investigació i la resolució de les estructures detectables es relacionen de manera inversa. Treballant en la zona subsuperficial aquests canvis de l'escala de treball de metres a desenes o centenars de metres poden ser important per poder assolir els objectius i la resolució de cada estudi.

En funció del rang de freqüència de cada instrument, aquest mètode electromagnètic s'anomena diferent (Fig.3.4). Així doncs, per a freqüències baixes o períodes grans (10^{-6}- 1Hz) el mètode s'anomena magnetotel·lúric, MT, usat en estudis a nivell cortical i de mantell. Per a freqüències mitjanes (1 - 10^5Hz), el mètode s'anomena audiomagnetotel·lúric, AMT, emprat en estudis a nivell de conca o locals. Per a altes freqüències (>10^4), el mètode s'anomena radiomagnetotelluric, RMT, usat per a caracteritzar en detall els primers metres dels subsòl.

Les característiques matemàtiques del tensor d'impedàncies permeten determinar la dimensionalitat geoelèctrica del subsòl. Si les estructures geoelèctriques només canvien en la vertical el medi seria 1D. Si canvien en la vertical i al llarg d'una direcció, el medi seria 2D (perpendicular 'strike' geològic regional). En el cas més general, on el medi seria 3D, la resistivitat canvia en les tres direccions. L'anàlisi de la dimensionalitat de les dades audiomagnetotel·lúriques és molt important per realitzar una correcta decisió del tipus dimensional de modelat a utilitzar, per així assumir el tipus d'error que es cometrà quan per exemple s'aproximin medis 3D amb algorismes 2D. Per tal de determinar la dimensionalitat de les dades audiomagnetotel·lúriques s'ha emprat l'aplicació WALDIM, desenvolupada per Martí (2006), basada en la informació que contenen els 7 paràmetres invariants del tensor d'impedàncies (Weaver *et al.*2000), controlant els paràmetres llindar (Taula 3.2).

La resistivitat aparent i la fase són emprades per començar el procés de modelització i inversió per tal d'obtenir models de la distribució de resistivitat en l'espai 1D, 2D o 3D. Els codis d'inversió i de modelat que s'usen més habitualment són bidimensionals, on s'utilitzen els modes TE i TM conjuntament per a crear models 2D. Tanmateix en el món real tridimensional, els models 2D no sempre son totalment acceptables, ja que poden incloure efectes laterals 3D (Ledo, 2006; Queralt *et al.* 2007).

Per tal d'aproximar medis 3D a models 2D d'una manera vàlida, s'ha utilitzat el codi DetREBOCC (Pedersen and Engles, 2005) basat en el codi REBOCC (Siripunvaraporn and Egbert, 2000), que utilitza el determinant del tensor d'impedàncies (eq.3.8) en l'algorisme de inversió. El determinant del tensor de impedàncies és invariant a la rotació i per tant, és independent de la direcció de mesura. Els models obtinguts a través de la inversió del determinant del tensor de impedàncies no es veuen afectats per cossos laterals finits, i per tant, no inclou efectes 3D. Per contra, els models generats tenen un caràcter més regional dins de cada escala de treball (determinada per la freqüència i resistivitat del medi).

El mètode electromagnètic està basat en l'assumpció de la propagació vertical de les ones electromagnètiques a través del sòl. Tot i ser un mètode de camp natural, sovint existeix poca senyal o existeix soroll electromagnètic. En aquests casos s'utilitza una font controlada per tal de millorar la relació senyal-soroll. La font controlada ha de posicionar-se en la zona de camp llunyà, és a dir, suficientment lluny per tal d'acomplir la premissa de mesura d'ona plana. Quan una font electromagnètica se situa en la zona de camp proper o en la zona de transició les mesures no aporten informació de la resistivitat del subsòl sinó que el senyal dependrà de la distància a la que està situada la font en relació a l'estació. Les relacions matemàtiques que descriuen el comportament dels camps electromagnètics mesurats generats per dipols electromagnètics horitzontals han estat recollides (Pfaffhuber, 2001) per tal d'estudiar l'efecte d'una font situada en camp proper sobre les dades.

L'equip de mesura emprat en les aplicacions hidrogeofísiques presentades en la segona part de la memòria, és l'StrataGEM EH4 system© de Geometrics (Geometrics 2001) (Fig. 3.6). És un instrument de mesura tensorial electromagnètic de font natural i artificial amb un rang de mesura de 10 a 92000 Hz. El sistema està composat per quatre elèctrodes d'acer inoxidable i dues bobines d'inducció. La font controlada està composta per dos dipols magnètic horitzontals amb un moment magnètic de 400 Am^2 que emet 14 freqüències, de 800 a 64000 Hz.

Els efectes de la senyal electromagnètica situada a la zona de camp proper o a la zona de transició són fàcilment detectables. S'han observat experimentalment els efectes de les

mesures en camp proper fent proves de variació de la distància font-receptor. En camp proper s'observa un valor en les fases de 90º, mentre que la resistivitat aparent presenta una recta de pendent negatiu de 45º (Fig 3.8 i Fig. 3.9). Quan s'està en la zona de transició, la resposta és una situació intermitja, i tot i que les fases tendeixen cap als 90º és més difícil de discernir. Per altra banda, s'ha evidenciat la sensitivitat de l'aparell. En una mateixa mesura, la distancia transmissor-receptor pot ser massa petita (observant-se efectes de camp proper en les baixes freqüències), i massa gran per a obtenir senyal de la font per a les altes freqüències. En alguns casos, doncs, cal establir un compromís amb distancia per tal de rebre senyal de la font sense estar en el camp proper o saber eliminar les freqüències afectades si s'està en camp proper. És important remarcar que les mesures obtingudes quan la font està situada una distancia ideal en la zona de camp llunyà presenten una millora important.

Part II

La segona part de la memòria de tesi doctoral inclou tres capítols 4, 5 i 6. Corresponen a tres avaluacions de diferents sistemes aqüífers a tres escales de treball diferents. En tots ells s'ha usat la combinació de diferents tècniques geofísiques amb informació hidrogeològica. Cada estudi té el seu caràcter diferencial per la disparitat dels objectius a assolir, i per tant, en la metodologia seguida. Tot i això, tots tres capítols tenen un tret comú, l'audiomagnetotel·lúrica com a eina geofísica principal que, conjuntament amb informació hidrogeologica i d'altres mètodes geofísics (ERT, sísmica, gravimetria i magnetometria), pot proporcionar millores en els models finals obtenint informació hidrogeològica-estructural més continua i contrastada.

Capítol quatre, Aplicació hidrogeofísica: el sistema aqüífer de la Tordera. Aquesta primera aplicació hidrogeofísica es centra en l'estudi multidisciplinari d'un aqüífer fluviodeltaic porós afectat extensament per un procés d'intrusió marina. L'estudi s'emmarca dins el projecte d'investigació del Ministerio de Educación i Ciéncia "Tomoelect: Desarrollo para la caracterización eléctrica de aqüíferos" REN2002-04538-C02. Les dades hidrogeològiques, magnetotel·lúriques, de sísmica de reflexió i de refracció han estat avaluades conjuntament per a construir models espacialment més continus de propietats i processos dels sistema aqüífer. S'han creat models 2D i 3D, els que s'han validat amb dades litològiques i hidroquímiques. A més, s'ha realitzat el monitoratge d'un perfil audiomagnetotel·lúric cada quatre mesosper tal de visualitzar la dinàmica estacional de la falca de intrusió salina. Finalment, s'han comparat els

models de resistivitat obtinguts amb els mètodes de DC superficial, AMT i FDEM tant pel que fa a la seva resolució com a la profunditat d'investigació de cada mètode.

La conca hidrològica de la Tordera té una superfície de 894 km^2 situada al nord de les Serralades Costaneres Catalanes (CCR), a la costa nord-oriental de la Península Ibèrica (Fig. 4.1). Les CCR es defineixen com un sistema de *horts* i *grabens* de direcció NE-SW constituïts per un basament Paleozoic sota una cobertora Mesozoica discordant. El basament de la zona d'estudi està compost quasi totalment per granits emplaçats durant l'orogènia Herciniana posteriorment afectats per l'orogènia Alpina. En particular, s'observa com el traçat de la Tordera i l'espai deltaic estan controlats per aquests sistemes de falles extensives post-alpines i les seves conjugades que travessen les serralades. El sistema aqüífer fluviodeltaic de la Tordera està composat per materials detrítics Neògens i Quaternaris. En particular el processos periglacials a les vessants de les serralades emergents durant el Pleistocè varen cursar intensiva erosió i meteorització, i conseqüentment, varen aportar una gran quantitat de materials detrítics al sistema fluvial i deltaic (Rovira *et al.*, 2005).

El règim fluvial de la Tordera canvia substancialment des de la seva capçalera, on el riu porta aigua i sediments contínuament, vers la zona litoral, on el règim fluvial és efímer i durant la major part de l'any no existeix circulació superficial. El model conceptual del sistema aqüífer està compost per quatre unitats aqüíferes limitades per un basament granític (Geoservei, 2001). De dalt a baix, es defineixen: un aqüífer superficial lliure, un aqüitard, un aqüífer profund semiconfinat, i només restringit a la zona més propera a la línia de costa, s'ha definit un sistema aqüífer basal.

El sistema aqüífer de la Tordera ha estat considerat durant les últimes dècades com un recurs estratègic per al desenvolupament econòmic i social de la zona. El desenvolupament industrial, turístic i urbà de la zona ha incrementat substancialment la demanda d'aigua potable. Així doncs, l'equilibri aigua dolça-aigua salada s'ha trencat degut a les excessives extraccions induint la intrusió d'aigua salina terra endins arribant a salinitzar alguns pous d'extracció. L'aqüífer profund, és el que sustenta la major part de les extraccions i per tant, és l'aqüífer més afectat per la intrusió salina. Per tal de poder abastir la demanda d'aigua, existeix una planta dessaladora (ITAM Blanes) la qual pot tractar un màxim de 10 Hm^3/any. Aquesta quantitat no ha estat suficient per frenar la intrusió salina, sobretot en anys repetits d'escasses precipitacions. Actualment s'està estudiant l'ampliació de la planta per tal de poder aportar un total de 20 Hm^3/any.

L'estudi hidrogeofísic pròpiament dit va començar amb la recopilació de totes les dades hidrogeològiques i geofísiques disponibles, és a dir, informació litològica dels pous d'extracció, resultats d'anàlisis hidroquímics, així com la recopilació de dades geofísiques anteriors: sísmica i sondejos elèctric verticals. L'anàlisi de les dades hidrogeològiques, la informació de pous i de piezòmetres, va ser una tasca costosa, ja que es va evidenciar que les descripcions litològiques en molts punts eren de poca qualitat, subjectives i poc rigoroses. Es tracta de pous construïts per l'abastament des de la dècada dels 60 fins a la actualitat i que per tant provenien de fonts molt diverses. A més, els pous estan distribuïts de manera no homogènia amb una penetració molt desigual. Amb totes les dades litològiques es van construir les superfícies de les unitats aqüíferes definides en el model conceptual amb l'aplicació *GoCad,* construint un model 3D simple, per tal de comparar els models hidrogeològics amb els geofísics (Fig. 4.6).

Les anàlisis hidroquímiques de dos piezòmetres (W-04 i W-06), durant la primavera del 2004 (coetanis als nostres registres audiomagnetotel·lúrics), van evidenciar una afectació salina important del sistema. Les mostres corresponents a l'aqüífer profund presentaven alt contingut en ió Cl^- (16650 ppm Cl^- i 1350 ppm Cl^- respectivament) (Taula 4.2). La posició d'aquests piezòmetres, a 500 m i 1200 m respectivament de la línia de costa, indicarien l'abast de la zona de transició aigua marina aigua fresca. Soler *et al*. (2006) van presentar el model de barreja Cl^-/Br^- (Fig. 4.3), on es suggereix que la mostra del piezòmetre W-04 conté un 80% d'aigua salina, mentre que la mostra del piezometre W-06 conté un 8%. D'altra banda, en el pou Malgrat-1, just en la línia de costa, es va realitzar un registre vertical de conductivitat (IGC), que mostra una estratificació de la cunya de intrusió marina al voltant dels 50 m de profunditat. Aquests resultats mostren la morfologia i abast de la falca d'intrusió marina i la zona de transició.

Les dades geofísiques anteriors a la realització d'aquesta tesi, les quals han estat analitzades, provenen de diferents campanyes de sondejos elèctrics verticals (SEV) dels anys 1969, 1994, 1995, 1996, 2002, i de perfils sísmics adquirits per l'Institut Cartogràfic de Catalunya PS1 i PS4 (Fig.4.5) (Teixidó, 2000). Durant el desenvolupament del projecte s'han adquirit dos perfils de tomografia elèctrica un al llarg del riu i un paral·lel a la línia de costa coincidint amb els perfils sísmic analitzats, un perfil electromagnètic en el domini del temps (TDEM) coincidint amb el perfil sísmic i elèctric PS1. Finalment, s'han realitzat 47 sondejos d'AMT distribuïts en malla en la zona oest del delta i 42 sondejos en el perfil de monitoratge (Fig.4.5).

Tant a partir de la tomografia elèctrica com dels sondejos elèctrics verticals s'observa que al llarg del curs del riu actual (perfil PS4) la intrusió marina i la seva expressió geoelèctrica com un front continu, estava restringida als 500 primers metres de la costa. Tot i això

s'observen zones de baixa resistivitat en profunditat desconnectades d'aquest front. Les dades de camp audiomagnetotel·lúriques (pseudoseccions de freqüències de la resistivitat aparent del determinat del tensor de impedàncies) (Fig. 4.8), suggereixen l'existència d'una zona de baixa resistivitat a l'oest del delta. Introduint les dades litològiques i hidroquímiques es pot afirmar que en la zona occidental del delta existeix un abast major de la intrusió a través d'un paleocanal corresponent a una antiga fase deltaica que podria induir la intrusió salina lateralment al curs actual de la Tordera.

A partir de les anàlisis preliminars dels models hidrogeològics, dades i models geofísics, s'evidencia que el model hidrogeològic 3D creat és massa groller i per tant no es pot comparar directament amb els models geofísics. Els models geofísics han de ser validats i comparats amb dades hidrogeològiques sobreimposades.

Aquests estudis preliminars van situar les bases per a les futures línies d'investigació, ja que els SEVs ens aporten informació puntual, i tant aquest com els perfils de tomografia elèctrica no aportaven la profunditat de investigació requerida. Per tant, es va proposar de treballar conjuntament les dades hidrogeològiques, les dades d'AMT i els perfils sísmics per tal de crear models geoelèctrics i hidrogeològics més detallats i continus.

La dimensionalitat de les dades audiomagnetotel·lúriques del delta de la Tordera ha estat estudiada amb l'aplicació WALDIM (Fig.4.9). El resultat confirma la tridimensionalitat de les dades, i per tant, per modelar vàlidament aquest espai geoelèctric 3D s'han creat models 2D amb el codi DetREBOCC, així com un model invers 3D.

Els perfils sísmics PS1 i PS4 han estat reprocessats per tal d'obtenir una millor imatge de sísmica de reflexió i model de tomografia sísmica de velocitats (Benjumea *et al.* 2006). La informació sísmica ha estat utilitzada sobretot per ajudar a determinar la posició del basament en els models audiomagnetotel·lúrics 2D (Fig.4.12 i 4.13). En un procés de prova i error s'ha anat ajustant el basament geoelèctric audiomagnetotel·lúric al basament sísmic sempre que es millorés l'ajust de les dades audiomagnetotel·lúriques a la resposta del model. Val a dir però, que tot i la millora dels models d'AMT, el basament sísmic i geoelèctric presenta discrepàncies en certs llocs de poques desenes de metres.

Els perfils audiomagnetotel·lúrics PS1 i PS4 tenen una disposició quasi perpendicular i per tant, d'ells es pot inferir una idea de la tridimensionalitat de les estructures geolèctriques. La interpretació dels models ens porta a distingir dues zones clares. Una correspon al basament que correspon a una zona resistent en profunditat d'entre 80 i 150m (depenent de la zona), i l'altre

correspon al sistema aqüífer. El sistema aqüífer, presenta un rang de valors de resistivitat molt ampli (1-1000 ohm·m). Es poden distingir clarament 1) les zones amb una alta afectació per intrusió marina ja que presenta valors de resistivitat molt baixos, i 2) les zones amb aigua fresca i granulometria grollera que presenten una resistivitat relativament elevada. En els casos amb valors de resistivitat intermitjos, i per tant, en els casos de presencia d'argila o contingut rellevant d'aigua salada, els models geofísics són més difícils de interpretar. Tot i que s'ha presentat una proposta de model hidrgeolèctric (Fig. 4.19), en llocs claus seria necessària informació complementaria, ja sigui a partir d'informació litolgòica, hidroquímica, o de la informació de la continuïtat de les estructures geoelèctriques que aporta el model 3D. Val a dir, que en els registres geològics no s'ha descrit el grau de desenvolupament i la potència de la zona d'alteració del granit, el que explicaria en part les discrepàncies entre la posició del basament elèctric i sísmic.

Els següent quadre resum presenta les facies hidrgoelèctriques que s'han interpretat.

Granulometria	**Tipus de dipòsit**	**Resistivitat**
Grollera	Fluvial	1000-100
Mitja	Plana deltaica	100-40
Fina	Plana d'inundació Argiles prodeltaiques	40-10

El perfil de monitoratge audiomagnetotel·lúric s'ha realitzat al llarg del paleocanal camí preferent de la intrusió marina. L'objectiu principal era provar la sensibilitat del mètode audiomagnetotel·lúric per poder mesurar canvis estacionals de la zona de transició de la falca de intrusió marina. Primerament, es presenten models que simulen un aqüífer amb tres casos d'afectació d'intrusió marina per crear dades sintètiques (Fig. 4.15). Els models inversos produïts a partir de les dades sintètiques ajuden a la comprensió dels models reals en la resolució i detall de les estructures geolelèctriques observades.

L'experiment natural de monitoratge es basa en la mesura d'un perfil d'uns 1700 m, compost per 7 sondejos. El perfil s'ha mesurat cada quatre mesos, des del 2004 fins al 2006. P per tant tenim 7 imatges 2D en el temps (M-1 a M-7) (Fig.4.15). La inversió de les dades s'ha realitzat a través del codi DetREBOOC amb el mateix model inicial en tots els perfils per tal de potenciar només els canvis de resistivitats deguts a canvis en la concentració de clorurs de l'electròlit. La seqüència dels models 2D mostren tendències interessants al llarg d'aquests dos

anys i que estan d'acord amb l'estat hidrològic del sistema revisat a través de les sèries piezomètriques i pluviomètriques mensuals.

La validació dels models 2D audiomagnetotel·lúrics PS1, PS4 i M-1, s'ha realitzat a través d'informació del registre litològic continu i de les anàlisis hidroquímiques en els tres nivells de profunditat de mesura dels piezòmetres W-04 i W-06 (Fig. 4.17). Els valors de resistivitat que presenta el model audiomagnetotel·lúric concorda amb la contribució tant de la litologia (en especial del contingut d'argiles) com del quimisme de l'aigua continguda (contingut en clorurs).

El model 3D audiomagnetotel·lúric invers, s'ha calculat usant el codi de modelització WSINV3DMT (Siripunvaraporn *et al.*, 2005), que es troba en un estat final de desenvolupament i test. Val a dir però, que no és esperable obtenir automàticament resultats vàlids dels models tridimensionals obtinguts amb aquest codi (Siripunvaraporn, 2006). En un procés de prova d'assaig i error cal analitzar les estructures geoelèctriques obtingudes ajustant la respostes del models a les dades, així com validant els possibles models amb totes les dades hidrogeològiques disponibles per tal d'obtenir un model final més satisfactori.

Primerament, s'ha creat un model d'un sistema aqüífer amb una zona rectangular simulant un camí preferent de intrusió marina (Fig.4.20). Calculant el problema directe s'han obtingut dades sintètiques. Aquestes dades sintètiques son les dades d'entrada de la inversió 3D per a observar quin tipus de resolució, morfologies geoelèctriques s'obtindrien i detectar possibles problemes numèrics de l'algorisme d'inversió tridimensional (Fig. 4.21).

Després de moltes proves, el model final té 35 cel·les (E-W) x 35 (N-S) x 15 cel·les verticals amb una potencia creixent, i una profunditat màxima de 300 m. En la modelització tridimensional inversa de les dades de camp s'han invertit 8 períodes i quatre components (les no diagonals). S'ha utilitzat un model inicial construït a partir dels models 1D de les dades i s'ha imposat el mar. Aquest paràmetres d'entrada s'han considerat per tal d'ajudar a l'algorisme d'inversió en la convergència numèrica amb un temps raonable.

El model obtingut amb l'algorisme d'inversió tridimensional s'ha sotmès a un procés iteratiu d'assaig i error calculant les respostes del model (Mackie and Madden 1993) comparant-les amb les dades mesurades. Així s'ha comprovat l'existència d'algunes estructures geoelèctriques i s'ha millorat l'ajust entre ell model i les dades. El model final (Fig. 4.23) ajusta el determinant del tensor d'impedàncies amb un RMS total de 6.8 en la resistivitat i un 5.2 de

les fases, considerant un 5% d'error en les components de la impedància (que correspon a un error de 10% en la resistivitat aparent i 2.9º en les fases).

El tret més destacat de la interpretació del model 3D és la visualització de la distribució de la intrusió salina, la qual està controlada estratigràficament a través del paleocanal a l'oest del delta, però també estructuralment a través del basament. En particular s'observa una zona alta de basament a la desembocadura actual del riu i per tant, la intrusió està bloquejada (Fig. 4.23).

S'ha comprovat la validesa tant dels models inversos 2D com del model 3D. Els models 2D i els mateixos talls dels models 3D presenten, en general, les mateixes morfologies tot i que hi ha certes diferències en la profunditat dels límits geoelèctrics i en els valors de resistivitat, degut al problema d'equivalència dels models geofísics (Fig.4.24).

En els perfils PS1 i PS4, s'han obtingut models de resistivitat elèctrica audiomagnetotel·lúrics, de tomografia elèctrica de resistivitat i electromagnètics en el domini del temps. Per tant, es poden observar les diferencies en resolució i profunditat d'investigació de cada mètode, visualitzant així les capacitats i habilitats de cada tècnica (Fig.4.25).

Capítol cinquè, Aplicació hidrogeofísica: La Soutte, Vosges. Aquesta aplicació hidrogeofísica es basa principalment en l'estudi audiomagnetotel·lúric de la Soutte, un laboratori natural hidrogeofísic, situat al nord est de França. L'objectiu principal de l'estudi a la Soutte és obtenir un model de mesoescala que serveixi de marc per a les altres aplicacions geofísiques que s'estan portant a terme en aquesta zona. En aquest cas, un model 3D directe i models 2D inversos estudien una zona de recàrrega d'un aqüífer fisurat. A més, s'ha combinat els mètodes audiomagnetotel·lúric i tomografia elèctrica de resistivitat per visualitzar les diferents escales de resolució d'aquests dos mètodes geofísics.

L'estudi de sistemes aqüífers fisurats és complex degut a la seva heterogeneïtat en la distribució i densitat de facturació. La fracturació controla l'emmagatzematge i la transmissió de fluids en aquests medis de baixa permeabilitat. Actualment, la caracterització detallada dels medis de baixa permeabilitat tridimensional és molt important no només pel reconeixement dels recursos hídrics explotables, sinó com també pel seu possible ús com a dipòsits subterranis.

La Soutte és un laboratori hidrogeofísic natural instrumentat per l'equip de recerca "Proche surface" de l'EOST, ULP, per desenvolupar-hi expermients hidrogeofísics. La Soutte se situa als SW de la ciutat d'Strasbourg, (França), al flanc oest del graben continental del Rhin, en el domini estructural del Vosges. Es tracta d'una zona d'unes 9 ha aproximadament a una altitud de 950 m amb una pendent vers el centre del *graven* d'un 5%. La zona d'estudi està situada sobre el basament Hercinià, composada de roques volcàniques devonianes intruïdes per mircrogranits porfiroides (Carbonífer Superior) (Fig.5.3). En superfície, aquests materials han desenvolupat un sòl d'alteració que pot presentar espessors de més de 2 metres. Al sud del camp experimental, existeix el naixement d'una riera, és a dir, la zona d'estudi correspon a la zona de captació i capçalera del riu Ehrn, un afluent del Rhin. Pel que fa a les zones potencialment aqüíferes, es poden definir 1) aqüífers penjats en superfície desenvolupats en el sòl d'alteració i 2) zones fracturades utilitzades com a zones de transferència d'aigua vers l'aqüífer regional del Rhin.

Les dades geofísiques en que es centra l'estudi són 31 sondejos audiomagnetotel·lúrics distribuïts en malla de 50 metres de pas, i perfils de tomografia elèctrica de resistivitat (Fig. 5.4) (Behaegel, 2007). Tanmateix, només s'ha presentat el model de tomografia elèctrica de resistivitat coincident amb línia 4 audiomagnetotel·lúrica, ja que presenta una llargària d'uns 300 m i una profunditat suficient per ser comparades amb els models audiomagnetotel·lúrics.

L'anàlisi dimensional de les dades audiomagnetotel·lúrica conclou la tridimensionalitat de les dades (Fig.5.6). Aprofitant aquest fet i que els sondejos estaven distribuïts en un '*grid' 2D* s'ha creat un model directe 3D. El model 3D directe es crea seguint un procés de prova i error per tal d'ajustar les dades a les respostes del model, en aquest cas calculades amb l'algorisme d'inversió de Mackie and Madden (1993). Per intentar simplificar el temps de treball el model inicial considerat va ser un model d'interpolació del models 1D de tots els sondejos. El model final ajusta el determinant del tensor d'impedàncies amb un RMS total de 5.43 en la resistivitat i un 3.95 de les fases considerant un 5% d'error en les components de la impedància.

El model 3D final mostra estructures geoelèctriques que es podrien associar a hidrogeofàcies diferents (Fig.5.7 i 5.8). Així s'observa una zona superficial fins a uns 30 m de fondaria que mostra baixa resistivitat associada a zones de sòl d'alteració i/o fractures superficials amb alt contingut en aigua i/o argila. Per sota, segellant aquesta primera capa es visualitza una zona de resistivitat major i ,per tant, de menor alteració o fracturació. Cap a uns 100 m de profunditat, s'observa una zona de baixa resistivitat que podria ser associada a fractures o zona de discontinuïtat litològica per on podria existir circulació de fluids. I

finalment, en profunditat fins al límit de resolució del model, existeix un domini més homogeni i resistiu i per tant, menys fracturat.

S'ha realitzat un anàlisi de sensitivitat de la zona de baixa resistivitat en profunditat, ja que aquesta estructura geoelèctrica va ser un resultat inesperat (Fig.5.9). S'han calculat diferents models 3D, amb i sense aquesta zona de baixa resistivitat i s'han examinat els ajustos de les dades de camp amb les respostes dels models. El model 3D directe sense la zona de baixa resistivitat, crea un únic domini resistiu en profunditat, el qual ajusta molt pitjor les dades, ja que les respostes presenten un caràcter massa resistiu. Per tant, aquesta zona de relativa baixa resistivitat ha d'existir per poder ajustar les dades.

Les tècniques geofísiques de tomografia elèctrica de resistivitat (DC superfície) i audiomagnetotel·lúrica (AMT) produeixen models de resistivitat elèctrica del subsòl, però per tal d'observar la complementarietat de les dades s'ha transformat les dades de tomografia elèctrica al domini de les freqüències a partir d'una llei empírica proposada per Meju *et al.* (1999) (eq 5.1) (Fig.5.10 i 5.11). Les mesures d'AMT i DC de superfície s'han comparat tant a nivell de dades en el domini de les freqüències com amb els models il·lustrant la diferent resolució i profunditat de investigació de cada tècnica. El perfil de resistivitat aparent de DC superficial presenta una alta densitat de mesures en comparació dels sondejos audiomagnetotel·lúrics, tanmateix el rang de freqüències mesurades és menor que la de l'AMT. Cal remarcar la existència de solapament entre ambdues tècniques, en el rang de freqüències d'entre 10^4 i 10^5 Hz. En aquest rang de freqüències s'observen les mateixes estructures geoelèctriques (Fig. 5.10).

Els sondejos de AMT permeten estudiar els sistemes aqüífers des de desenes de metres fins a pocs centenars de metres enllaçant la dinàmica superficial, poc detallada, amb les parts més profundes del sistema aqüífer. D'altra banda, els perfils de tomografia elèctrica, degut a la seva separació entre elèctrodes de 5m, en aquest cas, proporciona imatges detallades superficials fins a poques desenes de metres. La complementarietat d'aquestes dues tècniques obre les perspectives de les tècniques inversió conjunta per obtenir models que satisfacin els dos tipus de dades. Integrant els dos tipus de dades s'obtindrien models més profunds amb una millor resolució de les estructures geoelèctriques superficials.

Capítol sisè, Aplicació hidrogeofísica de Spring Valley, Nevada, USA. Aquest capítol presenta una aplicació hidrogeofísica portada a terme a Spring Valley, una vall de 110 km de longitud situada al desert de Nevada, Estats Units d'Amèrica (Fig.6.1). L'objectiu principal de l'estudi audiomagnetotel·lúric és aportar informació estructural de la morfologia de les falles normals que limiten la conca extensiva de Spring Valley per a la construcció del model hidrogeològic de la conca.

Spring Valley es situa a la regió estructural de *Basin and Range*, caracteritzada per un sistema de *horsts i graven* de direcció N-S. Aquestes conques extensives d'edat Neògena estan reblertes de materials detrítics i volcànics. D'altra banda, les serralades presenten litologies molt diverses degut a la gran extensió longitudinal, i per tant, per l'evolució geològica diferencial de cada zona des del Precambrià (Fig.6.1 i 6.2). En la zona d'estudi, el basament està compost per sèries molt potents de materials Precambriàns i Paleozoics constituïts per unitats calcàries, quarsites, pissarres, dolomies, esquistos i/o roques cristal·lines en funció de la seva situació dins la conca. Hidrogeològicament, es considera que els sistemes aqüífers estan organitzats en valls que es relacionen a traves de zones fracturades. Els aqüífers principals se situen en les roques calcàries paleozoiques, i els sediments volcànics i detrítics que rebleixen les conques.

Durant els anys 2005 i 2006 s'han realitzat diverses campanyes d'AMT amb les que s'han pogut construir cinc perfils audiomagnetotel·lúrics distribuïts al llarg de la vall, en el flanc oest de la conca (Fig. 6.3). La direcció de les estructures geològiques N-S de la zona feia pensar que la dimensionalitat de les dades audiomagnetotel·lúriques podria ser 2D. Tanmateix, degut a la escala de treball i segurament a la disposició de la falla principal no és sempre estrictament N-S, tots els perfils excepte un presenten un caràcter tridimensional.

Els models audiomagnetotel·lúrics han estat creats amb el codi DetREBOCC per tal d'aproximar un medi 3D a perfils bidimensionals. El prefil B també s'ha modelat amb el codi REBOCC invertint els modes TE i TM conjuntament. El model 2D invertit amb els modes TE+TM i el mode determinant presenten una gran similitud en les principals estructures geolèctriques, validant així la utilització del codi que permet invertir amb el determinant del tensor d'impedàncies (Fig.6.5).

Els perfils geològics preexistents, els models de gravimetria i dades de magnetometria han ajudat en la interpretació dels models audiomagentotel·lúrics per tal de delimitar la conca i localitzar falles principals (Fig.6.7). La posició i morfologia de la falles principals limitants de la conca extensiva són clarament visualitzades en els models de resistivitat, ja que el basament presenta resistivitats superiors als sediments que rebleixen la conca. Per altra banda, dins del

rebliment de la conca es poden observar 1) zones de baixa resistivitat les quals es podrien associar a zones aqüíferes o amb contingut elevat d'argiles i 2) zones anòmalament d'alta resistivitat que podrien ser associades a calcretes. A més a més, s'han pogut caracteritzar les zones amb sediments volcànics que presenten una resistivitat característica. La taula 6.2 mostra les unitats geoelèctriques que s'han caracteritzat a través del models de resistivitat, on l'interrogant denota on seria necessari tenir informació addicional per tal de fer una interpretació més correcta.

Dominis geoelèctrics	**Resistivitat ohm·m**	
	Saturats	No saturats
Sediments detrítics	10- 40	100-1000
Materials volcànics	10-20 (?)	10-20 (?)
Basament	~ 100 (?)	> 600

Conclusions

La hidrogeofísica; eina multidisciplinar en l'avaluació de sistemes aqüífers

La hidrogeofísica és una disciplina científica que ha sorgit en els darrers anys amb el repte d'assolir un major grau de coneixement del medi subterrani integrant dades hidrogeològiques i geofísiques. L' estat de desenvolupament de la hidrogeofísica, els objectius i les línies de recerca actual, s'han presentat en el desenvolupament d'aquesta tesi.

Des d'una perspectiva hidrogeològica, existeixen diverses estratègies d'utilització de mètodes geofísics d'una manera efectiva. La tria del tipus d'instrumentació per a cada investigació depèn sobretot dels objectius de l'estudi, la resolució i precisió desitjades, les condicions del medi, el temps, el pressupost, els recursos computacionals i la informació prèvia de que es disposa.

La multidisciplinarietat de la hidrogeofísica és un dels seus punts forts per tal de crear models hidrogeològics més complerts i detallats. Les dades hidrogeològiques han de ser considerades com a punts de control i de calibració de les dades geofísiques, i per tant els models geofísics han d'estar en acord amb les dades hidrogeològiques com la millor garantia de la bondat i qualitat dels models geofísics finals. Per altra banda les dades geofísiques proporcionen informació més contínua tant temporal com espacialment, la qual cosa pot completar la informació puntual hidrogeològica. Per tant, és evident que ambdues disciplines tenen un gran potencial en complementar-se.

D'entre els molt diversos mètodes geofísics que poden ser utilitzats en les avaluacions de sistemes aqüífers, els mètodes elèctrics i electromagnètics són els més utilitzats a l'hora de caracteritzar processos i paràmetres hidrogeològics. La resistivitat i la permitivitat elèctrica depenen altament del tipus de material, l'estructura de l'espai porós, el contingut en aigua i la seva qualitat. Per altra banda, els mètodes sísmics, gravimètrics i magnetomètrics poden ajudar en la caracterització estructural del medi, límits i estructures internes que controlen la circulació del fluid subterrani.

El mètode Audiomagnetotel·lúric

La sensibilitat als processos i paràmetres hidrogeològics, un gran ventall d'escales de treball i que l'AMT és un mètode geofísics 3D real, confereixen a aquest mètode una gran capacitat per a la seva aplicació en les investigacions hidrogeològiques.

La font controlada. El soroll (electromagnètic) cultural, és una de les principals limitacions de les dades electromagnètiques sobretot a prop de zones habitades, que és on les problemàtiques mediambientals són presents. Per tal de millorar la proporció senyal-soroll, l'instrument d'adquisició audiomagnetotel·lúric que s'ha emprat treballa amb un parell de dipols magnètics horitzontals (HMD) com a font artificial. La millora de les dades usant la font a prop de zones habitades ha estat comprovada. La font, però, s'ha de col·locar en la zona de camp llunyà per a acomplir l'assumpció d'ona plana, i no introduir efectes de camp proper si la distància receptor transmissor és massa petita en funció de la resistivitat del medi. Experimentalment s'ha comprovat la signatura característica de situar el HMD en camp proper, on la corba de resistivitat aparent presenta una pendent negativa de 45º, mentre que les fases es situen a 90º.

El disseny de la campanya de camp. La modelització inversa audiomagnetotel·lúrica ustilitzant dades sintètiques, tant en 2D com en 3D, és un pas clau abans de portar a terme una campanya de camp. Aquests models serveixen per a planificar més eficientment la campanya, ja que amb ells es pot obtenir un informació preliminar sobre la resolució, morfologies esperables i profunditat de investigació de cada medi. Per tant són útils per tal d'assegurar l'acompliment dels objectius particulars de cada estudi.

L'anàlisi de la dimensionalitat. L'anàlisi de dimensionalitat de les dades audiomagnetotel·lúriques és un pas important per tal de triar el tipus de modelització multidimensional adient. Els estudis hidrogeofísics presentats corresponen a medis tridimensionals, i per tant, la correcta aproximació a aquests medis seria a través de models tridimensionals. Tanmateix, s'han obtingut bons resultats usant l'aplicació 2D DetREBOOC per tal d'investigar zones 3D. L'algorisme d'inversió utilitza el determinant del tensor de impedància, ja que matemàticament és invariant sota rotació i, per tant, és útil quan les dades no són totalment 2D. Els models 2D creats amb el mode determinant presenten una bona qualitat evidenciada en 1) la validació dels models 2D amb la litologia i les mostres hidroquímiques, i en 2) la similitud entre els models 2D i els corresponents talls del models inversos 3D.

Resolució de les estructures. Les estructures geoelèctriques presents en els models inversos han d'estar revisades i analitzades abans de poder acceptar el model final. Aquest procés s'anomena anàlisis de sensibilitat. El procés segueix iterativament un esquema de prova i error modificant les estructures i resolent el problema directe per obtenir millors ajustos entre les dades i les respostes del model. Al mateix temps, si es tenen dades hidrogeològiques o altres dades geofísiques, també poden ajudar en l'ajust entre les dades i la resposta dels models constrenyent el problema d'equivalència dels models geofísics. L'anàlisi de sensibilitat de les estructures geoelèctriques clau dels models 2D i 3D del estudi dels sistemes aqüífer de la Tordera, La Soutte, i Spring Valley han estat realitzades per tal de millorar els models finals.

Models 3D. La correcta aproximació als medis geoelèctrics tridimensionals és construir models 3D. Tant els models 3D directe com els 3D inversos són unes eines de treball molt valuoses per a obtenir una avaluació completa dels sistemes aqüífers. Els models 3D permeten obtenir una visió global de les propietats i processos dinàmics del sistema, mentre que els models 2D només proporcionen informació parcial i limitada. La creació dels models 3D inversos i directes és un procés temporalment costós degut al gran nombre de paràmetres a computar. No obstant, s'ha utilitzat un model inicial construït a partir de la interpolació dels models 1D, el que ha estat una eina eficient tant en resultats com en el temps de convergència numèrica. El model inicial ajuda a l'algorisme matemàtic en la busca d' un model 3D que ajusti les dades. Malles més fines, més períodes i més estacions, haurien millorat els models 3D que s'han presentat, tot i que el temps de computació hauria augmentat substancialment.

Monitoratge audiomagnetotel·lúric. S'ha provat que el mètode audiomagnetotel·lúric és un mètode geofísic prou sensible per a caracteritzar canvis dinàmics dins d'un sistema aqüífer. En concret, l'AMT ha estat capaç de monitorar els canvis hidroquímics estacionals deguts al moviment de la cunya de intrusió marina i, per tant, de la seva zona de transició. La seqüència dels set models geofísics presentats està en acord amb l'estat hidrològic dels sistema.

Aplicacions hidrogeofísiques

A la segona part de la memòria de tesi s'han presentat tres estudis hidrogeofísics a tres escales diferents. L'AMT, conjuntament amb d'altra informació hidrogeològica i geofísica, pot esdevenir una eina importat per millorar el modelat hidrològic, la planificació, la gestió i el control dels recursos i reserves de les agües subterrànies.

Escala conca-local. L'avaluació del sistema aqüífer de la Tordera tenia com a objectiu principal investigar hidrogeofísicament un sistema fluvio-deltaic i el seu estat d'intrusió salina. La contaminació per intrusió salina és una de les grans problemàtiques de la gestió de les aigües subterrànies d'aquesta zona. En l'aproximació hidrogeofísica, el model hidrogeològic que vam crear a partir de la recopilació de descripcions litològiques és massa groller per a ser comparat amb els models geofísics, ja que aquest últims són molt més continus. Per tant la calibració i validació dels models geofísics s'ha fet a patir de dades hidrogeològiques superposades. L'estudi multidisciplinari es centra bàsicament en el treball conjunt de les dades hidrogeològiques, models sísmics i models 2D i 3D audiomagnetotel·lúrics. Això ha permès obtenir imatges geoelèctriques de qualitat que poden enllaçar-se a hidrofàcies característiques. Tant els models 3D com els 2D mostren clarament l'estat d'intrusió d'aigua salina del sistema i els seus controls. Per una banda la intrusió salina progressa preferentment per un paleocanal a la zona oest del delta, però també està controlada estructuralment per la morfologia del basament. En particular, en la direcció del riu actual el basament es troba en una posició molt més superficial que a l'oest del delta, és a dir, fa de barrera en aquesta direcció. L'experiment de monitoratge audiomagnetotel·lúric ha visualitzat els canvis estacionals de la posició intrusió salina i de la seva zona de transició al llarg d'aquest camí principal d'intrusió.

Escala local. La Soutte (França) és un laboratori natural hidrogeofísic situat sobre un medi fisurat en el que s'han analitzat les dades audiomagnetotel·lúriques i de tomografia elèctrica de resistivitat. El model d'AMT directe 3D revela zones geolèctriques característiques. En superfície s'observa una zona de baixa resistivitat associada a aqüífers penjats superficials, corresponent al desenvolupament del sòl d'alteració on coexisteixen un gran contingut en aigua, argila, arena i zones fisurades. En profunditat (~100 m), s'observa una altra zona de baixa resistivitat, el que sugeriria l'existència d'una zona fracturada usada com a zona de transmissió vers l'aqüífer regional del *graven* del Rhin. Les zones més resistents del model s'associen a material més massiu.

L'anàlisi de les dades i models audiomagnetotel·lúrics i de tomografia elèctrica de resistivitat mostren la resolució i profunditat d'investigació de cada tècnica. La creació de models utilitzant ambdós conjunt de dades milloraria els resultats finals obtenint una bona profunditat d'investigació mantenint una alta resolució en la zona més superficial. La inversió conjunta és un dels reptes i camps de desenvolupament actual de la hidrogeofísica.

Escala regional-conca. L'estudi hidrogeofísic de Spring Valley, a la regió estructural de "Basin and Range" als Estats Units, es centra en la interpretació conjunta dels models

aduiomagnetotel·lúrics, gravimètrics i les dades de magnetometria. L'objectiu principal és determinar la morfologia de la conca per a la creació del model hidrològic de gestió i explotació dels recursos hidrologics de la vall. Els cinc models 2D audiomagnetotel·lúrics mostren els canvis més importants de la morfologia de la falles principals que limiten de la conca extensiva així com les característiques del rebliment de la vall. S'han pogut delimitar el basament, els diferents materials detrítics amb zones saturades i/o argiloses, les calcretes i els materials volcànics.

Perspectives de futur

De la mateixa manera en que es van assimilar els mètodes sísmics dècades enrere per tal de determinar estructures, el mètode audiomagnetotel·lúric ha de passar un procés de normalització i acceptació entre la comunitat geocientífica com a una bona eina per visualitzar i caracteritzar estructures i propietats dels materials geològics, hidrogeològiques, ambientals i d'enginyeria civil. Per aquesta raó els geòlegs i geofísics han de treballar conjuntament per tal de poder extreure tota la informació possible de les dades i models. La sensibilitat en la resolució i precisió de les estructures geoelèctriques pot complementar la informació puntual litològica hidroquímica i la clàssica informació estructural sísmica per tal de crear models amb més informació de les propietats del medi.

El món real necessita la creació de models tridimensionals on s'inscriuen tant les estructures, propietats del medi subterrani, com la caracterització de la dinàmica del processos. El mètode audiomagnetotel·lúric és un mètode 3D real i, per tant, seria esperable que s'incrementés la seva utilització per a crear models 3D. Els models d'AMT inversos estan encara en un estat de desenvolupament i test on encara s'han de fer moltes millores per tal d'assegurar bons resultats més ràpidament. Models més grans, és a dir, models amb malles més fines, més períodes i més sondejos, tant en el Tordera com en La Soutte, proporcionarien millors resultats.

El desenvolupament de les relacions petrofísiques per tal de quantificar propietats del medi subterrani, és una de les perspectives més importants i l'objectiu últim que la hidrogeofísica ha de resoldre. En les tres aplicacions hidrogeofísiques, l'avaluació quantitativa hidrogeològica dels models geofísics no s'ha presentat ja que no existeix una relació o llei que resolgui tots els casos. En general, les relacions es deriven comparant una gran quantitat de dades geofísiques i hidrogeològiques o utilitzant lleis generals assumint valors estàndard per a

cada tipus de medi. En els tres casos d'estudi presentats les relacions petrofísiques no han estat generades degut a les poques dades hidrogeològiques i geofísiques superposades tant en l'espai com en el temps. Per completar totalment les avaluacions del sistemes aqüífers de la Tordera, La Soutte i Spring Valley, encara s'ha de treballar en les relacions petrofísiques i poder obtenir les propietats hidrològiques del sistema.

Part I
Introduction and fundamentals

1. Introduction
2. Hydrogeophysics
3. The audiomagnetotelluric method

Chapter 1. Introduction

The shallow subsurface of the earth is an extremely important geological zone that yields much of our water resources, supports our agriculture and ecosystems, and influences our climate. This zone also serves as the repository for most of our wastes. Some authors refer to this zone as "the critical zone" (Slater et al., 2006) where complex interactions exist between processes in hydrogeology, geochemistry and geobiology. Safe and effective management of our natural resources is a major challenge, that is, not to overexploit and pollute the aquifer systems. Expansion of the population and economical growth require greater volumes of fresh water, and at the same time emphasize the need to protect and sustain known supplies and sources. Economical growth is usually experienced at the expense of the environment. However, future tendencies focus on minimizing this impact, given that water resources and reservoirs are crucial for modern life development. To better identify groundwater resources, its biological and chemical characteristics as well as its boundaries and flow properties have to be assessed with sufficient accuracy. Well and bore holes alone cannot achieve this objective. They provide core sampling, in situ test and piezometric measurements but are invasive methods that can modify water circulation, and may provide too sparse information. Geophysical techniques are non-invasive, cost-effective and can be performed with high spatial sampling. That is, geophysics have an enormous potential for complementing hydrogeological data. Nonetheless, direct measurements (hydrogeological data) are required as the hard data to calibrate, validate and use on the petrophysical relationships linking geophysical models with hydrogeological properties.

The hydrogeophysics discipline has emerged in recent years to investigate the potential that geophysical methods hold for providing quantitative information about subsurface hydrogeological parameters and processes. Hydrogeophysical investigations strive to move beyond the mapping of geophysical "anomalies" by providing quantitative information that can be used as input into flow and transport models. Hydrogeophysics as many other geoscientific disciplines is based on the previous experience associated with the mining and petroleum industries. However, its working scale has to be modified for its applicability to the near surface zone where the pressure, temperature and depth conditions are different, and the contrasts are subtle compared to deeper features. In addition, geological characterization, from a hydrological perspective, concerns the

dynamics of the water through the subsurface. Geological structure, transport and storage of water are the key parameters to understand hydrological processes.

Different hydrogeological problems could benefit from geophysics. Among them are the determination of the aquifer geometry (bottom, top and lateral boundaries), characteristics of fractured rocks (location of faults and fissures, characteristics of fluid circulation), knowledge of the hydraulic properties of the aquifer (porosity, clay content, transmissivity, permeability) quality of the water (fresh, salty, polluted), and monitoring dynamic processes (seawater wedge dynamics or seepage through the vadose zone).

Geophysical methods can perform at different scale lengths, and thus attain different resolutions. This versatility ranges from regional watersheds to catchments studies, and from airborne studies to surface and borehole methods. The choice of a particular techniques or acquisition approach depends mainly on the objective of the investigation relative to the sensitivity of the geophysical method, the desired resolution, conditions at the site, time, funds, and computational resources available for the investigations. However, the integration of hydrogeological data with geophysical data is essential to provide a better understanding of the underground media over various scales.

The present thesis has been divided into two main parts. Part I has a theoretical character where the novel hydrogeophysical discipline has been reviewed. In particular, electrical and electromagnetic methods have been critically reviewed given that the electrical resistivity has a high capability on providing information of hydrological properties and processes. The audiomagnetotelluric method (AMT) has been discussed with a special insight, presenting an ideal suitability for aquifer systems appraisal. The AMT system used on the subsequent aquifer appraisals has been tuned up. The equipment and its controlled source have been tested to ensure the optimal efficiency. Part II is composed of three different hydrogeophysical case studies at different scales where AMT plays a key role on the approach to each aquifer system.

1.1. Part I

Chapter two, ***Hydrogeophysics***, aims to review the actual state of the hydrogeophysical discipline showing the paramount perspectives of the geophysical methods applied to the hydrogeology discipline. Hydrogeophysical importance relies on its multidisciplinarity. That is, the

joint interpretation of geophysical and hydrogeological data to get better approach and more constrained/reliable hydrogeologic models. A general overview of the geophysical methodology is demonstrated from instrumentation to modelling processes, as well as the kind of hydrogeological objectives that could be solved with the different geophysical methods. The principal geophysical methods that have actually been applied to hydrogeology problems are reviewed, as well as their challenges, limitations and concerns. In particular, electric and electromagnetic methods that provide electrical resistivity models have been examined in detail. The electrical resistivity is considered, given that this property is highly controlled by the hydrogeological properties of the media (lithology, porous structure, water content and quality). However, the complexity of the property contribution of the geophysical response made the transfer step from geophysical model to hydrological properties a complex issue. This research will continue to be undertaken to find out a reasonable solution.

Chapter three, ***Audiomagnetotelluric method (AMT)***, presents further insights of the AMT frequency domain method. Firstly, theoretical basics of the AMT method, investigation depth and magentotelluric family methods (frequency recording capability) are reviewed. Further on, the determinant mode modelling process is discussed in order to obtain a reasonable approach of three-dimensional media along two-dimensional profiles. This chapter demonstrates in detail Stratagem EH4 equipment, in particular, source effects, optimal transmitter receiver distance, and signal improvement of controlled electromagnetic source.

1.2. Part II

Chapters four, five and six are three different aquifer appraisals at three different scales, using a combination of different geophysical techniques, as well as hydrogeological information. Each case study has its own and different character due to its diverse objectives and therefore its different approach. However, as a common treat, audiomagnetotellurics is presented as the main geophysical tool that could provide a better hydrogeologic-structural approach in conjunction with other geophysical methods including direct current (DC), seismic, gravity and magnetometry. Tordera extensive hydrogoephysical study is developed on the Geoelec project framework REN2002-04538-C02 (Marcuello and Plata, 2005). La Soutte and Spring Valley case studies are the result of two international stages performed during 2004 and 2006 respectively. The former stage was conducted at l'Institut Physique du Globe, Ecole et observatoire des Sciences de la Terre, Strasbourg, Université Luis Pasteur within Proche Surface research group. The latter stage was held at the Unite States Geological Survey, with the Geophysical Unit Menlo Park research group.

Chapter four, ***Hydrogeophysical application: Tordera deltaic aquifer, Spain,*** is a hydrogeophysical application carried out on a porous aquifer media extensively affected by seawater intrusion. This chapter presents a multidisciplinary approach to a fluviodeltaic aquifer system. Hydrogeological information, audiomagnetotelluric (AMT), seismic reflection and velocity tomography models have been evaluated together to provide spatially continuous information about aquifer properties and processes. Two and three-dimensional inverse models have been obtained and validated with hydrogeological data. In addition, an AMT experiment has been performed every four months (from 2004 to 2006) along the same profile to monitor seasonal seawater changes along the main seawater intrusion path. Finally, direct current, time domain electromagnetic (TDEM) and audiomagnetotelluric collocated models are presented.

Chapter five, ***Hydrogeophysical application: La Soutte, Vosges***, ***France*** is based on the Audiomagnetotelluric study on "La Soutte", natural hydrogeophysical laboratory. In this case, 3D AMT forward and 2D inverse models look into a small scale catchment area, aimed to provide a mesoscale framework for other geophysical applications carried out on the site. Combined use of AMT and DC surface resistivity has been also used to image different resolution and work scale of each method. DC and AMT joint inversion would improve final models, enlarging investigation depth while retrieving better shallow resolution.

Chapter six, ***Hydrogeophysical application: Spring Valley, Nevada***, ***USA*** presents the hydrogeophysical application carried out on Spring Valley, a 110 km long valley on the Nevada Desert aimed to provide a structural framework for water resources exploration and hydrological modelling. The target work scale is a large watershed basin with high variability of geological environments. Five 2D AMT profiles along the valley, together with gravity and magnetometry data have been analysed to map the aquifer bounding structure and sediment infill in a typical Basin and Range setting. Faults, stratigraphy, and estimates of depth to basement are valuable information for assessing groundwater potential.

Water is essential for life. It has been and will continue to be a hot topic in both the political and scientific fields for years to come.

Chapter 2: Hydrogeophysics

This chapter introduces the hydrogeophysics discipline and its significant contribution to the near surface environmental applications. An overview of the hydrogeological objectives that benefit from geophysics is presented. The full scope of hydrogeophysics is examined here, from instrumentation and modeling methods to the relationship between the geophysical signal and rock physical properties. In this chapter special emphasis is focused on the electrical resistivity property given that its response depends primary on the soil characteristics and water content. Several other geophysical techniques with high potential for the hydrogeophysical field are also described. Basics of the geophysical methods and schematic field procedures are briefly reviewed, including the main concerns and limitations. Finally, the hydrogeophysical challenges as petrophysical relationships, geophysical-hydrogeological integration and improvements on the current technologies are presented.

2.1. Introduction

Hydrogeophysics has emerged over the last decade as one of the more challenging disciplines in near-surface geophysics, aiming to improve the simultaneous use of geophysical and hydrogeological measurements. It can be described as the use of geophysical measurements for mapping subsurface features, estimating properties and monitoring processes that are important to hydrological studies, such as those associated with water resources, seepage through out the vadose zone, contaminant transport, and ecological and climate investigations (Rubin and Hubbard, 2005).

Natural heterogeneity and the large spatial variability of hydraulic parameters control groundwater dynamics: seepage within the vadose zone, water storage and the spread of contamination. Conventional sampling techniques for characterizing or monitoring the shallow subsurface typically involve collecting soil samples or drilling boreholes from which to acquire hydrological measurements. Direct measurements are typically sparsely distributed or acquired at an inappropriate scale. When the scale of the study area is large relative to the scale of the

hydrological heterogeneity or when the hydrogeology is complex, data obtained at point locations or within wells may not capture key information about the field-scale heterogeneity. Geophysical datasets can provide more dense 2D/3D information, are non invasive, are acquired faster than hydrologic measurements, and are cost-effective. Geophysical surveys therefore are often beneficial in improving hydrogeological knowledge.

Many recently published studies combining both disciplines, hydrology and geophysics, have achieved accurate subsurface characterization and have successfully monitored hydrologic processes with high temporal and spatial resolution over a wide range of spatial scales (Schwinn and Tezkan, 1997; Unsworth *et al.*, 2000; Krivochieva and Chouteau, 2003; Meju *et al.,* 2003; Goldman and Kafri, 2004; Pedersen *et al.,* 2005). Hydrogeophysics provides a meaningful perspective that many water agencies and councils have recently demanded (CUAHSI, 2005). Indeed, the interest in hydrogeophysics within the scientific community is reflected in the number of special sessions focusing on hydrogeophysics that have taken place during many recent conferences and workshops:

- 3rd NMR Madrid, 25 - 27 October 2006. International workshop on the magnetic resonance sounding method: a reality in applied hydrogeophysics,.
- SEG 2006. Annual meeting New Orleans. Geophysical monitoring for groundwater management.
- 18th EMIW, Spain. Session on EM Application for Environmental Studies. Review paper: Near surface electromagnetic characterization of hydraulic conductivity: from petrophysical properties to aquifer geometries, Slater (2006).
- SEG NSG section, 2006, Vancouver. Summer research workshop on Hydrogeophysics
- 19 th SAGEEP 2006, Seattle. Session on Watershed Geophysics.
- 11 th EAGE near-surface 2005, Palermo. Hydrogeophysics workshop.
- 2005 AGU Fall Meeting. Creation of the Near-Surface Geophysics Focus group (NS).

In the scientific literature, recent important contributions include: “Hydrogeophysics” (Rubin Y. and Hubbard S., 2005, Eds.); “Near-surface Geophysics” (Buttler D.K., 2006, Ed.); the special section on hydrogeophysics of The leading Edge June 2006, vol.25 nº6, from the Society of Exploration Geophysics; the essay from Slater *et al.* (2006) on Eos; the special

volume of the Hydrogeology Journal "The Future of Hydrogeology" (13 nº 1, March 2005) containing many geophysical contributions.

2.2. Hydrogeologic objectives

Geophysical data are used to assist in meeting a wide range of hydrogeological objectives taking advantage of the fact that the different geophysical techniques are sensitive to different properties and scales (Table 2.1). The work of Pellerin (2002), Guérin (2005), CUAHSI (2005), Hubbard and Rubin (2005), and Auken *et al.* (2006 a) among others, in reviewing the main geophysical applications to hydrogeological systems is drawn on in the following summary. The main hydrogeological objectives to be solved by geophysical methods can be categorized into three main areas: hydrogeological mapping, hydrological parameter estimation and hydrological process monitoring.

1) **Hydrogeological mapping** aims to define aquifer geometry, water table level, basement and boundaries, the fresh-salt water interface, contaminant plumes, fault and fracture zones, thermal aquifers (Goldman, 2003; Krivochieva and Chouteau, 2003; Arango, 2005; Falgàs *et al.*, 2005; McPhee *et al.*, 2006). Mapping provides a qualitative approach to deriving the main features at any desired work scale. The most common approach is to integrate the sparse borehole data that provide direct information, with the less invasive and more laterally continuous geophysical data to extrapolate information away from boreholes. However, problems could appear relatives to the chosen geophysical technique on matching the coarser resolution provided by a volumetric geophysical measurement with the finer resolution provided by the punctual borehole measurements (mesoscale gap). In addition to the scale problem, much literature has dealt with the heterogeneity of the subsoil as a main problem in estimating representative effective parameters over determined aquifer volumes. Sánchez-Vila *et al.* (2006) has published an extensive review of the main concepts and approaches to determine effective volumetric and representative hydraulic permeability. Hydraulic permeability is largely controlled by the heterogeneity of the subsurface, and the delineation of geological structures that constitute preferential flow paths, such as paleochannel and fractures become highly important.

2) **Hydrological parameter estimation** provides a quantitative approach to estimating the water content, water quality, and volumetric-effective parameters. Given the

difficulty of obtaining sufficient hydrologic data (pumping tests, hydrochemical analysis), geophysical properties are calibrated with co-located hydrological data, either at the field-scale using well logs or in the laboratory, to provide quantitative estimation of hydrogeological parameters (Mazác *et al.*, 1990; Wempe, 2000; Guérin *et al.*, 2001; Jarvis and Knight, 2002; Ferré *et al.*, 2005; Tullen *et al.*, 2006). The derived petrophysical relationships are extrapolated across the aquifer system and are used as input to numerical flow and transport models, assisting with subsurface management decisions.

The key parameters required to model groundwater flow and contaminant transport are hydraulic conductivity (K) and porosity (Φ). The porosity is defined as the volume fraction occupied by the pore space V_p in relation to the total volume.

$$\phi = \frac{V_p}{V_t} \tag{2.1}$$

In a saturated media, the hydraulic conductivity (K, m/s) determines the rate at which fluid flows through a saturated porous medium and can be defined for an homogeneous isotopic materials as:

$$K = \frac{\rho_w g k}{\mu} \tag{2.2}$$

where ρ_w (kg/m^3) is the density of the pore fluid, g (m/s^2) is the gravitational acceleration, μ (Ns/m^2) is the fluid dynamic viscosity, and k is the hydraulic permeability (m^2). K depends on the properties of the medium through k (pore size distribution and surface area, pore connectivity, and tortuosity) and on the fluid type through ρ_w, and μ.

Petrophysical relationships link geophysical properties with hydraulic conductivity (K), permeability (k) or porosity (Φ), and with water saturation and water quality. Much of the basis for estimating k or Φ assumes that the geometric parameters of the above equation (eq. 2.2) can be replaced with equivalent measurable geophysical effective properties using for instance electrical resistivity, dielectric constants, or porous acoustic relationships. As discussed below in considering the challenges facing hydrogeophysics (section 2.5), the derivation of petrophysical relationship is one of the main topics of research due to its complexity.

3) **Hydrological process monitoring** consists of imaging subtle geophysical property changes, caused by natural or forced systems. In general, water content and water quality changes are monitored (Park, 1997; Slater *et al.,* 1997; Singha and Gorelick, 2005; Tezkan *et al.,* 2005). Time-lapse measurements image the dynamic transformations and thus have the potential of investigating the flown and transport processes. Analysis and interpretation of the time dependent surveys is based on the comparison of geophysical data or models at the same location. Time–lapse measurements present inherent problems mainly associated with study scale in comparison with the dynamic property assessed, such as repeatability and accuracy on soundings location. These problems may introduce uncertainty into the results while looking for quantitative rates of change. Survey repeatability refers to the possibility of reacquiring surveys at different times where observed changes are only due to changes in the dynamic conditions of the subsurface (e.g. water content). Equipment, cultural noise and modeling procedures may produce variations on data and models on time spaced surveys. At the same time, time-lapse models decrease the repeatability uncertainty on the geophysical measurement and on data inversion procedures if constraining unchanging targets are retrieved on all the models. Problems related to the sounding location accuracy are related to the study scale length. In detailed shallow surface studies identical positioning plays a major role in performing quantitative comparisons, while in more regional surveys not being acquired exactly in the same position still allows larger scale changes to be observed.

Geophysical Methods		Obtained properties	Hydrogeological objectives
Airborne Satellite	Remote sensing Aeromagnetic Electromagnetic	Gamma radiation, Thermal radiation, Electromagnetic Reflectivity, gravity, Electrical resistivity	Bedrock mapping, faults, hydrothermalism, aquifer bounding characterization n and regional water quality
Surface	Seismic Refraction	P-wave velocity	Bedrock mapping, water table, faults
	Seismic Reflection	P-wave reflectivity and velocity	Stratigraphy, bedrock and faults delineation
	Electrical Resistivity DC Electromagnetic (TDEM, FDEM, CSEM, AMT) IP	Electrical resistivity Electrical resistivity Complex electrical resistivity	Aquifer zonation, water table, bedrock, fresh and salt-water interfaces and plume boundaries, estimation of hydraulic conductivity, estimation and monitoring of water content and quality Hydraulic conductivity
	GPR	Dielectric constant values and dielectric contrast	Stratigraphy, water table, water content estimation and monitoring
	NMR		Water content, mobile water content, pore structure
Cross hole	Electrical Resistivity DC GPR	Electrical resistivity Dielectric constant	Aquifer zonation, estimation monitoring of water content and water quality
	Seismic	P-wave velocity	Lithology, estimation and fracture zone detection
Well bore	Geophysical well logs	Many properties such as electrical resistivity, seismic velocity, and gamma ray	Lithology water content, water quality, fracture imaging
Laboratory	Electrical resistivity seismic, dielectric x-ray	Many properties such as electrical resistivity, seismic velocity, dielectric constant, x-ray attenuation	Development of petrophysical relationships, model validation and instrument sensitivity

Table 2.1: Main hydrogeophysical methods classed by investigation scale, its measured properties and the hydrogeological objectives (Modified form Rubin and Hubbard, 2005)

2.3. Geophysical methodology

This section provides a general overview of the main components of the methodologies used in geophysical studies. Types of geophysical equipment, modeling, interpretation procedures and links between geophysical data and rock physical properties have been reviewed.

2.3.1. Work scale

Advances in technology over the last decade have resulted in an exponential increase in the number and diversity of available geophysical instrumentation, adapted to different study scales. The study scales range from satellite, remote sensing and airborne, to surface and cross-hole, and at a more detailed scale well logs and laboratory measurements (Figure 2.1). Satellite, remote sensing and airborne geophysics work at regional scales, providing data which can be used to draw conclusions about the regional subsurface architecture. It could also be used to identify areas of interest for carrying out more detailed ground based surveys. At the other extreme, borehole geophysics provides continuous profiling or point measurements at discrete depths, and can be related to the physical and chemical properties of the surrounding wall rock, the fluid saturation of the pore spaces in the formations, the fluid in the borehole, the well casing, or any combination of these factors.

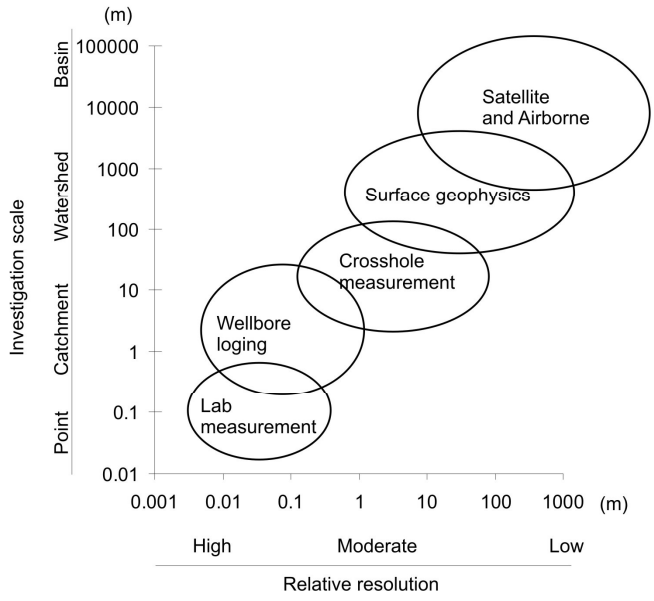

Figure 2.1: Schematic diagram of field geophysical length scale resolution and study objective scale (Modified form Rubin and Hubbard, 2005).

Prior to any geophysical survey, the compromise between resolution and work scale has to be assessed in order to choose the appropriate instrumentation and field survey design to achieve study objectives.

Because different geophysical techniques and different equipment are sensitive to different properties and scales, a combination of these is often used to characterize the subsurface. In addition, integration of complementary geophysical data sets with direct hydrogeological measurements can provide a better characterization of the subsurface at different resolutions and scales (Meju, 2000; Choudhury and Saha, 2004; Pedersen *et al.,* 2005).

2.3.2. Geophysical modeling, inversion and interpretation

Geophysical data can be used to extract either qualitative or quantitative estimates of the subsurface characteristics. The qualitative approach uses raw geophysical data to provide effective properties of a characteristic ground volume. It is often used for preliminary mapping or to assess relative changes. These raw data images are a smooth image of the subsurface, neither the properties values nor the depth position could be considered as true. Geophysical data require specific data processing and analysis for each technique before modeling and inversion processes can be performed. Careful data analysis can provide further accuracy of the final models or constrain the specific modeling approach, such as the dimensionality inversion (Ledo *et al.*, 2002 a; Martí *et al.,* 2004; Ledo, 2006).

The most important objectives of applying geophysical methods is to obtain quantitative information over the subsurface model space. The transformation from raw data to an estimated geophysical model is usually achieved using numerical forward modeling and inversion procedures, to provide a description of the subsurface fitting the observed data. Joint inversion of different geophysical sets (Gallardo and Meju, 2003; Bedrosian, 2006; Linde *et al.*, 2007) is used to constrain the possible subsurface models with multiple independent data sources, using either a deterministic approach, or a probabilistic approach such as stochastic inversion methods (Deutsch and Journel, 1998; Rubin and Hubbard, 2005; Gómez-Hernández, 2005).

Modeling and inversion

The numerical methods used in the modeling and inversion methods relate the observed geophysical responses to hypothetical subsurface structures that could generate them (Tarantola, 1987). The forward problem moves from an input model, m, towards the data

responses, d, (Figure 2.2). Forward modeling is a trial and error process that computes the responses of an input model, comparing the responses with measured data, modifying the model where the data are poorly fitted and then re-computing the responses until a satisfactory fit is obtained.

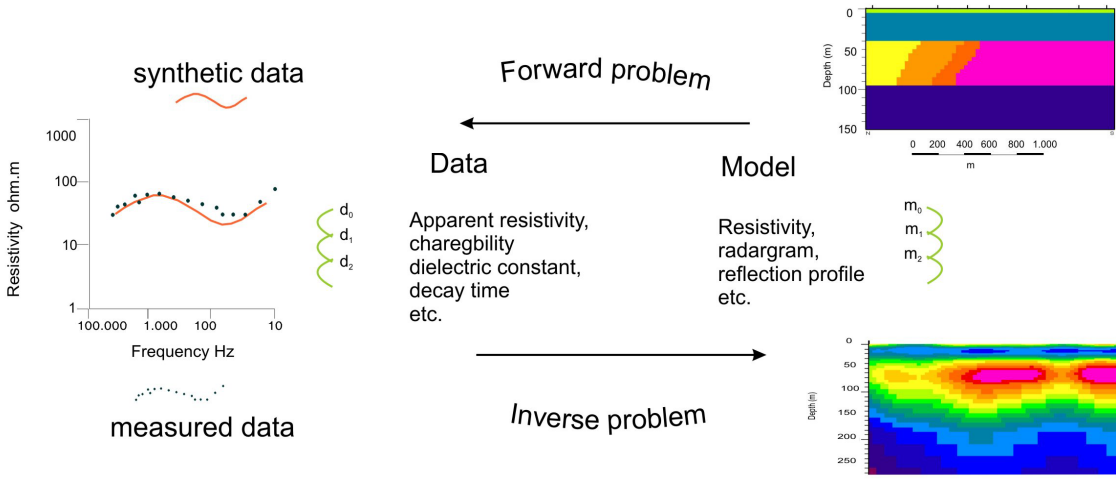

Figure 2.2: Flux diagram showing the forward and inverse processes. On the left an example of calculated and observed data and on the right created and inverted models.

The inverse problem is the search for a model, m, that reproduces the measured data, d, progressing in the opposite direction of the forward problem. In general, the inverse problem involves an automatic iterative process that searches for the best model, progressively reducing the misfit between the measured data and synthetic data from the model with each iteration. The iterative process proceeds until either a predefined threshold misfit value is reached or until an acceptable model is obtained. Inversion strategies used aim to achieve better numerical convergence, more stable solutions, three-dimensionality inverse modeling, and to reduce the computational time (Spichak and Popova, 2000; Zyserman and Santos, 2000; Haber *et al.*, 2004; Siripunvaraporn *et al.*, 2004; Avdeev, 2005; Haber, 2005; Siripunvaraporn *et al.*, 2005 a).

Forward modeling of a set of different expected models is essential before any survey to help designing the most appropriate survey configuration. The expected geophysical responses can then be compared with the instrument resolution (Maurer and Boerner, 1998). On the other hand, inverse models derived from synthetic data obtained from the forward modeling will allow the user to determine the expected resolution of the survey.

Interpretation accuracy

The model resulting from the modeling process provides an image that has to be considered as the estimated model, and never as the true model, given that it carries inherent uncertainties. All geophysical data is subject to errors (i.e. cultural noise, equipment noise), and it is therefore important not to overfit data, introducing artifacts into the models. Moreover, numerical processes and coarse discretization tend to provide regionally smooth models; however natural boundaries are usually sharp, thus the model itself will be an approximation. Finally, a study of the sensitivity of the model is required to provide confidence in the subsurface image. It is also desirable for the estimated model to be in accord with any available and realistic petrophysical, geological or well log data (Binley and Kemma, 2005).

2.3.3. Electrical properties

Geophysical techniques allow the detection of contrasts in rock properties such as density, resistivity and seismic velocity to map the subsurface. All these properties depend on the subsurface: lithology, porosity, structure and degree of porous connection, pore fluid chemistry and water content (Figure 2.3).

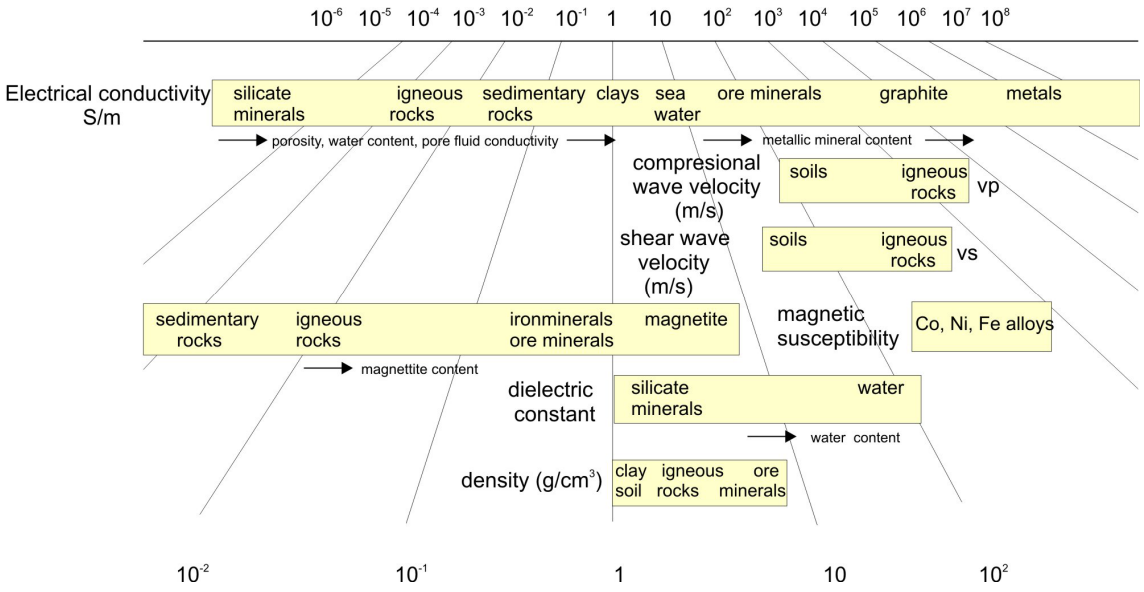

Figure 2.3: Scale ranges of rock properties, electrical conductivity, s and p-wave velocity, magnetic susceptibility, dielectric constant and density. (Modified form The Berkeley course on applied geophysics).

Table 2.1 summarizes important geophysical methods from a hydrogeological perspective, the properties that can be inferred and the hydrogeological objectives that can address with them. In addition, Figure 2.3 shows the typical ranges of values observed for the different properties (conductivity, density, P-S-wave velocity, etc.) that can be derived from geophysical measurements. And as can bee seen in Figure 2.3, electrical conductivity has the widest range of values and therefore provides the potential for better discrimination of material and processes occurring within the subsurface (Figure 2.4).

Electrical and electromagnetic (E&EM) methods are the most commonly used geophysical approaches for determining hydrogeological parameters and processes, and are presented in detail in this thesis (sections 2.4.4 to 2.4.9). E&EM are particularly suitable for hydrological studies in the vadose and saturated zones, given that the electrical properties of subsurface materials are highly dependent on lithology, water saturation, biochemistry of the fluid and movement of this fluid. Figure 2.4 presents the electrical resistivity variability of the different geological materials.

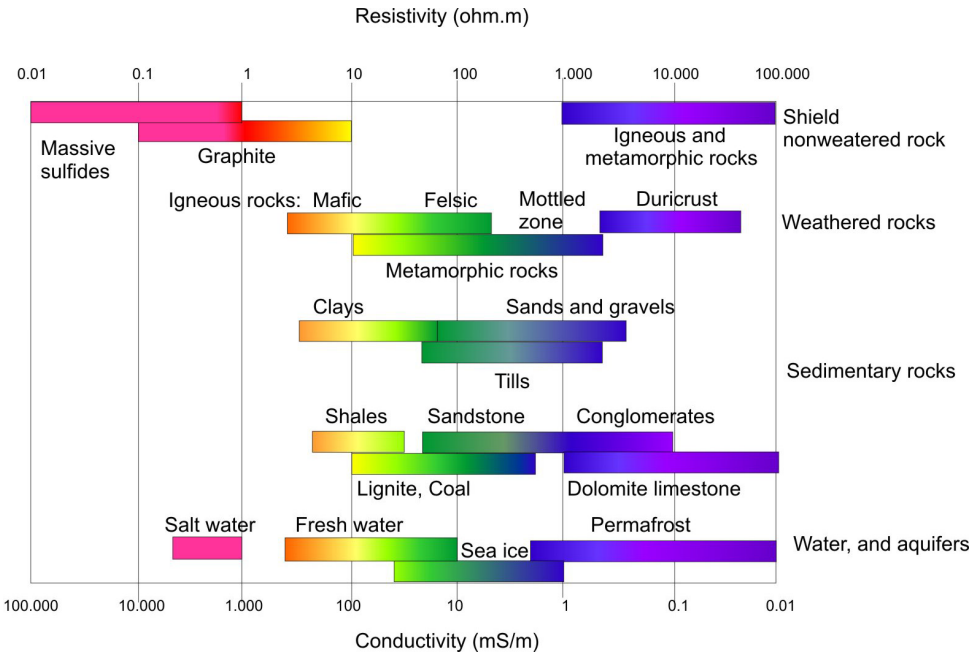

Figure 2.4: Electrical resistivity and conductivity of Earth materials (modified from Palacky, 1988).

When an electrical current naturally exists or is externally applied, the mobile charge carried within the soil starts to flow, and the differential charge distribution is measurable as a

potential difference. Using the constitutive relationships, the conductivity $\sigma^{(1)}$ (S/m) is the ratio of the current density $\vec{J}$ (A/m^2) to the electric field strength $\vec{E}$ (V/m)

$$\vec{J}=\sigma\ \vec{E} \tag{2.3}$$

similarly,

$$\vec{D}=\varepsilon\ \vec{E} \tag{2.4}$$

where the permittivity ε (F/m) is the ratio of the electric displacement $\vec{D}$ (C/m^2) to the electric field strength $\vec{E}$. Electrical conductivity describes how free charges flow to form a current when an electric field is present and the electrical permittivity describes how charges are displaced in response to an electric field.

The measured geoelectrical properties of Earth materials may be presented by a frequency (ω) dependent effective property (σ_{eff}, ε_{eff}) or frequency dependent complex property (Ward and Hohmann, 1988) expressed as

$$\sigma_{eff}(\omega)=\sigma'(\omega)-i\sigma''(\omega) \tag{2.5}$$

and

$$\varepsilon_{eff}(\omega)=\varepsilon'(\omega)-i\varepsilon''(\omega) \tag{2.6}$$

where ω represents the angular frequency proportional to the frequency f (Hz=s^{-1}) defined as:

$$\omega=2\pi f \tag{2.7}$$

Conductivity and similarly permittivity can be expressed as a magnitude and a phase angle that relates the in-phase and the out-of-phase measurement components, also dependent on ω:

(1) Electrical conductivity σ (S/m) and electrical resistivity ρ (ohm·m) are related by $\rho=1/\sigma$ and will be both used to refer to the electrical geophysical measurements.

$$|\sigma| = \sqrt{(\sigma')^2 + (\sigma'')^2} \tag{2.8}$$

$$\theta = \tan^{-1}\left(\frac{\sigma''}{\sigma'}\right) \tag{2.9}$$

where σ', σ'', ε' and ε'' denotes the real' and imaginary" electrical components that refers to the ohmic conduction, faradic diffusion, dielectric polarization, and energy loss due to polarization respectively. Equations 2.5 and 2.6 imply that there is more than ohmic conduction contributing to what is measured as electrical conductivity, and there is more than dielectric polarization contributing to what is measured as effective permittivity or stored energy in the system. A point of divergence in the literature is found in the assumptions that are made about the relative importance of these four parameters in order to extract values from the measured data.

Complex electrical conductivity or resistivity and complex permittivity contain the same information expressed differently and are related by the following expression:

$$\sigma^* = \frac{1}{\rho^*} = i\omega\varepsilon^* \tag{2.10}$$

where * indicates a complex number and the complex components are related as:

$$\sigma_{eff}(\omega) = \sigma'(\omega) + \omega\varepsilon''(\omega) \tag{2.11}$$

and

$$\varepsilon_{eff}(\omega) = \varepsilon'(\omega) + \frac{\sigma''(\omega)}{\omega} \tag{2.12}$$

σ' corresponds to the pore-filling electrolyte and the surface conduction due to ionic migration at the electrical double layer (EDL) (Purvance and Andricevic, 2000). It represents the ohmic conduction current (energy loss) detected by the DC resistivity and EM induction methods. σ'' is related solely to the fluid-grain interface (Slater, 2006), related to the polarization (energy storage) term measured with induced polarization techniques.

When modeling electrical behavior of Earth materials at frequencies greater than 100 kHz it is commonly assumed that $\frac{\sigma''(\omega)}{\omega} = 0$ and $\sigma'(\omega) = \sigma_{DC}$ (Knight and Endres, 2006) therefore equations 2.11 and 2.12 can be rearranged as:

$$\sigma_{eff}(\omega) = \sigma_{DC} + \omega\varepsilon''(\omega) \tag{2.13}$$

and

$$\varepsilon_{eff}(\omega) = \varepsilon'(\omega) \tag{2.14}$$

For low frequency electrical measurements, $\sigma'(\omega) \neq \sigma_{DC}$ and σ'(ω) is taken to be the source of the frequency dependence governing the electrical behavior, where two specific end-member cases can be defined:

1) When fluid conductivity dominates the electrical behavior, that is ionic conduction dominates $\sigma'(\omega) > \omega\varepsilon''(\omega)$, thus the electric loss term $\varepsilon''(\omega)$ can be neglected and effective resistivity can be formulated as

$$\sigma_{eff} = \sigma'(\omega) \quad (2.15) \qquad \text{and} \qquad \varepsilon_{eff}(\omega) = \varepsilon'(\omega) \tag{2.16}$$

2) When energy loss dominates the electrical behavior (fluid grain interface effects, ionic migration on the EDL) $\frac{\sigma''(\omega)}{\omega} > \varepsilon'(\omega)$ equations 2.11 and 2.12 can be expressed as

$$\varepsilon_{eff}(\omega) = \frac{\sigma''(\omega)}{\omega} \quad (2.17) \qquad \text{and} \qquad \sigma_{eff}(\omega) = \omega\varepsilon''(\omega) \tag{2.18}$$

Further insights into the petrophysical implications of the mixed electrical behaviors described above are provided on the section challenges of hydrogeophysics (2.5.1), given that it is a highly important research field currently under development.

Electric field strength can be determined through measurements of the potential difference which is a parameter measured by geophysical instruments. The potential difference, in turn can be defined as proportional to an apparent resistivity or permittivity. The apparent

property, either effective or complex, has to be inverted to obtain estimated value as a function of depth, or can be used directly as a preliminary and qualitatively approximation of the representative values of a subsurface volume. The following sections present the main electric and electromagnetic methods used where resistivity or permittivity can be inferred.

2.4. Geophysical methods

The following sections of this chapter present a brief summary of the geophysical techniques that may help solving hydrogeological questions. E&EM methods can provide direct hydrogeological information, whereas seismic, gravity and magnetic methods mainly provide complementary structural information (Table 2.1). In addition, the main advantages and concerns of each method are considered, as well as examples of hydrogeophysical case studies where geophysical methods have been efficiently applied to hydrogeological problems.

Complete reviews of the main geophysical methods applied to near-surface environments have been summarized in Hydrogeophysics (Rubin and Hubbard Eds., 2005), Near-surface Geophysics (Buttler, 2006). Previous reviews of E&EM methods for near surface investigations include Nobes (1996), Pellerin and Alumbaugh (1997), Tezkan (1999), Pellerin (2002), Pellerin and Wannamaker (2005), and Auken *et al.,* (2006 a).

2.4.1. Direct Current methods (DC)

DC methods are based on the injection of a current into the ground, to measure the generated electrical field as a potential difference. The experimental configuration of the electric resistivity method consist of four electrodes. Two of them are the current electrodes, AB, where a current I(A) is injected and the other two are the potential electrodes, MN, where a potential difference ΔV(V) is recorded. The potential difference measured depends on the current applied, the resistivity of the subsurface medium and the geometric factor (k) determined by the array configuration (distance between electrodes). The following expression relates these parameters to the apparent resistivity ρ_a:

$$\rho_a = k\frac{\Delta V}{I} \tag{2.19}$$

defined as the resistivity of a homogenous Earth to which the measure is equivalent. The apparent resistivity has to be inverted to obtain estimated resistivity versus depth.

Many electrode configurations are commonly used for ground-surface surveys, Schlumberger, Wenner, Dipole-dipole, where the electrode separations relate to the investigation depth and lateral resolution, according to the sensitivity distribution of each arrangement (Roy and Apparo, 1971; Edwards, 1977; Gabàs, 2003). There are numerous electric prospecting arrays depending on number of electrodes and its distribution on the ground. The most appropriate survey configuration (vertical electrical sounding, electrical resistivity tomography ERT or DC surface, cross-borehole) will strongly depend on the specific objectives of the project.

DC resistivity surveying is one of the most widely used methods given that field survey acquisition, processing and interpretation are relatively easy to perform. DC resistivity cannot easily determine the relative importance of electrolyte and surface conductivity on the bulk measured resistivity (Slater, 2006; Binley and Kemma, 2005; Purvance and Andricevic, 2000). However procedures for estimating hydraulic permeability and porosity have been attempted widely and will be discussed below.

Vertical electrical soundings (VES)

Vertical electrical sounding (VES) consist of a symmetric geoelectrical array that can be used to determine the electrical resistivity of the subsurface. Increasing progressively the spacing between the current electrodes AB, while keeping the potential electrodes MN at the same position, provides a sounding curve corresponding to the apparent resistivity versus depth of at single location. The wider the electrode spacing, the deeper is the investigation depth. Although the VES method is still widely used (Choudhury and Saha, 2004), nowadays VES is regarded as an outdated techniques as there are alternative instrumentation and electrode configurations that can provide 2D or 3D images of the subsurface more time-effectively.

Electrical surface imaging (DC or ERT)

Electrical surface imaging (DC surface) called as well Electrical Resistivity Tomography (ERT), combines surface profiling with vertical soundings using a multi-electrode array to produce 2D or 3D images of the subsurface resistivity. The measurements are acquired along profiles using a large number of electrodes placed equidistantly, allowing the electrodes to

be current and potential electrodes alternately. The procedure is repeated for as many combinations of source and receiver electrode positions as is defined by the survey configuration to create a full set of measurements (Figure 2.5). In new instrumentation developments continuous recording systems has been implemented that consist of fixed-electrode configurations taking measurements continuously as the instrument is towed over the ground such as for example the "Ohm-mapper" system (Geometrics) or "Paces" system (Sørensen, 1996).

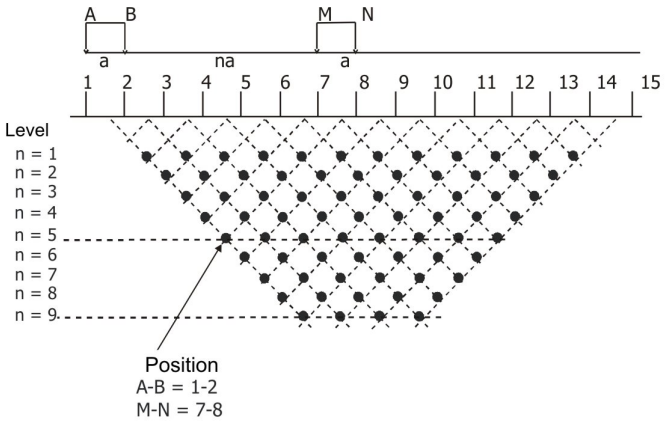

Figure 2.5: Measurement distribution of a surface resistivity arrangement that built the resistivity pseudo-section.

Measured data are presented as a pseudo-section in which the apparent resistivity is assigned to the midpoint of the four electrodes for each survey level (related to the spacing between current and potential electrodes) (Figure 2.5). The pseudo-section provides a smooth image of the 'true' resistivity structure with depth, so does not reproduce correctly either the electrical resistivity contrast between structures, or its exact spatial position. Solving the inverse problem is necessary to obtain the estimated resistivity with depth.

ERT is widely used in applications relating to hydrogeological problems (Slater *et al.*, 2002; Mota *et al.,* 2004; Auken *et al.,* 2006 a; Wilson *et al.*, 2006). Work scales may vary from 2-5 m up to 50-100 m depending on the electrode spacing and the resistivity of the ground, and limited by the strength of the current injected. DC has been used mainly to map static hydrological properties, structure or hydraulic pathways as well as to monitor temporal properties associated with changes in moisture or water quality.

2.4.2. Induced Polarization (IP)

Induced Polarization, IP, allows the spatial distribution of the subsurface resistivity characteristics to be determined in a similar manner to the DC method. However, IP is capable of determining the geophysical signal contribution from the pore fluids and from the fluid-grain interfaces that contribute to the real and imaginary parts of the electric conductivity. Given that IP is sensitive to the processes at the fluid-grain interface (effective clay content or internal surface area), it has been used to establish petrophysical relationships with hydraulic permeability (Knight and Nur, 1987; Purvance and Andricevic, 2000; Slater, 2006).

IP measurements are made in the field using a four electrode arrangement using non-polarizing electrodes. The measurements are based on recording the polarization and potential difference that occurs after applying a current in either the time or the frequency domain. Time-domain IP measures the decay voltage as a function of time after stopping the current injection (Figure 2.6, left). The gradual voltage decrease is a complex function of the electrical charge polarization at the fluid-grain interface and the conduction within the pore fluid (Binley and Kemma, 2005). The measurements are used to obtain an IP apparent resistivity and an apparent chargeability m_a

$$m_a = \frac{1}{(t_2 - t_1)Vp} \int_{t1}^{t2} V(t)dt \tag{2.20}$$

where Vp is the primary voltage and the integral measure the decay secondary voltage with time.

In the frequency-domain mode, after injecting an alternating current of characteristic angular frequency, the resistivity magnitude and the phase-shifted voltage of the complex electrical resistivity is measured (or the time delay between the transmitter current signal and the received voltage signal is measured) (Figure 2.6). A more challenging method is the Spectral Induced Polarization (SIP) involving the injection of current at different frequencies normally ranging between 0.1 to 1000 Hz. The complex resistivity, composed by a spectrum of impedances is obtained after applying a Fourier transform to derive apparent resistivity and phases as a function of frequency.

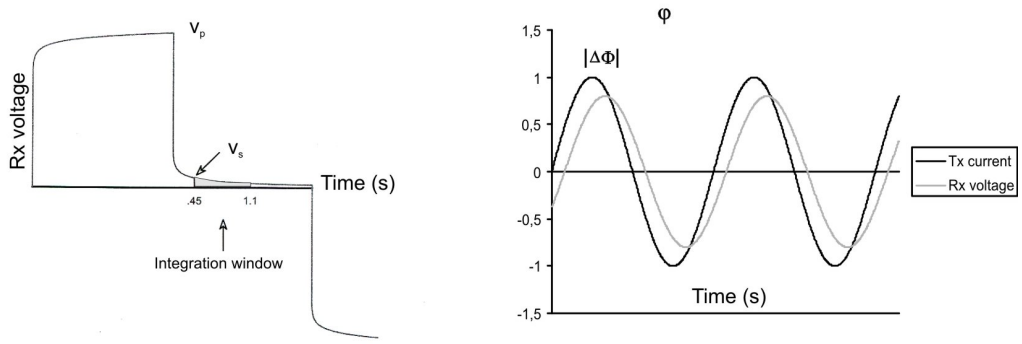

Figure 2.6: Left, Time domain IP waveform showing the primary voltage V_p, the secondary voltage V_s, and the integration window. On the right, frequency domain IP waveform showing IP response defined as a phase lag in the received waveform (Modified after Zonge *et al.*, 2006).

SIP has been reported to provide better results for extracting information on the pore-fluid conductivity and the fluid-grain interface (specific surface area) (Slater and Lesmes, 2002). It has been found to show a very close dependence on the specific surface area of pore volume ratios of soils, which represents the inverse of the hydraulic radius and exerts a critical control on hydraulic permeability (Slater, 2006). Although SIP provides better predictive estimates of hydraulic permeability, great disadvantages exist when compared to the DC applications due to the fact that 1) data acquisition and interpretation is more complex, 2) coupling effects and high noise-signal ratio and 3) physiochemical interpretation is still not fully understood (Slater and Lesmes, 2002).

2.4.3. Self Potential (SP)

SP is a geoelectrical natural field method based on the measurement of electric potentials generated by natural electrokinetic processes (composed by electrocinetism, electrothermalism and electrochemism among other phenomenon) usually when an electrolyte flows in a porous medium (Revil and Pezard, 1999). The spatial distribution of electric potential measured using non-polarizable electrodes allows the mapping of the steady-state current flow. A pore fluid is in chemical equilibrium with the rock matrix, resulting in an ion accumulation at the pore fluid interface known as the electrical double layer (EDL). Thus, when a fluid flows through a porous medium, so do the charged ionic species, resulting in the generation of an electrical current. If no other external electric current sources exist, the convection current is balanced by conduction current so as to maintain a constant electric charge. The conduction current is responsible for the measured SP signal. In this case, the measured potential V is

related to the fluid pressure, P, through the Helmholtz–Smoluchowski equation, (Darnet and Marquis, 2003):

$$\overline{\nabla} V = C \overline{\nabla} P \tag{2.21}$$

where C is the SP cross-coupling coefficient (V Pa^{-1}) that depends mainly on the water content, electrical conductivity, permittivity and dynamic viscosity.

SP has been commonly used for the monitoring of hydraulic processes and consists of the continuous measurement of the electric potential differences between two unpolarizable electrodes using high impedance voltimeter. This dipole is usually aligned along the direction of the water flow. In addition, to ensure a good electrical contact between the electrode and the medium, an electrically conductive solution (e.g. salty water with clay) is usually added around the electrode. The electrokinetic effects of water flow during pumping tests have been shown to generate surface Streaming Potential (SP) anomalies of several tens of milivolts that are well correlated with the geometry of the water table (Darnet, 2003). SP measurements have been used to estimate aquifer hydraulic properties, flux direction, and hydrothermal circulation near volcanic zones to forecast or characterize possible volcanic crises (Sailhac and Marquis, 2001). However, the main concerns about the method relate to low signal-to-noise ratios, and scale issues. In addition, more detailed investigations need to be conducted on the specific contribution of each elecrokinetic effect on the final measurement in order to have a better understanding of the results.

2.4.4. Electromagnetic methods: fundamentals

The principle behind electromagnetic methods (EM) is governed by Maxwell's equations that describe the coupled set of electric and magnetic fields change with time: changing electric currents create magnetic fields that in turn induce electric fields which drive new currents (Figure 2.7).

Most of EM techniques presented here (CSAMT, TDEM, FDEM, GPR and NMR) use a controlled artificial electromagnetic source as a primary field that induces a secondary magnetic field. However, other EM methods use the Earth's natural electromagnetic fields as well (AMT). Natural EM waves are generated by thunderstorm activity in the frequency range of interest to hydrogeophysical studies 1Hz to 1 MHz.

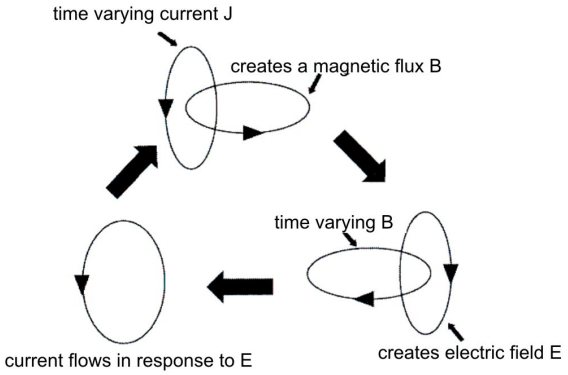

Figure 2.7: Wave nature of electromagnetic fields. A moving charge of current creates a magnetic field *B* which induces an electric field *E* which in turn causes electric charges to move and so forth (modified after Annan, 2005).

Combining the laws of Ohm, Ampere, and Faraday and the constitutive relationships results in a wave equation, which relates electromagnetic responses to rock physics in order to quantify material properties (Everett and Meju, 2005):

$$\nabla^2 B - \underbrace{\mu_0 \sigma \frac{\partial B}{\partial t}}_{\text{I}} - \underbrace{\mu_0 \varepsilon \frac{\partial^2 B}{\partial t^2}}_{\text{II}} = \mu_0 \nabla J_s \qquad (2.22)$$

where B (T) is the magnetic field, μ_0 (H/m) is the magnetic permeability, σ electrical conductivity (S/m), ε (F/m) electric permittivity, J (A/m^2) is the source current distribution, and t (s) is time. For most hydrogeophysical applications the Earth is generally considered to be nonmagnetic and μ_0 taken as the magnetic permeability of free space $\mu_0=4\pi.10^7$ H/m. In highly magnetic soils or in the presence of ferrous metal objects this assumption can break down.

Referring to the equation (2.22), term I is the energy dissipation relating to the electromagnetic diffusion and term II is the energy storage describing wave propagation,. The frequency of the electromagnetic waves controls the contribution of both diffusion and propagation phenomena through the Earth. The diffusion regime (< 100 kHz) is prevalent when term I is larger by several orders of magnitude than the wave propagation term (II), also called the quasi-stationary approximation. In the diffusion regime the propagation term II could be ignored and the electric permittivity plays no further role in the discussion of the AMT, TDEM, FDEM methods. In a similar manner, when the propagation term is bigger than the diffusion one (frequencies >1MHz), the conductivity effect is minor, in this situation the GPR is highly

effective. However, problems can occur when both effects make contributions to the response of the recorded induced currents.

Advantages of EM geophysical methods

The electromagnetic methods are sensitive to electrical resistivity and electric permittivity over a volume of ground where induced electric currents are present. Among the subsurface based geophysical methods that sense bulk electrical and effective properties of the ground, EM provides deeper penetrations depth capability and greater resolving power (Everett and Meju, 2005). EM methods are cost effective, relatively easy to operate in the field, and a variety of data processing options are available, ranging form the construction of apparent resistivity curves or pseudosections for a fast subsurface evaluations, to 1-D and 2D forward and inverse modeling. 3D inverse modeling is not yet fully developed although research is moving forward rapidly in this field, where new codes are being tested. However, the main concerns in all EM methods are cultural noise sources such as power lines, pipelines and DC trains among others, that screen and disturb the geophysical signal.

Electromagnetic induction methods are the most widely used and versatile geophysical methods in hydrogeology studies at different scale ranges. This diverse set of techniques and instruments available provides the possibility of conducting cross-scale investigations. Airborne electromagnetic methods are used to obtain regional survey information from watershed to basin scales and can be implemented either from a helicopter or a fixed-wing aircraft and operated in either the frequency or the time domain. Surface geophysical methods can investigate greater depths and on higher resolution (from local studies to basin scale). At a detailed resolution scale in depth there are borehole and cross-hole arrays available. Selection the appropriate technique will be strongly influenced by study objectives, time, founds and computational facilities.

2.4.5. Time Domain Electromagnetic (TDEM)

TDEM is an inductive method in which a strong direct current is usually introduced through an ungrounded loop, Tx, and is abruptly interrupted after a specific time. The secondary fields due to the induced eddy currents in the ground are measured with a suitable receiver loop, Rx, in the absence of the primary field. Changes in the polarization of the vertical, and sometimes also the horizontal components of the secondary magnetic fields are measured within different time gates after the primary inducing current is turned off. The signal recorded by the receiver is called the transient, and several hundreds of transients are typically recorded and

averaged to reduce the effect of EM background and instrumentation noise. The transmitter and receiver loops (Tx, Rx) can either be separated by some distance, as in offset-loop sounding, or not, as in a central loop configuration, which is most commonly used and where no reversal sign is recorded (Figure 2.8).

The amplitude of the current flow decreases as a function of time both downwards and outwards away to the Tx due to the resistivity of the soil. The magnitude and distribution of the decaying transient depends on the resistivity of the ground and the instrument configuration. In the early stages (after the shutdown), the induced voltage is time-invariant and proportional to the near surface resistivity value, whereas at later times the time dependent voltage v(t) decay asymptotically (Spies and Frischknecht,1991).

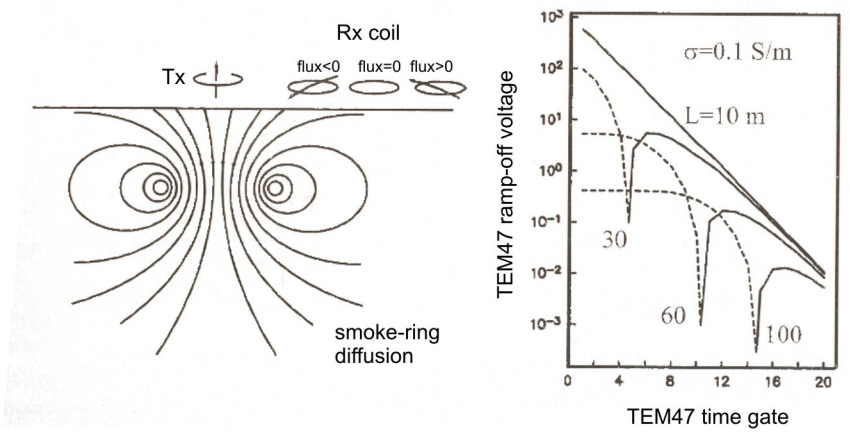

Figure 2.8: On the left, transmitter and receiver coil and electromagnetic waves distribution in the Earth's interior. On the right, transient decay curves for a loop-loop system at different separation distances over a uniform halfspace (0.1 S/m). The transient time of the sign reversal increases with increasing Tx-Rx separation from 10, 30, to 60, to 100 m. Dashed line negative voltage, solid line positive voltage (from Everett and Meju, 2005).

Conversion of v(t) to apparent resistivity curves at late stages depends on the loop configuration, and for instance in a central loop configuration is defined by:

$$\rho_a = \frac{kM^{2/3}}{v(t)^{2/3} t^{5/3}} \tag{2.23}$$

where k is a constant, M is the transmitter coil moment (current per area transmitted that for a circular loop $M=2\pi r^2 I$), t is time and v(t) is the output voltage from a single- turn receiver coil of area one m^2.

Investigation depth is function of recording time and loop radius (transmitter moment and turn-off time) at the expense of shallow resolution; however the signal must be strong enough compared with the EM background and instrumental noise in order to be measurable (Fitterman and Stewart, 1986, Nabighian and Macnae, 1991). The extent of the EM noise limits the time length of the recording and consequently limits the investigation depth. Enlarging the transmitting loop affects the sounding curve at early times, making the calculations difficult for the first layer where mathematical approaches assumes late stage decay at all the times. Furthermore the first layer has to have a minimum thickness to be detectable due to the inherent instrumentation delay in starting sampling after the current turnoff.

Time-domain electromagnetic data can provide information from shallow to relatively deep, up to 500 m and are used mostly for qualitative preliminary interpretation of the resistivity distribution in an estimated range depth. Inversion methods are established only for 1D parametrization due to a more stable solution. TDEM is still limited by the lack of applicability of the algorithms for the inference of 2D and 3D structures. TDEM is a good method for resolving the position of conductors; however it is a poor technique for distinguishing resistivity contrasts in high resistivity ranges (Auken et al, 2006 b). Transient electromagnetic systems have also been adapted to helicopter and aircraft, used to acquire extensive and dense surveys (Sørensen and Auken, 2004). TDEM has been used to delineate the depth to basement, hydrostratigraphy (Fitterman and Stewart, 1986; Krivochieva and Chouteau 2003) and buried valley aquifers (Steuer, 2006). It is particularly good at mapping conductive targets, such as clays (Auken *et al.*, 2006 b) or seawater. It has been used to determine clays as a structural indicator of aquifer pollutant susceptibility, or to detect salt-water freshwater interfaces (Guérin *et al.*, 2001; Goldman and Kafri, 2004), where porosity and site specific relationships have been studied using measured water resistivity.

2.4.6. Frequency domain electromagnetic (FDEM)

The frequency domain electromagnetic method, FDEM, is based on the injection of an alternating current of a given angular frequency through an ungrounded loop with a characteristic frequency. The primary field of the Tx loop will induce eddy currents in all conductors present in the Earth. The response at the Rx loop contains contributions from both

the primary magnetic flux from the transmitter loop and the secondary magnetic fluxes generated by the induced currents. The out of phase ratio of the secondary to the primary magnetic fields are used to estimate the apparent conductivity σ_a:

$$\sigma_a = \frac{4}{\omega \mu_0 L^2} \frac{H_{si}}{H_{pj}} \tag{2.24}$$

The primary field, H_{pj}, is known precisely since the Tx and Rx characteristics are under the control of the experiment. Profiling is performed by measuring the apparent resistivity of the depth volume as a function of frequency at the Tx-Rx midpoint positions (Figure 2.9). There are many different coil configurations, which include both horizontal co-planar for mapping horizontal features and vertical co-axial to delineate vertical structures. The different configurations provide different sensitivities in the horizontal and vertical directions. Investigation depth depends on the coil separation as well as the frequency of the applied current and has been qualitatively determined as the 0.75 times the transmitter-receiver loop spacing for a horizontal electromagnetic dipole configuration and 1.5 times the spacing for a vertical dipole (CUAHSI, 2005) at a fixed frequency.

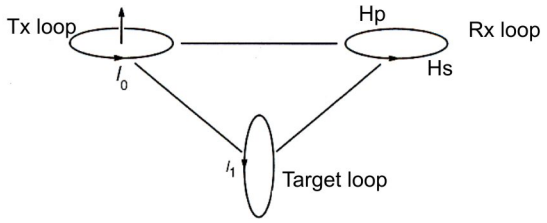

Figure 2.9: Geometry of a typical loop-loop system. Coils can operate either in a vertical or horizontal configuration, achieving different investigation depth and lateral resolution**.**

Systems have been improved by the development of multiple frequency transmitter capabilities. In general, new instrumentation can measure from 3 to 6 frequencies that provide different effective penetration depths, and providing better resolution in depth. FDEM has been widely used as profiling method mainly for providing qualitative interpretation or 1D smooth inversion. Quantitative inversion is complex due to the coupling effects of the primary and secondary fields and calibration of the coil interferences is therefore complex. Other concerns relate to the problem of extremely low resistive first layer limiting penetration depth.

While frequency domain electromagnetic method has a lower penetration than TDEM, the surveys are easy to perform and the instruments are light and easily portable with a fixed coil separation. Airborne frequency domain electromagnetic methods, similar to TDEM, provide fast data acquisition, and therefore more time and cost effective surveys. FDEM surveys have been used for qualitative preliminary interpretation of subsurface resistivity distribution for an estimated depth range depending on each frequency. Research fields currently focus on imaging the first tens of meters of the subsurface and to identify flow pathways (Geonics, 1999), saline soils (Himi *et al.,* 2002; Arranz *et al.,* 2004), mapping clay content, UXO, and is often used in precise agriculture investigations (Pellerin and Wannameker, 2005).

2.4.7. Audiomagnetotelluric (AMT)

Audiomagnetotelluric (AMT) is a natural source electromagnetic technique working in the frequency domain that allows the determination of the resistivity distribution of the subsurface. The fundamentals are common to the magnetotelluric method (Simpson and Bahr, 2005) applied at higher frequencies (> 1 Hz). AMT is based on the simultaneous measurement of the temporal fluctuations of the horizontal electric and magnetic fields on the Earth's surface. The transformation from the time to the frequency domain is achieved by a Fourier type transform or a wavelet transform (Trad and Travassos, 2000; Arango 2005) that computes the frequency content of the signal within a particular time interval.

AMT instrumentation consists of two pair of electrodes laid out perpendicularly to each other and two coil magnetometers aligned in the orthogonal directions. From the ratios of any of the electric and magnetic field components in the frequency domain we can define the complex impedance as $Z_{ij}(\omega)=E_i(\omega)/H_j(\omega)$, where i and j are two perpendicular directions. The relation between the horizontal electrical and magnetic fields in the frequency domain can be written as:

$$\begin{pmatrix} E_x(\omega) \\ E_y(\omega) \end{pmatrix} = \begin{pmatrix} Z_{xx}(\omega) & Z_{xy}(\omega) \\ Z_{yx}(\omega) & Z_{yy}(\omega) \end{pmatrix} \begin{pmatrix} H_x(\omega) \\ H_y(\omega) \end{pmatrix} \tag{2.25}$$

The impedance components can be scaled to obtain the apparent resistivity, similar to that used in DC resistivity techniques, and the impedance phase:

$$\rho_{a,xy}(\omega) = \frac{1}{\omega\mu}\left|\frac{E_x(\omega)}{H_y(\omega)}\right|^2 \quad (2.26) \qquad \varphi_{xy}(\omega) = \tan^{-1}\left(\frac{E_x(\omega)}{H_y(\omega)}\right) \quad (2.27)$$

The investigation depth is a function of the electrical resistivity of the Earth and angular frequency, ω, of the EM field. A reasonable measure of the penetration scale length, is the skin depth, which corresponds to the distance in which the amplitude of the incident electromagnetic field has attenuated by a factor of 1/e. In a uniform half-space the skin depth, in meters, is given by:

$$\delta \approx 501\sqrt{\frac{\rho}{f}} \quad (2.28)$$

The measured apparent resistivity and phase data must be inverted to obtain the Earth's electrical resistivity distribution. Plane wave methods, of which AMT is an example, have significant advantage in comparison to other EM methods. Multidimensional modeling capabilities are well developed from traditional crustal-scale MT studies and are directly applicable to hydrological problems, at higher frequencies. Presently there are several 2D inversion codes (Siripunvaraporn and Egbert, 2000; Rodi and Mackie, 2001), and 3D inversion codes are beginning to be used (Siripunvaraporn *et al.,* 2005 a).

In hydrogeophysical applications, the AMT method is starting to be used. It has been used for the delineation of static properties, aquifer geometries and boundaries (Krivochieva and Chouteau, 2003; Linde and Pedersen, 2004 b), structural and stratigraphycal characterization, in thermal aquifers (Manzella *et al.,* 2004; Arango, 2005), and seawater intrusion problems (Falgàs *et al.*, 2005; Unsworth, 2006). Monitoring of dynamic processes has recently been implemented on oil leakages (Tezkan *et al.*, 2005) and seawater-freshwater dynamic interface movement.

AMT is ideally suited for hydrogeological investigations given the sensitivity of electrical resistivity to the subsurface lithology, the presence of water and its quality. It can be implemented rapidly, it can achieve high investigation depths with reasonable resolution and it provides a true 3D measurement. In this thesis AMT plays a significant role used as the principal geophysical technique that, together with complementary information is used to improve our knowledge of aquifer systems.

2.4.8. Ground Penetrating Radar (GPR)

The ground penetrating radar (GPR) is an electromagnetic method that measures the transmission and reflection of high frequency (1MHz to 1 GHz) electromagnetic waves within the Earth. The method is effective in low-loss materials in which energy dissipation is small compared to the energy storage, and therefore GPR waves respond within the propagation regime (eq. 2.22). When the EM waves reach a boundary, the incident wave is partially transmitted and partially reflected, and GPR measures the velocity, v, and the energy attenuation, α, as the arrival time of reflected energy. Electromagnetic wave velocity and the reflection of the EM energy are primary controlled by the dielectric constant, ε, and the conductivity, σ, of the medium.

$$v = \frac{1}{\sqrt{\varepsilon\mu}} \qquad (2.29) \qquad \text{and} \qquad \alpha = 0.5\frac{\sigma}{\sqrt{\frac{\mu}{\varepsilon}}} \qquad (2.30)$$

GPR data provide a subsurface reflection time versus spatial position. Variations in the reflection amplitude and time-delay indicate variations in the propagation velocity and energy attenuation. Resolution and penetration depth of the resulting GPR images depend on the use of different antenna frequencies and the conductivity of the medium. Typically, higher frequencies increase the resolution at the expense of the depth of penetration, while electrical conductivity of the subsurface has a significant impact on the attenuation of the EM energy. In general investigation depth is not greater than 10-20 m for most geological media.

GPR instruments are commonly composed of a transmitter and a receiver, with a fixed spacing among them. Surveys usually are organized in regular grid to achieve 2D and 3D coverage. GPR surveys can be performed using a surface-based system where the transmitter and receiver antennas are moved across the Earth's surface (reflection survey), in a cross-hole system where the antennas are positioned in separate boreholes (transilumination survey) or a combination of the two.

There are many GPR contributions to hydrogeological applications (Knight, 2001) since the presence or absence of water dominates the GPR response through the dielectric constant, ε, where many time lapse GPR surveys focus on moisture-fluid movement recognition (Loeffler, 2005). GPR has also been considered useful because of its ability to delineate fine-scale stratigraphic structures which have importance on the groundwater flow. However, clayey

materials and saline soils provide low penetration and conductivity estimation has been recently derived from observations of the energy attenuation. Quantitative interpretation is a subject of current research, and typically site- specific relationships has been developed.

2.4.9. Nuclear Magnetic Resonance (NMR)

Nuclear Magnetic Resonance (MNR) is a fairly new electromagnetic geophysical technique used for directly investigating the water content, mobility, and pore-structure parameters controlling the hydraulic permeability. The fundamentals of the method rely on the excitement of the hydrogen protons of water with an external electromagnetic source transmitting at the resonance frequency of the protons (Larmor frequency, f_L, around 1-3 kHz, depending on the local Earth magnetic field) (Figure 2.10). The Larmor frequency is defined by:

$$f_L=\gamma B_0/2\pi \tag{2.31}$$

where γ=0.2675 Hz/nT, is the gyromagnetic ratio of hydrogen protons and $\omega_L= 2\pi f_L$ is the angular frequency.

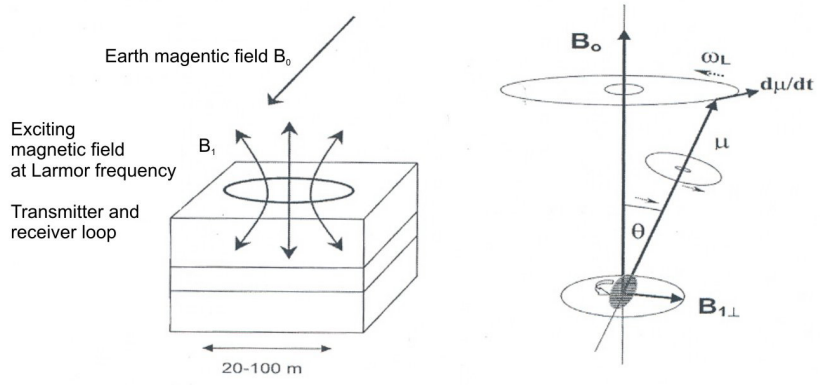

Figure 2.10: On the left NMR instrument application. On the right detail of the hydrogen proton deflection due to the induced current at the Larmor frequency (from Yaramanci *et al.*, 2005).

Protons of hydrogen atoms in the water molecules have a magnetic moment that is aligned with the local magnetic field B_0. When another magnetic field, B_1, is applied the axis of the precession movement is deflected (Figure 2.10, right). When B_1 is removed the protons generate a relaxation magnetic field emitting an electromagnetic signal that decays with time (Figure 2.11). The device is composed of one loop that works as a transmitter and a receiver system. An alternating current is applied within the loop with the angular Larmor frequency at

specific intensity. After the current is switched off, a potential difference or voltage v(t), which is frequency and time dependent, is induced in the loop. The signal v(t) is usually approximated by:

$$v(t) = E_o e^{-t/T} \cos(\omega_L t + \varphi) \tag{2.32}$$

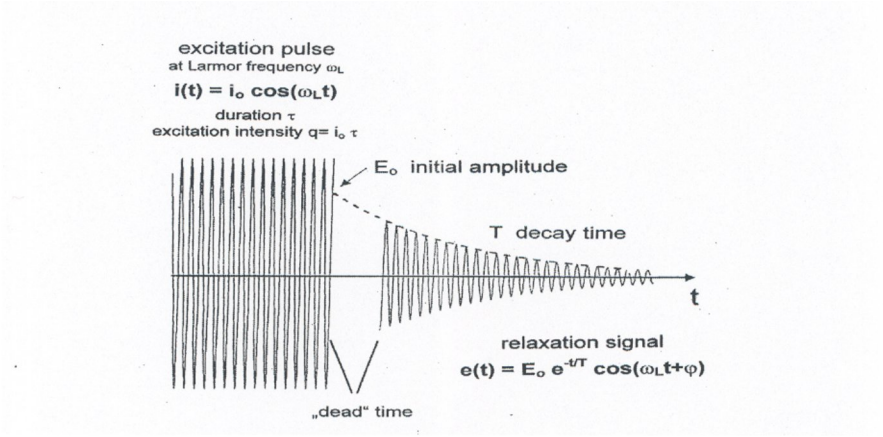

Figure 2.11: Input and output signals of NMR (from Yaramanci *et al.*, 2005).

The initial amplitude E_0 at t=0 is related to the water content for a non-conductive medium, while the decay time, T, is related to the mean pore size (or grain size), and the hydraulic conductivity of the material. Decay times are shorter for materials with finer grains sizes (60ms-300ms) than for the coarser sizes (300-600 ms for gravels). At the other extreme, in clay materials water is bounded by a strong molecular attraction and has a very short relaxation time (< 30 ms) that can not be detected by the NMR.

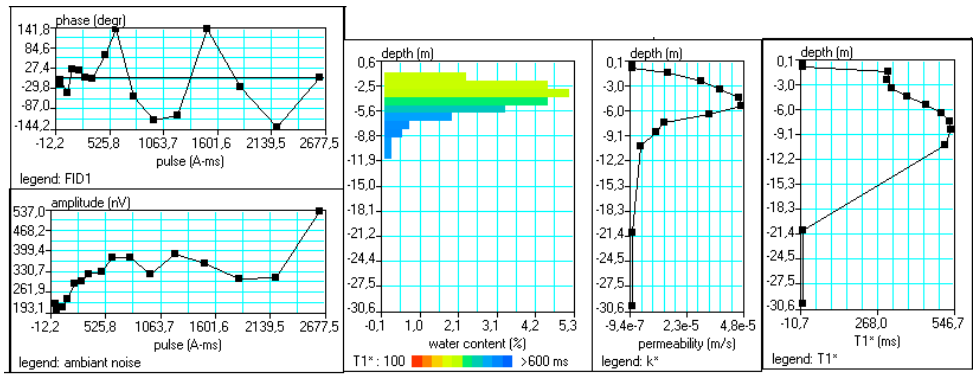

Figure 2.12: Typical data (left) and inversion models (right) of an NMR sounding on La Soutte (Behaegel 2006), where water content and permeability have been estimated.

NMR measurements are conducted for different excitation intensities (q), recording the initial amplitude $E_0(q)$ and the decay time T(q). The primary parameter obtained through inversion of the NMR data is the density distribution of hydrogen atoms, which is directly related to the water content (Figure 2.12). In terms of petrophysical approaches, the currently available quantitative expressions that describe of the relationship between the decay time and flow-property parameters are of an empirical nature. Approximation of the hydraulic conductivity relationships can be addressed simply by the pore size hydrologic relationship and site specific proves. For instance, Yaramanci *et al.* (1999) have proposed a hydraulic conductivity estimation given by $K \sim T^4$, where K is hydraulic conductivity in m/s, and T is decay time in milliseconds.

The resolution and accuracy of the NMR method decreases with depth, and depends mainly on the intensity of the current applied (i.e., higher strength and/or longer pulse time). Increasing the intensity increases the investigation depth as long as the injected current time << decay time. In the studies carried out by Lubczynsky and Roy (2003) the high intensity of the applied current allowed subsurface characterization to more than 80 m depth. Nonetheless, the main concerns are related with EM noise given the low signal to noise ratio.

NMR has the potential to become a powerful tool for groundwater exploration, with many contributions to date having produced petrophysical characterization, data inversions procedures and successful case studies (Lubczynski and Roy, 2003; Legchenko and Shushakov, 1998; Plata and Rubio, 2002; Keating and Knight, 2007). Yaramanci *et al.* (2005), considering the capability of NMR as a direct indicator of water and soil properties, suggest that an improvement will be achieved through the development of joint inversions or joint interpretations of NMR with electric and electromagnetic methods as a means of decresing the uncertainty in the results in conductive media. The induction effects need to be considered to improve the inversion and modeling process in order to account for the primary field modification in the presence of conductive structures. Other important research are the regularization and inversion procedures considering that nowadays only 1D inversion are mainly used.

2.4.10. Shallow seismic methods

Seismics is a commonly used geophysical method that can provide structural and additional complementary information about the aquifer systems. Seismic methods are based on the generation of an elastic wavefield that propagates through the ground, returning to the

surface where several detectors record its spatial-temporal variation. Developed for locating and mapping oil reservoirs, seismic methods can also be used as a tool for high-resolution mapping of shallow geologic targets (Hunter *et al.*, 1984; Steeples and Miller, 1990).

Seismic waves include body waves (P-waves and S-Waves) that travel three-dimensionally trough solid volumes, and surface waves (Love waves and Rayleigh waves) that travel as a boundary wave near the Earth's surface. P-waves are the first waves recorded due to their higher velocity, and are the most commonly used and easiest waves type to work with. The velocity of propagation of various types of elastic waves, and their frequency content, are related to both the elastic properties and mass density of the medium in which the waves are traveling. The propagation velocity is given by the product of the wave frequency and the wavelength, $v = f\lambda$, where the P-wave and S-wave propagation velocities are defined respectively by:

$$v_p = \sqrt{\frac{k + \mu\frac{4}{3}}{\rho}} \qquad (2.33) \qquad\qquad v_s = \sqrt{\frac{\mu}{\rho}} \qquad (2.34)$$

where k is the bulk modulus, μ is the shear modulus, and ρ is the density of the material through which the waves are propagating. Fluids have no shear strength, their shear modulus is zero, and S-waves therefore cannot propagate through fluids. Since the velocity is a physical property intrinsic to each Earth material, higher frequencies result in shorter wavelengths and better resolution. The upper frequency limit for near surface studies is generally about 1KHz.

Seismics involves measurement of the travel time between the generation of a seismic pulse and its arrival as a wave train at different geophones located at known distances away from the source. Wave propagation is described by several mechanisms: time delay, dispersion, attenuation, reflection, refraction and interference. When a seismic energy source (e.g. sledgehammers, explosives or vibration devices) is activated, energy radiates in all directions prompting wave refraction or reflection at geological interfaces (Figure 2.13).

When the seismic refraction method is used, the waves corresponding with headwaves originating at geological interfaces are recorded at the surface as the first arrivals (Figure 2.13). Surface seismic refraction methods are focused on travel-time data sets which provide information about seismic velocity. Inversion routines are used to determine velocity as a

function of depth, and are based on Snell's law and ray theory (Pelton, 2006). From a hydrogeological point of view, P-wave seismic velocity can improve our understanding of changes in fluid saturation (e.g. mapping water table) and locate interfaces with large acoustic contrasts, such as the bedrock-soft sediment interface. Velocity changes are related to lithology, pore-fluid type and pressure changes (Rubin *et al.,* 1992).

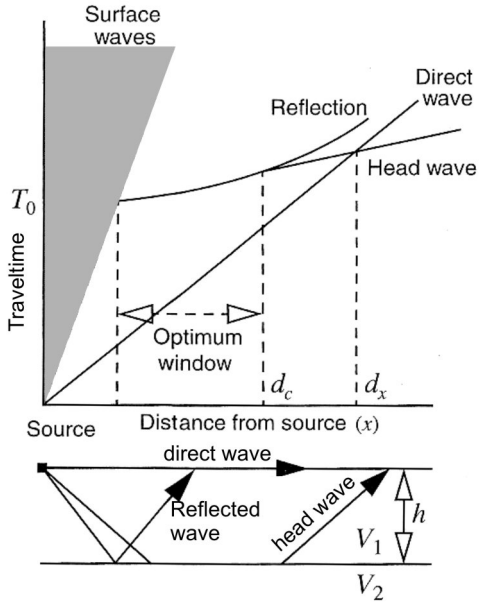

Figure 2.13: Geometric relationships between surface, reflected, direct and refracted (headwave) waves (From Pelton, 2006).

Seismic reflection methods are based on the isolation and processing of reflections from the boundaries of geologic units to provide a time image of the subsurface called seismic section. The amount of seismic energy that crosses an interface depends upon the acoustic impedance, Z_i :

$$Z_i = \rho_i v_i \tag{2.35}$$

where ρ_i the density and v_i is the seismic velocity of each layer i. Reflection seismic will provide a direct image of the impedance contrasts within the subsurface, in two-way-travel time, provided three criteria relating to the subsurface materials are satisfied: acoustic impedance contrasts must be present, the dominant frequency of the data must be high enough so the direct waves and refractions will not interfere with the reflections, and finally the wave-field must be

sampled adequately in space and time, using appropriate experimental design (Figure 2.13). The generally accepted vertical-bed resolution limit is given by the ¼ λ wavelength criterion for the dominant frequency. The dominant wavelength for seismic reflections normally increases with depth due to the velocity typically also increasing with depth. The dominant frequency always decreases with depth due to the attenuation of high frequencies.

When possible, vertical seismic profiling, VSP, is conducted in boreholes, allowing the accurate determination of the one-way travel time of seismic waves to various geologic units, as well as the attenuation and acoustic impedances. Surveying is preformed using a string of hydrophones placed in a borehole, with the source placed on the surface.

In shallow seismology, the main concerns are the interference of refractions with reflections, the presence of air-waves, and the presence of surface waves that need to be efficiently filtered or muted (Steeples, 2005). Inaccurate velocity estimations also induce errors in the depths estimated in the seismic profiles.

Seismic applications to hydrologic problems have focused on mapping the bedrock, delineating confining units, resolving sedimentology and stratigraphy, detection of geologic faults, evaluating karst conditions, mapping landslides' base, determining the degree of saturation and the water table depth which may help constrain other geophysical techniques (Gallardo and Meju, 2003; Jarvis and Knight, 2002; Rubin *et al.*, 1992). Novel approaches also include S-wave methods, three-component recording methods with orthogonal mounted geophones, surface wave analysis (SASW, MASW), acquisition and processing of 3D surveys, the combined use of GPR and high resolution seismics and development of relationships between seismic properties and rock physical properties.

2.4.11. Gravity and Magnetic

Gravity and magnetics are potential field methods that in hydrogeophysical applications are generally used in support of the regional interpretations of other geophysical measurements. An extensive review of both methods can be found in Blakely (1995).

Gravity prospecting consists of the measurement of variations in the vertical component of the gravitational field of the Earth. Data require extensive processing and correction for non geological effects and for subsurface geological variation (e.g. topography, location, day and time) before they can be modeled. Gravity data traditionally have been used to

determine the subsurface configuration of structural basins, made possible by the large density contrast between basin infill and bedrock. Gravity data inverted to produce basement depth estimates are more sensitive to shape than depth (i.e. Jachens and Moring, 1990). The main hydrogeological applications of gravity data are to estimate maximum aquifer thickness in basins to constrain water flow models, to distinguish carbonate from sandstone aquifers (difficult when using geoelectrical methods), and in the case of microgravity, to measure the total mass of water in a conceptual column and therefore to examine changes in the mass balance of water (Gehman *et al.*, 2006).

The magnetic method utilizes the variation in the strength of the Earth's magnetic field that reflects the spatial distribution of magnetized material throughout the subsurface. Magnetization occurs naturally in materials and rocks, and depends on the quantity of the magnetic minerals and on the strength and direction of the permanent magnetization carried by these minerals (magnetite, pyrrhotite). Although magnetic data do not respond directly to the presence of water, they can contribute to the understanding of the geologic controls on the groundwater systems. Magnetic surveys can be useful in hydrogeological studies due to their ability to determine basin geometry, to delineate igneous intrusions that my affect groundwater flow, and to identify shallow local magnetic anomalies caused by faults, paleochannels, eolian deposits or man-made features, intrasedimentary faults, and hence the compartimentation or connection within the aquifer system (Grauch, 2001).

2.4.12. Well logging

Borehole geophysics includes all methods that make continuous profiles or point measurements at discrete depths down a borehole. The measurements are made by lowering different types of probes into the borehole. Logging probes enclose the sensors that are connected to a cable that is pulled upward while data are recorded. The measurements are related to the physical and chemical properties of the surrounding rock, to the pore fluid, to the fluid in the well, the well casing or any combinations of these factors. Many geophysical logging techniques were initially developed by the petroleum industry, and later adapted for the hydrogeological discipline. Once a well is drilled, geophysical well logging is able to make several different physical measurements (acoustic, electric, nuclear) that can provide information on lithology, thickness, continuity of aquifers, porosity, bulk density, resistivity, groundwater chemical and physical characteristics, fluid movement parameters, and integrity of the well construction. The most commonly used log types that provide those properties are SP, resistivity, gamma-ray, gamma-gamma, neutron, elastic wave propagation, cement bond log,

acoustic televiewer, borehole television, caliper, temperature, fluid conductivity, flowmeter, fluid transparency or turbidity. Korb *et al.* (2005) present a complete summary of hydrogeophysical applications of log probes facilities.

In terms of the limitations of borehole geophysics, the main concerns are related to borehole characteristics, most of the logs need uncased wells, fluid-filled wells, or require isolation packers. Laboratory analysis of cores and fluid is essential either for direct calibration of the logs or to verify calibrations used to estimate hydrological parameters.

2.5. Hydrogeophysical challenges

There are three main research topics where special effort is required in order to fulfill the potential of hydrogeophysics: 1) Petrophysical relationships, 2) Integration of geophysical and hydrogeological measurements and 3) Improvement on the geophysical methodologies.

2.5.1. Petrophysical relationships

Estimation of hydrogeological parameters using geophysical data is a new and current area of research, with which several challenges are associated. Firstly, geophysical properties may be associated with more than one hydrogeologic condition (as described above, effective conductivity versus fluid conductivity and surface specific conductivity, or electrokinetic effects) that can lead to misinterpretation. Secondly, the scale of sampling from the hydrogeologic data is different to the geophysical datasets (cores, well lithologic description, seismic, DC, GPR). In addition, geophysical data are often dependent on the array geometry and measurement direction whereas hydrogeologic data is commonly measured at a single point. However to estimate hydraulic parameters over the space the dense, cost-effective geophysical datasets are needed to provide a better understanding of the hydrologic systems and processes.

The link between the hydrogeological parameters and the geophysical properties measured is non universal for geological materials. The most common strategy is to infer a site specific empirical relationship between the geophysical measurement and the parameter of interest using collocated hydrogeological and geophysical data. Under controlled laboratory conditions petrophysical parameters can often be defined more completely and more accurately (Ferré *et al.*, 2005). For example, soil and water resistivity measurements and granulometric

analysis of core samples can be performed in the laboratory and used to extrapolate the geophysical results over the entire basin site (Keller, 1988; Mazáck *et al.*, 1990; Purvance and Andricevic, 2000; Guérin *et al.*, 2001) (Figure 2.14). Similarly, geophysical well logs can be used to define hydrogeologic parameters such as hydraulic conductivity and effective porosity given that neutron density or acoustic logs can be calibrated in porosity units (used basically in oil reservoir modeling).

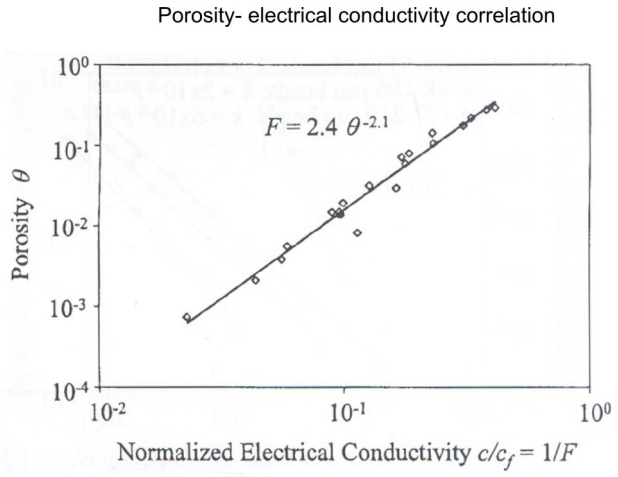

Figure 2.14: Archie type petrophysical relationship. F is formation factor and θ is porosity extracted from laboratory studies. C is conductivity and C_f is the fluid conductivity. Linial regression is derived and subsequently applied at the same locality, when only one of the two variables is known (form Purvance and Andricevic, 2000).

Resistivity models

While electrical resistivity is the most commonly used property from which to infer porosity, Φ, or hydraulic permeability, k; no general petrophysical relationship has been reported. The well knowed Kozeny-Carman equation (eq.2.36) has been commonly used to estimate the hydraulic permeability in a porous medium, replacing the porosity and/or the specific surface area S_p with an electrical measurement. Kozeny-Carman relationship states:

$$k = \frac{\phi \quad r^2}{aT} \tag{2.36}$$

where r is the radius of the pore space (m) (inverse of specific surface area S_p of the porous volume), a is a shape factor and T is the tortuosity defined as the ratio between the effective

fluid transmission path length (L_a) and the macroscopic length of the sample (L). The tortusosity has been related (Nelson, 1994) to the electrical formation factor F (defined below).

$$T = \left(\frac{L_a}{L} \right)^2 \propto \phi F \tag{2.37}$$

and consequently equation 2.36 can be rearranged as:

$$k = \frac{1}{aFS_p^2} \tag{2.38}$$

Quantitatively, the rock resistivity response is principally due to the pore fluid conductivity (related with F) and pore surface conductivity (related with the S_p) since most of the rock materials are fundamentally electrical insulators (Purvance and Andricevic, 2000). However defining the correct equivalent effective property of the geophysical measurement is not simple.

For a clay free environment the widely used relationship that relates porosity, formation resistivity ρ and fluid resistivity ρ_w can be approached with Archie's law (Archie, 1942):

$$\rho = a\rho_w \phi^{-m} \tag{2.39}$$

The formation factor is a structural parameter defined by:

$$F = \frac{\phi^{-m}}{a} \tag{2.40}$$

where m is the Archie cementation factor. Keller (1988) among others, provides tables for the a and m parameters for different materials obtained by analysis of a collection of samples analysis. Considering eq 2.39 and 2.40, can be obtained eq.2.41 that relates the fluid resistivity and the formation resistivity to the structural parameter F (Figure 2.14).

$$F = \frac{\rho}{\rho_w} \tag{2.41}$$

In this clay free case, pore fluid resistivity provides the main contribution to the bulk resistivity. Inverse and direct relationships between hydraulic permeability and resistivity could be established. In a saturated media the higher the hydraulic permeability the lower the electric resistivity within the same rock type due to increasing effective porosity and a negative linear log K-log ρ relationship results (continuous lines in Figure 2.15).

On the other hand, hydraulic permeability and electrical resistivity are directly proportional to the grain size (the rock type), and increasing grain size increases both the electrical resistivity and the hydraulic permeability and a positive linear log K-log ρ relationship results (dashed line in Figure 2.15).

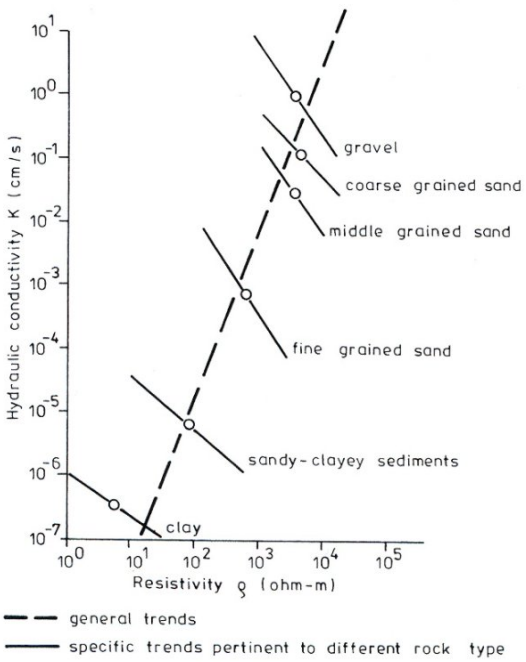

Figure 2.15: Relationships between hydraulic conductivity and resistivity for different rock types (direct correlation) and within a specific rock types (inverse correlation) (from Mázac *et al.*, 1990).

In addition, Archie's law fails on predicting Φ where clay minerals are present. The presence of clay strongly influences porosity, permeability and resistivity given that clay is characterized by a high cation exchange phenomenon (Waxman and Smits, 1968), and high

specific surface area. In clayey environments the dominant contribution to the bulk resistivity is due to surface conductivity. In general, the higher the clay content the lower the resistivity and the lower the hydraulic permeability (Figure 2.15, Figure 2.16, left). Porosity decreases increasing clay content until the effective porosity is reduced given that it reduces connected porous. Thereafter the porosity as non connected porous space increases increasing clay content (Figure 2.16, right), reflecting the total porosity.

In Figure 2.16 shows the relative impact on resistivity provided by clay content and salinity (fluid resistivity). For a given clay content two types of behaviors are seen, 1) when the effect of high clay content dominates the bulk resistivity, even with increasing salinity (horizontal trend line in Figure 2.16 left), and 2) when salinity dominates the bulk resistivity, which follows the 0% clay content and water line trends. In low clay materials, fluid dominated behavior is attained at lower salinity concentrations.

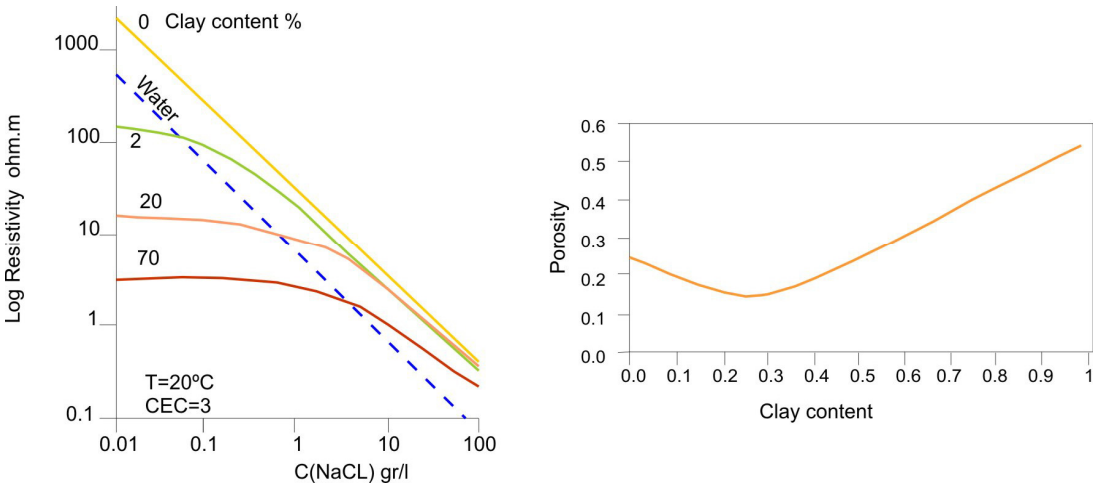

Figure 2.16: Left, resistivity versus salinity concentration (C_{NaCl}) for samples with different clay content samples showing two different dominant resistivity process. Right, the relationship between porosity and clay content. Total porosity decreases due to increasing clay content up to a critical point, where after it starts to increase, and conversely effective porosity decreases (modified form Shevnin, 2006).

The fundamental limitation of most of the effective resistivity geophysical measurements is to determining the relative importance of the both resistivity contributions, due to the electrolyte or the surface specific conductivity, thus the real and imaginary parts of the complex resistivity (section 2.3.3). In many studies the Hashin-Shtrikman bounds (HS) are used to restrict the solutions (Hashin and Shtrikman, 1962; Wempe, 2000). The theoretical (HS) bounds for electrical resistivity provide upper and lower limits for the resistivity–porosity

relationship in a multi-constituent media. The upper bound HS^+, describes the case where the conductive material is perfectly interconnected, whilst the lower bound HS^- describes de case where the conductive material is confined within isolated pockets.

Several research groups are working on the improvements in determining k based on IP and SIP, where the real an imaginary parts of the electric conductivity can be inferred independently and used in the Koezeny-Carman relationship for F and S_{por} respectively (Purvance and Andricevic, 2000; Binley *et al.*, 2005; Slater, 2006) (Figure 2.17).

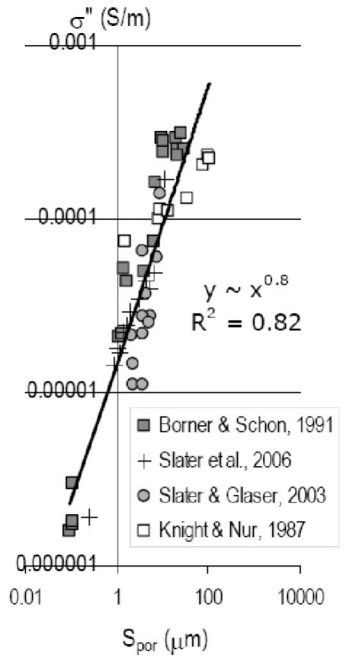

Figure 2.17: Compilation of measurements of specific porous surface area S_{por} and imaginary electric component σ'' from different materials and studies, showing a consistent relationship (from Slater, 2006).

Permittivity models

There is no general theoretical relationship between permittivity and hydraulic conductivity. Since permittivity is strongly controlled by water content due to the large contrast between the permittivity of the water (80), the air (1) and minerals (aprox 5), the apparent permittivity data contain information about the water content variation or water-filled porosity. Secondary factors affecting the permittivity responses of rocks and soils include the effective shapes of the pores and grains, fine scale lamination, temperature and salinity of the saturated solution (Lesmes and Friedman, 2005). The Complex Refractive Index Model expressed as the

CRIM equation (Wharton *et al.*, 1980), is one of the most widely used models to predict the porosity of water saturated materials from their measured permittivity:

$$\sqrt{\kappa^*} = (1-\phi)\sqrt{\kappa_s^*} + \phi\sqrt{\kappa_w^*} \tag{2.42}$$

where k^* denotes the dielectric constant as a complex number defined by the ratio of $k = \varepsilon/\varepsilon_0$, with ε_0 being the permittivity of a vacuum. The dielectric constants k_s, k_w, and k_a are the dielectric constants of the solid grains, pore water and air respectively. In saturated soils, permittivity ε_{eff} and ε_s, depend on the porosity and effective pore/grain shapes, and therefore permittivity measurements can potentially be used to constrain parameters in a permeability prediction formula, that is calibrated using pore/grain sizes that are determined empirically in the laboratory.

Introducing grain shape and porous space permittivity considerations in CRIM equation, more complex models MG (Maxwell-Garnett) and SS models (self-similar) has been developed. Lesmes and Friedman (2005) made and extensive review of permittivity models on both saturated and unsaturated media. In the later condition, Topp relationship (Topp, 1980) relates the permittivity and the volumetric water content as a three phase model. The Topp equation expresses the effective relative permittivity as a function of volume water content θ:

$$\kappa_{eff} = 3.03 + 9.3\theta + 146\theta^2 - 76.6\theta^3 \tag{2.43}$$

Although the Topp model is generally the most reliable relationship (Lesmes and Friedman, 2005), Archie's law, Topp and CRIM equations all fail in the estimation of k in fine textured soils, where these latter equations under predict the water content.

2.5.2. Integration of geophysical and hydrogeological measurements

To perform the integration of geophysical measurements with hydrogeological measurements, the scale problem has to be considered, as well as the non uniqueness and uncertainty of the geophysical models, and which specific petrophysical relationship is most appropriate for each case study. Thereafter, integration and estimation approaches can be applied that focus on defining the spatial distribution and the magnitude on the aquifer system.

The first step is to obtain reliable geophysical models with which to translate geophysical properties into hydraulic parameters. The second step is the quantitative conversion of the geophysical property to hydrological properties that may be obtained 1) via direct mapping using a petrophysical relationship, the so called deterministic approach, or 2) by applying stochastic methods, such as geostatistics or Bayesian techniques (Deutsch and Journel, 1998; Gómez-Hernández, 2005; Rubin and Hubbart, 2005), the so called probabilistic approach. The most general way to integrate a priori information and data for non-linear problems is to apply stochastic inversion methods where the resulting models parameters is given by a probability distribution. The probabilistic weight of each element is considered in the iterative posterior inversions to improve the models. These geostatistical and simulating methods include Montecarlo simulation, neural networks, fuzzy logic, and Bayesan methods. Computational time and a priori distributions of model parameters are the main concerns.

Joint inversion procedures

Hydrogeophysical research is increasingly turning to joint inversion strategies in which multiple geophysical datasets and/or geophysical-hydrological datasets, are processed simultaneously to produce more realistic estimates of the hydrologic parameters that satisfy all the available datasets , e.g., DC+GPR, DC+NMR, DC+AMT, GPR+Seismic (Bedrosian, 2006; Linde *et al.*, 2006; Gallardo and Meju, 2003). Thus joint inversion methods are configured either as a coupled inversion of geophysical and hydrological data or as a coupled inversion of multiple geophysical data.

When two datasets are both sensitive to the same physical property, the simultaneous inversion is achieved by minimizing the misfit of both datasets (Linde, 2005). On the other hand, if the geophysical datasets are sensitive to different physical property final models will provide complementary information at the same location point. Joint inversion of hydrogeological and geophysical data is expected to improve the final hydrogeological final model. Hydrogeological data calibrates the hydrogeophysical variables based on the assumption that any relevant hydrogeological structure has a geophysical signature (Slater, 2006).

2.5.3. Geophysical methodology improvement

Over the last decade instrumentation has gone through a significant improvement in many aspects. Guérin (2005) has reviewed the novel instrument prototypes within the hydrogeophysical scientific community, and the case studies carried out with them, showing its potential. Remarkable effort has expended in the diversification of the measurable properties

recorded from the subsurface that can provide independent complementary information at different time and scales. However, further advances in the geophysical technology are required to improve the sensors, sensitivity, depth resolution, and portability. Few remarks about geophysical improvement are listed below:

1) Development of multidimensional inversion and 3D acquisition devices to provide valid 3D models. Currently, 3D environments (except from a few cases of 3D DC or AMT measurements) are approached using 2D profiles or dense 1D spatial sampling which only provide partial information of the study area.

2) Better resolution at all depths. Geophysical methods usually results in and inverse relationship between depth of investigation and target resolution, that is high resolution at shallow depths and vice versa. Multiscale measurements will provide more detailed models at greater depths.

3) Advancements will provide very large datasets due to high resolution sampling or due to more continuous data acquisition. Therefore inverse modeling processes need to improve in order to handle these large datasets with less computational time.

4) Cultural noise is one of the main geophysical concerns during data acquisition in urban areas, where most environmental hydrogeophysical problems are investigated. Much more research is needed to minimize coupling effects and noise limitations (Guérin, 2005; Post, 2005).

5) Geophysical instrumentation is usually composed of several components: transmitter, receiver, console, and batteries, which results most of time in large devices with significant total weight that are not easy to transport. Smaller and more portable equipment would contribute greatly to improve field procedures.

6) New communication capabilities such as satellite or mobile phone technology will provide data in real time from permanent arrays used to monitoring hydrodynamic processes. While some projects have had access to these technologies, is currently not economically viable for more modest projects.

Chapter 3: The Audiomagnetotelluric method (AMT)

In this chapter, further insight into the audiomagnetotelluric method (AMT) is presented, given that this PhD study is strongly based around the use of AMT in hydrogeological investigations. In particular, AMT principles, data dimensionality analysis and modelling processes use in the subsequent chapters are reviewed here. Furthermore, AMT instrumentation used in hydrogeophysical applications is also presented here, and described in detail in respect to resolution, accuracy and sensitivity of the equipment.

3.1. Audiomagnetotelluric principles

As introduced on the section 2.4.7 the Audiomagnetotelluric method, AMT, is an electromagnetic induction technique used to determine the resistivity distribution of the Earth's subsurface. There are two hypotheses or approximations that must be considered:

a) The quasi-stationary approximation: displacement currents can be neglected since conduction currents dominate the electromagnetic behaviour. The dominant diffusive process makes it possible to obtain responses of volumetric averages of the measured Earth resistivity.

b) The plane wave hypothesis: The primary electromagnetic field is a plane wave that propagates vertically towards the Earth surface (z direction).

The primary electromagnetic source energy, which can be either natural or artificial, penetrates into the Earth inducing secondary electric and magnetic fields. The contribution of both electromagnetic fields is recorded on the surface. Natural EM waves, generated by thunderstorm activity, provide frequency signals higher than 1Hz, that are used on the AMT method. Frequencies lower than 1Hz are caused by large scale ionospheric currents, created by the interaction between the solar wind and the magnetosphere (Kaufman and Keller, 1981; Vozoff, 1991) and are used in MT crustal and lithospheric-asthenospheric scale studies. In cases of weak signal (e.g. the death band) or when affected by electromagnetic noise, controlled

artificial sources provide a stable, dependable signal, resulting in higher precision. However, controlled sources can also complicate interpretation by adding source effects when station is not located in the far field zone.

Traditionally, controlled sources consisted of grounded electric dipoles ranging in length from 500 m to 2 km used in deep studies (Goldstain and Strangway, 1975; Sandberg and Hohmann, 1982). In shallow experiments, it is more advantageous to use horizontal magnetic dipoles given that they are expected to provide better plane-wave conditions (Pedersen *et al.*, 2005). Horizontal magnetic dipoles present less coupling effects in the presence of conductive structures and are smaller and easier to install.

The measurements are carried out by two pairs of electrodes and two or three magnetic induction coils oriented orthogonally (Figure 3.1).

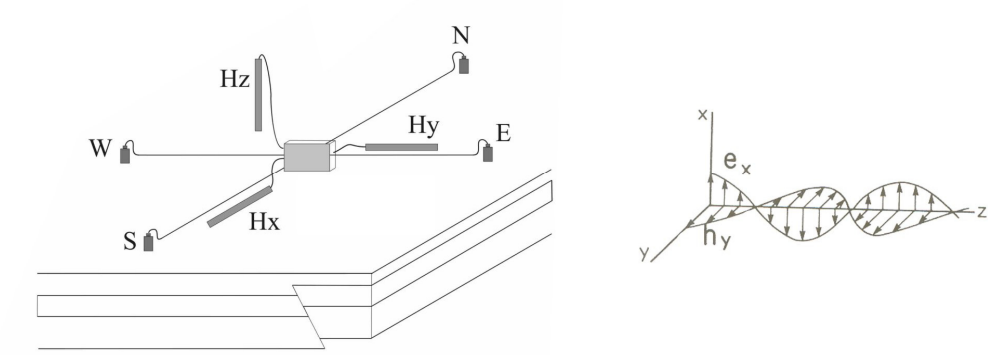

Figure 3.1: Sketch of an AMT receiver array. Electrodes are located N, S, E, and W, and the induction coils H_x and H_y are oriented NS and EW respectively. H_z is emplaced vertically. On the right, is shown the electric and magnetic field propagation into the Earth.

Recorded electric and magnetic time series are transformed into the spectral domain through a fast Fourier transform (FFT), or using wavelet transforms (WT) (Zhang and Paulson, 1997, Trad and Travassos, 2000). Arango (2005) presents a detailed comparison between the FFT and WT methods in AMT. The wavelet transform is presented as advantageous due to its more accurate positioning in the spatial (time) and frequency domains. However, temporal-spectral transformations based on the Fourier Transforms (Figure 3.2) are most widely used.

In both cases, the transformation process decomposes the time series into a complex linear combination of sine and cosine functions that provides a frequency and amplitude characterization of the data.

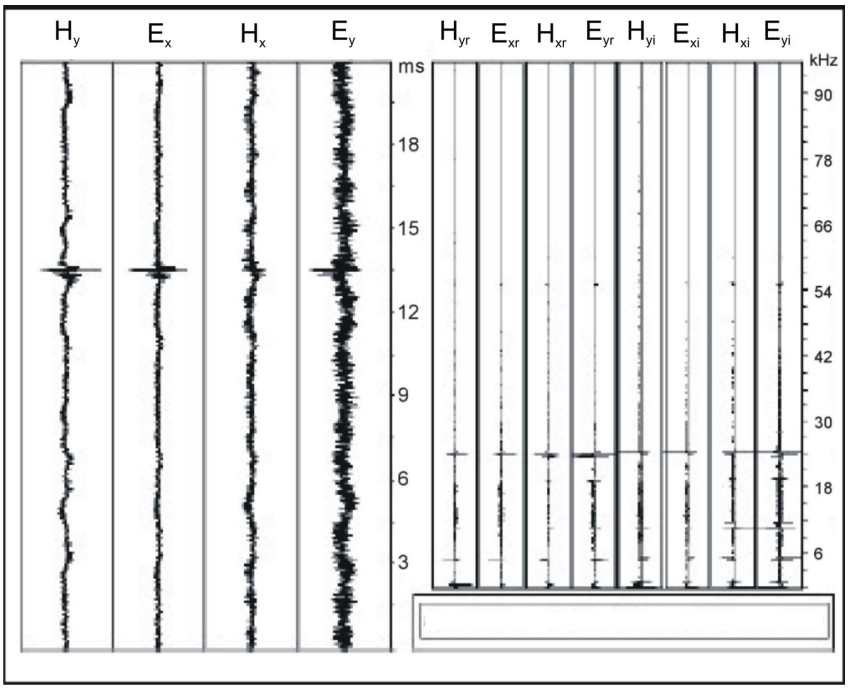

Figure 3.2: Time series of the electric and magnetic data components, on the left, and their FFT transforms on the right. Subindices r and i denote real and imaginary components respectively of the complex electric and magnetic fields. Image extracted from the Imagem application of the StrataGem Instrument (Geometrics, 2000).

The magnetotelluric transfer functions relate the simultaneously measured fluctuations of the horizontal electric and magnetic fields at given frequencies. From the relationships between the electric and magnetic components in the frequency domain we can define the complex impedance tensor as :

$$\begin{pmatrix} E_i(\omega) \\ E_j(\omega) \end{pmatrix} = \begin{pmatrix} Z_{ii}(\omega) & Z_{ij}(\omega) \\ Z_{ji}(\omega) & Z_{jj}(\omega) \end{pmatrix} \begin{pmatrix} H_i(\omega) \\ H_j(\omega) \end{pmatrix} \tag{3.1}$$

where i and j are two perpendicular directions and ω is the angular frequency.

The impedance components can be scaled to obtain the apparent resistivity, ρ_a, (eq.3.2) and phase, φ, (eq.3.3) for given frequencies to provide data curves used in AMT interpretation (Figure 3.3).

$$\rho_{a,ij}(\omega) = \frac{1}{\omega\mu}\left|Z_{ij}(\omega)\right|^2 \tag{3.2}$$

$$\varphi_{ij}(\omega) = \tan^{-1}\left(\frac{Z_{ij}^{I}(\omega)}{Z_{ij}^{R}(\omega)}\right) \tag{3.3}$$

Superscripts R and I denote the imaginary and real part of the impedance element, respectively.

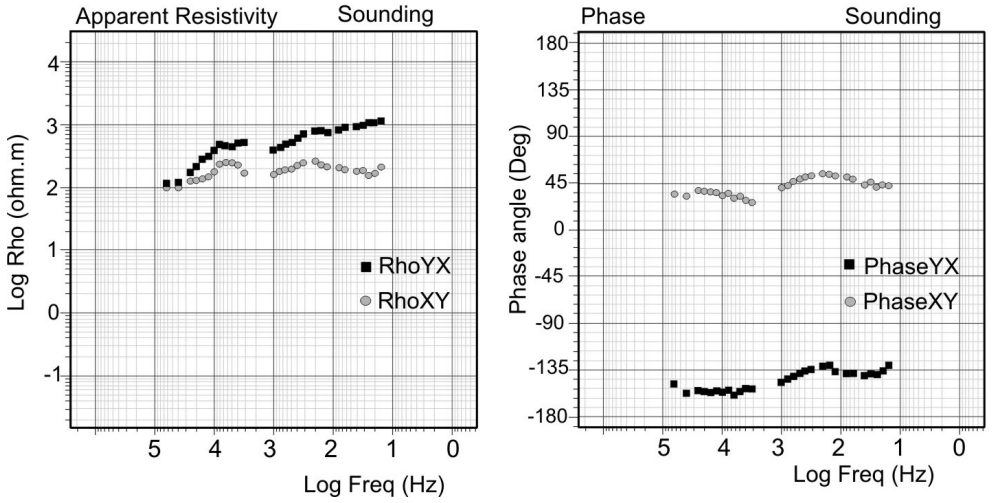

Figure 3.3: Example of apparent resistivity and phase angle frequency dependent curves corresponding to the off-diagonal components Z_{xy} and Z_{yx}.

3.2. Investigation depth: Skin depth

Investigation depth can be roughly estimated using the skin depth parameter (δ). The skin depth is defined as the frequency dependent depth at which the electromagnetic field amplitude at the Earth's surface is attenuated by a factor of e in a homogeneous medium.

$$\delta \approx 501\sqrt{\frac{\rho}{f}} \quad \text{in meters.} \tag{3.4}$$

It is worth mentioning that depending on the measurement frequency range and thus investigation depth, MT methods are named differently: Magnetotellurics (MT), Audiomagnetotelluric (AMT), and Radiomagentotellurics (RMT) (Figure 3.4). MT measures in the frequency range 1 to 10^{-6} Hz, where studies focus on imaging crustal and mantle geological targets. Natural electromagnetic source energy is usually adequate to ensure full frequency spectrum. Low frequency signals however, require longer measurement time than AMT and RMT methods.

In the mesoscale frequency range, from 1 to 10^5 Hz, the method is referred to AMT. A controlled electromagnetic source is commonly used at higher frequencies to prevent low signal-to-noise ratios where cultural noise and weak natural signal may be present. The study scale varies in depth from a few meters to hundreds of meters, and is useful on hydrogeology, mining, tectonics, stratigraphy, or vulcanology studies, among other applications (Figure 3.4).

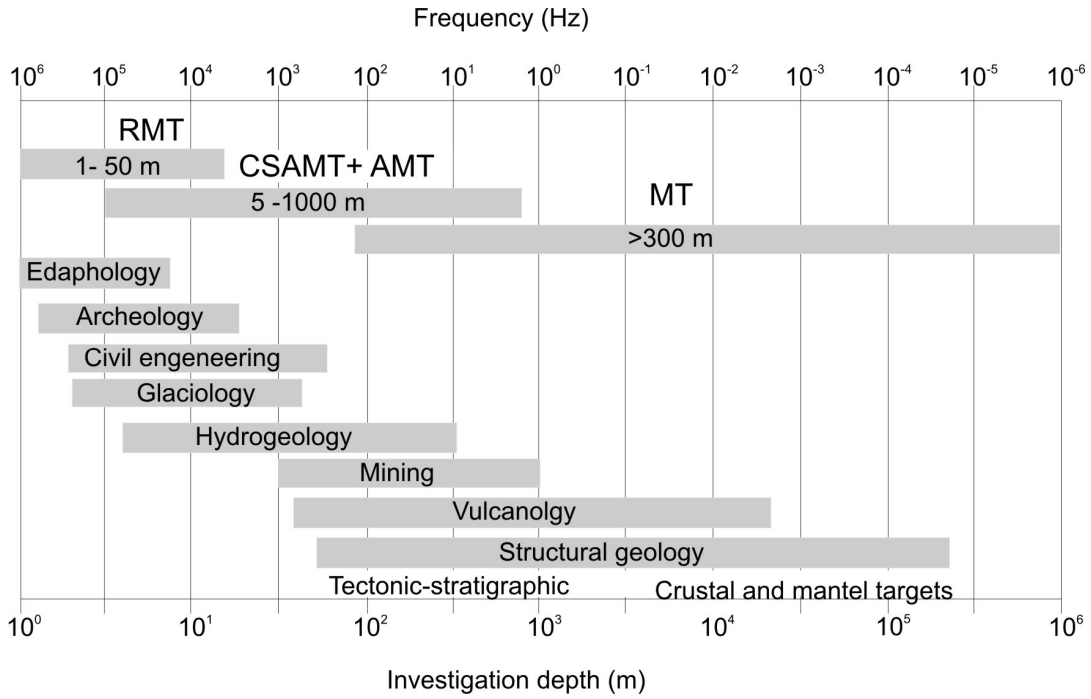

Figure 3.4: General overview of the investigation depth of the different magnetotelluric techniques and some of the main fields of application. Frequency-depth limits are non strict.

And finally, at the very shallow scale, allowing characterization in detail within the first tens of meters of depth, RMT measures in the frequency range of 250-15 KHz using a radiotransmitter. RMT may be applicable to studies of subsurface hydrogeology, edafology, archaeology, surface civil engineering, and precision agriculture. However, there are only few prototypes among the scientific community (Tezkan, 1999; Bastani, 2001; Tullen *et al.*, 2006).

In terms of hydrogeophysical applications, the RMT and AMT methods are suitable given that these instruments record over a high enough frequency range to allow a detailed investigation of the shallow subsurface, as shown by eq. 3.4 and in Figure 3.4.

Equation 3.4, shows that investigation depth depends not only on frequency but also on the resistivity of the subsoil. Figure 3.5, illustrates the significant change in investigation depth due to the variable frequency and resistivity of the subsurface which, when working at shallow depths becomes very important. In a 100 ohm·m homogenous halfspace high frequencies (10^5 Hz) start sampling at 30 m depth and the investigation depth may reach more than 500 m deep, whereas for a 1 ohm·m halfspace high frequencies start sampling at less than 5 m depth and the investigation depth is limited up to 150 m at 1Hz. In practice, the subsurface is never a perfect homogeneous halfspace so that the predicted depth based on skin depth and an average resistivity value for the area provides only a rough and preliminary estimate to the investigation depth.

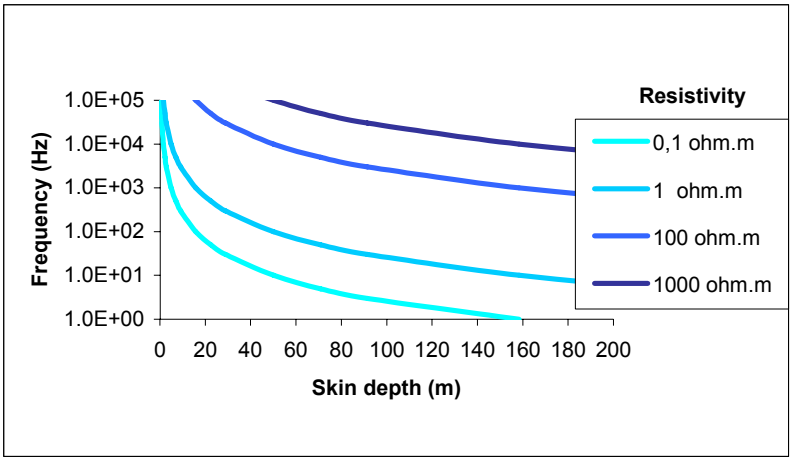

Figure 3.5: Frequency versus investigation depth given by the skin depth relationship.

The AMT frequency band (100 kHz to 1 Hz) allows investigation within mesoscale range from meters to hundreds of meters, making the method ideally suited to hydrogeological

studies on a watershed and basin scale, whereas the frequencies in RMT restrict its investigation to shallow depths and the hydrogeophysical studies to local catchments.

3.3. The control source: near field effect

The AMT method is based on the assumption that electromagnetic waves propagate vertically through the Earth, and therefore the controlled source has to be located far enough away from the receivers to fulfil this assumption. Traditionally, horizontal and vertical electric dipoles have been used as controlled sources and the mathematical description of the electromagnetic field behaviour when recording in the far field or the near field has been derived for that specific case (Zonge and Hughes, 1988; Boerner, 1992). In the work of Pfaffhuber (2001) horizontal magnetic dipoles HMD expressions are developed in the far field and in the near field zones based on Ward and Hohmann (1988) EM theory formulation. The results are presented on the table below, showing the dependence of the specific fields components over a 1D earth on $\omega\mu\sigma$ and on r (transmitter-receiver distance) using a horizontal magnetic dipole HMD as the artificial electromagnetic source.

	Near field	**Far field**
$\mathbf{E_h}$	$\omega\mu\sigma\frac{1}{r^2}$	$\sqrt{\omega\mu}\frac{1}{\sqrt{\sigma}}\frac{1}{r^3}$
$\mathbf{H_h}$	$\frac{1}{r^3}$	$\frac{1}{r^3}$

Table 3.1: Source field geometry in the near field and far field zones using a HMD as the artificial electromagnetic source. (From Pfaffhuber, 2001).

The far-field zone is essentially the area free from non-plane wave source effects, or where source effects constitute less than 10 percent of the total response in the apparent resistivity and phase parameters (Zonge and Hughes, 1988). Far from the source, in the far field zone where the induction number ($r/\delta<1$) is low, both, the E_h and H_h fields decay proportionally to $1/r^3$, and resistivity is thus independent of the transmitter-receiver distance (r).

In the other extreme, the near field zone is defined as the area where the E and H fields are completely saturated and where the plane wave assumption is no longer fulfilled. Close to

the source, in the near field zone where the induction number is high ($r/\delta >> 1$), E_h decays as $1/r^2$, and H_h as a $1/r^3$, and the resistivity values are related to the distance from the source. At intermediate distances, in the transition zone, E decays as $1/r^2$, and H decays at an intermediate rate between $1/r^3$ and $1/r^2$, and thus this is the intermediate case where both distance and subsoil resistivity contribute to the response.

By substituting the expressions of table 3.1 into equations 3.2 and 3.3 for each component it can be seen that in the near field zone the apparent resistivity decreases with decreasing frequency.

$$\rho = \omega \mu \sigma^2 r^2 \tag{3.5}$$

In the source test experiment these predictions have been observed (section 3.6.1).

3.4. Dimensionality

The mathematical properties of the impedance tensor allow the geoelectrical dimensionality of the subsurface to be determined which may be 1D, 2D or 3D. Dimensionality analysis has been proved to be highly important before multidimensional modelling process, given that many 3D environments have been approached with 2D models, not being totally acceptable in some cases (Ledo *et al.,* 2002 a; Ledo, 2006; Queralt *et al.*, 2007).

In a stratified medium, the 1D case, resistivity changes only with depth and the impedance tensor is independent of the measurement orientation of the field components. The diagonal components of the impedance tensor, Z_{xx} and Z_{yy}, are null and the antidiagonal components have the same magnitude but with opposite sign i.e., $Z_{xy}=-Z_{yx}$

$$\begin{pmatrix} E_x(\omega) \\ E_y(\omega) \end{pmatrix} = \begin{pmatrix} 0 & Z \\ -Z & 0 \end{pmatrix} \begin{pmatrix} H_x(\omega) \\ H_y(\omega) \end{pmatrix} \tag{3.6}$$

In the 2D case, geoelectrical changes occur with depth as well as in a direction perpendicular to the geologic strike direction. Maxwell equation's can be decoupled into two different polarization modes, TE and TM with respect to the electrical strike direction. The TE

mode (transverse electric) is defined when the horizontal component of the electric field E is parallel to the strike direction and the horizontal magnetic field H is perpendicular. Conversely, the TM mode (transverse magnetic) is defined when the horizontal magnetic field H is parallel to the strike direction and E is perpendicular. In both TE and TM modes, only one of the horizontal components of the electric and magnetic field is null, and thus the impedance tensor is reduced to its off-diagonal components, not equal in magnitude.

$$\begin{pmatrix} E_x(\omega) \\ E_y(\omega) \end{pmatrix} = \begin{pmatrix} 0 & Z_{TE} \\ Z_{TM} & 0 \end{pmatrix} \begin{pmatrix} H_x(\omega) \\ H_y(\omega) \end{pmatrix} \tag{3.7}$$

The impedance tensor can not be expressed as eq.3.7, but rather as the general impedance tensor (eq.3.1), when measurements are not performed along the electrical strike direction. However it is possible to rotate the measurement axes to an angle θ so that the diagonal components of the magnetotelluric tensor become zero and the axes are parallel and perpendicular to the geoelectrical strike direction. The strike angle can be obtained from the observed MT impedance using several methods: Strike (Groom and Bailey, 1989; McNiece and Jones, 2001), Phase Tensor (Caldwell *et al.*, 2004), WALDIM (Weaver *et al.,* 2000; Martí *et al.,* 2004).

The 3D case represents the most general type of geoelectrical structure where resistivity changes in all directions and the impedance tensor contains all the horizontal electric and magnetic field components independently of the measurement direction, and is expressed by the general equation (eq.3.1).

3.4.1. Data distortion

Data distortion is produced by the presence of three-dimensional local scale structures, located in the shallow subsurface, producing an anomalous charge distribution over its surface area. Distortion may be galvanic or inductive (Berdichevsky and Dimitriev, 1976), but the inductive distortion can generally be ignored due to its small magnitude. Galvanic distortion is frequency independent and its effect on the electric field may be of the same order of magnitude as that of the regional electric field, and is thus considered as an additional anomalous electric field. Galvanic distortion is a complex problem in AMT field surveys, where the impedance tensor is affected by a distortion matrix. In the simplest cases in 1D, and in some 2D cases where measurements are performed in the TE and TM directions, its effect is called static shift.

In practice, static shift is a vertical displacement of the apparent resistivity curves, where the phase angle curve is not affected.

There is no numerical method to correct for the static shift and it is necessary to use information from other geophysical methods that are not affected by static shift such as TDEM (Pellerin and Hohmann, 1990; Meju, 1996; Krivochieva and Chouteau, 2003; Meju 2004), using the tipper data (Ledo *et al.*, 2002 b), or comparing all the survey responses with a priori geological or geophysical information.

3.4.2. WALDIM

Most of the methods used to characterize the dimensionality of the geoelectrical structures are based on rotational invariants, that is a set of parameters computed from the observed AMT tensor that do not depend on the direction of the measuring axes (Bahr, 1988; Szarka and Menvielle, 1997; Weaver *et al.*, 2000;). As an alternative, Caldwell *et al.* (2004) introduced the magnetotelluric phase tensor, defined as the relationship between the real and imaginary parts of the MT tensor. Martí (2006) analysed these different methods, highlighting their strengths and weaknesses and proposed the WAL invariant approach (Weaver *et al.*, 2000) as the best method to extract maximum information from the regional MT tensor while considering accurate invariant thresholds (Martí *et al.*, 2004). In addition, Martí *et al.* (2004) developed a Visual Fortran 2000® application, termed WALDIM, as a tool to automatically perform dimensionality analysis on a set of raw or synthetic MT data.

Case	**Geoelectrical dimensionality**
1	1D
2	2D 3D/2D only twist 3D/2D general galvanic distortion twist + shear
3	3D 3D/1D2D galvanic distortion over a 1D or 2D structure non recoverable strike direction Undeterminable due to strong distortion

Table 3.2: Summary of the WALDIM analysis scheme. TheWALDIM application is used in all the AMT aquifer appraisals presented after as one of the first steps of the data analysis.

The main functions of WALDIM program are to determine the data dimensionality, following the WAL criteria, according to the data errors and the threshold. Eight different dimensional cases can be obtained, divided into three general situations: 1D, 2D, and 3D, the latter including the case of undeterminable dimensionality due to strong distortion.

3.5. Modelling

AMT multidimensional techniques are well developed using existing MT modeling processes directly applied at higher frequencies. Forward modeling codes can resolve 1D, 2D (PW2D Wannamaker *et al.*, 1987; Pek and Verner, 1997), and 3D structures (Mackie and Madden, 1993) using the time consuming trial-an-error approach. Inversion codes also exist for computing 1D and 2D and 3D responses. Important 2D inversion codes include 2D Occam (Constable *et al*., 1987), RRI (Smith and Booker 1991), RLM2DI (Mackie *et al.,* 1997), REBOCC (Siripunvaraporn and Egbert, 2000), NLGC (Rodi and Mackie, 2001) or DetREBOCC based on REBOCC code, modified by Pedersen and Engels (2005). 3D inverse codes are still in the development stage and many codes are currently being tested with synthetic data and simple models. Recently, WSINV3D has been publically released (Siripunvaraporn *et al.,* 005), however computational time and other mathematical issues are still matters of concern.

3.5.1. The Determinant mode of the Impedance Tensor

Most of the inversion codes listed above are based on the combined inversion of TE and TM modes to retrieve 2D geoelectrical models. However, in the real three-dimensional world the resulting 2D models may fail on the good correspondence between the measured data and model response. As a result many authors use only one of the two modes (TE or TM) in the inversion process.

In practice, many 3D environments are tackled using 2D profiles due to computational limitations or survey geometry along a line making it impossible to compute a 3D model. Most of these 2D profiles include 3D effects in the final model that can lead to misinterpretation (Ledo *et al.,* 2002a; Ledo, 2006). Pedersen and Engels (2005) proposed the use of the determinant of the impedance tensor (eq.3.8) as a useful tool for computing routine inverse

models when is not possible to determine principal strike direction, given that the determinant is invariant under rotation.

$$Z_{\det}(\omega) = \sqrt{Z_{xx}Z_{yy} - Z_{xy}Z_{yx}} \tag{3.8}$$

The determinant mode reduces the distortion effects caused by shallow heterogeneities and non-finite lateral structures, and the phase is not affected by galvanic distortions (Berdichevsky and Dimitriev, 1976). The determinant inversion generally allows a good data fit while at the same time resolving reasonably well both resistive and conductive structures along any profile. Estimated resistivity values lie much closer to the true subsurface resistivity in between the extreme resistivities predicted by individual TE and TM mode inversions (Pedersen *et al.*, 2005). The determinant mode has been successfully tested in several studies (Chouteau *et al.*, 1994; Linde and Pedersen, 2004 a/b; Pedersen *et al.*, 2005; Linde, 2005).

In the hydrogeophysical applications discussed subsequently (chapters 4, 5, and 6), the analyzed environments show mainly three-dimensional behavior due to the scale and heterogeneity characteristics of the subsurface media. In order to cope with the three-dimensionality, the determinant of the impedance tensor has been used to visualize the data as apparent resistivity and phase. The inversion procedure has been done using DetRebocc (Pedersend and Engels, 2005) that allows the inversion of the determinant of the impedance tensor using the REBOCC code (Siripunvaraporn and Egbert, 2000).

3.6. Limitations

G.H.Hohmann (1984) in his class notes discussed on the limitations and future of the MT method, and those thoughts are still valid to some degree: “MT method was invented by Tikhonov (1950) and by Cagniard (1953) in the early 1950’s. Since then, the method has been refined considerably but problems are still present, primarily with noise in the measurements and lack of an adequate interpretation. Improvements in data collection, data processing and three dimensional numerical modelling should solve some of theses problems”. Artifacts are inherent in every inversion algorithm due to noise, undersampling and three-dimensionality, and thus inverse model results that provide a good data fit should not be regarded as the only

possible answer. A geologically reasonable model that fits the data is our best assurance that we have produced a credible model.

Cultural noise may be considered as a main limitation when no filtering is possible. The use of an artificial source can help to improve the data quality. However, in the high frequency range, the near-far field transition distance is relatively small, and thus, in order not to impose significant near-field effects on the acquired data, rigorous field survey procedures including R-T testing must be followed.

In terms of resolving power with respect to targets of interest, attention has to be given to a priori geological assumptions, mesh size and data dimensionality. In general, shallow targets demand dense site spacing, denser meshes and use of appropriate sensors for the period range. Spatial aliasing is the term used to describe undersampling where adequate resolution of the targets is not achieved because the measurement sites are located too far apart in a heterogeneous media. Investigation targets size increases with depth due to increasing recording frequency, while target resolution decreases. As seen in the skin depth section ground resistivity can change the investigation depth and consequently the resolution of the retrieved information for the same frequency range. Data should be modelled using rigorous pertinent dimensional code so as not to include three-dimensional effects in widely used 2D profiles. 3D inverse models are still on testing state and main concern relays on computational time, and usefulness for appropriate interpretations.

AMT models provide information on bulk resistivity alone, which in terms of interpretation cannot be directly linked to any lithology, porosity of the media, or hydraulic permeability without a priory hydrogeological information. Resistivity measurements are affected simultaneously by lithology, fluid presence, and structure of the pore spaces. Further research needs to address this issue on the study of petrophysical relationships in order to quantitatively convert resistivity into rock physical properties.

3.7. Instrumentation tune up

The Audiomagnetotelluric equipment used on the hydrogeophysical applications developed on this Thesis is the StrataGem EH4 system from Geometrics©. The technical characteristics and equipment tune up for field surveys are exposed on the next sections.

3.7.1. StrataGem EH4

StrataGem EH4 system©, is a four-channel, natural and controlled-source tensor system recording in the range of 10 to 92000 Hz (Geometrics, 2000). The system is composed of 4 buffered active high-frequency dipole and stainless-steel electrodes and 2 induction coils connected to an AEF receiver (Figure 3.6), that transmit magnetic and electric time series data to the console where the data are stored.

To improve the signal-to-noise ratio where cultural noise may be present or where the natural signal is weak, an unpolarized transmitter (800 to 64000 Hz) comprised of two horizontal-magnetic dipoles with a magnetic moment of 400 Am^2 is used. The transmitter needs to be located far enough away from the receiver to fulfil the plane wave assumption, but close enough to provide adequate signal strength. AMT+CSAMT tensor measurements may be treated using standard MT processing techniques.

Using Imagem software, the recorded time series (Stratagem Yfile) are converted to complex cross-spectra using an FFT (Stratagem Xfile). A least-square cross-spectral analysis (Geometrics, 2000) is then used to derive the transfer function (impedance) that relates the observed electric fields to the magnetic fields (Stratagem Zfile).

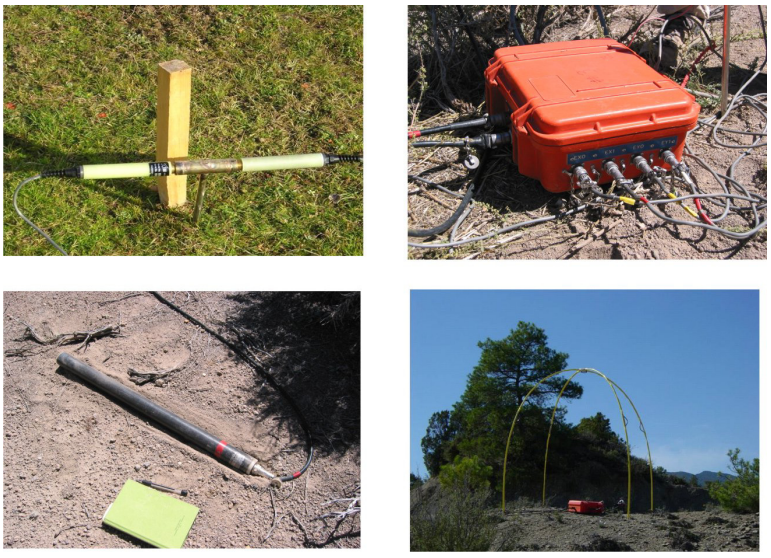

Figure 3.6: Pictures illustrating the different components of the StrataGem system. From left to right and top to bottom is shown an electrode, the AEF receiver box, an induction coil, and the controlled source.

3.7.2. Source test experience

Once the StrataGem equipment arrived at the department it was necessary to tune up the equipment to get a better knowledge of the capabilities of the instrumentation. In particular, three main issues related with the StratGem controlled source has been explored: 1) to identify the source transmitting frequencies, 2) to recognize the non plane wave effects due to the source proximity, and 3) to verify the signal improvement resulting from using the controlled source and assessing the sensitivity of the equipment.

1) Transmitted frequencies

Fourteen independent frequencies are transmitted sequentially by the horizontal magnetic dipole at: 800, 1000, 1400, 2000, 3000, 4000, 6000, 8000, 12000, 16000, 24000, 32000, 56000 and 64000 Hz. This frequency range is termed the controlled source frequency band (CS band in the figures). To assure that the source transmits signal at the specified frequencies, a wavelet spectral analysis was conducted following the procedure developed by Arango (2005) (Figure 3.7).

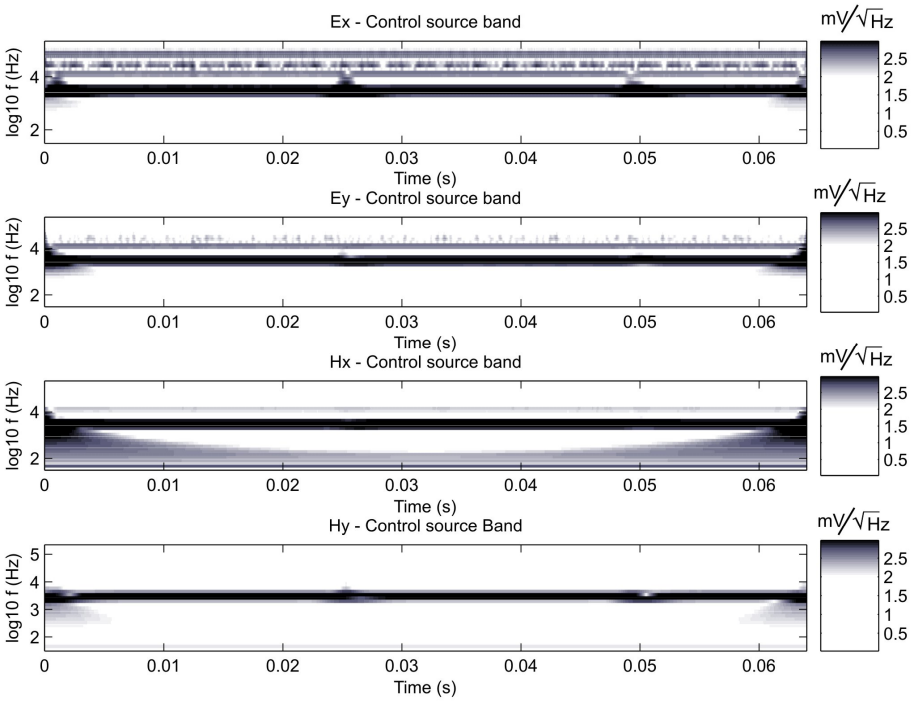

Figure 3.7: Frequency domain spectral analysis based on the Morlet wavelet transform showing the 4 AMT data components (courtesy of C. Arango.). The dominant frequency appear as a high amplitude band at one specific frequency (black line), that corresponds to one of the fourteen frequencies transmitted by the controlled source.

The AMT sounding analysed consist of a fully saturated near-field source signal to ensure that only one transmitted frequency is the main frequency content at each transmitter time, since in the test case characterization of the subsurface resistivity is not important. The existence of fourteen different frequencies transmitted was confirmed on all the components (E_x, E_y, H_x , H_y). In the same way as Figure 3.7, 13 other plots were generated to confirm the presence of signal energy at all the specified transmitter frequencies.

2) Near-field effect

The source effect is easily recognized by the distortion of apparent resistivity and phase given that near-field effect is the result of the changing dependence of E_i and H_j on the impedance tensor. In order to determine the near-far field distances several soundings on the same location were recorded increasing receiver-transmitter (R-T) distance.

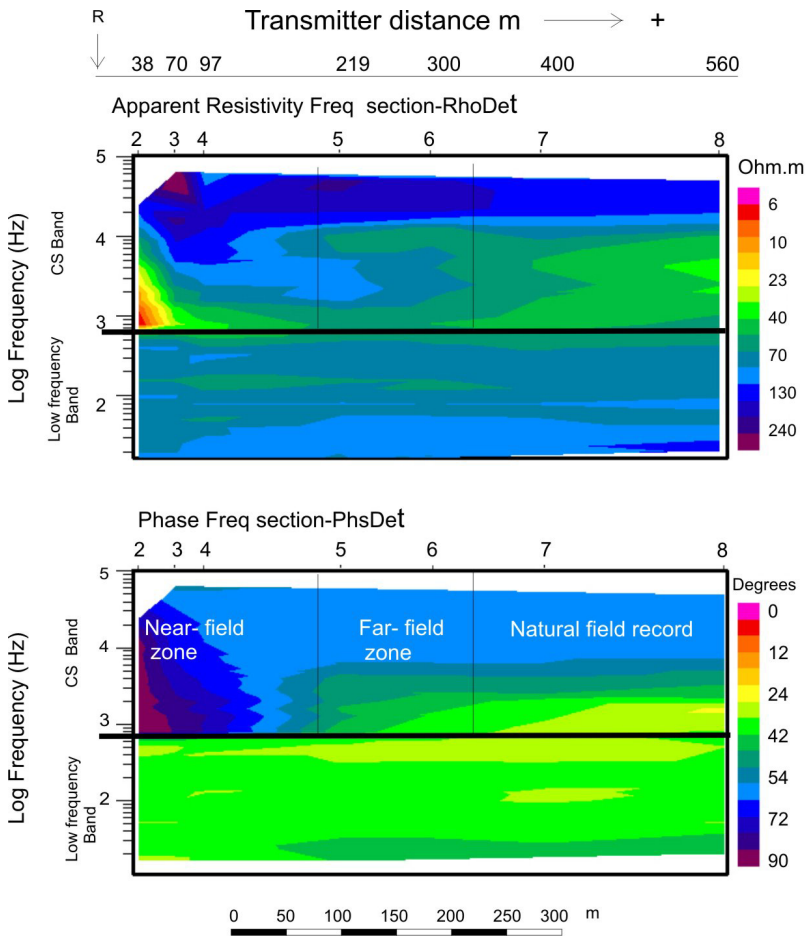

Figure 3.8: Pseudosections of the apparent resistivity and phase of the impedance tensor determinant. Soundings are spaced according to transmitter-receiver distance. The horizontal black line at 800 Hz, divides the controlled source band (higher frequencies) from the low frequency band, and highlights the behavior change with and without the source.

Figure 3.8 shows pseudosections of the apparent resistivity and phase of the determinant of the impedance tensor for the same sounding position with different R-T distances. Given that the soundings are at the same site, "distances" between soundings shown in Figure 3.8 correspond to increasing R-T distances from left to right. The pseudosections illustrate the transition from the near-field zone (sounding 2, 3, and 4) to the far field zone (sounding 6 and 7) and beyond (soundings 7 and 8) where the transmitter is too far away to provide any noticeable effect.

The near field zone is clearly recognized on the left of the pseudosections (Figure 3.8) where the source is at 38, 70 and 100 m (soundings 2, 3 and 4 respectively). The near field effect is apparent in the phase section where phase values reach 90º and where the resistivity values display a negative slope of 45º (see section 3.3). Figure 3.9 shows the apparent resistivity and phase for sounding 2, where the recorded signal contains near-field effects in both the phase and apparent resistivity. There is a gradual resistivity and phase shift from sounding 2 to sounding 4 (Figure 3.8).

Sounding 4 is a singular case, where not all the controlled source frequencies are affected by the non plane wave effects (Figure 3.8). Source influences can be observed in the lower frequency position of the CS band, where the phase shifts towards 90º, but is not seen in the higher CS frequencies.

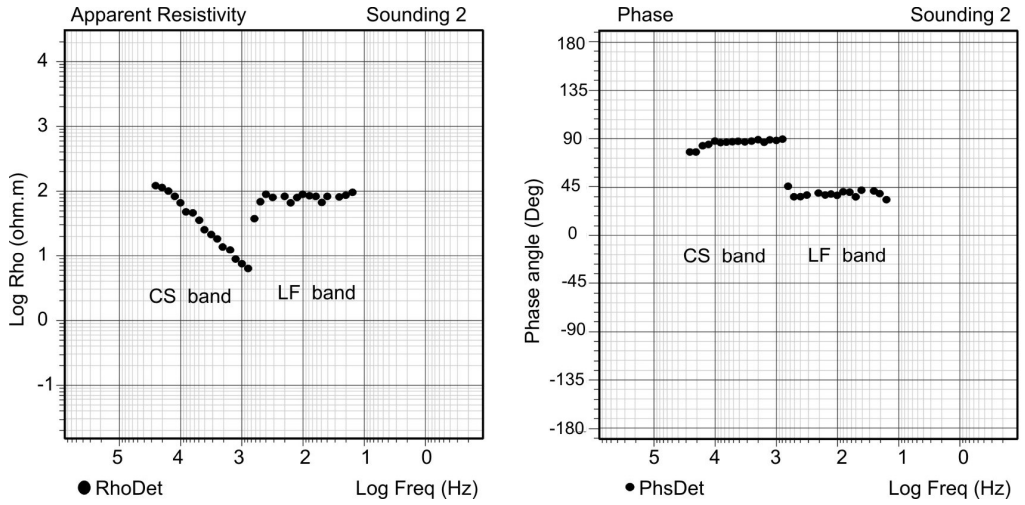

Figure 3.9: Detail of the apparent resistivity and phase angle curves on a sounding affected by non plane wave effects. Apparent resistivity curve has a 45º slope and phase angle of 90º due to coherent noise. There is a sharp transition form the CS band to the natural EM band.

These observations illustrate the sensitivity of the instrument to R-T distance within the high frequency recording range. Measurements recorded within the far-field and near-field zones may only be separated by a few tens of meters. Therefore a compromise between R-T distance and signal strength has to be achieved so as to avoid near-field effects, in particular in the lower spectrum of the CS band, while still being close enough to record adequate signal strength at highest frequencies.

3) Source quality improvement

A far field response is apparent in the data of soundings 5 and 6, where the transmitter is located at 200-300 m, and therefore at this specific site this R-T distance would be the ideal for surveying this area (Figure 3.8).

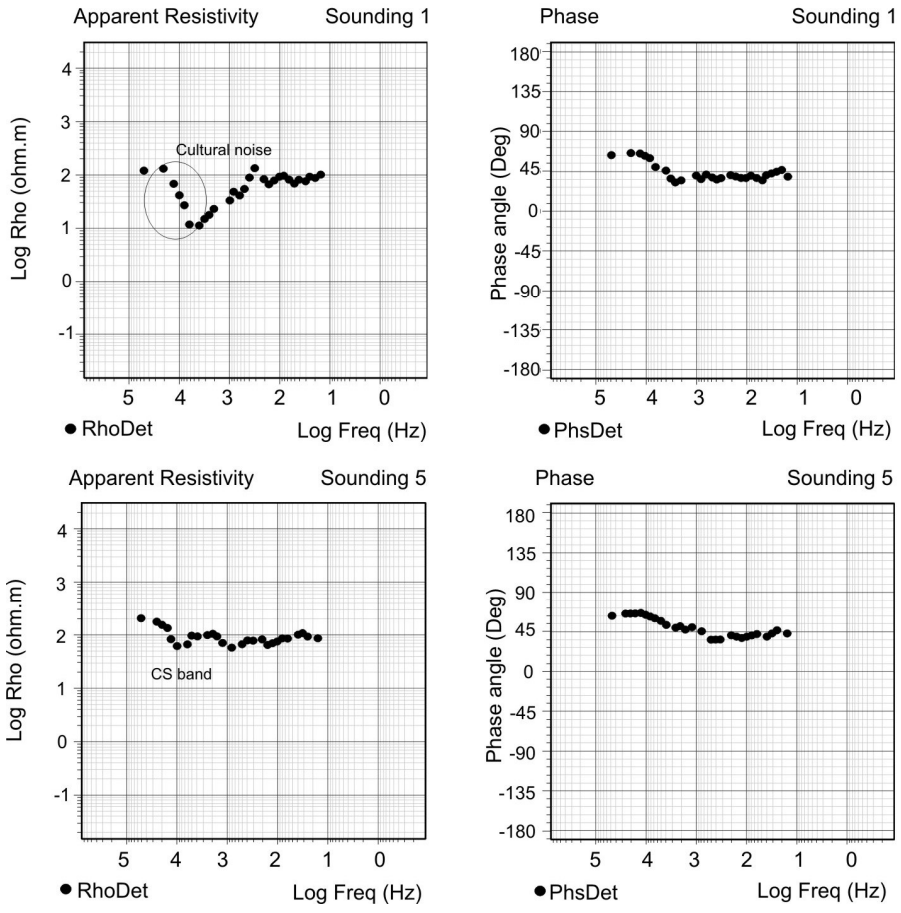

Figure 3.10: Soundings 1 and 5 recorded without and with the controlled source respectively. Curve comparison shows significant improvement in the data quality on sounding 5 where the source is located at an optimum distance.

The data of sounding 5, recorded on the far-field zone, can be compared with that of sounding 1 which was acquired without using a controlled source and recording the natural EM signal only (Figure 3.10). Sounding 1 is characterized by high noise data on CS Band as seen in the apparent resistivity curve of the determinant of the impedance tensor. The phases however, are characterized by reasonably good data quality. Sounding 5, acquired with a plane wave source, displays better data quality, showing the importance of using the transmitter in noisy areas (Figure 3.10). Similar improvement can be expected in the case of a weak EM natural signal where the source can substitute for the absent natural signals.

The source test experience has evidenced that the controlled source located at optimal distance improves data otherwise data will include controlled source near-field effects or equipment will not receive enough signal strength. In any new survey different environmental conditions can be found and thus a far-field near-field optimal distance test should be done to ensure good data quality. Tordera, La Soutte and Spring Valley far-field distances has been tested before progressing on the survey acquisition.

Part II

Hydrogeophysical applications

4. La Tordera, Spain
5. La Soutte, France
6. Spring Valley, USA

Part II: Hydrogeophysical applications

The first part of the memory presents the hydrogeophysical discipline, and the hydrogeological objectives that could be reached with the combination of both hydrogeological and geophysical datasets. An overview of the geophysical approach to the hydrogeological media has been also presented, from field to modeling and interpretation steps. In addition, the most important hydrogeophysical methods have been documented, with the special emphasis on AMT (Chapter 3). The goodness of the geophysical methods to complete hydrogeological data is unquestionable; however there are many challenges that have to be improved and resolved. Many aspects from instrumentation accuracy, data processing, and computational skills have still to be improved, to fully develop the hydrogeophysical discipline.

In the following part of the memory (part II) three different hydrogeophysical applications entitled La Tordera, La Soutte and Spring Valley are presented. These following chapters are three case study result of the PhD study development. La Tordera is the main hydrogeophysical application since Tordera aquifer system was one of the study areas of the Geoelec project (Marcuello and Plata, 2005), where my PhD scholarship was associated. Whereas La Soutte and Spring Valley case studies are the result of the two stages with different geophysical research groups, one in France and the other in USA. These experiences have provided the possibility to know different hydrogeological contexts, to learn diverse geophysical techniques and associated problems and to discuss hydrogeophysial advances from other perspectives. To work with other advanced research groups has enriched extensely my hydrogeophysical background.

These three multidisciplinary studies investigates different aquifer systems at different resolution scales, from a local catchment (La Soutte) to local basin aquifer system (La Tordera) and a larger watershed scale (Spring Valley, Nevada). Each project responds to a specific objective and therefore methodology followed present different approaches. However in all three cases AMT has been used as the principal geophysical data set that helped with other different geophysical techniques reach a higher degree of knowledge. The Tordera application is based on the appraisal of a fluviodeltaic aquifer system north of Barcelona, where exist an extensive seawater intrusion problem. Aquifer system therefore is developed on a porous media

where significant withdrawal are performed. La Soutte is a small catchment area near Strasbourg, France, where the team 'Proche Surface' EOST has its hydrogeophysical experimental field site. Aquifer system is fissured in nature on granite and volcanoclastic materials. Main importance relay on the knowledge of the hydrodynamic transfer zone form the surface and perched aquifers towards the regional Rinhegraben aquifer. Spring Valley in Nevada, USA, is larger scale hydrogeophysical approach to detect the main basin boundaries controlled by the frontal range of the Basin and Range region of the USA. Extensive studies of gravity magnetic and AMT are being carried out by the US Geological Survey to delineate those characteristics. Main aquifer units are developed on a porous and karstic media, where the geophysical investigations correspond to a water exploration phase. Geophysical models are being used as a complementary tool to built up the valley hydrologic model.

Chapter 4. Hydrogeophysical application: Tordera aquifer system

In this chapter, a multidisciplinary approach to a fluviodeltaic aquifer system integrating several geophysical methods with hydrogeological data is presented. Hydrological information, Audiomagnetotelluric (AMT) and seismic reflection and refraction models have been evaluated together to provide spatially continuous information about aquifer properties and processes. 2D and 3D AMT inverse models have been obtained as well as an AMT time-lapse monitoring experiment has been conducted. In addition, DC resistivity and TDEM measurements have been carried out and a comparison of resolution and investigation depth among EM methods is presented.

Tordera aquifer system appraisal has been developed on the framework of Geoelec project REN2002-04538-C02 **Tomografia geoeléctrica: desarrollo para la caracterización de acuíferos,** where my PhD scholarship is associated.

4.1. Introduction

Characterization of groundwater resources and reservoirs require high resolution and high precision methods in order to resolve natural heterogeneity at different scales. In particular, groundwater management needs highly detailed characterization especially in porous coastal aquifer systems in semiarid climates that are under hydrological pressure. Groundwater resources in deltaic aquifer systems are controlled by 1) its tectono-sedimentary evolution that determines the aquifer boundaries and the aquifer units (distribution of coarse to fine detritic materials), and 2) anthropogenic pressure over the aquifer system. Geological and hydrogeological characterization is a difficult task when only scarce information is available. Moreover, the characterization is critical for salt-water intrusion problems where seawater migration is largely controlled by the heterogeneity of the subsurface. This chapter presents a multidisciplinary study focused on the characterization of hydrogeological parameters and

processes of a deltaic aquifer system using mainly hydrogeological information, audiomagnetotelluric (AMT) and seismic data.

The Tordera aquifer system was chosen because it was supposed to be hydrogeologically well constrained and previous geophysical survey data was available. However, complex issues have been observed on the quality of the available lithological data, transforming a simple geophysical validation experiment into a fully hydrogeophysical approach of a porous aquifer. In addition, the Tordera delta has gone through a salt water intrusion process, where salt water encroachment has an extensive presence inland on the deep aquifer. The main objectives of the present work are 1) to use different geophysical techniques to characterize the aquifer system (in particular, AMT and seismic techniques), 2) to integrate the geophysical results with the hydrogeological information to build a more complete hydrogeophysical model (to establish the thickness and continuity of the aquifer units, morphology and depth to the basement), 3) to characterize the seawater encroachment state and dynamics of the aquifer system, and finally 4) evaluation of those independent geophysical methods AMT, TDEM, surface DC and seismic profiles to determine its strengths and limitations on hydrogeology problems.

4.2. Hydrogeological setting

The Tordera basin (894 km^2) is located in the northern part of the Catalan Coastal Ranges (CCR) in the northeastern coast of the Iberian Peninsula (Figure 4.1) situated 60 km northeast of Barcelona. The CCR can be defined as a complex system of asymmetric horsts and grabens that extends parallel to the present day SW-NE coast line. The horst domains are essentially composed of Paleozoic basement and a discordantly overlying Mesozoic cover (Roca, 1996). All graben domains are infilled by Miocene and younger sediments, divided by two parallel ranges, the Prelitoral and the Litoral Ranges.

The Tordera River morphology and deltaic space (21 km^2) is structurally constrained by faults (Figure 4.1). These morpho-structural expression of the CCR is the result of the post-alpine distension that affect the Catalan margin with SW-NE normal faults and its subsequent subdivision of the main structural unit into minor blocks at right angles. The CCR basin bedrock consists of plutonic and metamorphic rocks. On the study area, bedrock is composed by granites

emplaced during the Hercynian orogeny and later affected by the Alpine orogeny (Enrique, 1985).

Periglacial processes on hillslopes during the Pleistocene Epoch caused intensive rock weathering. Since then, considerable amounts of sandy material have been released from the bedrock and easily moved into the streams (Rovira *et al.*, 2005). Thus, fluviodeltaic sedimentary cover from the Neogen and Quaternary period is building up a fluviodeltaic depositional system of transition facies, from continental to marine. Deltaic evolution show different phases, morpholgically observed on the coastline and prodeltaic front (Serra and Valois, 2007). The detritic material comprises clay & silt with varying size in prodelta region and floodplain material to coarse gravels in the channels that constitute the heterogenic aquifer system.

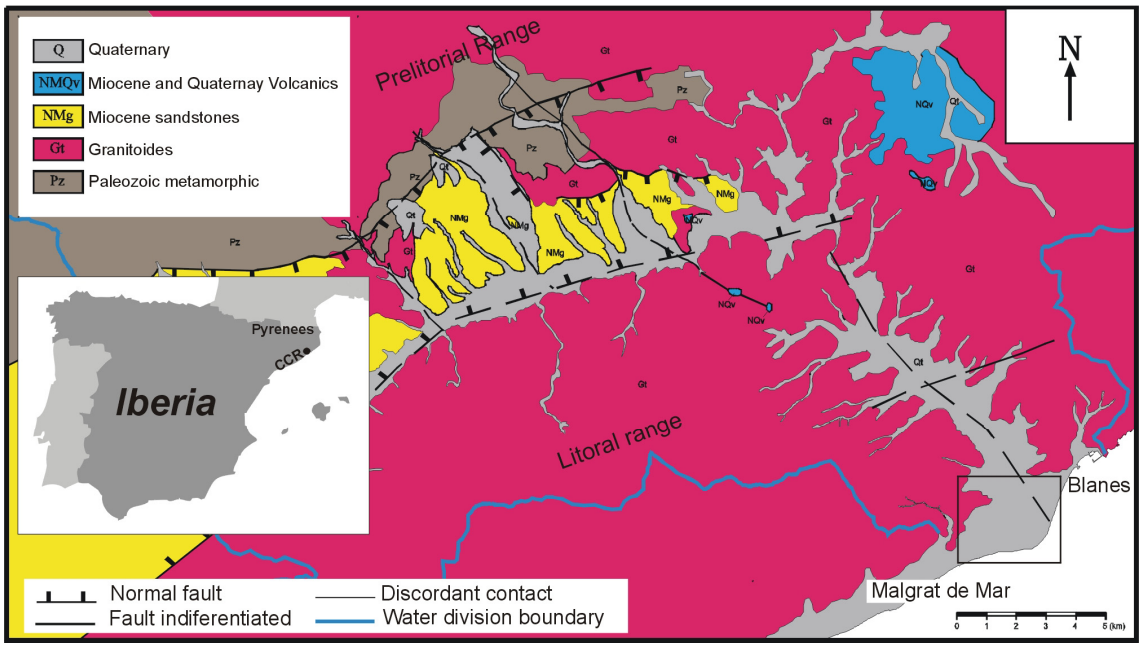

Figure 4.1: Study area situation. Simplified geologic map of the Tordera basin derived from 364, 365, and 359 maps Serie Magna 1:50.000 IGME (Modified from Geoservei, 2001), and the satellite map locating main geological structures on the north-eastern Iberian peninsula: Pyrenees, and Catalan Coastal Ranges.

The climate is classified as sub-humid Mediterranean with maritime trends (Sala, 1979). Mean annual rainfall ranges from 1000 mm in the catchments and recharge areas to 600 mm along the coast. River changes its fluvial regime, shifting from a quasi-continuous water and sediment circulation in the upper parts, to an ephemeral flow pattern in the lower sections, where on the deltaic region most of the time there is no surface water circulation.

Aquifer system conceptual model is composed of 3 or 4 aquifer units depending on the author. Here we present four units from shallow to deep: a free upper aquifer above an aquitard, a deep semi confined aquifer and a basal aquifer system restricted near the shoreline (Geoservei, 2001). Tordera aquifer system is considered as a strategic aquifer for the management planning of regional hydrologic resources. During the last decades, water demand has increased substantially and the seawater wedge has progressed inland reaching some water-supply wells. The deep semi-confined aquifer bears excessive withdrawals due to tourism, domestic and industrial activities, and therefore the deep aquifer is the most affected by the seawater intrusion influence. In order to reduce freshwater extractions a salt water plant (ITAM Blanes) was built and it began its activity during the fall of 2002, with a maximum treating capacity of 10 Hm^3/ year. Not being sufficient to satisfy the water demand and to reduce the salt water encroachment, on June 2005 the Environmental Ministry approved the facility to be extended for a final treatment volume of 20 Hm^3/year. However this second phase development is still in its study phase.

4.3. Hydrological context

This next section introduces the structural aquifer framework and the seawater encroachment situation. Firstly, the hydrologic conceptual model and its associated hydraulic parameters from the literature are presented. Secondly, the hydrochemical analyses of selected wells are presented to provide a general overview of the distribution of seawater wedge far-reaching inland.

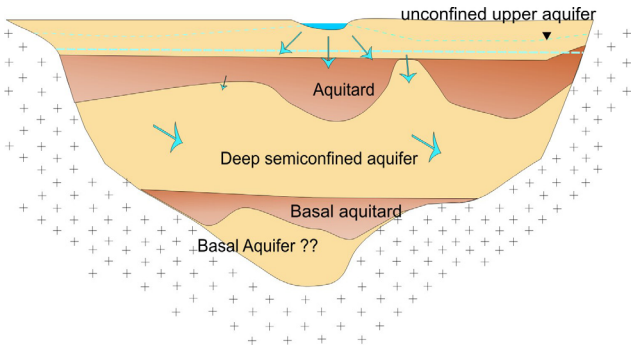

Figure 4.2: Tordera hydrogeologic conceptual model composed by: an upper free aquifer, a deep semiconfined aquifer, and a basal aquifer. Arrows show and ideal water flux, river is mainly influent where vertical recharge flows from the upper aquifer to the deep aquifer and from the upper basin aquifer zones.

4.3.1. Conceptual model and hydraulic parameters

The conceptual hydrological model (Figure 4.2) comprises four main units (Geoservei, 2001): 1) an upper unconfined aquifer that covers the entire delta, the thickness of which can vary from 6 to 20 m, 2) an aquitard with maximum thickness of 25 m, 3) a deep semi-confined aquifer with high hydraulic conductivity, and 4) a basal aquifer restricted near the shoreline as a consequence of a substantial increase in sedimentary thickness from 80 m to more than 180 m. This feature can be related to a vertical displacement fault aligned NE-SW along the regional fault strike of the Catalan Coastal Ranges. However, this simple conceptual model does not show neither the lithological heterogeneity nor the discontinuities of the hydrological units.

Aquifer unit	**Hydraulic permeability K (m/d)**	**Hydraulic transmissivity T(m^2/d)**	**Storage coeff. S**	**Porosity Φ**
Upper free	200-3000	160-9500	0.2	0.2
Deep semiconfined	50-1400	1050-4300	$6.23*10^{-5}$ – $0.5*10^{-3}$	0.3
Basal	100	150-880	$1.01*10^{-2}$	0.1
	Vertical permeability	**Leakage factor B (m)**		
Aquitard	$4.5*10^{-1}$-$5.6*10^{-2}$	340-500	$1*10^{-2}$	0.1

Table 4.1: Comparative table of hydrologic parameters built as a summary of precedent Hydrologic Tordera studies: REPO (1971), PHPO (1985), Teixidó, T. (2000), Geoservei (2001), Casas and Rahola, (2003), Guimerà *et al.* (2003).

Deltaic aquifer system has been described with total resources of 43 Hm^3/y (Teixidó, 2000). The upper aquifer is used mainly for agriculture, whereas deep aquifer, which is the largest source of freshwater, bears most of the industrial and water supply extraction. In general terms, the upper aquifer recharges the deep aquifer through the aquitard and higher permeability windows in addition to the upper system contributions. Aquifer system‘s piezometry is highly influenced by pumping, direct precipitation and river inputs. During summer, there is the maximum extraction and minimum recharge prompting sinking on the head levels. The deep aquifer presents continuous negative cones due to excessive withdrawal for water supply (Galofré *et al.*, 1998). Piezometric levels show a low hydrodynamic gradient ($2\text{-}3.35.10^{-3}$), typical of deltaic zones and groundwater flux direction is roughly NW-SE (spring 2003)

following to the river direction (Casas and Rahola, 2003), nonetheless anomalies are expected nearby water supply zones so that flux is highly influenced by the extractions.

Compilation of hydraulic parameters has been done for different resources (Table 4.1). Variability of all these parameters show the heterogeneity of the system, since the transmissivity responds to the average volume nearby the well.[(1)]

4.3.2. Seawater hydrochemical state

Antropic pressure over the aquifer system results on the imbalance between input and output of the system, that reflects a hydric deficit compared with the estimated total resources enhancing the progress of the seawater wedge. Saline water is a major concern in this zone, for this reason salt net control was completed on this area with 6 multi-tube piezometers during 2003; however, no analysis has been done on these wells since 2004. The lithology and hydrochemistry of W-04 and W-06 wells have been used for the calibration and validation of our geophysical data and models due to its closeness (section 4.11).

Hydrochemistry analyses are available on the Catalan Water Agency ACA interactive webpage (Http://mediabient.gencat.net/aca). W-04 and W-06 are two multi-tube piezometers that provide three lectures in depth where anomalous high Cl^- ion concentrations were measured. Table 4.2 shows the lectures on depth of the Cl^- ion concentration in May. Our first AMT survey was carried out at the same period and thus hydrochemical data was used on posterior joint interpretation (section 4.11).

Focusing on the chlorine ion concentration on spring of 2004 (Table 4.2), it is seen that Tordera fresh water ranges between 100-120 ppm Cl^-, that in resistivity terms corresponds from 7 to 15 ohm·m respectively. In contrast, there are some records of 16000 ppm Cl^- and 1350 ppm Cl^-, which may indicate significant seawater content in the samples.

(1) Most of the transmissivity values T (m^2/dia) shown on table 4.1 were obtained from hydraulic tests at different wells derived from the pumping rate Q (l/s), and the well drawdown s (m), qualitative approach (Custodio and Llamas, 1996) $T = \frac{Q}{s}100$

Hydrochemical and head values of the aquifer system related to the seawater intrusion process have been controlled due to the increasing water demand. For instance, Teixidó (2000) show the head values evolution from the period of 1983 to 1995, where a decrease of the head level on piezometer B2-b is seen, around 500 m to the shoreline. Even though the well is away from the shoreline and from the main extraction zone, the well show a piezometric drawdown [(2)] that was interpreted as a substitution of 50-60% fresh water with saline water assuming linear changes from fresh water density (1 g/cm^3) to high density saline water (1.25 g/cm^3) (Custodio and Llamas, 1996).

Piezometer	Depth	Cl^- ppm	µS/cm	ohm·m
W-04	3-15 m	129.7	1361	7.31
	22-45 m	348.9	1306	7.6
	53-80 m	**16653**	33408	0.29
W-06	3-11	90	632	15.84
	15-49	111.3	680	14.705
	51-68	**1355**	4261	2.34

Table 4.2: Chlorine concentration, laboratory electrical conductivity lecture and its translation to electric resistivity**,** on piezometers W-04 and W-06. (10 ohm·m = 1 µS/cm**).**

In order to quantify the seawater amount in the water samples using a more rigorous methodology Soler *et al.* (2006) computed a Cl^-/Br^- mixing model for the piezometrers W-04 and W-06. This hydrochemistry tracer approach has been used successfully by many other workers (Custodio and Herrera, 2000, and references therein).

[(2)] Being x % of seawater content, [Cl] chlorine ion concentration on the seawater, on the well and freshwater. Water density changes, γ (g/cm^3), due to x are considered on the well to obtain the non affected piezometric level $H_{freshwater}$.

$$[Cl_{seawater}]x + [Cl_{freshwater}](1-x) = [Cl_{well}];\quad x\gamma_{seawater} + (1-x)\gamma_{freshwatr} = \gamma_{well};$$

$$H_{freshwater} = \frac{(\gamma_{well} - \gamma_{freshwater})}{\gamma_{freshwater}} z + \frac{\gamma_{well}}{\gamma_{freshwater}} H_{well}$$

As end members, they have used on one hand the Mediterranean seawater Cl^- and Br^- concentration to establish the 100% of seawater content and on the other extreme the minimum values of Cl^- and Br^- concentration from the sampled wells as the freshwater (0% of seawater content). Derived from Figure 4.3, it can be seen that W-04 shows almost 75% of seawater content and W-06 around 8%. In addition, radioactive isotope analysis has been carried out ($^{228}Ra/^{226}Ra$, and H^3) for dating purposes. Results suggested that water residence time ranges from months to years ruling out the hypothesis of the presence of high chlorine concentration inland due to trapped paleowaters (Soler *et al.*, 2006).

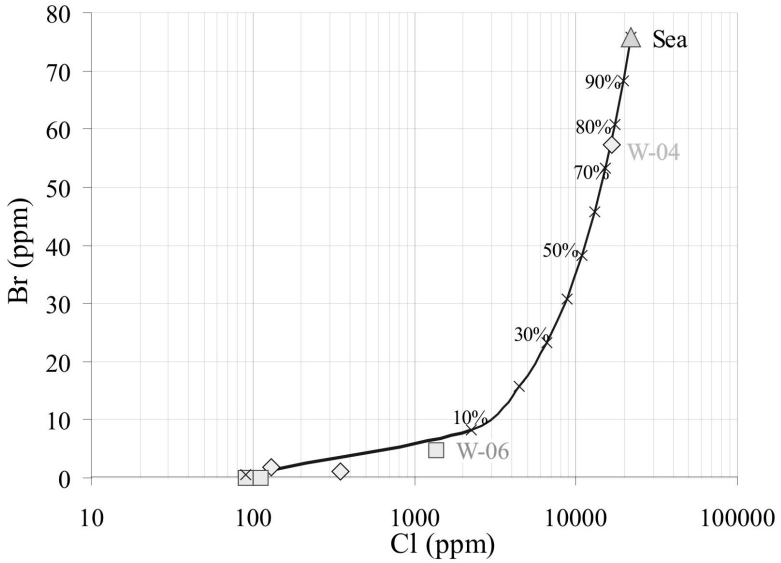

Figure 4.3: Tordera seawater-freshwater Cl^-/Br^- mixing model. Diamonds and squares shows three hydrochemical lectures on depth of W-04 and W-06 where percentage of seawater could be derived. For specific location of W-04 and W06 see Figure 4.5.or Figure 4.10. (Modified form Soler *et al*., 2006).

In spring 2006, l'Institut Geològic de Catalunya (IGC), carried out a well log temperature and conductivity record on Malgrat-1 well located near the shoreline (Figure 4.4) (see Figure 4.5 for exact location). Electric conductivity values image water column stratification from shallow up to 50 m. From that point on, extreme high conductive values are measured corresponding to seawater (50000 μs/cm- 35000 ppm Cl^--seawater) showing a typical stratified seawater wedge structure.

From the electrical conductivity record of Malgrat-1 well, and the hydrochemistry analyses from W-04 and W-06 it could be inferred that high ion chlorine concentration is due to the seawater encroachment that presents a characteristic stratification at 50 m depth near the

shoreline. Moving inland, from Malgrat-1 to W-06, 1200 m further inland, a meaningful decrease on the chlorine concentration depicting the seawater transition zone is observed.

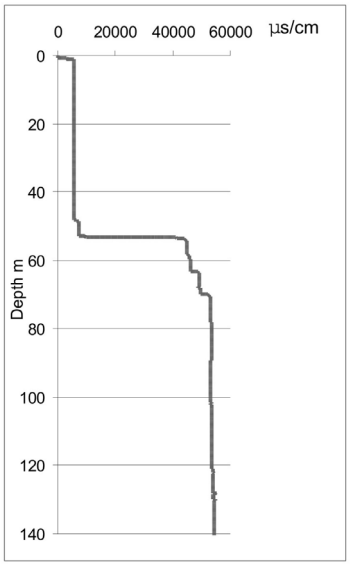

Figure 4.4: Electrical conductivity well log record on Malgrat-1. Seawater wedge is clearly differentiated and found around 50 m depth. See Figure 4.5 for specific location. (IGC, B. Benjumea personal communication, 2006).

4.4. Geophysical data

This section presents previous geophysical information and new geophysical surveys carried out during the research project development 2003-2006.

4.4.1 Previous geophysical projects

- In 1969 Geofisa-Prohidro SA, carried out 80 VES over the lasts 10 km of the Tordera and over the deltaic zone. The array geometry corresponds to Schlumberger with AB/2 ranging from 0.5 to 240 m.
- In 1994, 1995 and 1996, the Servei Geològic de Catalunya carried out VES surveys with 28 soundings of Schlumberger configuration with a maximum AB/2 of 320 m.
- In 1994, the Servei Geològic de Catalunya acquired reflection seismic profiles.

- In 2002, L'Institut Cartogràfic de Catalunya conducted new VES survey on the northwestern deltaic zone. New reflection and refraction profiles were also acquired.

All these above surveys were analyzed processed and interpreted in Teixidó (2000).

- FDEM surveys were carried out by Himi *et al.* (2000) and Arranz *et al.* (2004).

4.4.2. New geophysical surveys

During the project development several geophysical surveys have been carried out: 1) DC resistivity and TDEM surveys following the preexistent seimic profiles PS1 and PS4 2) AMT survey carried out in a 2D grid covering the western deltaic zone, where 2D and 3D models has been produced. In addition, seismic lines have been reprocessed.

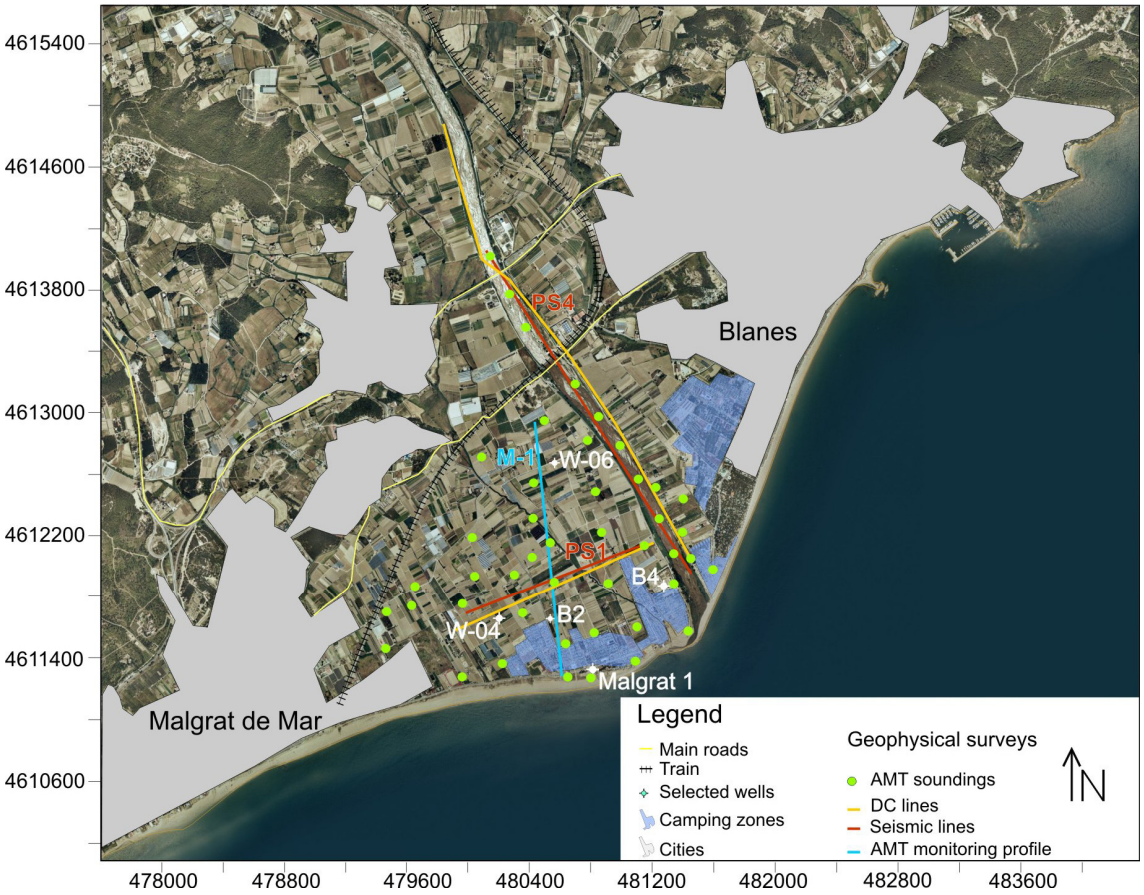

Figure 4.5: Study area situation map where geophysical surveys presented on the following sections are located. Also principal geographic features are drawn, that is, urban and camping zones, main roads and train line.

DC surface resistivity

During 2003-2005 three DC surveys were carried out by the Institutlo Geologico y Minero de España (IGME) within the project REN2002-04538-C02 (Marcuello and Plata, 2005). Data acquisition was planned on coincident locations with the seismic lines PS1 and PS4 and the 2D AMT models later presented (orange lines on Figure 4.5). DC resistivity equipment used was ABEM Terrameter SAS 4000, with 60 electrodes.

In winter 2003, two DC profiles were carried out along the river line following PS4 seismic profile (Figure 4.5). Due to maximum flow in the river, survey could not be completed. so that a gap of 300 m between two DC profiles reminded. After preliminary consideration of the results, another profile was acquired (December 2004) when river was dry to connect the earlier two profiles. As a result a unique profile of 3300 m was built with a Wenner's configuration, and electrode spacing of 15 m. Other arrays were tested with Schlumberger and dipole-dipole methods in order to notice different vertical and lateral responses (Marcuello and Plata, 2005). During the second phase survey, in December 2004, a profile of 1500 m length was acquired coincident with PS1 and another one along the beach on the eastern riverside in front of the saltwater treatment plant wells were carried out. Wenner configuration and 15 m electrode spacing was used similarly to the previous DC surveys (Marcuello and Plata, 2005).

AMT surveys

During spring 2004, the AMT survey was carried out over the deltaic zone, composed of 37 sites. Survey was planned on a 2D grid with a homogeneous spacing of 250 m, however, due to agricultural activities location was modified with availability. To complete the survey, another 10 soundings were acquired in summer of 2005, along the riverbed when the river was dry. Moreover, every four month, from spring 2004 to spring 2006, we have surveyed the same line for control and monitoring purposes with a total of 7 sites each time. Thus a total of 89 soundings, 47 on a grid and 42 on the monitoring line compose the AMT data set available over the Tordera deltaic zone.

Three different 2D models were obtained (see Figure 4.5 for specific location), two of them coinciding with PS1 and PS4 seismic lines and the third one is the time-lapse sea-water monitoring line along the main sea-water path (M-1). Finally an AMT 3D inverse model has been created (section 4.12).

'Stratagem EH4 system' equipment (Geometrics, 2000), has been used for AMT recording (92000 Hz to 10 Hz). Every survey receiver-transmitter distance tests settled optimal

distance from110 to 170 meters due to the low resistivity of the area. Electrode dipole length was at most 20 m, with an array orientation NS-EW, for convenience given that rotation could be performed a posteriori, if a preferential strike angle could be retrieved.

Seismic

Seismic profiles PS1 and PS4 (Teixidó, 2000) have been reprocessed to obtain seismic velocity models and to improve seismic reflection images (section 4.7-4.8). PS1 extends transversally across the western part of the delta ENE-WSW and PS4 follows the riverbed NNW-SSE (Figure 4.10). PS1 and PS4 meet at their eastern and southern most parts respectively. The total profile length was 1460 m for PS1 and 2400 m for PS4.

Seismic data was acquired using a 48-channel digital seismograph, 40-Hz geophones and 5 m shot and receiver spacing. A roll-along system enabled an end-shooting geometry along the profile. Some center spread shots were additionally carried out for refraction purposes. Low-energy explosives (pyrotechnic noisemakers) were employed as seismic source. The conversion of a time seismic section into a deep section has been carried out using stacking velocities.

TDEM

In December 2004 a TDEM survey was conducted by GEOGNOSIA S.L. The survey was along the profile PS1 of 1500 m length. TDEM profile is composed of 15 soundings spaced 100 m. PS4 soundings line was acquired in summer 2005 and is composed by 27 soundings. Equipment used was EM Zonge using ZT-30 transmitter that introduces continuous current (from 24 a 120 volts) alternating polarized cycles. The receiver, GDP-3Z^{II} multichannel, could work on the frequency domain or time-domain, and uses TEM-3 antenna. Two different configuration arrays were used in the survey, central loop and out of loop. In all the soundings has been used one single loop of 100 m x100 m, 256 cycles with 8 Hz emission frequency and intensity around 6 A. Models were obtained considering conservative parameters performing 1D smooth inversion (Marcuello and Plata, 2005).

4.5. Initial hydrogeophysical appraisal

The first step on the hydrogeophysical appraisal was to perform an accurate data analysis of all geophysical and hydrogeological data available, where partial and preliminary conclusions were extracted.

4.5.1 Reconstructing the hydrologic conceptual model

Complementary to the existing Tordera hydrological models (FCIHS, 2002; Guimerà *et al.*, 2003) we proposed a hydrogeological model following the hydrogeological conceptual aquifer units (Figure 4.6). The main objective of this model was to have a three-dimensional framework for location of hydrogeological and geophysical data and models, and thus to have a three-dimensional platform for validation and calibration of the geophysical results.

Summary of all good quality lithology records were analyzed together. Data quality of some of the well was doubtful so that it was decided to exclude them. Lithologic information compiled was classed under 11 different lithologies to unify all the records that came from different sources and times (Figure 4.6). This collecting effort made the joint interpretation easier to build up a consistent hydrogeological model based on hydrological conceptual model. *GOCAD* (Earth decisions) software was used for its capabilities of exact location and visualization of multiple different geo-information over the three-dimensional space (Figure 4.6).

Nonetheless is important to mention that the hydrogeological model carries remarkable uncertainties due to interpolation to build up the surfaces. Important lack of information has to be accounted for using those lithological based models due to; 1) well log records present variability on the quality given that these wells were drilled as a water supply wells and there are no cores , 2) well distribution is not homogeneously sparse, 3) in most of the cases well penetration depth is shallow, only the seawater treatment wells located on the shoreline reach more than 150 m. Theses wells do not attain the granite and it is suggested a high displacement fault roughly W-E, dipping southward and 4) no weathering granite thickness has been reported on any lithologic record.

Considering these uncertainties comparing hydrogeological and geophysical models, is possible to conclude that the hydrogeological model is too coarse to be compared with the geophysical models. Validation and calibration of the created geophysical models have to be done with collocated hydrogeological data (section 4.10).

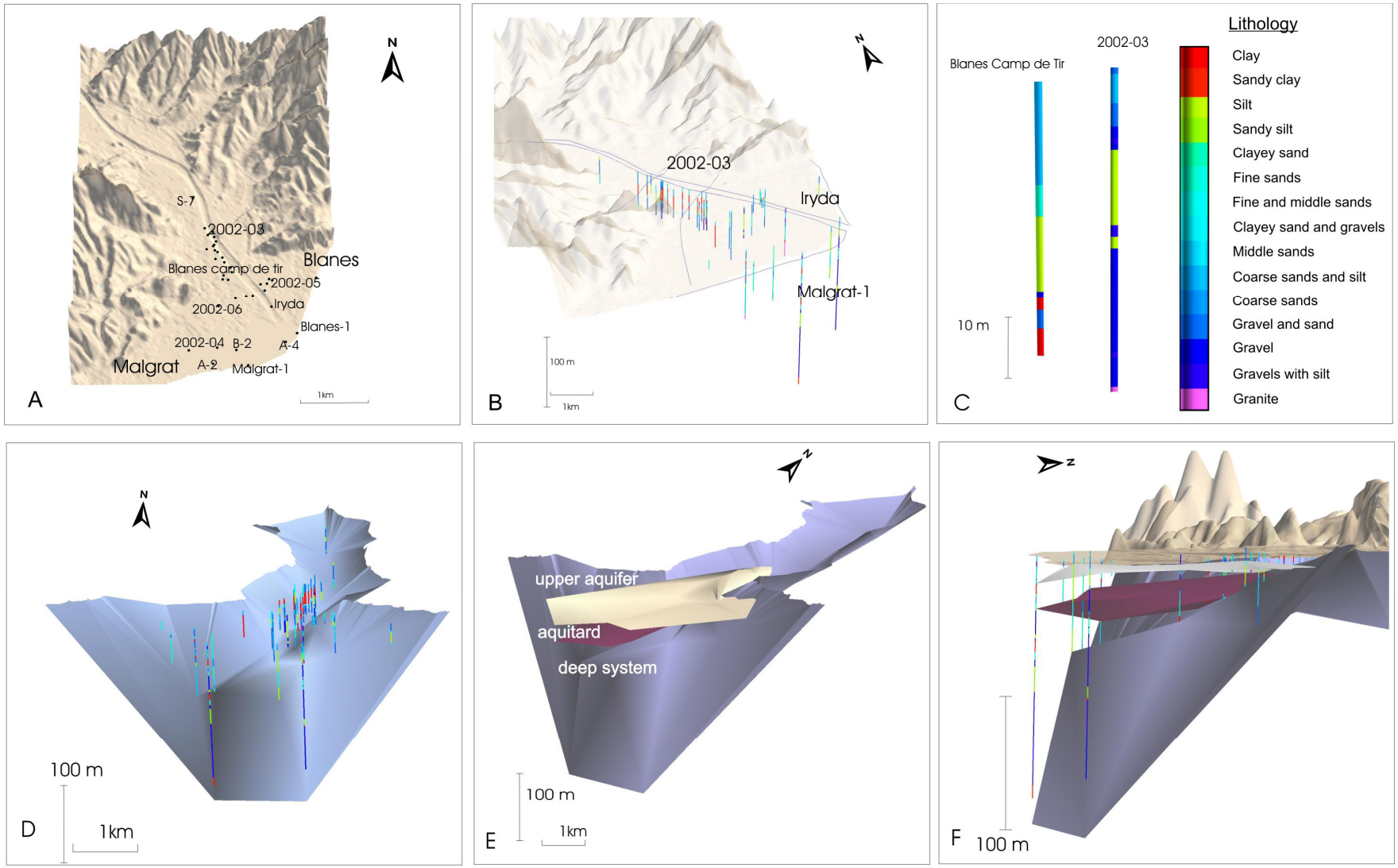

Figure 4.6: Sketch of the lithological data process to built the 3D hydrological model, vertical scale x10. A) Well location over the digital elevation model. B) 3D view of the lithology in depth. C) Lithological legend example. D) Basement granite surface. E) Aquifer units interpreted surfaces. F) Western view of the generated surfaces.

4.5.2. Hydrogeophysical interpretations

First geophysical data considered are earlier VES, the new DC profiles along the riverbed and first AMT survey. Vertical electrical sounding surveys (1994, 1995, 1996 and 2002) were analyzed and inverted to obtain resistivity on depth that together with the first two DC profiles along the river line, and first AMT survey data (37 soundings) over the western deltaic zone, were used as a starting point of the geophysical characterization of Tordera aquifer system. Main results were summarized in Falgàs *et al.*, 2005 included in the book 'Groundwater and Saline intrusion', Publicaciones del Instituto Geológico y Minero de España, Serie Hidrogeología y Aguas Subterráneas nº15.

Following are the conclusions by VES and DC resistivity surveys: Along the riverbed, seawater intrusion and its geoelectrical expression as a continuous intrusion front is restricted to 500 m from the shoreline. However, there are low resistive zones further inland around 80-100 m depth that might be related with saline water encroachment.

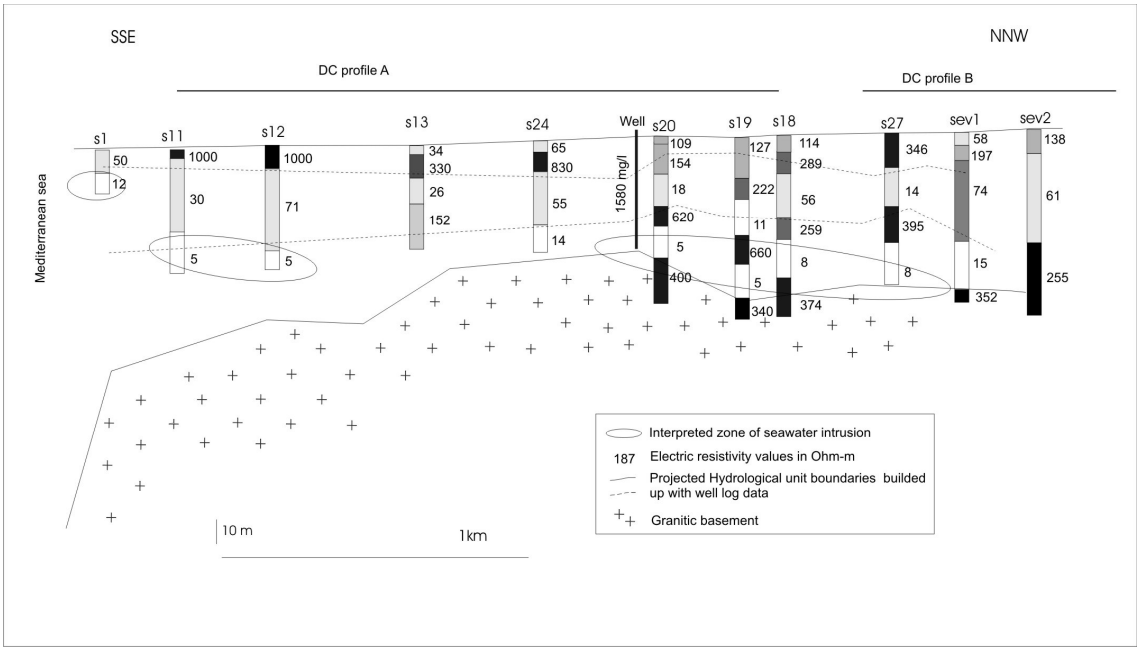

Figure 4.7: Geoelectrical cross-section along the river obtained from VES data. Dashed lines are the projection of the aquifer units model built up with lithologic data. Chlorine information is from ACA monitoring salinity net control (February, 2003).

Figure 4.7, shows that 1D VES models along the river intersected with the hydrological unit surfaces of the *GOCAD* model. In general, it could be said that *GOCAD* aquifer units are a

coarse approach to the true heterogeneity and thus to the electrical resistivity values. Ellipses remark zones with low resistive values that may be related with the seawater encroachment given that sandy sediments are reported.

In addition, according to deltaic AMT raw data (frequency pseudosections), the existence of a low resistive zone on the western deltaic zone was envisaged. This low resistive zone was associated with a main seawater path induced by a paleochannel oblique to the actual riverbed, allowing the lateral presence of saline water inland (Figure 4.8).

Since depth of penetration in VES was limited providing punctual information and DC profile did not attain the required depth, seismic and AMT jointly with hydrogeological data played a key role in this research project. Additionally, DC and TDEM profiles were carried out on coincident locations following the previous seismic and AMT lines.

4.6. Seismic profiles (PS1 and PS4)

PS1 and PS4 seismic profiles were carried out during 2000 (Teixidó, 2000). PS1 extends transversally across the western part of the delta ENE-WSW direction and PS4 follows the riverbed in NNW-SSE (Figure 4.5, Figure 4.10). Seismic velocity models and improved seismic reflection images has been obtained after data reprocessing (Benjumea *et al*., 2006). The total profile length was 2400 m for PS4 (Figure 4.13) and 1460 m for PS1 (Figure 4.14). Since profile PS1 was acquired in two different phases without overlapping, lack of information can be seen at the cross between both phases due to surface-wave muting (Figure 4.14). On the other hand PS4 present bad reflection quality on its northern zone, and has not been considered (Figure 4.13). However, first arrivals traveltimes can be identified to obtain the velocity tomography model.

4.6.1. Seismic refraction tomography

First arrival travel times have been identified for the total of 302 and 239 shot gathers along PS1 and PS4, respectively (Benjumea *et al*., 2006). The database created for travel time data and geometry (position of sources and receivers for each trace) are processed to obtain an initial velocity model through the Delta t-V method (Gebrande and Miller, 1985) included in Rayfract package. This model is the initial input for the tomographic inversion using Wavepath

Eikonal Traveltime WET algorithm (Schuster and Quintus-Bosz, 1999), to obtain a velocity model. Figure 4.13 (b) and Figure 4.14 (b), shows the result for profile PS-1 and PS-4.

Tomographic models show an irregular maximum depth due to the acquisition mode. However, general trends can be extracted. Near-surface sediments (up to 10 m) are characterized by velocities between 500 to 1450 m/s. Below, a zone with velocities varying between 1450 and 1750 m/s is characterized by a variable thickness along the profile up to 60 m. At depth high-velocity zones (>3000 m/s) are observed. Low velocity values (<1450 m/s) can be interpreted as dry or not fully saturated sediments. Thus, we can define the water table as the transition zone between 1450 m/s to 1500 m/s. Materials with velocities ranging from 1450 m/s and 1750 m/s can be considered as water-saturated unconsolidated sediments. In depths, high-velocity values indicate an increase in compactness associated with consolidated materials and basement.

4.6.2. Seismic reflection processing

Seismic reflection data processing has been carried out with Promax software. Data processing for these near-surface high resolution reflection profiles has been done following standard procedures: amplitude scaling, band-pass filtering, CMP sorting, velocity analysis, and stacking (Benjumea *et al.* 2006).

Seismic reflection data shows good quality in the sectors with a near-surface water-table or surface fine material. However, strong amplitude coherent noise interferes with the reflection signals (guided waves) in areas where the water table contact is located at depths greater than 5 m, or coarser grain materials are present near-surface. In order to attenuate guided waves linear-moveout has been applied that yields data with nearly horizontal guided waves. In this way, they can be discriminated from reflection amplitudes on the FK domain. After removing coherent noise with an FK filter, inverse Fourier transform is applied and linear-moveout terms are removed on the time domain. Time to depth conversion has been carried out using stacking velocities hence depth uncertainty is expected to increase with depth. This depth must be considered as approximate. Figure 4.13 and Figure 4.14 shows the result for profile PS-1 and PS-4. Main reflectors and changes on reflectivity behavior have been used as structural indicators in the joint interpretation of AMT-resistivity models with seismic features.

4.7. AMT data analysis

AMT data analysis comprises four main steps: time series processing, removing noise effects on the sounding curves, frequency pseudosection evaluation, and geoelectrical dimensionality assessment. These analysis moves from the full time series record to the final data to be used on the multidimensional inversion and interpretation. Given that this is the first application chapter the step by step data analysis process will be exposed. Similar process has been performed on the next chapters mentioning only main differences (chapter 5 and 6).

4.7.1. Data quality analysis and frequency pseudosections

Cultural noise is an important problem while working near populated areas. Tordera deltaic zone is an agricultural area, nearby two main populated villages that are linked by a DC train. Therefore, in spite of using controlled EM source, cultural noise is still present. Good data quality has been obtained over the deltaic zone, only three of the 89 AMT soundings, have been rejected due to noise expression on the records.

Firstly, time-series have been analyzed using Imagem software (Geometrics, 2000) where specific time windows affected with electromagnetic noise can be erased. Thereafter the impedance is recomputed to obtain the new frequency apparent resistivity and phase curves. This is followed by data analysis of sounding curves of apparent resistivity and evaluation of phase angle. Data points affected by cultural noise has to be removed, however data gaps could be created due to affected sequential frequencies. Apart from few cases, where the sounding is too much affected by cultural noise, AMT frequency data in surplus present enough information to retrieve the main geoelectrical targets after time series and sounding curve analyses.

Frequency pseudosections analysis has been performed using the apparent resistivity ρ_a from the impedance tensor determinant for different frequencies (Figure 4.8). This parameter has several properties that make it suitable for preliminary interpretation when dealing with 3D environments (Vozoff, 1972; Ledo, 2006).

Pseudosection interpretations

Figure 4.8 shows the apparent resistivity pseudosection for selected frequencies used for all survey sites. Higher frequencies show shallow structure response whereas lower frequencies correspond to deeper zones (skin depth phenomenon, see chapter 3). It is possible to extract

valuable information from the extremely low resistivity targets that can be associated with seawater content. In the higher frequencies, pseudosections reveal that seawater intrusion is restricted to the shoreline and along the riverbed in the upper aquifer system unit. In contrast, in the lower frequencies, deeper in the aquifer system, a low resistivity tongue is observed on the western deltaic area above a high resistivity feature. This decrease in resistivity coincides with the location and depth of one of a main ancient deltaic paleochannel (described above) working as a preferential seawater path. The deepest high resistivity region reflects the granite basement.

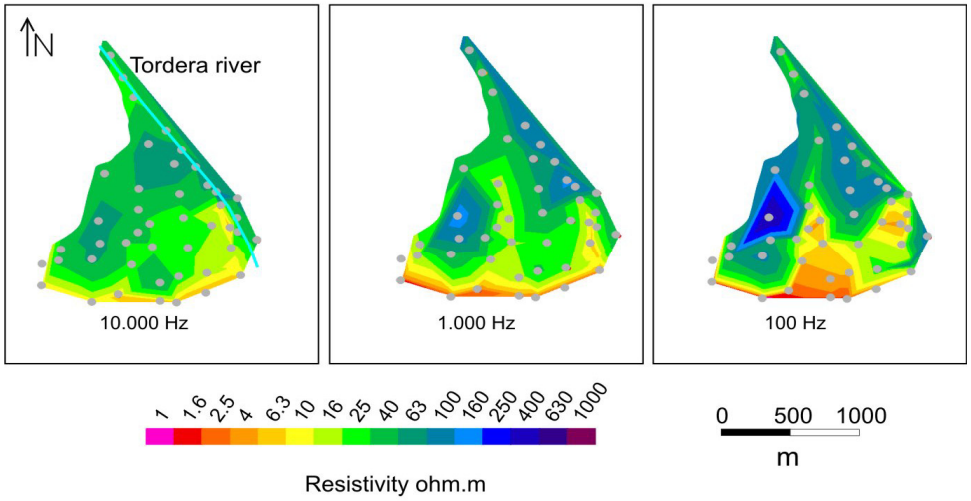

Figure 4.8: 2D grids of apparent resistivity (ρ_a) from the impedance tensor determinant for selected frequencies using all AMT Tordera sites.

4.7.2. Dimensionality

Impedance tensor dimensionality has been determined using WAL invariants (Weaver *et al.*, 2000) following the scheme proposed by Martí *et al.* (2006) using the WALDIM application. Threshold value considered is 0.15, however 0.1-0.2 proposed as extreme values has been also tested revealing similar results. Results of the analysis show that AMT data presents mainly 3D behavior, already imaged through the frequency pseudosection.

Figure 4.9 presents four plots showing the dimensionality classed by decades where arrows represent the assessed strike direction. Arrow size is inversely proportional to the error on the determination of the strike, that is the bigger the arrow the more reliability on the strike appraisal. In spite of the main three-dimensional geoelectrical behavior, there are some sites where a 2D behavior could be estimated. Strike direction retrieved is NE-SW, nonetheless 2D

strike angle cannot be used giving that no general trend on all sites all frequencies could be inferred.

3D AMT data has to be modeled and inverted accordingly to its dimensionality in order not to induce artifacts on the 2D profiles due to finite lateral bodies. Nevertheless, 2D profiles are much easier to visualize and more easy to compare with the other geophysical techniques that produce 2D images, and therefore are still needed. 3D inversion codes are in their infancy and to built 3D forward trial and error fitting models is time-consuming. These reasons motivated the implementation of the determinant of the impedance tensor to create preliminary 2D models to work with the seismic and DC resistivity lines.

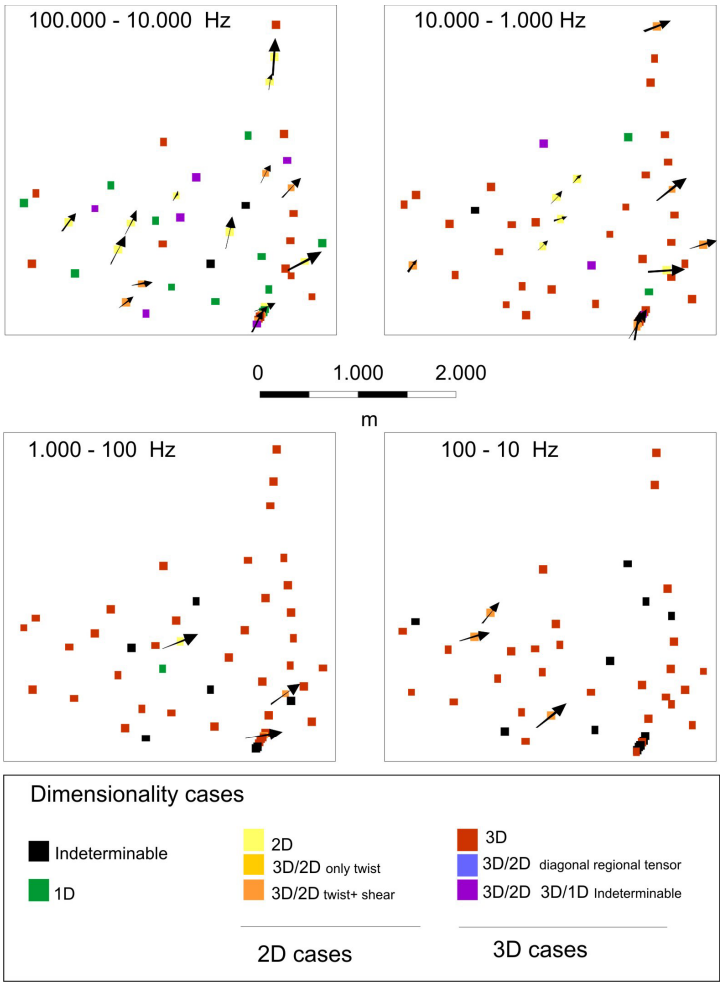

Figure 4.9: Dimensionality result of the Tordera AMT dataset grouped in 4 period bands. The arrows indicating the strike direction are scaled by the inverse of the error in the determination of the strike.

The 2D inversion of the impedance tensor determinant makes a reasonably good approximation to 3D structures in many cases (Pedersen and Engels, 2005; Ledo, 2006). Therefore before starting with the 3D inverse model creation, three different models have been created using the determinant model as first approach (Figure 4.10). Models thus obtained provide a more regional structure owing to the nature of the determinant inversion. Further considerations could be found on Chapter 3 and 4.8.1 section.

4.8. AMT-seismic models

In this section, are presented PS1 and PS4 2D AMT models collocated with the seismic lines to work on ensemble. AMT inversion process and sensitivity tests are firstly presented, where the seismic velocity tomography model and reflection profiles have an important role. And afterwards, AMT models, seismic reflection and velocity tomography are analyzed and used jointly for hydrogeologic interpretation.

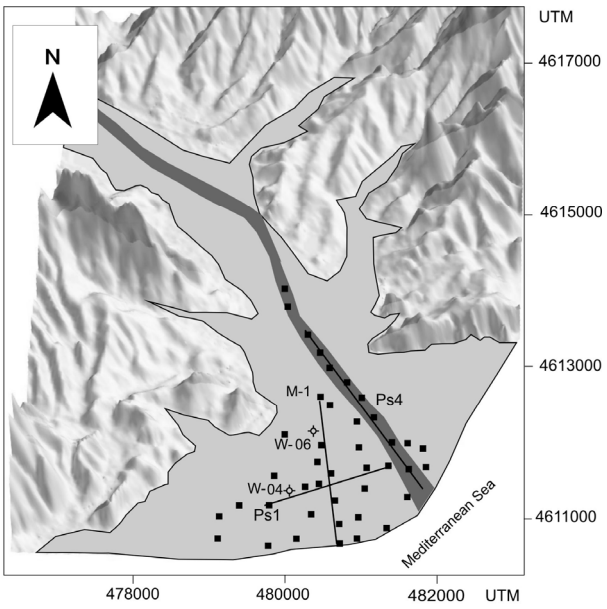

Figure 4.10: Schematic map showing the AMT survey over the deltaic zone, PS1 and PS4 seismic DC resistivity and AMT models, M-1 AMT model, and locations of W-04 and W-06.

4.8.1 Inverse modeling

Electrical resistivity models have been created using the inversion algorithm proposed by Siripunvaraporn and Egbert (2000) (REBOCC) and modified by Pedersen and Engels (2005) (DetREBOCC) to use the impedance tensor determinant components (Figure 4. 11, Figure 4.16). The determinant of the impedance tensor provides a good compromise that allows for a good data fit while at the same time resolving high and low resistivity structures reasonably well along the profile. The determinant mode has been successfully tested in several studies (Pedersen *et al.*, 2005; Pedersen and Engels, 2005; Linde and Pedersen, 2004 a/b).

In the inversion process, we used a 100 Ω.m half space initial model with an error floor of 5% for resistivity and phases. Owing to the nature of the inversion determinant mode, models may provide the regional geoelectrical targets ruling out finite lateral structure reducing 3D artifacts. The RMS[(3)] as a primer quality indicator obtained for all the 2D models are between 3 and 5 that indicates a relatively good data fit. However after the total acceptance of the released inverse models, sensitivity test of the main geoelectrical structures has to bee done.

4.8.2. 2D Model sensitivity tests

Model sensitivity of certain geoelectrical structures has been realized to ensure their presence on the inverse models (Figure 4.12). Sensitivity tests increase the reliability of the models and also increase their accuracy given that inverse models are modified for a better model-data fit as a trial and error process, computing the forward model with Wannamaker *et al.* (1987) algorithm.

Model sensitivity for the boundary between highly resistive basement and the low resistivity structure associated with seawater intruded areas has been done, giving that the extensive deep low resistive structures on depth would seem to image basement deeper (see section 4.9.1 for further details).

[(3)] Total RMS is computed for M sites and N frequencies following the expression $RMS = \frac{1}{MN}\sqrt{\sum_{i=1}^{N}\sum_{f=1}^{M}\left(\frac{x_{meas} - x_{model}}{\delta}\right)^2}$, where δ is the error of the measured variable (x_{meas})

In addition, given that seismic data provides basement information the electrical resistive basement has been adapted according to the seismic one accepting the change when getting a better data fit. Nonetheless, seismic and AMT basement position do not match perfectly and differ in some zones a few tens of meters away.

Mediterranean Sea influence on AMT data and models has also to be tested in order to avoid lateral effects on the models. PS4 profile incorporates the sea on the SE end of the profile. No significant changes on the data-model fit are recognized, even on those sites closer to the coast. This can be explained by the high frequency range used and the low electrical resistivity of near surface structures, being all the sites located more than 1-2 skin-depth distance from the shoreline and not affected by the presence of the coast. Figure 4.12, shows the comparison between data and final model responses for both profiles after the sensitivity test.

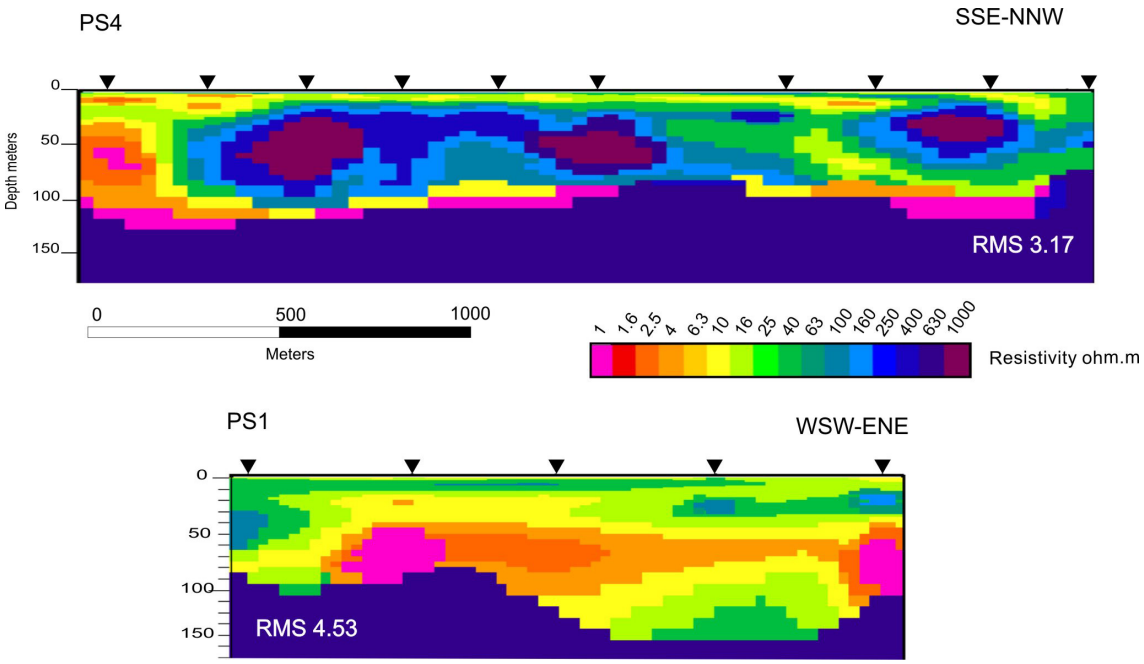

Figure 4. 11: 2D resistivity models obtained from the inversion of the impedance tensor determinant. Top PS4 and bottom PS1 AMT models.

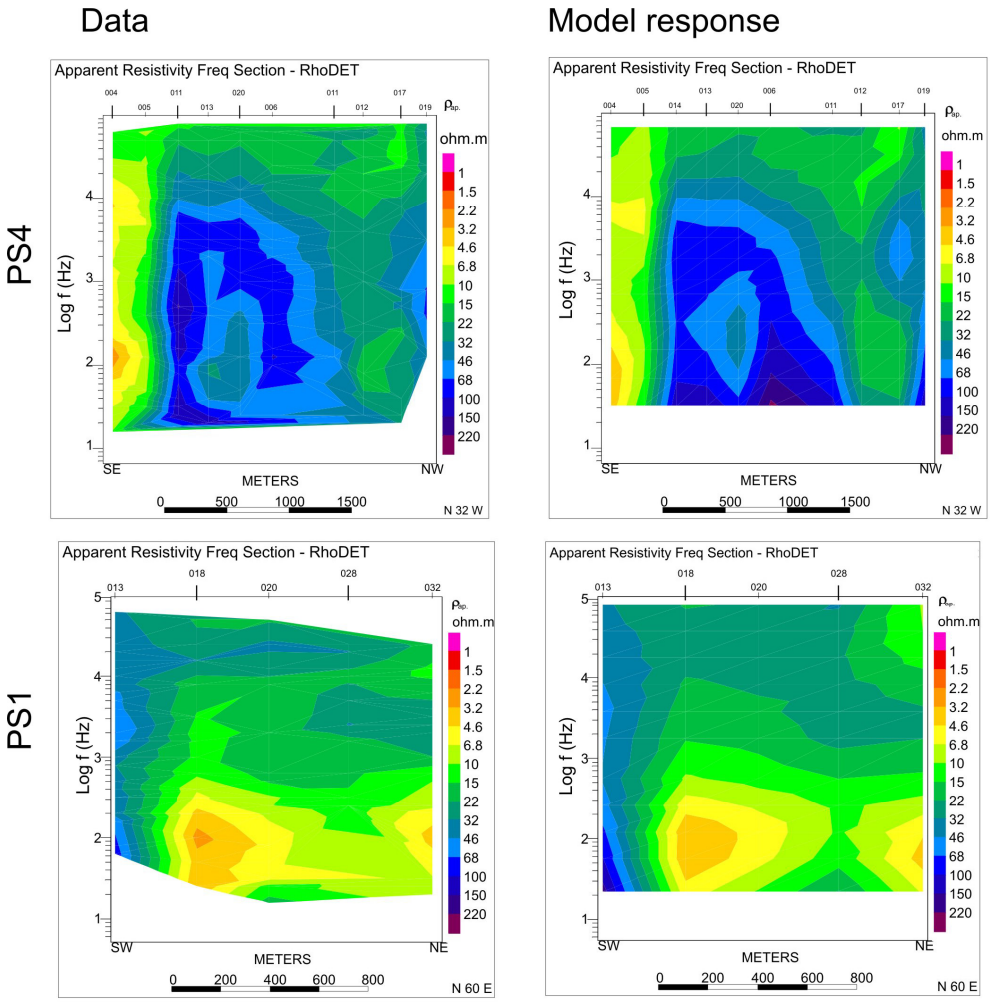

Figure 4.12: Comparison of AMT data pseudo-section (left) and AMT final model responses (right) for PS1 and PS4 lines.

4.8.2. Interpretation

Figure 4.12 presents the goodness of the created models (data and response of the model), whereas Figure 4.13 and Figure 4.14 present PS4 and PS1 final 2D AMT models. Its perpendicular orientation allows getting a three-dimensional idea of the heterogeneity of the system. Two main zones can be assessed: 1) a deep zone with almost homogeneous resistivity >600 ohm·m from 80 to 150 m depth, that represents the basement, and 2) an upper part with a highly variable resistivity area, ranging from 1 to 1000 ohm·m due to its hydrofacies and seawater content, that represents the aquifer system. On the other hand, AMT model gives the evidence that hydrological model created using the well interpretation (Figure 4.6) does not reproduce the true heterogeneity of the system.

Basement

Highly resistive fresh granite basement was slightly modeled on the preliminary AMT models due to the low resistivity of the entire area (Figure 4.12 data). Therefore, reflection and refraction seismic data has been a useful tool to determine the position of the fresh granite basement on the geoelectrical profiles, as has been exposed on the above AMT sensitivity test section.

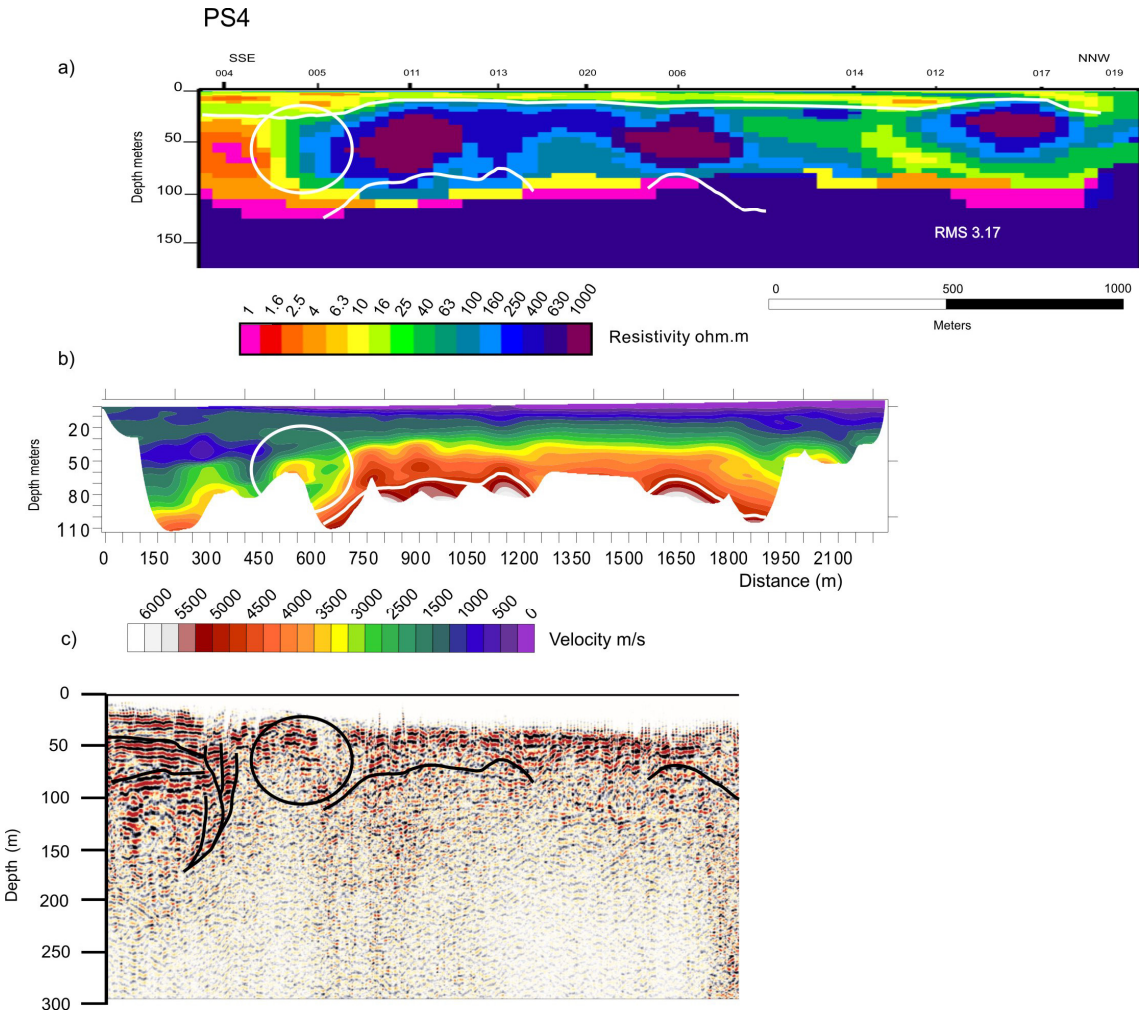

Figure 4.13: PS-4 AMT model (a) seismic refraction model (b) and seismic reflection profile (c). Lines denote the main discussed features, basement, deep aquifer, and near surface aquifer-aquitard system.

Basement definition in the PS4 model has been done with the reflection and refraction models (Figure 4.13). Near the shoreline, reflection data exhibits a very high signal-to noise ratio locating the basement up to 150 m deep. The lateral boundary of this thick sequence of coherent and continuous reflections may indicate the presence of a main faulting zone (Figure 4.13c). From 400 to 650 m, reflection data show a deterioration of the coherency signal with

depth (white circle on Figure 4.13c). The velocity model (Figure 4.13b) shows a thick sequence of low velocity materials not reaching the basement in this section. Taking into account refraction tendencies, AMT basement model is located around 100 m deep (Figure 4.13a). Further discussion about this specific spot is done in the aquifer system section related to the lateral resistivity sharp transition. And finally, from 650 m onwards (NNW of the profile), basement depth from tomography velocity model has been imposed. Considering high velocities around 4500 m/s, the basement can be delineated around 80 m depth; however the AMT basement is located at deeper depths.

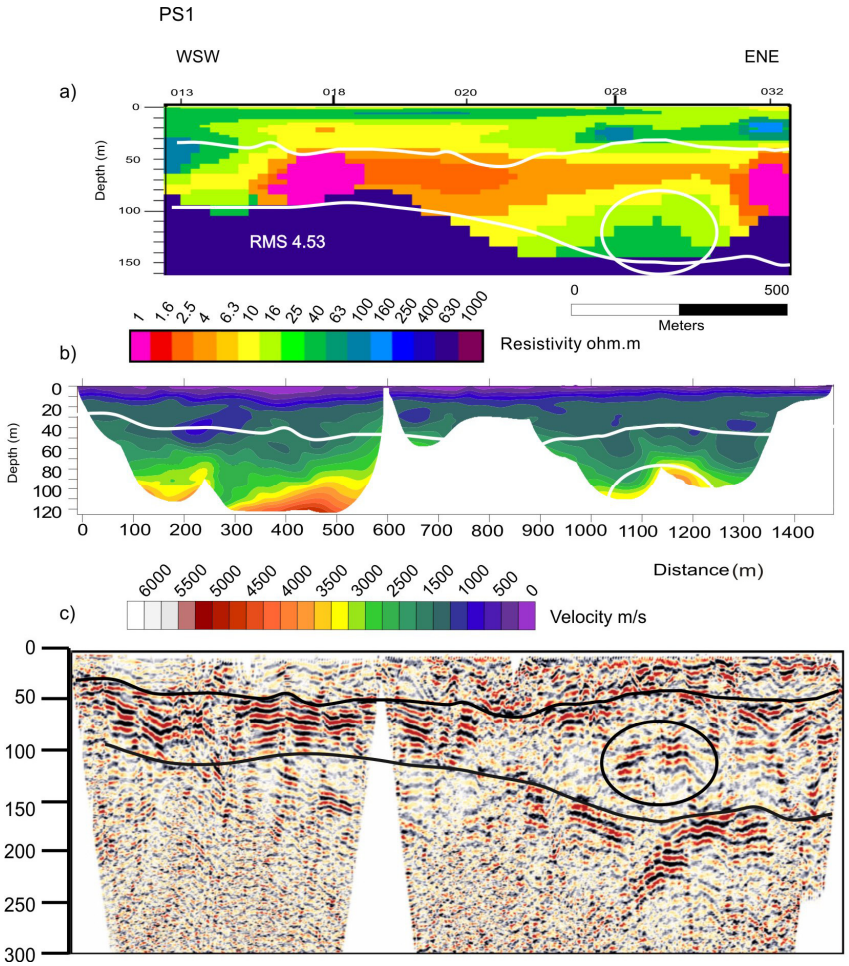

Figure 4.14: PS-1 AMT model (a) seismic refraction model (b) and seismic reflection profile (c). Lines denote the main discussed features, basement, deep aquifer, and near surface aquifer-aquitard system. The same scale of Figure 4.13 has been used for a better comparison.

The basement along PS1 has been recognized throughout the reflection model. It can be depicted along the profile as a gentle slope that dips from 100 m on the WSW to 150 m on the ESE (Figure 4.14c). Due to the seismic array geometry and thick deposits of low velocity material, the velocity tomography model cannot reach the high velocity materials associated

with the fresh granite basement. However, a high velocity gradient is seen on the western zone (Figure 4.14 b).

Basement reported from geophysical methods is located deeper than the position described by the water supply wells, therefore a thick weathered zone may exist yielding fresh granite basement in a deeper position. Its morphology gives an indication of gentle slopes that might be produced by fault activity and weathering evolution.

Aquifer system

Looking into the aquifer system, PS4 AMT model shows an upper zone up to 30 m of thickness (Figure 4.13 a) marked by the upper white line. This area includes the free upper aquifer and the aquitard where the resistivity varies from 10 to 40 ohm·m. Low to medium velocities are present in this area providing control on the transition from unsaturated to saturated materials. Below, a wide high resistivity target from 100 to 1000 ohm·m is imaged north of site-005 that might correspond to the deep semiconfined aquifer composed of medium to coarse gravels containing fresh water. A dramatic resistivity change is observed between sites 005 and 004 from a high to low resistive area. The seismic velocity model also imaged a lateral change in this zone, increasing the thickness of the low velocity material. In addition, the reflection profile presents an incoherent and non-continuous reflection character at depth, which may be misinterpreted as the basement depth. All these indicators may be the result of main hydrofacies change from more sandy seawater bearing sediments to clay dominated sediments, confining the seawater wedge in this direction. Another low resistive zone (<4 ohm·m) appears almost continuously above the basement. It disappears when basement is high enough to exercise a structural limit. This low resistive target appears again below site 17, that can be understood as a lateral brackish water flow, observed previously on the apparent resistivity pseudo-section (Figure 4.8). Those zones have been modeled on the sensitivity test analysis as a result of electric-seismic basement location.

The PS1 model meets PS4 in its southern part. Its main feature could be seen as the lateral extension of PS4, nevertheless, specific features have been assessed. As in the previous model, an upper zone where the resistivity range going from 10 to 40 ohm·m is observed belonging to the aquifer and aquitard units. This zone coincides with a chaotic and low amplitude reflection zone up to 50 m depth on the reflection profile (Figure 4.14). Below, a low resistivity zone in the entire deep semiconfined aquifer is imaged, related to seawater bearing sediments. The main lowest resistivity target is located between sites 15 and 20 on the WSW zone of the profile, where high-amplitude reflections are observed. Thus, estimated resistivity,

relatively low velocity values in the seismic tomography model, and reflection characteristics indicate that the main seawater intrusion path is associated with the paleochannel position. Around 100 m depth at a distance of 1200 m estwards, a high amplitude reflection area hummocky and discontinuous zone is observed. This zone correlates with a high velocity anomaly (black circle) that might correspond to a different lithology or more compact materials. With respect to the AMT model, higher resistivity values are observed in this zone than in the seawater influenced area, therefore suggesting the hydrofacies change hypothesis.

4. 9. Electrical monitoring of seawater wedge dynamics

Previous hydrogeological and geophysical information presented have provided a static image of the seawater intrusion state over the aquifer system, suggesting a seawater intrusion affection on the western delta related with a an ancient paleochannel (Teixidó, 2000; Falgàs *et al.*, 2005). The present AMT monitoring experience aimed to observe the seawater fresh-water interface dynamics along this preferential seawater path.

In the next section, sensitivity and expected resolution of the AMT synthetic models, and the field monitoring experiment with the models' sequence have been studied. The monitoring profile, 1753 m length composed of 7 AMT soundings that have been surveyed every four month, from April 2004 to May 2006.

4.9.1. Forward and Synthetic models

Effective electrical resistivity is mainly controlled by the pore fluid content in high saline electrolytes (Purvance and Andricevic, 2000). Therefore electrical resistivity time-variation values can be associated to seawater variation conditions. To test AMT as a sensitive method to monitor changes in fluid electrical resistivity we created several synthetic models comparables to the seawater wedge dynamic seasonal movement (Figure 4.15). Models were inspired on the aquifer geometry and hydrogeophysical-geoelectrical facies in three different situations A, B and C. Models represent dynamic seawater geoelectrical changes from 'A' far-reaching seawater influence to 'C' a restricted seawater wedge situation, and 'B' a middle situation between A and C. Site location of the created model are the same as location of August 2005 (M-5) monitoring profile to regard the influence on the irregular distance among sites.

Models A, B and C, from shallow to deep areas are composed of a low resistive layer (16 ohm·m) of 10 m thick, over a 100 ohm·m layer of 40 m thickness. Below, there is the seawater intruded region of the aquifer system where A, B and C models differ on resistivity distribution enhancing different seawater contents of the seawater–freshwater transition zone from 1 ohm·m (pink), 4 ohm·m (orange) and 10 ohm·m (yellow) to 100 ohm·m on the freshwater domain. A horizontal sharp transition with a high resistive zone indicating the basemen is located at 100 m depth.

Inverse models from synthetic data allow determining which electrical changes could be detectable. TE and TM forward response of the created seawater intrusion models are computed with the algorithm of Wannamaker *et al.* (1987). The synthetic data obtained are used to perform the TE and TM inversion numerical process. RLM2DI (Rodi and Mackie, 2001) code was used with a starting model a 100 ohm·m halfsapce and 5% of error floor.

Inversion models (Figure 4.15 below) provide valuable information about geoelectrical and structural morphologies, reliability on the retrieved targets, and how to perform correct interpretation of the models on that situation. Relatively good accuracy has been found on the following targets:

- A, B, C inverse models evidence that three different situations of the seawater encroachment. Low resistive region penetrates further inland in model A than model B and model C where it is more restricted.

- The upper part of the aquifer system (up to 50 m) is well resolved on shape, depth and resistivity value, that is the uppermost relative low resistive layer and the lower homogeneous high resistive layer. In general, the high resistive target is well imaged, however, the modeled value of 100 ohm·m appears a little more resistive to 160 ohm·m and some points of 250 ohm·m.

- The upper boundary of the seawater intruded region is well constrained and located at 50 m depth.

However, more interpretative features have been regarded on the following geoelectrical targets. These interesting features contribute notably to the understanding of AMT resolution:

- A gradual increase in resistivity is observed in basement rather than a sharp horizontal transition. Around 100 m deep (where the basement of the synthetic model is located), the low resistive areas tends to rise up its value. However, the lower the resistive value of the seawater encroachment layer, the lower the resistivity gradient. Therefore, due to the differential resistivity gradient, basement morphology is not regarded as a horizontal layer.

- Soundings distance is also a limiting factor where extensive low resistive areas are present. According to the inversion models it can be concluded that sounding 2 and 3 are located much far apart (400 m). The expected unique smooth lateral low resistive target is retrieved as the two isolated low resistive spots due to the lack of data coverage in between.

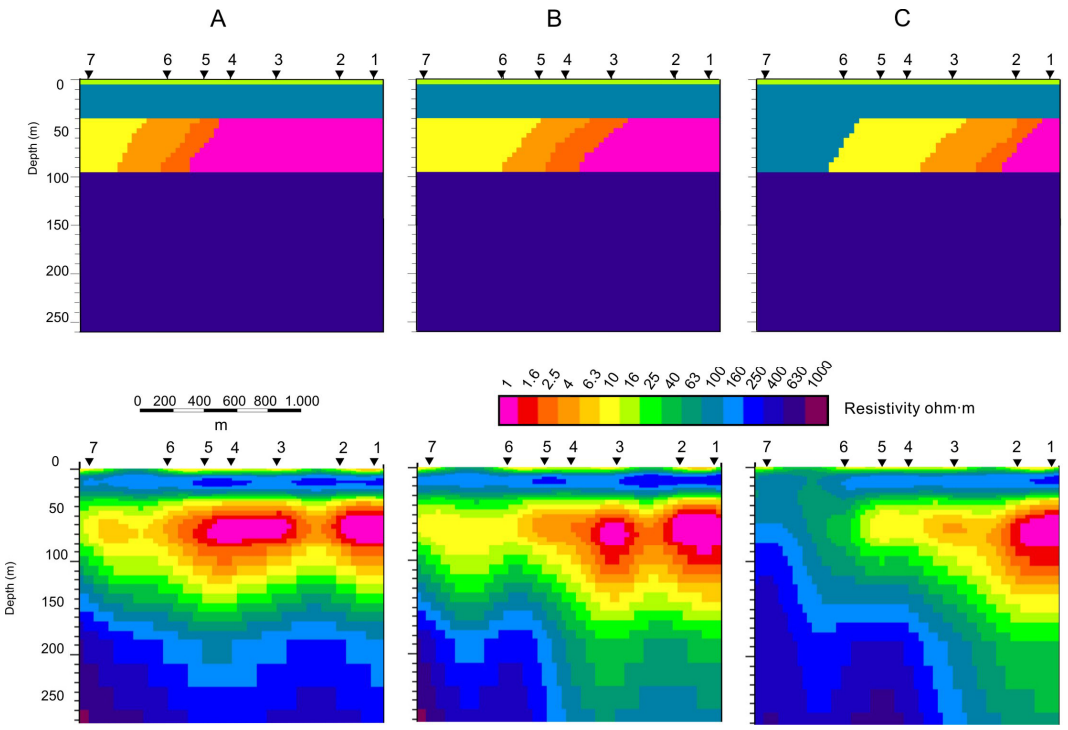

Figure 4.15: Seawater intrusion models simulating three different seawater encroachment cases. Above, A B and C created models and below the inverse models from the synthetic data.

Electrical resistivity time variation values are expected due to seawater variation conditions and therefore AMT method will be sensitive enough to reflect important changes in the electrical resistivity as a result of groundwater salinity changes.

4.9.2. Field experiment

The AMT monitoring experiment was conducted on the western Tordera deltaic zone from 2004 until 2006 to image the seawater-freshwater interface dynamics. Seawater-freshwater transition zone has been evidenced on the deep aquifer with the hydrochemistry and well log data from well Malgrat-1 and multi-tube piezometers W-04 and W-06. The interface distribution along the profile in the deep aquifer moves from the totally seawater content on Malgrat-1 (close to shore line) towards 75 % of seawater present on the W-04, 500 m from the shore line, to the 8% seawater content on the W-06, roughly 1200 m from the shoreline (Figure 4.5). The monitoring experience would like to image this transition zone and if possible to record its seasonal changes.

After preliminary analysis and interpretation of the apparent resistivity pseudosections (Figure 4.8) the monitoring line was delineated with seven soundings along the main seawater path (evidenced as the low resistive area on the frequency pseudosections). Every four month during 2 years the same profile has been recorded obtaining a total of 7 images along time. Location of the 7 sites is not exactly the same due agricultural works. Site deviations were the minimum possible from 50 m to 100 m at most. However, owing to the retrieved targets derived from the AMT determinant models this appraisal is considered valid for evaluating time-lapse model sequence. Taking into account sensitivity and accuracy resolution considered on the above synthetic proves, AMT models could be fully understood. In addition, considerations among evolution of geoelectrical tendencies, precipitations and head levels have been derived.

Models have been inverted using DetREBOCC code using the algorithm of Siripunvaraporn and Egbert (2000) and following the modifications and scheme proposed by Pedersen and Engels (2005). All monitoring models have been obtained using the same initial model to emphasize the variations only due to seawater content, considering a 5% error floor on the impedance component (10% on the apparent resistivity and 2.8º on the phases). Models RMS ranges from 3.3 to 4.8 showing a coherent and good data fit.

Interpretation

Figure 4.16 presents the seawater monitoring models. Most important geoelectrical target relay on the seawater bearing aquifer zone that present relative changes from one model to the other. In general, as described by PS1 and PS4 AMT models, an upper part up to 30-50 m is observed that presents a wide range of values composed of the upper aquifer and the aquitard. Below, it is seen a lower resistivity layer related to the seawater encroachment influence. And on the deepest position, it is regarded the relative high resistive zone representing the basement that has been adjusted to get a better data fit, as considered with the synthetic data inverse models.

The analysis of the 2D model sequence reveals tendencies of the seawater wedge associated with the deep low resistivity layer, in particular on their northern part. From M-1 model (4/2004- first survey) to M-2 (08/2004), seawater influence seems to retreat seawards. However, from M-3 (12/2004) to M-4 (04/2005) the conductive layer shows a progression towards inland. M-5 model (08/2005), achieve the maximum distance of seawater influence towards inland, and again M-6 and M-7 show a seawater regression (12/2005 and 05/2006 respectively).

Apart from the seawater influence movement, it is possible to discriminate the intruded upper aquifer from the seawater intruded deep aquifer on the southernmost areas of the model. Most of the profiles could be assessed for two different low resistivity structures as in the case of M-1 and M-2 models, whereas M-3 could not be differentiated due to noise effects.

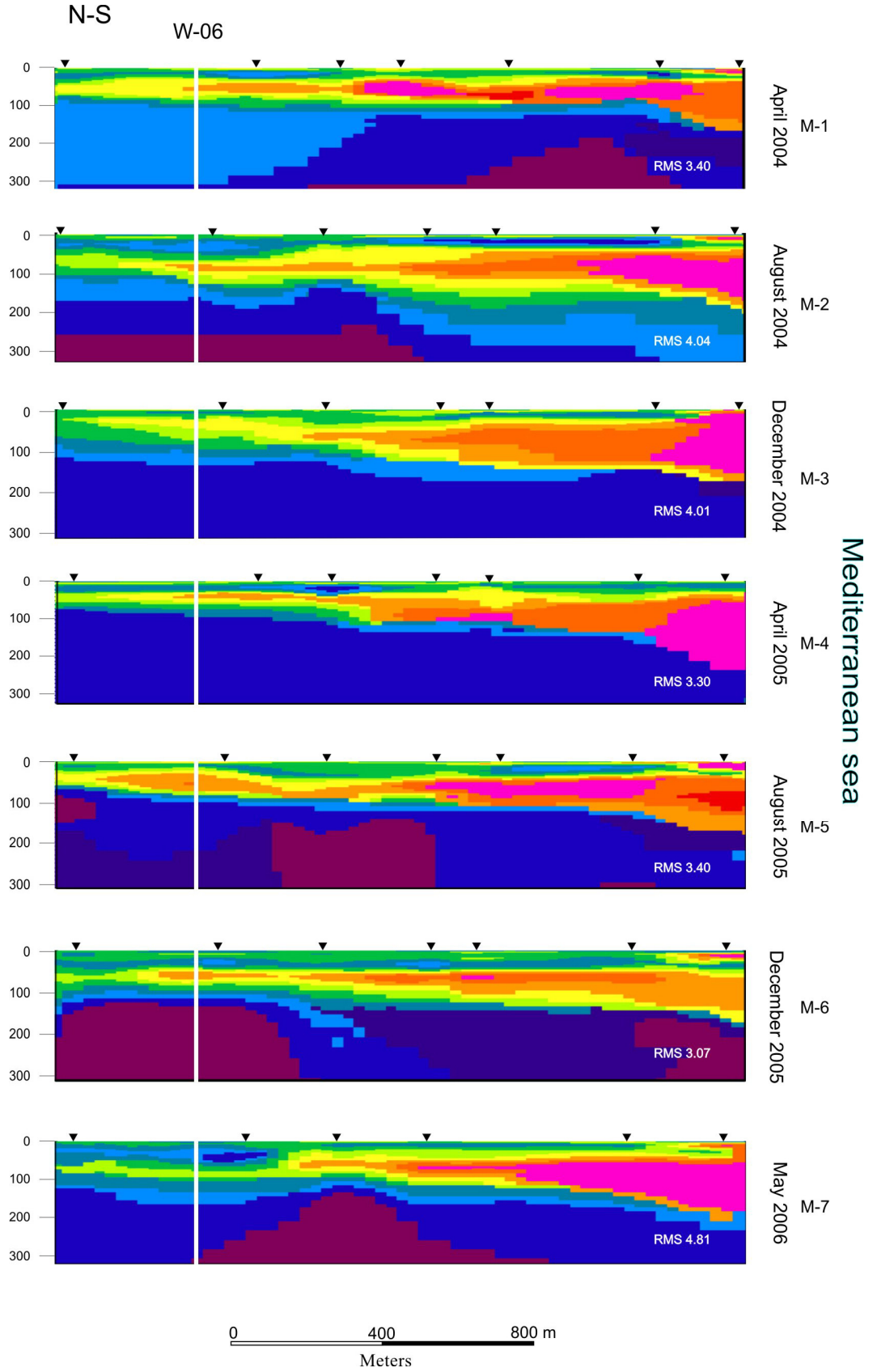

Figure 4.16: AMT monitoring sequence models from M-1 to M-7, resistivity values are same than Figure 4.15. White line corresponds to W-06 well, calibration among M-1 model and hydrochemistry analysis of W-06 is performed on following section 4.12. Resistivity colour scale is the same as Figure 4.15.

Electric, rainfall and piezometric level evolution

Computing precise and rigorous water balance is extreme difficulty. However, relation among hydraulic head levels, precipitations, and the AMT models are evaluated. Without accounting exact quantitative extraction, it has been observed that head level values shown a clear influence by precipitation.

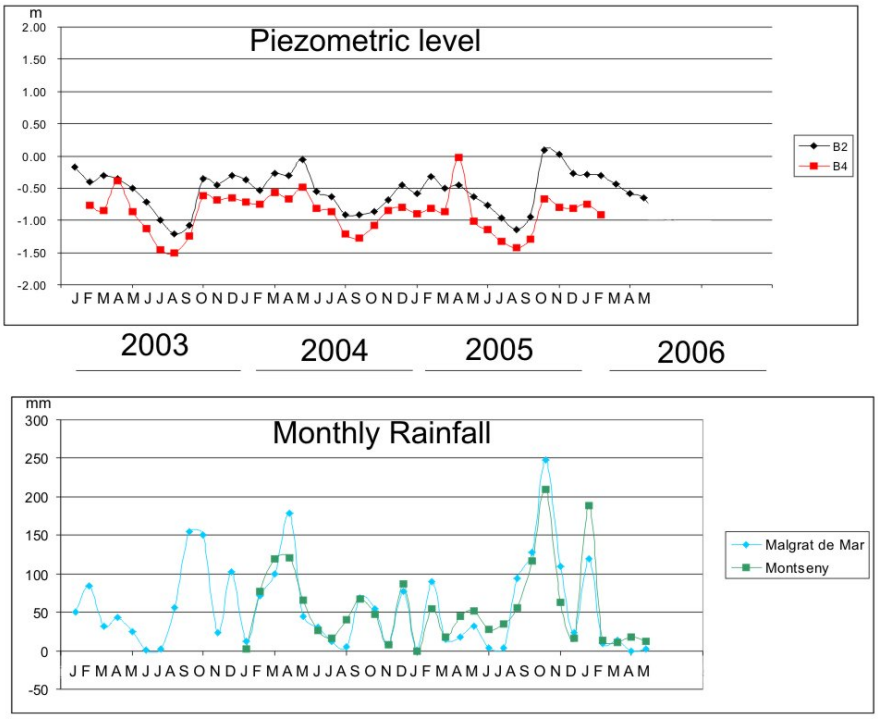

Figure 4.17: Piezometric levels (Http://mediabient.gencat.net/aca) on two piezometers and monthly rainfall from two weather station one on the catchment basin area (Montseny) and the other on the deltaic zone (Malgrat de Mar) information could be found at http://www.meteocat.com/marcs/marc_clima.html ("taules de dades mensuals").

Figure 4.17, present monthly precipitation of two different weather stations, one on the catchments zone of the Tordera basin (Montseny), and the other on the Deltaic zone (Malgrat) with monthly head level lectures from B2 and B4 piezometers (see Figure 4.5 for specific location) that measures the regional deep aquifer. Similar head values annual pattern is regarded on both B4 and B2 piezometers, but with a different base level due to precipitation and seasonal extractions. In general, in spring the head level starts to sink down due to the less quantity of precipitation attaining its minimum during summer time. When the hydrologic year starts (autumn), head level rise up recovering a stable relative high head level during winter in relation with the rainy seasons.

In more detail from 2003 to 2006, it could be seen those cycles, although different minimum and maximum levels are attained in relation to the different precipitation received. Summer 2003 was an extreme dry summer and head levels presented extreme low values, however fall 2003 provided good amount of rain restoring a good head level. During spring 2004, rains continued on a good rate not allowing the levels sink down. As a consequence, summer 2004 head levels decreased, however in minor degree due to continued precipitations. In autumn and winter 2004 precipitation continued at a low rate but continuously. AMT models M-1, M-2 and M-3 suggest a seawater retreat without of the head levels lowering during the summer due to the good amount of precipitation. However, spring and summer 2005 had scarce precipitation, so that the head level sank down and AMT model imaged a seawater intrusion progression inland (M-4 and M-5), presenting in July minimum head level. After the rainning episodes from autumn 2005, head levels started to recover and AMT model (M-6) imaged a slightly seawater retreat that continued on the model M-7. On this last model it is evidenced a time delay on adjusting the head level and seawater content, given that although the head level has started to decrease M-7 present seawater regression instead of progression.

Hydraulic response of the system clearly influenced on seepage of direct precipitation with less than one month time delay, particularly as evidenced in the rainny September and October months (Figure 4.17). However, equilibrium on salinity content makes the AMT resistivity response to present a higher time delay as regarded on the model sequence.

4.10. Hydrochemistry geophysical model calibration

In this section we present the calibration and validation of PS1 and M-1 AMT models with the piezometers W-04 and W-06. Presence of seawater content in both wells is around 40 m depth, but at different rates due to its position inland and therefore differential seawater content owing to the seawater transition zone nature. Multi-tube piezometer W-04 is located close to PS1 and W-06, 500 m to the north of the latter, is located on the northern part of our monitoring profile (Figure 4.10). These piezometers provide three independent lectures in depth from April 2004 that can be correlated with M-1 AMT model (Figure 4.18).

Figure 4.18 shows the comparison among lithology, water resistivity and bulk resistivity (AMT resistivity models). In W-04, the shallower zone (3-15 m), shows a value of 7.3 ohm·m (fresh water) in coarse sands that agree with the bulk resistivity of 40 ohm·m obtained in the 2D

model. Between 20 to 45 m depth, the water resistivity is 7.6 ohm·m in finer sand-clay interbeded layers. This lithology change is seen in the decrease in the bulk resistivity value (10 ohm·m). And finally in the deeper position from 50 to 80 m depth, the presence of 16000 ppm of Cl^- is recorded, that corresponds to a water resistivity of 0.29 ohm·m. This together with the reported coarse sands agrees with the recorded low bulk resistivity value of 1 ohm·m. Therefore, the geoelectrical model expresses a sandy aquifer zone with high seawater content.

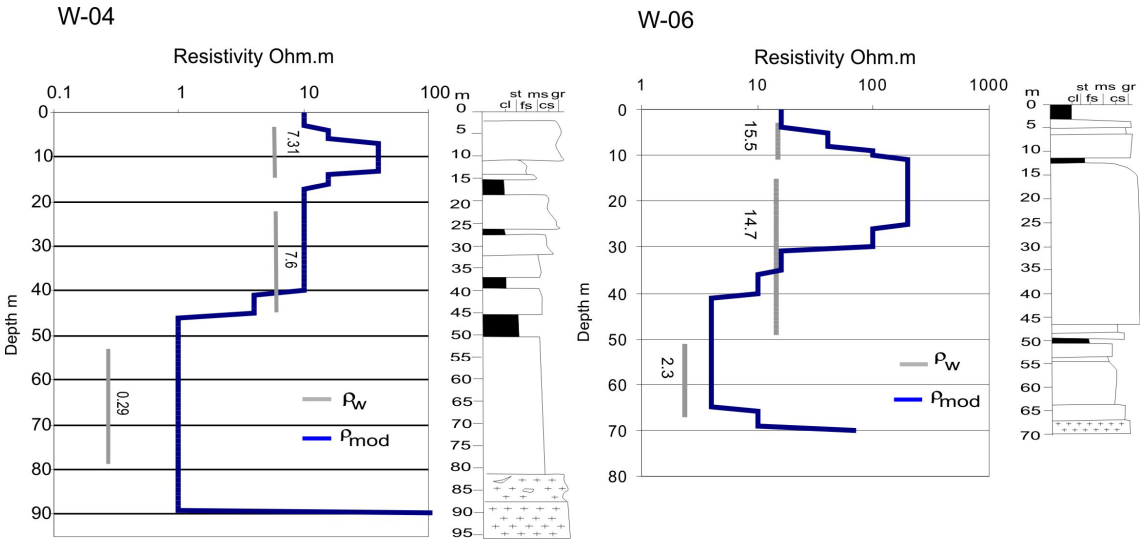

Figure 4.18: Water resistivity (ρ_w) and AMT bulk resistivity (ρ_{mod}) plots on wells W-06 and W-04. Water resistivity and AMT resistivity data are correlated in depth with lithologies. Lithologies, cl: clay, st: silt. fs: fine sands, ms: medium sands, cs: coarse sands, gr: gravels.

In the W-06, similar hydrochemistry trends are registered but in a minor degree giving that W-6 is located further inland and the seawater has less influence. The lithological log shows high amounts of coarse sands and gravels that may correspond to the paleochannel area. Water resistivity values of shallow (3-11 m) and middle lecture (15-48 m) are around 15 ohm·m, corresponding to fresh water. Evidencing seawater influence, water deep lecture (52-70 m) attains 2.3 ohm·m related with the higher chlorine concentration measured (1350 ppm Cl^-). The bulk resistivity value at shallow levels is around 10 ohm·m, fitting with clay observed in the first five meters. Below, the resistivity increases to more than 100 ohm·m, due to the presence of coarse gravel bearing fresh water. At around 40 m depth, a bulk resistivity decrease is observed. However, nor hydrochemical neither lithological evidence is observed. Below 52 meters, the bulk resistivity shows low resistivity values (4 ohm·m) and coarse sands are reported. Thus, the observed electrical resistivity values must be associated to the presence of seawater.

4.11. Hydrogeoelectrical models interpretation summary

Hydrogeoelectrical interpretation of PS1 and PS4 models has been constructed according to the resistivity models, hydrochemistry, lithology and the regional stratigraphical cross-sections (Geoservei, 2001). Hydrogeoelectrical models and hydrofacies electrical resistivity ranges has been summarized in Table 4. 3 and Figure 4.19.

Considering the AMT models, three different regions have been derived. These hydrogeoelectrical regions could be interpreted as three different fluviodeltaic hydrofacies.

Hydrogeophysical facies

Granulometry	**Deposit type**	**Resistivity (ohm·m)**
Coarse	Fluvial	100-1000
Middle	Delta plain	40-100
Finer	Flood plain Prodelta clays	10-40

Table 4.3: Hydrogeophysical facies derived from the 2D AMT models relating granulometry deposit type and observed resistivity on the models.

1) Delta plain deposits correspond to the shallow sediments, that usually contains fine sand and resistivity ranges from 40 to 100 ohm·m, 2) Finer deposits as flood plain deposits or prodeltaic clay deposits that present higher clay content (10-40 ohm·m) that may work as barrier or aquitards, and 3) Fluvial deposits composed of coarser sediments of the resistivity order from 100 to 1000 ohm·m are the main aquifer zones. In these later zones seawater encroachment may be easily induced due to high hydraulic permeability capacity showing low resistivity values (1-4 ohm·m). However, relatively low resistivity values (4 ohm·m to 10 ohm·m) cannot distinguish seawater wedge and transition zone from clayish zones. With geophysical data, additional hydrogeophysical information is required.

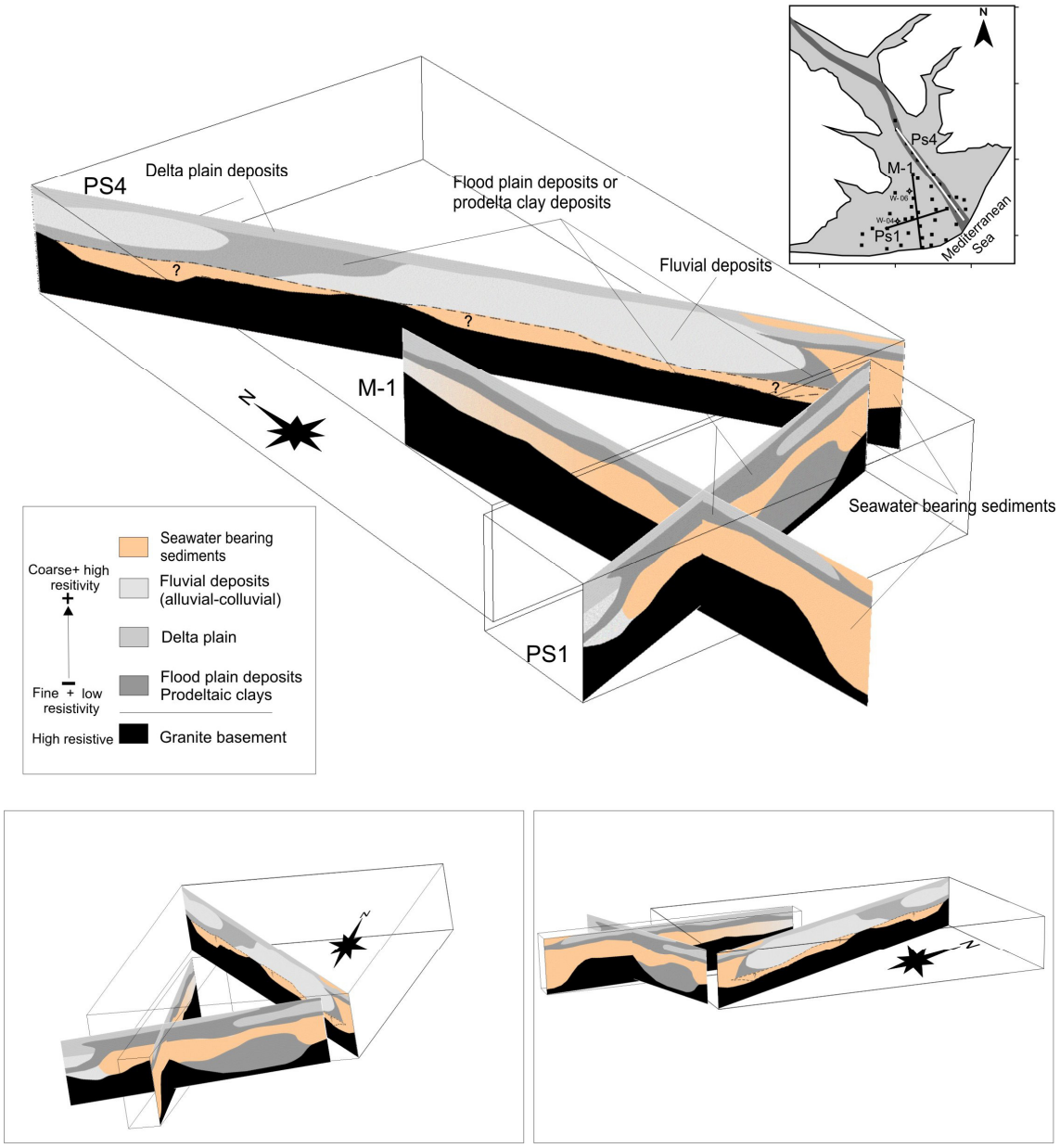

Figure 4.19: PS4, PS1 and M-1 interpreted hydrogeological cross-section showing main hydrofacies and interpreted seawater encroachment. Far reaching seawater intrusion or clayish sediment facies on the dashed line area, remains as an open question till additional hydrochemical information or lithological evidences of weathered granite can be obtained on this zone.

Petrophysical approach to Tordera model is still unresolved and was out of the scope of this work. Sedimentary record of Tordera fluviodeltaic system is composed of different grain sizes mixed with different clay contents. In addition, the seawater wedge affecting the deltaic zone could not be regarded as a sharp boundary but as a transition zone. Petrophysical relationship, where environment contains salt and clay are complex due to its cation exchange capacity (Waxman and Smits, 1968). For this reason, it is not easy to implement Archie's type

petrophysical relationship given that no extensive calibration of sedimentary analysis (grain sizes and clay content) and hydrochemistry records with electrical resistivity models have been done. So that the quantitative appraisal and the further step to infere hydraulic parameters from resistivity still have to be settled.

4.12. 3D Model

The AMT dimensionality analysis has shown a three-dimensional data behavior (4.6.2 dimensionality section). Correct appraisal to the Tordera deltaic aquifer system is to create a 3D model. Two different approaches could be performed: 1) solving the forward problem following a trial and error scheme or 2) resolving the inverse problem. Traditionally, the trial and error model fitting method has been used to build up the 3D models (see for instance chapter 5, Arango, 2005; or Martí, 2006) however it is a complex process and really time consuming. During 2006, WSINV3DMT (Siripunvaraporn *et al.*, 2005) inverse MT application was publicly released. We wanted to try out the software to create a 3D model with the full Tordera AMT data set.

WSINV3DMT (Siripunvaraporn *et al.*, 2005) is a full 3-D inversion program for magnetotelluric data. It is based on the data space Occam's inversion of Siripunvaraporn and Egbert (2000). The inversion seeks the smoothest minimum structure model subject to an appropriate fit of the data. Matrix dimensions depend on the size of the data set N, rather than the number of model parameters M, and thus computational costs are significant due to data space transformation (Siripunvaraporn, 2006). Computational limitations are therefore around memory and CPU requirements that can be too large for a standard single processor PC or workstation. WSINV3DMT is an inversion program that has to be perceived only as a tool that gives a model that possibly fit the data. Reasonable models are expected to be obtained after performing some work on the preliminary inversion model released. In other words, model and data parameters has to be adjusted several times before you could obtain a reasonable model computing the forward model that could be compatible with the area's geology (Siripunvaraporn, 2006).

This 3D inverse code therefore is in its test stage where users and developer have to work jointly to improve code and its results. All this preliminary and further considerations could be found on WSINV3DMT webpage http://mucc.mahidol.ac.th/~scwsp/wsinv3dmt/, and

also on the WSINV3DMT user webpage as a forum to share updates, questions and concerns http://www.gfz-potsdam.de/pb2/pb23/MT/projects/3dinv/where.

In Tordera AMT data survey, many different 3D models and strategies have been tested to achieve an acceptable model. To begin with, simple cases have been considered, coarse meshes, few periods and default parameters. The final model is composed of a mesh of 35x35x15, a total of 18375 cells, with central blocks of 100 x 100 m. The total model area is 3700 m x 3700 m with a depth of 230 m increasing block's thickness progressively, being the first block 5 m thick up to 40 m block thickness on depth. On the inversion process 8 periods have been used, within the period range of 10^5-10 Hz. Four components of the impedance tensor have been used on the inversion parameters, the non diagonals, given that diagonal parameters have lower quality. Inversion of four components has also been considered to liberate computational time.

```
TOTAL NUMBER OF DATA PARAMETER (N)  =   1568
        NUMBER OF STATION  (Ns)      =     49
        NUMBER OF PERIOD   (Np)      =      8
        NUMBER OF RESPONSE (Nr)      =      4
        ---------------------------------------------------
TOTAL NUMBER OF MODEL PARAMETER (M) =  18375
        NUMBER OF BLOCK IN X-DIR (Nx) =     35
        NUMBER OF BLOCK IN Y-DIR (Ny) =     35
        NUMBER OF BLOCK IN Z-DIR (Nz) =     15 (WITH AIR =   22)
        ---------------------------------------------------
```

Table 4.4: Data and model parameters used on the inverse 3D code. Log document generated by the code.

The number of data parameters (N) is smaller than the number of model parameters (M), one of the assumptions of better efficiency in WSINV3DMT inverse program. The default smoothing parameters has finally been used although other smoothing rates have been tested creating less defined resistivity model structures. Computational time with a PC Pentium D, 3.40 GHz and 1 Gb RAM takes 6 hours to create the sensitivity matrix and 4 hours for each iteration.

After different attempts, the initial model was created with the 1D models interpolated over the space to fill the 3D block cells, and imposing the Mediterranean sea following the coast line morphology and bathymetry, south-southeast of the model. Accounting seawater effect on the data and the model is compulsory for the reliability of the final model.

The preliminary inverse model obtained from the inverse program has to be readjusted after computing the forward response (Mackie and Madden, 1993) to get better data fit. Model targets improvement has to be done following a trial and error model-data fitting.

4.12.1. Synthetic 3D model

To understand the 3D inverse model response, a seawater intrusion aquifer model has been constructed. Important numerical problems can be observed, proving that sensitivity analysis of the geoelectrical targets is an important process to succeed to the posterior geoelectrical interpretations of the 3D inverse models.

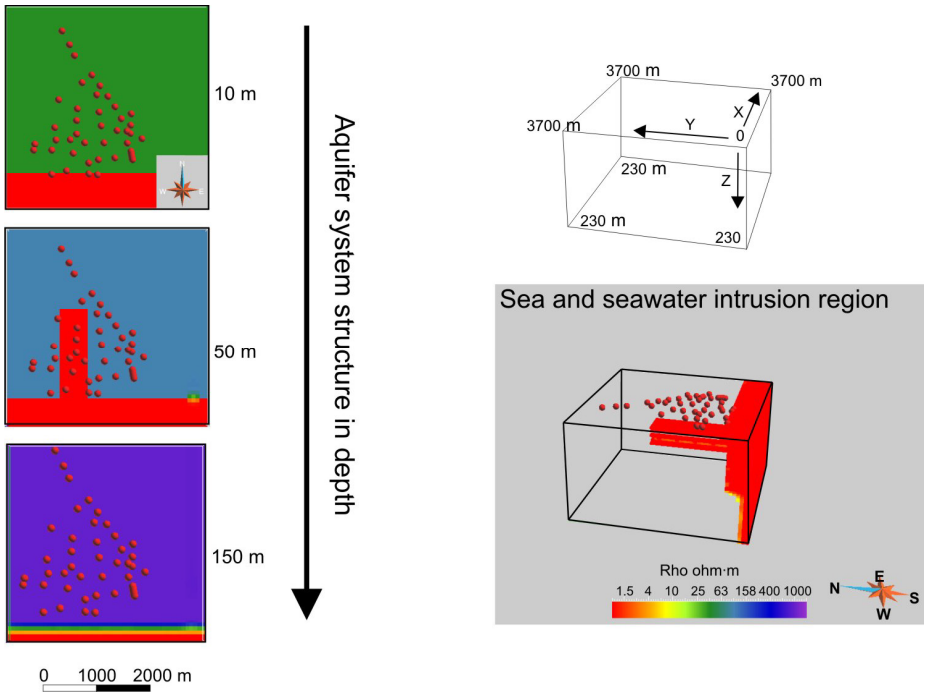

Figure 4.20: 3D model that simulates and ideal coastal aquifer with a rectangular homogeneous seawater path on depth. Red dots corresponds to the location where has been calculated the forward synthetic data.

The synthetic model is composed of 1) a seawater zone of 1 ohm·m on the southern area, 2) a 10 m thick layer of 40 ohm·m on surface, north of the sea, 3) below, a deep aquifer zone of 100 ohm·m of more than 100 m thickness has been modeled where 4) an ideal 1200 m length, 400 m wide and 40 m thick rectangular seawater intrusion path is included on the western part of the model. And finally 5) a deep high resistive basement has been modeled. Forward model data is calculated on the same location as the Tordera AMT survey soundings. Synthetic data obtained is used as input for the inverse modeling process (Figure 4.20).

First of all, it is important to mention that shape and depth boundaries of the main geoelectrical features could be retrieved, see for instance the low resistive rectangle (simulating seawater intrusion), or the position of the sea. However, other low resistive areas appear where no data coverage is available (N and NE of the model), so those are clearly numerical inversion artifacts (Figure 4.21 circles). Another electrical anomaly is related with ideal sharp limits. Sharp boundaries could not be obtained on the AMT inversion models. For instance, on the limit of the modeled seawater (Figure 4.21) spherical geoelectrical bodies appear where resistivity values are extreme. Those fake features may be the result of mathematical problems due to situation of the sites, too coarse mesh and in some cases not enough dense AMT sounding coverage.

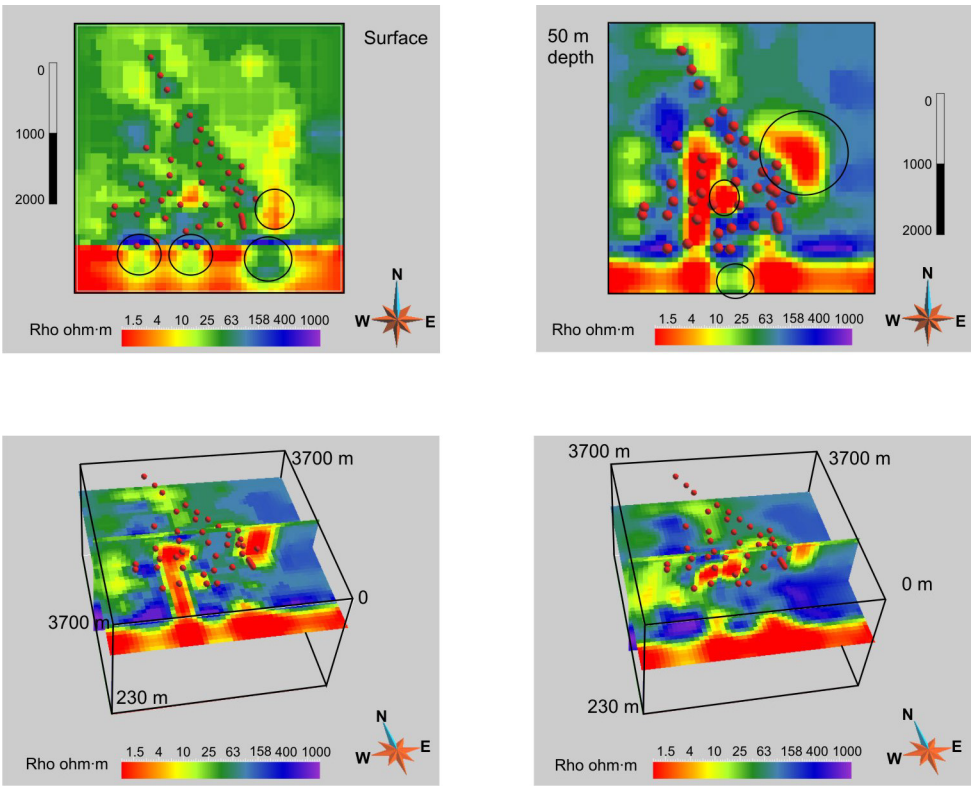

Figure 4.21: 3D inverse model from the synthetic data obtained with the created model Figure 4.20. The final model fits the determinant of the impedance tensor with a total RMS of a 4.5 in the resistivity and a 1.6 on the phases considering a 5% of error floor impedance component.

4.12.2. 3D Tordera model

3D AMT model obtained with the WSINV3DMT shows a RMS of 7.1 (Figure 4.22). As derived from the above considerations this 3D AMT model may show the main geoelectrical targets and additionally may carry artifacts, some of them clearly visible. In this specific case where sounding are too distant or no data coverage exist, mathematical procedures creates extreme low resistive values (circled zones Figure 4.22). Moreover, some work has to be done to obtain improvement of data-curve fit. Therefore it is compulsory to execute sensitivity test of the geoelectrical structures and work in a forward modeling process to obtain a better model data fit.

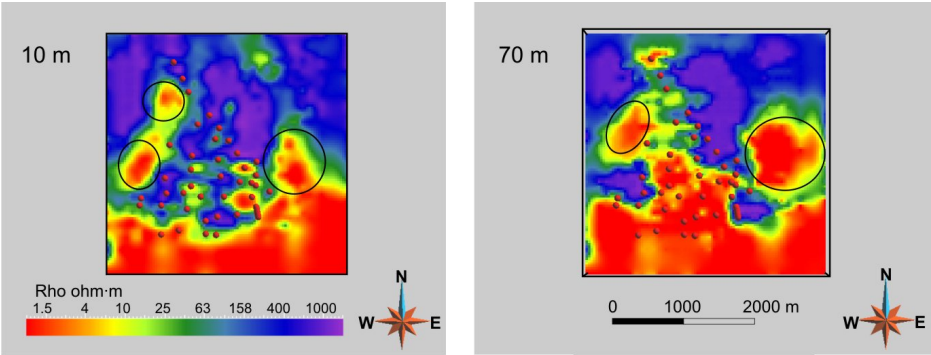

Figure 4.22: Preliminary 3D inverse model obtained from the WSINV3DMT with 7.1 RMS fitting TE and TM modes. Circles remarks the non data coverage zones where the code produces lateral low resistivity bodies.

The final model presented on Figure 4.23, obtained after testing sensitivity of key geoelectrical structures. The most important and visible geoelectrical targets are related to the seawater encroachment distribution, as well as basement morphology. Figure 4.23 A images the seawater influence inland as a continuum front following the coastline morphology (SW-NE low resistive area on the southern part of the model block). Besides to it a low resistive zone following the actual river line is observed up to the beginning of the PS4 AMT model line.

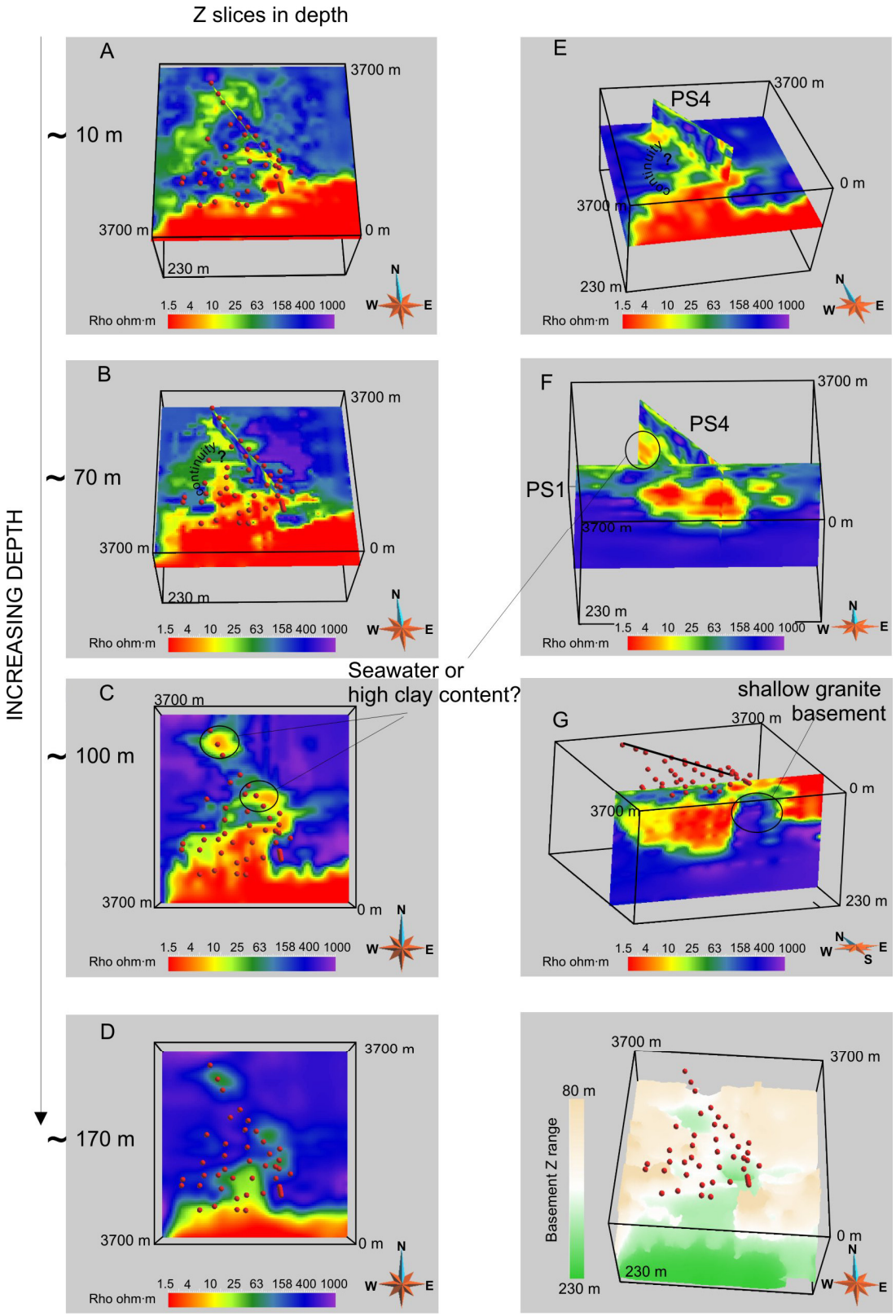

Figure 4.23: 3D inverse model showing relevant features. Z slices A, B, C, and D images, PS1 and PS4 lines E and F, and near shoreline basement geoelectrical target G. The final model fits the determinant of the impedance tensor with a total RMS of a 6.8 in the resistivity and 5.2 on the phases considering a 5% of error floor impedance component.

With the increase of depth (Figure 4.23 B around 70 m) seawater intrusion scenario changes entirely and correlates with what has been seen on the pseudosection and previous 2D models. Intrusion path is a wide zone located on the western area of the delta following an almost N-S direction. River line shows a high resistive zone to the near shore suggesting shallow basement that may protect aquifer from being affected in this direction (Figure 4.23 B, C, F and G) and thus seawater encroachment in depth may be induced from the western deltaic area. Far reaching seawater influence on the western intrusion path N-S direction is still an unknown, given that the lack of enough data in this direction. Imaging deeper (Figure 4.23 C and D, 100 and 170 m depth respectively) seawater intrusion influence starts to retreat seawards. It is possible to observe two low resistive spots where basement is modelled deeper, however it is difficult to conclude and relate its resistivity value with high clay content or seawater influence, giving the few hydrochemistry and lithology data available on that locations and depths.

Basement presents a high irregular paleorelief. In particular basement morphology is seen in Figure 4.23 C, E, F and G images, providing its importance as one of the main controls of the seawater intrusion.

Seawater intrusion on the Tordera Delta is obviously due to excessive withdrawls, however its distribution has a tectonosedimentary control with a meaningful basement control component. Seawater intrusion on the actual river line direction is limited due to shallow granite basement near the shoreline. On the western zone, where basement is deeper deltaic development presents a main paleochannel dominated by gravel and coarse material, and consequently seawater wedge can progress inland. In addition, near the shore line towards the south, modelled basement present a sharp deepening that may be related to CCR distension normal fault given that coincides with lithological observations. ITAM coastal wells does not reach the basement (>180 m depth).

4.12.3. 2D model versus 3D slices

PS4 and PS1 2D models and the collocated slice of the 3D model could be compared. In general, high similitude within retrieved geoelectrical targets could be observed (Figure 4.24) corroborating reliability with the 2D models, and validating the relevant work derived from them. However, it is obvious that 2D-3D models differ slightly given that mathematical process to obtain the final models has been different.

In general, it can be assessed that 3D model basement is better defined than 2D model basement. 2D model's basement has been constrained with seismic basement trying to locate shallower basement depth, whereas 3D model basement reproduce similar basement depth, where changes in basement depth is meagre with retrieval of good data fit.

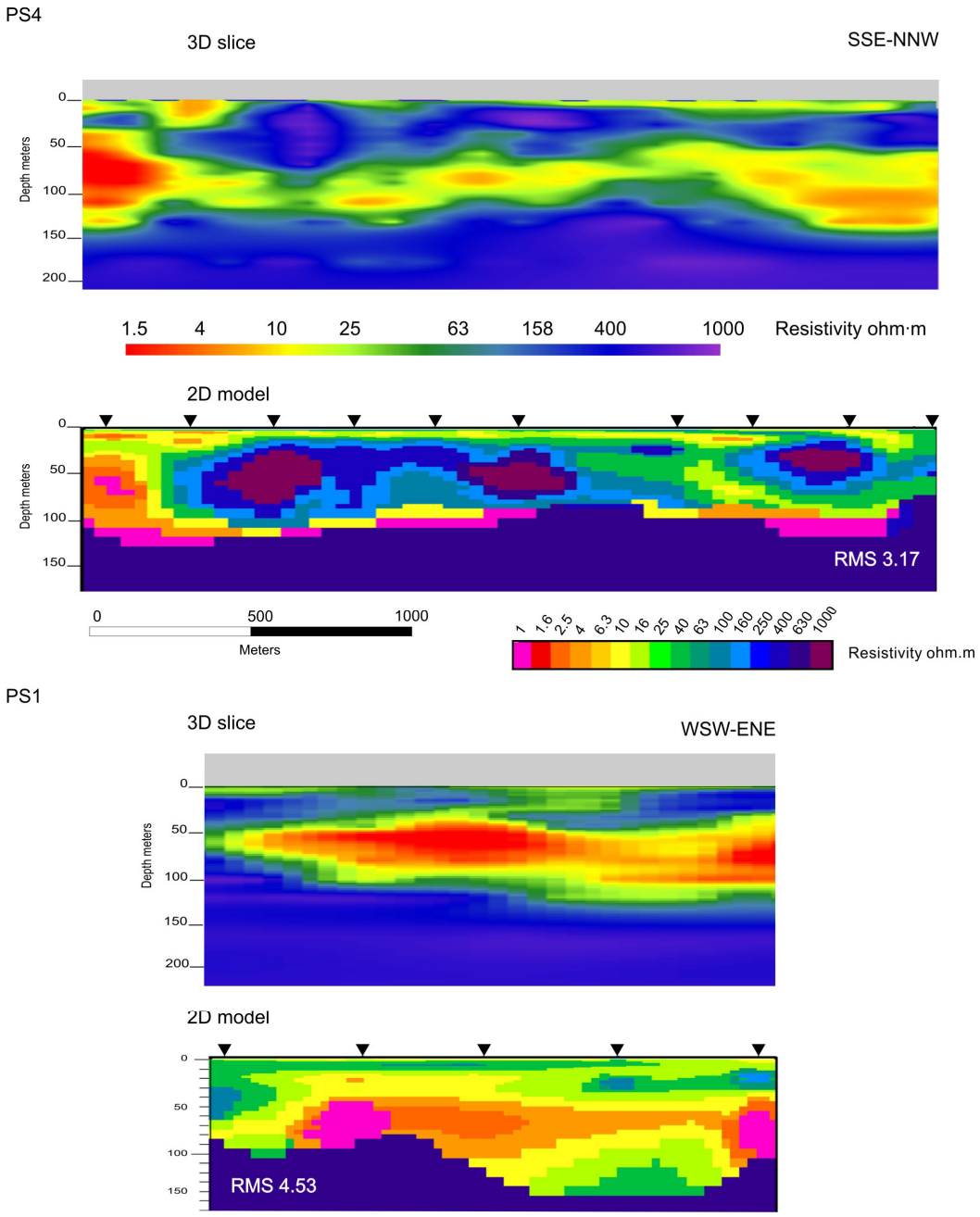

Figure 4.24: PS4 and PS1 3D inverse slice and 2D model. Images shows important similitude.

Different geoelectrical morphologies are regarded on low resistive zones of the aquifer system. In particular is significant on the low resistive zone at depth. For instance, PS4 3D low resistive deep zone is observed as a more wide area and slightly more resistive than on the 2D model, restricting the volume of high resistive freshwater aquifer unit. Similarly on PS1 3D model slice, the low resistive zone is more wide open than on the 2D model.

4.13. Comparison DC surface TDEM models with AMT models

In this section PS1 and PS4 resistivity models derived from AMT, DC resistivity and TDEM are compared.

DC resistivity models have been obtained with Profile-R designed for surface array resistivity profile imaging (Binley, 2003). The program uses finite elements method in forward modeling and inversion procedures. Profile-R is an inverse solution for a 2-D resistivity distribution based on computation of 3-D current flow using a quadrilateral finite element mesh. The inverse solution is based on a regularized objective function combined with least squares (an 'Occams' type solution). The code supplied has been compiled for Pentium processors with the visual interface of ZondRes2D (Kaminsky 2007, http://kaminae. boom.ru/Zond.htm).

TDEM data were acquired, processed and inverted by GEOGNOSIA S.L, so that model presented is the one presented in Marcuello and Plata, (2005). Models correspond to the interpolation of the 1D inverse models.

From the analysis of all models from the different origin, it can be clearly assessed that AMT, DC and TDEM retrieve the same main geoelectrical targets. In detail, it is possible to recognize important differences that should be consequence of different resolution and specific modeling procedures of each technique. Basement is clearly seen in the AMT models, giving that seismic basement has been tested on the sensitivity appraisal getting better data fit. Neither TDEM nor the DC models could provide a well defined high resistive basement on depth. DC electrode array distribution was 15 m spacing in order to attain higher depth while retrieving less detailed shallow information.

Resistivity values of the models, although similar present substantial differences from one model to the other. TDEM presents lower resistivity on the overall. DC presents moderate

values thus less resistivity contrast, whereas AMT presents a higher contrast of values, improving the resolution of more subtle structures.

PS4

Along line PS4 we have coincident AMT and DC resistivity and TDEM models. On the three models similar main geoelectrical targets are imaged (Figure 4.25), in particular a low resistive zone dominates the geoelectrical character of the southernmost part of the models toward the seawater. Towards the north, the overall geoelectrical targets could be described from top to bottom as high resistivity layer, a moderate low resistive and a wide high resistive zone. Laterally this later high resistive domain is interrupted by a moderate low resistivity zone (imaged clearly on the DC profile and AMT models). TDEM model length is too short to clearly recognize this feature. Basement as a high resistive domain is only imaged by the AMT model

Specific shape and geoelectrical bounding depth differs from AMT, DC and TDEM. The shallower high resistive zone on the DC model presents a 10 m thickness where on the AMT model is really thin, and TDEM cannot define it. The relative low resistive zone is imaged only by the DC and the AMT model. In general main geoelectrical targets depths are shallower for AMT models than DC and TDEM models.

TDEM presents the smoothest boundaries due to its 1D smooth inversion whereas AMT model boundaries are well defined and in a shallower position. Both issues are related due the different model mesh and modeling process used, giving that DC model has a coarser mesh than AMT and therefore DC model resolution is less accurate. DC shallower blocks are 10 m thick whereas AMT present 10 rows of 1 m thick increasing progressively the thickness.

PS1

PS1 line has also three geoelectrical coincident resistivity models AMT, DC, and TDEM model. Again in these models (Figure 4.26), the main geoelectrical targets are clearly observed, that is, a moderate resistive zone on the shallow surface, below a low resistivity zone, where shape and specific extreme resistivity values are slightly different. A shallow relative high resistivity zone and deep conducting zone boundary are well constrained and better defined on AMT model rather than on DC and TDEM, where boundaries are smoother. And again basement in TDEM and DC models could not be inferred. Taking into account the lithological AMT calibration (section 4.11) AMT structures depth fits better than DC and TDEM.

Given that TDEM model has been obtained from the interpolation of the 1D inverse models, PS1 model present less defined shapes among structures showing general trends as relative continuous tabular structures. On the other hand, DC presents a more irregular shape boundary between the shallow resistive and the deep low resistive zones. However, as considered in the PS4 line, the DC mesh is coarser than AMT mesh and therefore DC model retrieves more general trends.

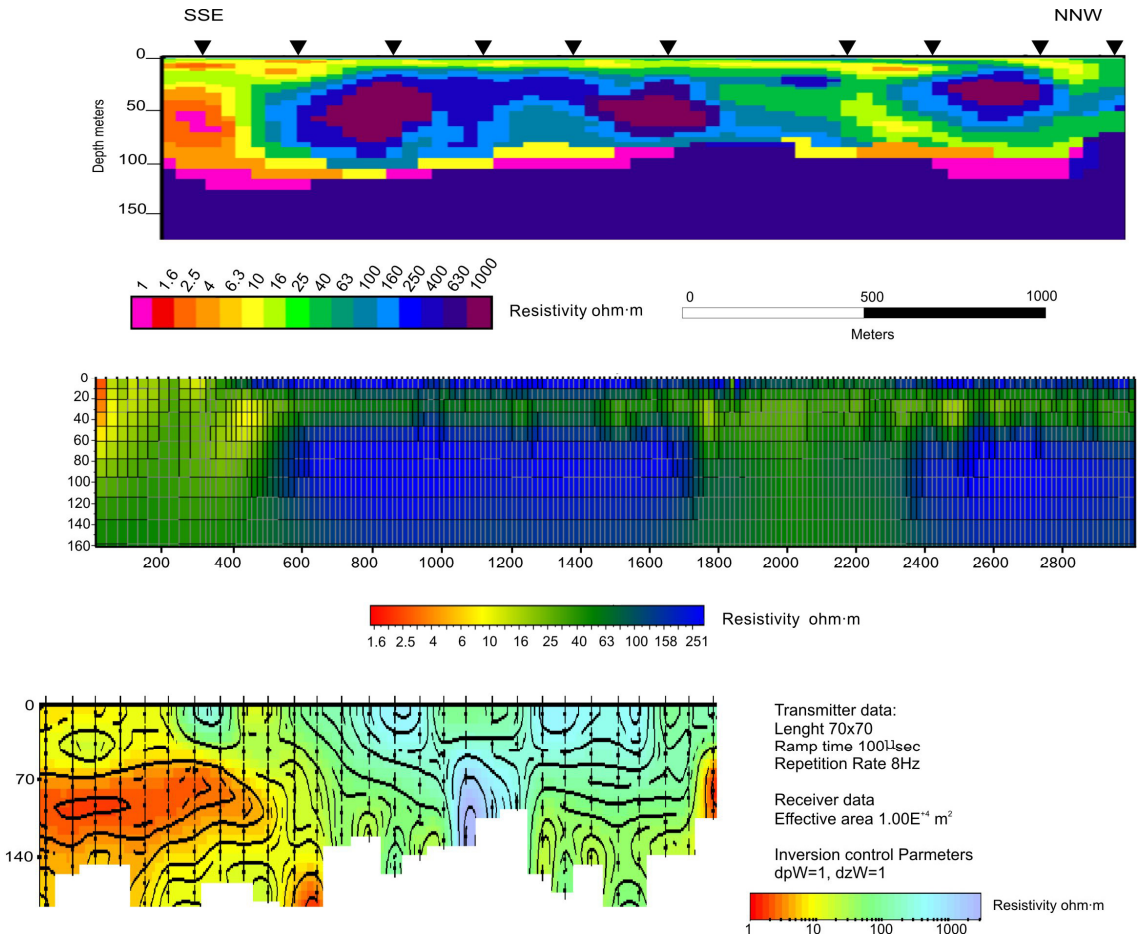

Figure 4.25: PS4 geoelectrical models. From top to bottom 2D AMT model and DC resistivity model. And TDEM model.

Therefore as a conclusion, although TDEM, DC and AMT models image the same geoelectrical targets, AMT present higher investigation depth while retrieving well defined structures. DC lose its high resolution capacity owing to the electrode spacing and does not reach the required depth penetration to image the basement. TDEM present the smoother models and only could detect the more general and regional trends.

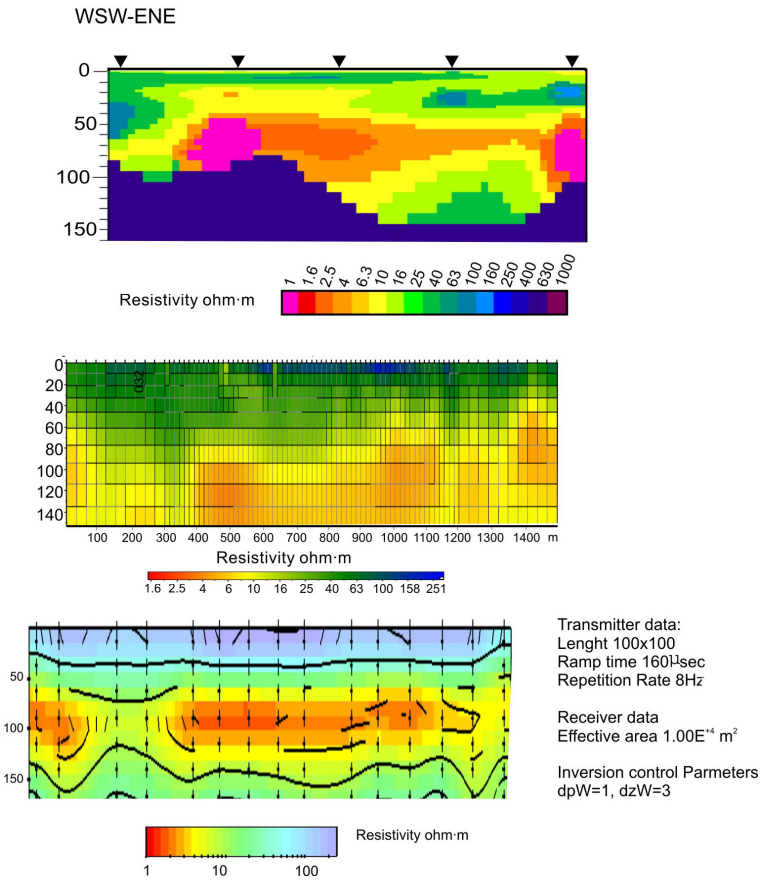

Figure 4.26: PS1 geoelectrical models. Above 2D AMT model, DC resistivity model on the middle position, and TDEM below.

4.14. Conclusions

Tordera aquifer system has been gaining a great importance during the last decades due to the economical growth of the area and therefore its water resources have played a strategic role in its development. However, as a collateral effect an environmental impact upon the aquifer system has been evidenced. The excessive withdrawals allow seawater wedge progression inland as observed from both hydrological and geophysical data.

Summary and compilation of all lithological and geophysical data available has been done in order to get the first hand knowledge of the hydrogeological and geophysical aquifer system ontext obtaining the following results:

1) Hydrogeological conceptual model obtained with the lithological well logs analysis shows clearly an information deficit on data coverage and therefore this model does not reproduce the true heterogeneity of the system.

2) Preliminary geophysical data has evidenced a seawater intrusion main path on the western zone of the delta.

In hydrogeological context, previous and preliminary geophysical data was used to delineate the future research lines using AMT, seismic and the hydrogeological data

The AMT data, although being acquired nearby populated areas shows good quality. Dimensionality analysis shows a three-dimensional geoelectrical behavior and therefore correct modeling process has to look into the three-dimensional modeling process. Nevertheless, three different 2D models have been created using the determinant of the impedance tensor as a first order approach of 3D environments on 2D profiles.

The 2D AMT models have been adjusted with the refraction and reflection seismic profiles obtaining a better data fit. AMT models PS1 and M-1 have been proved to be in accordance with lithological description and hydrochemistry measurement of W-04 and W-06 multi-tube piezometers. Validation and calibration of AMT with hydrogeological data has been done and shows the AMT capabilities to provide hydrogeological information. Therefore hydrogeological facies interpretation linking resistivity and position on depth has been done. However there are some uncertainties due to the scarcity of hydrogeological information to fully control all possible scenes over the deltaic space.

The monitoring experience has proved AMT method as a sensitive method to reflect changes in electrical resistivity as a result of groundwater salinity changes. In addition, this method has been ideally suited for the required resolution and investigation depth, from shallow units up to the basement. We have obtained seven models, every four month, from 2004 to 2006. Evolution tendency seems to be in accordance with the hydrological state of the aquifer system derived from the precipitations and system seasonal outputs.

The interpretation based on both 2D and 3D AMT models has shown the importance of testing the sensitivity and resolution of the models to control uncertainties on data and modeling procedures.

The recently released 3D inverse code WSINV3DMT (Siripunvaraporn *et al.*, 2005) has been used as a preliminary approach to the Tordera 3D geoelectrical model. The main geoelectrical targets, namely seawater distribution along the deltaic zone and basement morphology, could be assessed. Although more work still has to be done to extract all information contained on the 3D model is possible to state that 3D models provide the whole picture whereas 2D models provide only partial information. Seawater encroachment is clearly basement controlled, given that near the shoreline on the actual river line basement is on a relative shallow position constraining seawater wedge progression. On the western deltaic zone the basin is deeper on the overall and coarser material dominate the main ancient paleochannel zone that induces seawater wedge progression inland due to excessive withdrawals.

TDEM, DC and AMT models image the same geoelectrical targets, nonetheless AMT present higher investigation depth retrieved better defined structures. In this case DC loses its high resolution capacity owing to the electrode spacing and do not reach the required depth penetration to image the basement. TDEM present the smoother models and the more general and regional model due resulting model corresponds to the 1D interpolated inverse models, while other two techniques could provide 2D and 3D inverse models resulting more reliable models.

Petrophysical approach to the 3D model has still to be addressed. Complex issues on the electrical resistivity properties have still to be solved to fully constrain the clay and seawater transition zone. Extensive, precise and better hydrogeological information in key places are required to succeed in this ultimate goal.

Chapter 5. Hydrogeophysical application: La Soutte

The present chapter is the result of the collaboration between our research group with the Proche Surface research group of the Institut de Physique du Globe de Strasbourg, EOST-ULP, Strasbourg, and a three months stage hosted by the Proche surface group in the framework of the international exchange program granted by the Spanish Educational Ministry.

The work presented here is based on the Audiomagnetotelluric study at "La Soutte", a natural hydrogeophysical laboratory, near Strasbourg (France). In this case, 2D and 3D AMT models were obtained focusing on a small scale catchment area, aimed to provide a mesoscale framework for other geophysical applications carried out on the site. The combined use of AMT and DC surface resistivity has been used to image different scales.

5.1. Introduction

Characterization of fractured aquifer systems is complex from the hydrological perspective due to its heterogeneity on fault and fractured density distribution. In addition, three-dimensional characterization of near-surface aquifer systems is an important challenge for the society from an environmental perspective, not only for their use as water supply repositories but also as waste disposal systems. In this case study, Rhine graben ranges are the catchment and drainage areas towards the regional alluvial aquifer, so that hydraulic transmissivity capability of those zones is highly important to compute the income on the hydrologic budget.

The natural laboratory of La Soutte (SW of Strasbourg, France), emplaced over a fractured media, has recently been instrumented by the Proche Surface Geophysics team of EOST for hydrogeophysical experiments. Several geophysical methods retrieving different physical properties at different scales have been used in this natural laboratory: DC, Magnetism, Seismic, Georadar, Nuclear Magnetic Resonance (NMR), and Self-Potential (SP) monitoring lines. Granulometric analysis has also been done with 2 m deep boreholes, and have been

installed a weather station. Behaegel (2006) developed his PhD dissertation on the framework of this multi-geophysical datasets. With the aim to incorporate AMT and to do a comparison with DC data we carried out a survey using the Stratagem system from the Universitat de Barcelona during the summer of 2004.

5.2. Hydrogeological setting

The natural laboratory of La Soutte is located 50 km SW of Strasbourg (France), on the western flank of the continental Rhine graben (Figure 5.1), a long scale symmetric structure highly studied due to its importance within Cenozoic European tectonics. Relevant tectono-structural geologic literature can be found in Hirlemann (1974), Illes (1977), Illes and Fuchs (1974) and Dèzes *et al.* (2004).

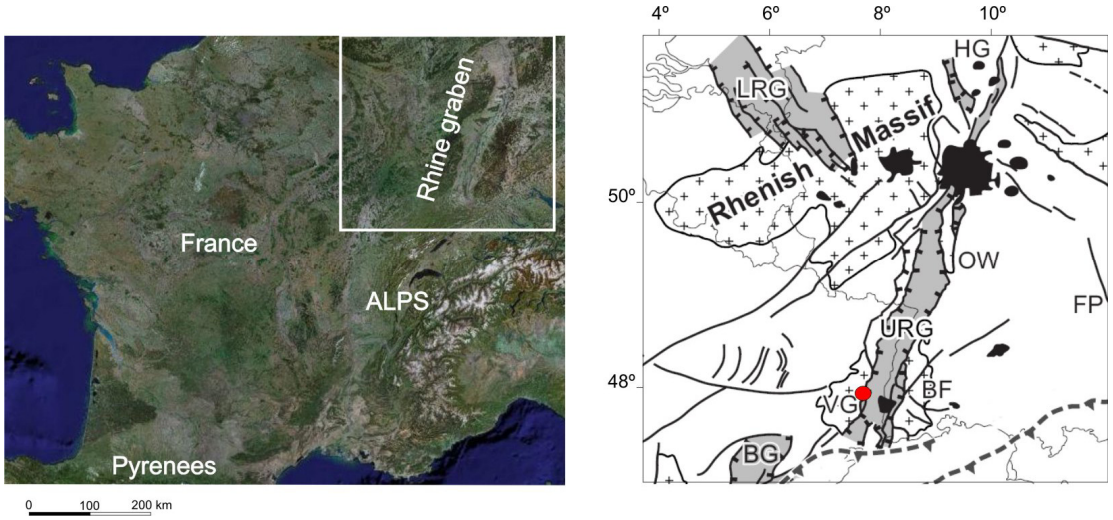

Figure 5.1: On the left, satellite image of France, the white rectangle corresponds to the right schematic geologic map. On the right, the European Cenozoic rift system (grey shading). Crosshatch pattern: Variscan massifs. Black: Later Cretaceous to Cenozoic volcanics. BF: Black Forest, BG: Bresse Graben, FP: Franconian platform. EG: Eger Graben. HG:Hessen Graben. LRG: Lower Rhine Graben. OW: Odenwald. URG: Upper Rhine Graben. VG: Vosgues. The red dot indicates the study area location, (modified form Ziegle *et al.*, 2004).

The Rhine graben is located on the northern European Cenozoic Rift System (ECRS), in the foreland of the Alps. Development of the ECRS began during the late Eocene mainly by the reactivation of Hercynian and Caledonian basement structures and fracture systems. The rifting

process is defined to be basement controlled given that rift valleys followed pre-existent weakness planes of the basement. On the Vosguien flank, where the study area is located (Figure 5.1), Hercynian basement presents shear zones parallel to the Cenozoic graben, as it is the prominent pre-existent weakness zone of Saint-Marie-aux-Mines fault, the Vosguien fault.

Actual Rhine graben morphology evolved as a product of two main stages of continental rifting. The first involves the creation of a N-S trending tensional rift valley, active from mid-Eocene trough to Lower Miocene. This first stage is related to the north-directed compressional intraplate stresses that originated in the Alpine and Pyrenean collision zones. The second stage is a period when the graben acts as a sinistral shear zone rotating the structure northeastwardly. The change in direction was initiated in the Upper Pliocene, related to the alpine uplift and extension. As a result, normal faults generally have split the graben segments, forming a mosaic of antithetic and synthetic tilted blocks, and thus basement and cover provides an image of a highly fractured structure, with a differential depth of compartment blocks deepening towards the centre of the Rhine graben (Figure 5.2).

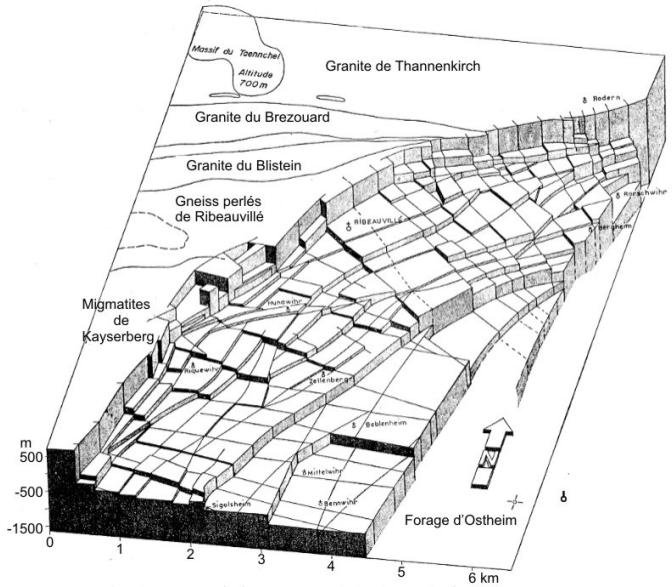

Figure 5.2: Block-diagram of the fracture field on the Haute Rhine, 20 km south of the study area. The Gres Vosgien formation (Busdsanstain) is the reference surface. Cover and crystalline basement present a highly fragmented structure. Although the crystalline basement fractures are less frequent, they are more important (From Hirlemann 1974).

La Soutte is an open square shaped zone of 9 ha at an altitude of 950 m, in the Vosgues Mountains located on the western flank of the Rhine graben that has a main slope of 5%

towards the Rhine graben center. The study area is located over the Hercynian vosguien basement, composed of Devonian volcanic rocks (pyroclasitcs), intruded by granite veins (microgranite porphyroides) Upper Carboniferous (Figure 5.3).

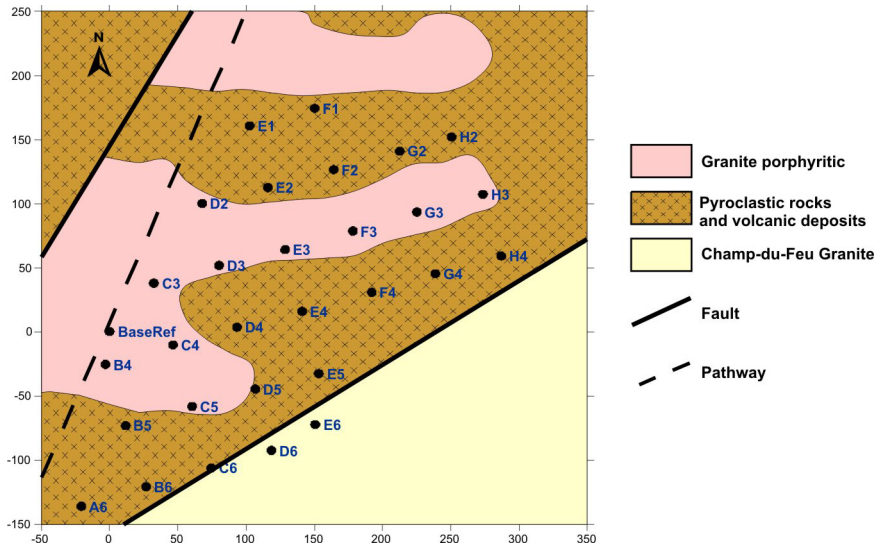

Figure 5.3: Geological map of La Soutte derived from the Geological map 1:50000 of the BRGM (271 Molsheim) and AMT sounding sites (Modified from Behaegel *et al.*, 2005). Map coordinates correspond to the DGPS local coordinates, Figure 5.4.

Regional structural-lithologic domains present a NE-SW direction due to the main fault's strike and compartmented blocks, however, inside the zone, the granite intrusion shows a three-dimensional structure. Above this fractured media have developed a thin weathering soil that presents thickness variability, from nonexistent to more than 2 m thick, evidenced by the presence of small outcrops and surface streams and springs.

La Soutte is the catchment area of the Ehrn River, itself an affluent of the Rhine, where there is a small stream on the southern zone of the study area (Figure 5.4). Potential aquifer zones correspond to perched aquifers within the subsurface weathered soil, and the fractured zones that may be used as catchments and drainage zones from the ranges toward the regional alluvial aquifer of the Rhine River Valley. Cenozoic graben fill can have more than 1000 m thicknesses, whereas Quaternary alluvial sediments are roughly 200 m thick.

5.3. Geophysical data

Topography of "La Soutte" has been measured in detail with local DGPS (Figure 5.4). Every 50 m has been marked with reference points as a positioning aid for the hydrogeophysical measurements. On Figure 5.4 those sites that have also been employed as AMT sounding survey sites are plotted.

The AMT survey was carried out in July 2004, the subsequent data analysis and modeling procedures started during the 3 month stage on the Institute Physic du Globe, Strasburg, ULP. 31 AMT soundings were acquired over a 2D grid having a step of 50 m with the StrataGem instrument, Geometrics (2001), that records a frequency range from 10 Hz to 92 kHz (Figure 5.4).

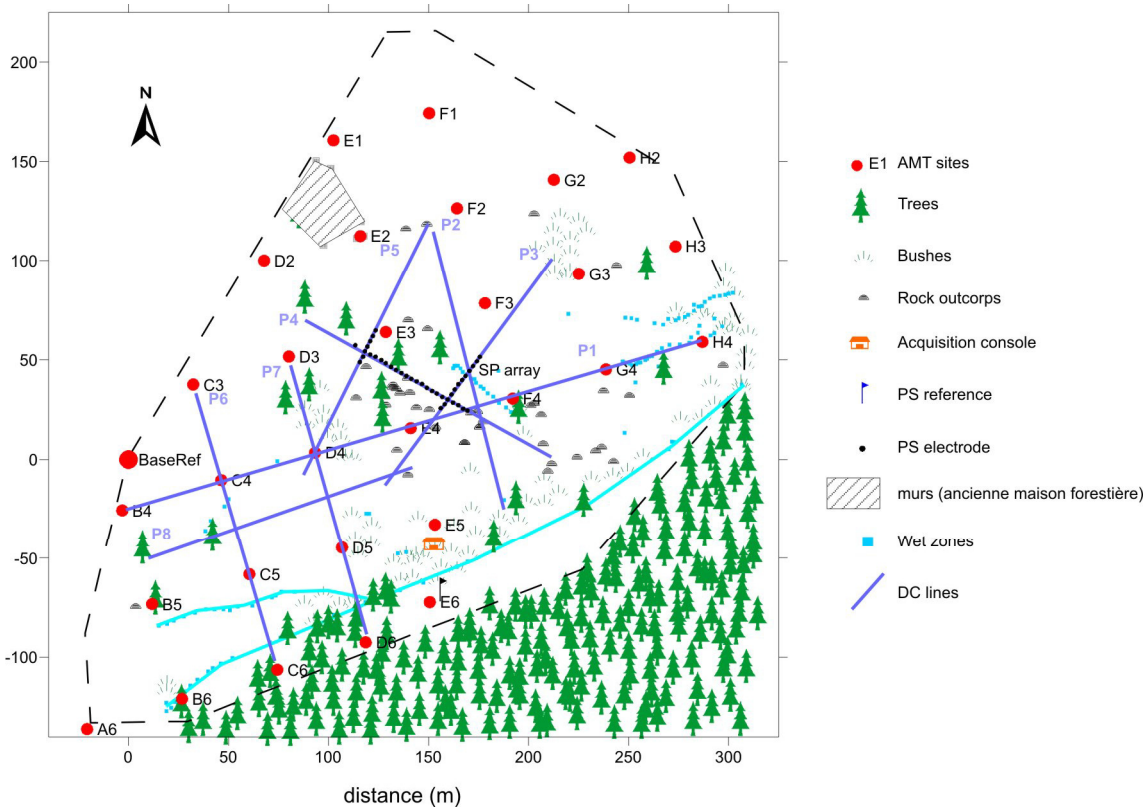

Figure 5.4: Local coordinate schematic DGPS positioning map of La Soutte, where AMT sites, DC resistivity lines, rock outcrop, streams and wet zones are shown.

Since AMT is a tensorial measurement and rotation can be easily performed towards the strike angle, induction coils and electrodes were oriented N-S, E-W, and a 20 m dipole electrode length was considered optimal. In general, high resistive materials impose an optimal

transmitter-receiver distance of around 300-400 m. However, this receiver-transmiter distance is the recording energy limit and thus, although electromagnetic source was used in some cases it was not totally efficient. Consequently, in some cases cultural noise is present on the data recorded, especially on the higher frequencies.

The DC surface survey was composed of 9 profiles, form 150 m to 300 m length (Figure 5.4). Acquisition equipment was a Syscal Jr system from IRIS Instruments using 48-electrodes. Profiles were acquired with Wenner-Schlumberger and dipole-dipole arrays with an electrode spacing of 3 m and 5 m, where investigation depth attains at most 20 m on the largest profile. DC resistivity data have been analyzed by the Proche Surface team and presented in the dissertation thesis of Behaegel (2006). In this thesis I only present line 4 following B4-H4 line, WSW-ENE direction (Figure 5.4) because is the largest profiles, and consequently attains enough investigation depth to compare AMT and DC surface data and models. This line has been used to show complementarities and disagreements of both geoelectrical methods, DC and AMT (section 5.5).

5.3.1. AMT Data analysis

AMT data were acquired within a 50 m 2D regular grid, thus a preliminary overview of the main resistivity patterns is easily imaged with data frequency pseudosections using the impedance tensor determinant. This parameter has several properties that make it suitable for preliminary interpretation when dealing with 3D environments (Vozoff, 1972; Ledo, 2006).

Qualitative preliminary analyses using data pseudosections provides general overview of the resistivity range and main geoelectrical targets, thus a few slices may provide the desired information. However, these data images are a smooth image of a possible estimated model and neither the values nor the depth position could be estimated from them.

Figure 5.5 presents four selected frequency pseudosections one for each decade of the apparent resistivity and phase of the determinant impedance tensor, thereby retrieving the main regional geoelectrical targets. The high frequency pseudosection represents the lowest apparent resistivity, in particular on the eastern area, whereas in the western zone there exist a high apparent resistivity area increasing its extension throughout lower frequency pseudosections. Apparent resistivity show a non 2D behaviour, suggesting a three-dimensional geoelectrical structure that correlates with the known geological structure of the study area and the dimensionality analysis presented in the following section.

No relevant static shift distortion has been observed on the AMT data soundings. Collocated AMT and DC data on the frequency domain (Figure 5.11) shows agreement on the resistivity values.

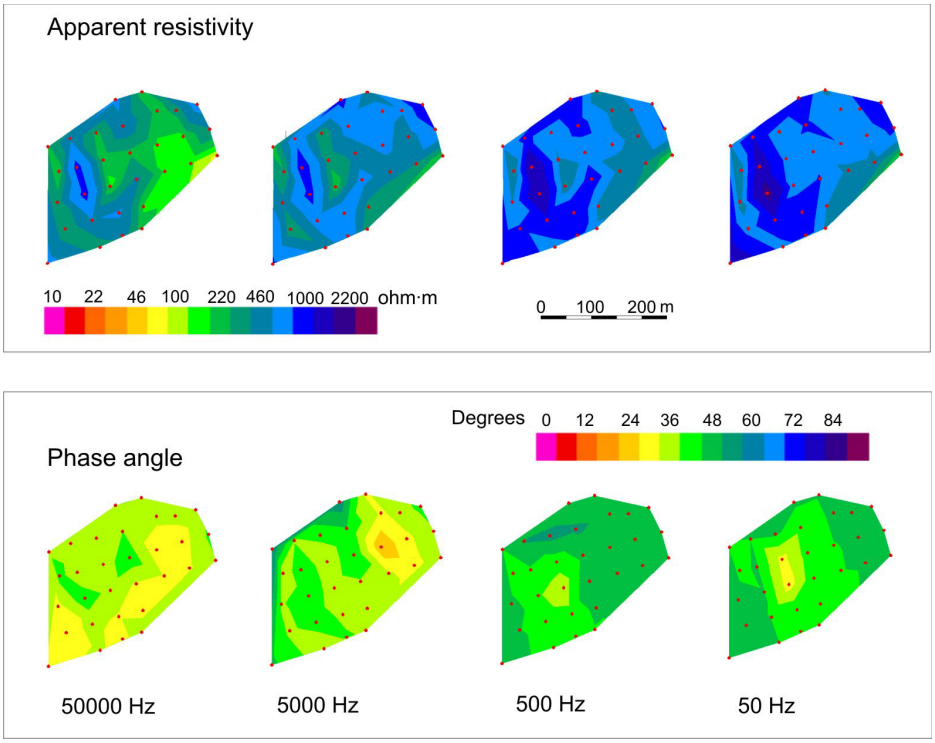

Figure 5.5: Frequency pseudosections for selected frequencies of the apparent resistivity (above) and phase angle (below) of the impedance tensor determinant.

5.3.2. Dimensionality

The *a priori* assumption of the strike direction owing to the Rhinegraben direction NE-SW was ruled out after dimensionality analysis. Site-by-site AMT data analyses has been done by computing WAL invariants (Weaver *et al.*, 2000) following the scheme proposed by Martí *et al.* (2004) (Figure 5.6), and by the classical Groom and Bailey (1989) decomposition method using the scheme proposed by McNeice and Jones (2001). Given that both methods show that the geoelectrical structures imaged by most sites are 3D only WALDIM dimensionality analysis is shown. This three-dimensional behaviour was already expected by the geologic map and the preliminary pseudosection data analysis (Figure 5.5).

In the WALDIM dimensionality analysis some sites with 2D trends could be identified (Figure 5.6), even though strike directions are different at each site and at each frequency

decade. A main geoelectrical strike direction cannot be retrieved, such that correct modeling process is only with a 3D model

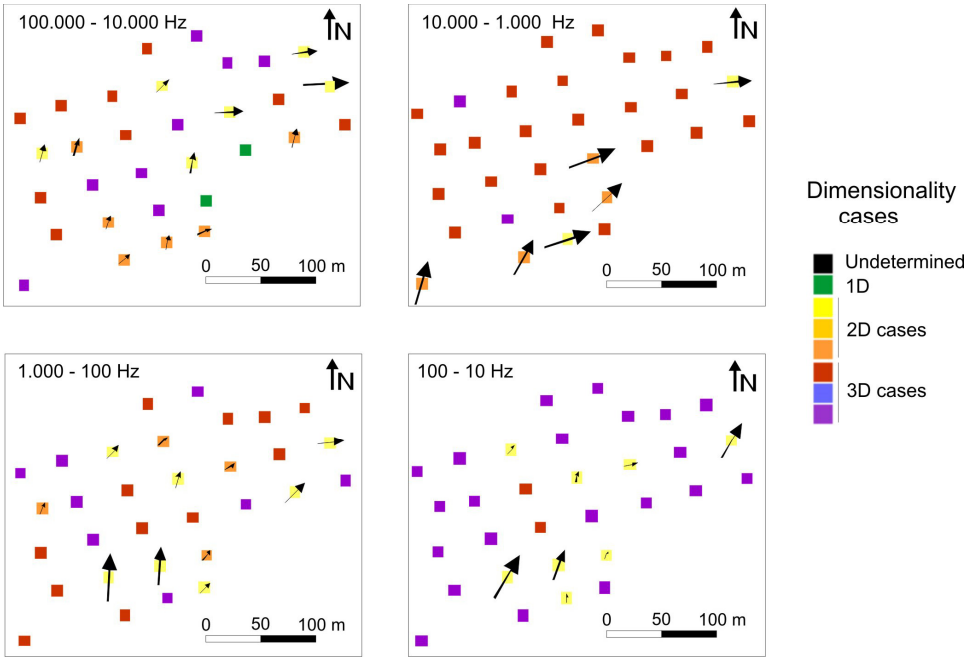

Figure 5.6: WALDIM dimensionality analysis showing the average dimensionality group for each decade. Arrow size is inversely proportional to the error determination of the strike angle.

5.4. AMT 3D model

The La Soutte 3D model is composed of a 3D grid of 20 cells (E-W) x 20 cells (N-S) x 15 vertical layers, with a 2 m top layer of increasing logarithmic thickness up to 400 m. The final model was obtained following a trial-and-error forward modeling process. The process involves creating an initial model, to compute the responses on the soundings locations, then by comparing the data and model responses remodifying the model where poor data-model fit exist. This iterative trial-and-error process has been performed as many times as was required to obtain a good data-model fit.

The initial model was built up using the 1D Occam's inversion models (Constable *et al.*, 1987) for each site, fitting the determinant data, and interpolating the 1D models over the space. The model responses were computed with the algorithm of Mackie and Madden (1993) at 13 frequencies between 10 Hz and 92 kHz. The final model fits the determinant of the impedance

tensor with a total RMS of 2.7 in the resistivity and 1.9 in the phases considering 5% of error floor impedance components (10% on the apparent resistivity and 2.8º on the phases).

5.4.3 Interpretation

To aid in the visualization and interpretation of the characteristic geoelectrical zones, the 3D AMT model was introduced into GOCAD (Earth Decisions). A cube was created by exporting the AMT model resistivity as XYZ and resistivity values of the center of each cell, Thereafter, horizontal and vertical interpolation on a densified mesh was done on the whole volume (Figure 5.7).

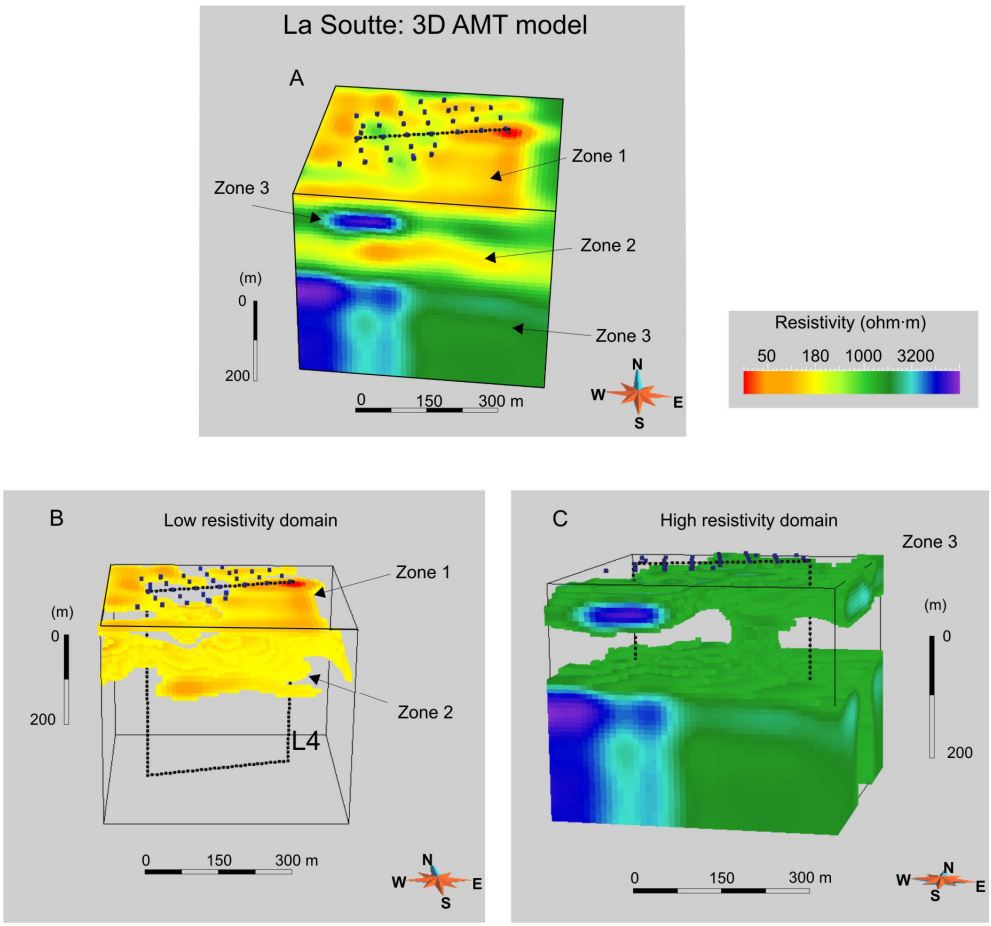

Figure 5.7: Images of the 3D AMT model. For a better situation sounding positions are depicted on the surface and line 4 profile as a rectangle. A: complete voxet. B: Highly resistive transparency image, to show the low resistivity zones. C: Low resistivity transparency image to show high resistive domain.

3D model resistivity values range from 50 to 10000 ohm·m, where changes should respond to the different hydrogeological targets. La Soutte lithologies are granites and volcanic

materials (high resistivity values) where fluid presence may be related to fractured zones and main faults (low resistivity values). Also as a low resistivity zone a top weathered soil layer was recognized that exhibits water and high clay content, where the impermeable zone induces small water floods. Interpretation of the AMT 3D model present a major step since no resistivity calibration of materials was done, however, the hydrogeological setting provides an excellent perspective. For a better three-dimensional comprehension, the main characteristics of the 3D model can be described as three different zones defined by depth and resistive structures illustrated in Figure 5.7 and Figure 5.8.

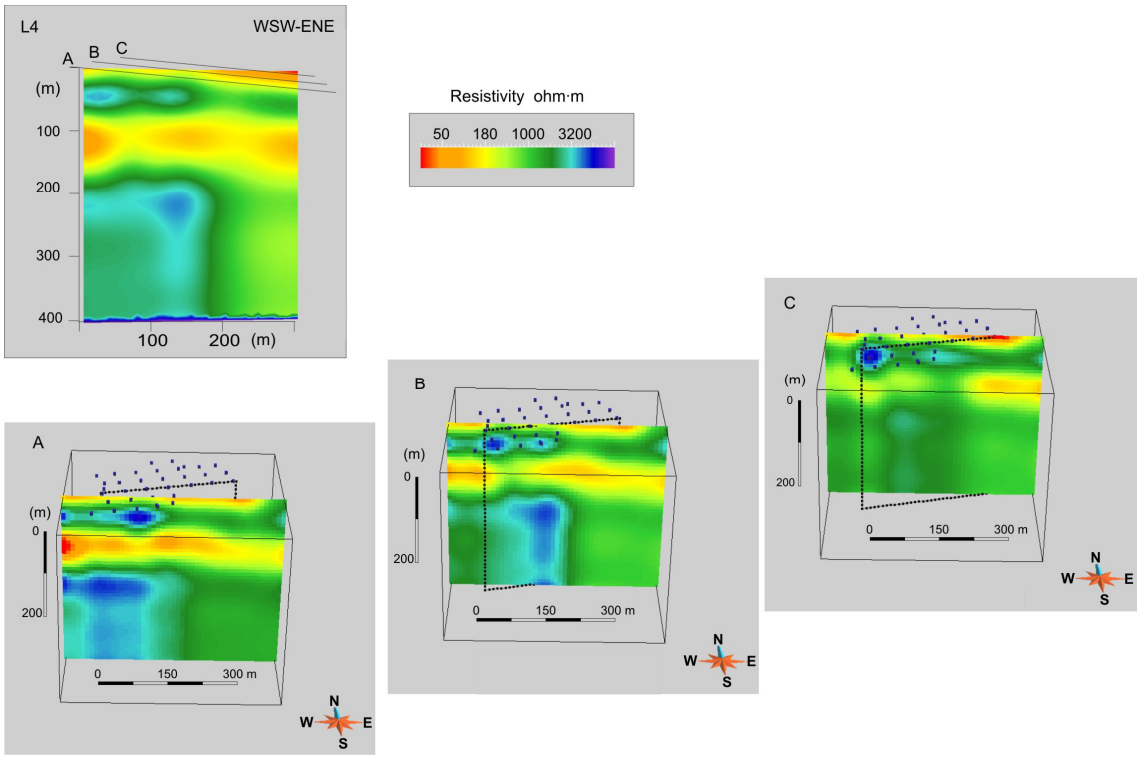

Figure 5.8: Slices derived from the 3D AMT voxet (Figure 5.7). On the top position is shown line 4 and the position of A B and C slices shown below. Line 4 cut A, B and C profiles in an oblique direction.

Zone 1, from surface to 15-30 meters, shows the most conductive zones that range from 50 ohm·m. Shallow position and resistivity values indicate the development of weathered soil and fractured rock areas containing clays and fluids. Although low resistivity values dominate on the shallow surface higher values also exist (up to 180 ohm·m), as seen by the low resistivity transparency image in surface gaps (Figure 5.7 B), implying less water or a less developed weathering layer.

Zone 2 is another relatively low resistivity zone, observed roughly from 80 to 150 m depth where resistivity values range from 100 to 180 ohm·m. Morphologically this zone is not continuous and not strictly horizontal (Figure 5.7 B). Position, shape and continuity are well imaged on the vertical slices that intersect L4 (Figure 5.8) where the relatively low resistivity domain decreases and diminishes northwards. Enhancing this latter statement the low resistivity transparency image (Figure 5.7 C), shows the high resistivity domain (zone 3) that extends its shallow position in depth to the northern part of the study area.

The Zone 3 high resistivity domain has two main depth zones from 30m to 80 m, and from 150 m to the end of the model.

The relatively low resistivity structure (zone 2) can be explained due to a 1) fracture zone related to the Rhine graben development used as a fluid circulation path, and/or 2) related to other granite intrusions and a change in mineralogy and weathering style. Conversely, middle and high resistivity values from 320 to 10000 ohm·m are predominant from 30 to 70 m (zone 3) and also in depth from 200 to 400 m. Interpretation must be related to a less fractured and weathered rock domain in comparison to the lower resistivity areas.

5.4.5. Sensitivity analysis

Model sensitivity of key structures was taken into account to ensure the presence or not of the main geoelectrical targets. In the 3D model, zone 2 was an unexpected result, because of the previous 2D models where a low resitivity structure was not obtained, therefore sensitivity tests has been conducted. Different 3D models with and without the low resistivity area were built to examine the data fit with new alternative models. While testing a model without the low resistivity zone (model B) creating a uniquely high resistivity deep zone (model B on Figure 5.9), model responses are shown to be too resistive (Figure 5.9). Model B fits the determinant of the impedance tensor with a total RMS of 6.4 in the resistivity and 1.9 in the phases considering 5% of error floor impedance components, and thus showing a poor fitting than the final model . Furthermore, 30 m thick horizontal layer of 320 ohm·m was included into the model. Given that this is a coarse simplification of the estimated low resistivity structure, the new models don’t fit all the curves and 320 ohm·m is still too resistive for most of the sites.

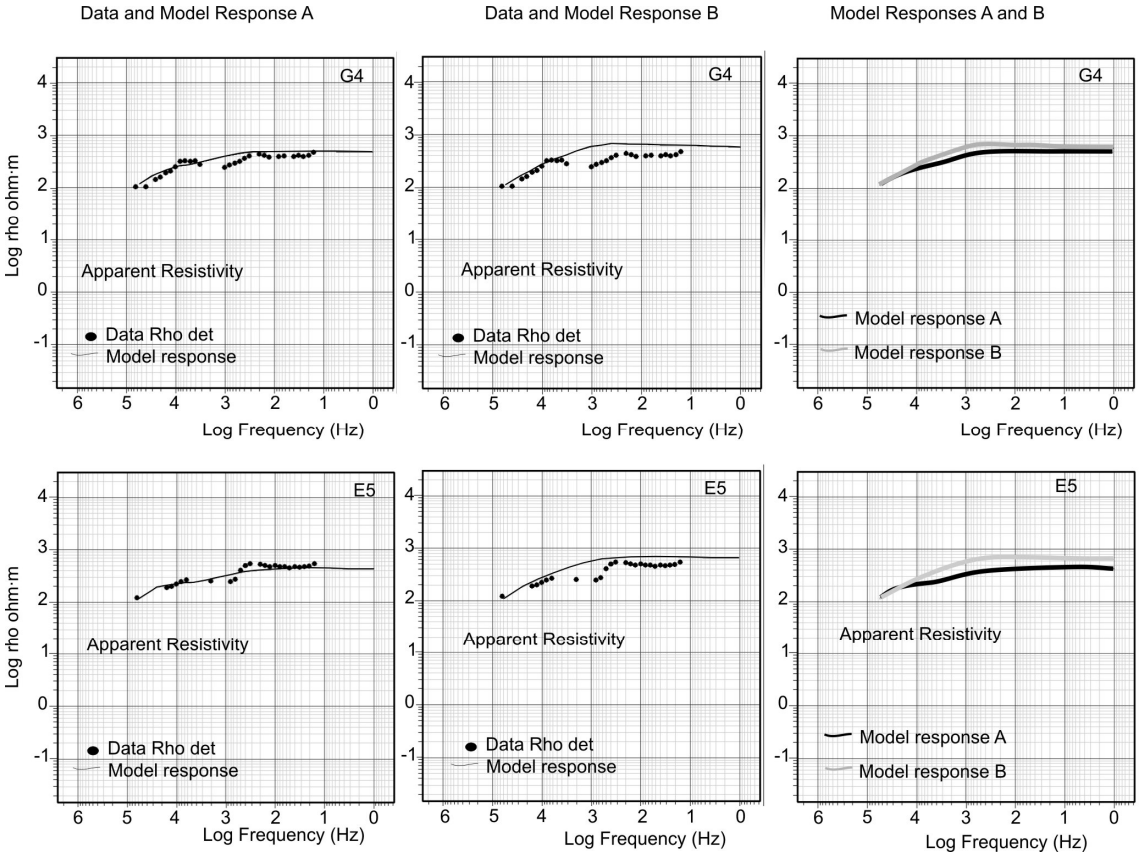

Figure 5.9: Sensitivity test of zone 2 low resistivity domain on two selected sites G4 and E5. From left to right is shown: data and model responses from the final model A, data and model responses from model B where the low resistivity zone in depth has been replaced with 1000 ohm·m high resistivity values, and a comparison of model A and model B responses.

5.5. AMT and Surface DC on the frequency domain

Integration of various methods to understand the complementary nature of them can be problematic. AMT and DC methods provide apparent resistivity of a determined volume of soil, thus, data and models may be consistent and comparable in the overlapped measurement zones. Since the DC surface survey electrode spacing was 3 and 5 m, and AMT frequencies were between 92 KHz and 10 Hz, it was obvious that DC gives shallow and detailed resolution in comparison with the AMT models. However, the complementary nature of both methods was not as evident regarding which volume is measured by each method. Comparison of both techniques can be done in the data space or in the model space (by comparing models).

5.5.1. Data space comparison

AMT and DC Line 4 was considered a good example for performing effective comparison of different methods and highlights the possibility of integration of both datasets to border the scale range while keeping shallow resolution (Figure 5.10). The DC apparent resistivity-pseudo-depth profile was transformed to the frequency domain.

A empirical law was proposed by Meju *et al.* (1996) and Meju (2004), which was derived from numerical modelling studies and by comparison with large amounts of experimental data from DC resistivity TEM and MT depth tests at coincident location in different environments. Conversion of AB/2 used in DC to the frequency domain is done by:

$$L = 355.9\sqrt{T\rho_a} \tag{5.1}$$

where T refers to the period, and L to AB/2 (one half of the electrode array length). Thus, T or its inverse, frequency, can be derived from every ρ_a and L measured, to built up a frequency pseudosection.

Regarding Figure 5.10, it can be assessed that DC data display a frequency range from 10^4 to 10^6 Hz where the majority of the data is located between 10^4 to 10^5 Hz. AMT frequency data range from 10^5 to 10 Hz. DC frequency transformation provides an irregular data distribution, especially in the top and bottom limits. This is well understood by the differential current penetration into differently resistive materials as related to depth-frequency attained. Overlap on the frequency records among AMT and DC data sections are around 10^4 to 10^5 Hz.

The DC profiles are composed of high density data in comparison to AMT data. In spite of this, both sections present the same resistive tendencies and correlate well. In particular, the overall resistivity changes are easily retrieved for the less detailed AMT data. For instance, the high resistivity zone on C4 or the low resistivity area on the shallow surface around G4 and H4 soundings.

Figure 5.11 shows the F4 AMT sounding with the corresponding DC resistivity sounding, illustrating another way of seeing the frequency overlap. Using both datasets of F4 soundings in the same scope, provides evidence for the enlarging capability of the frequency range.

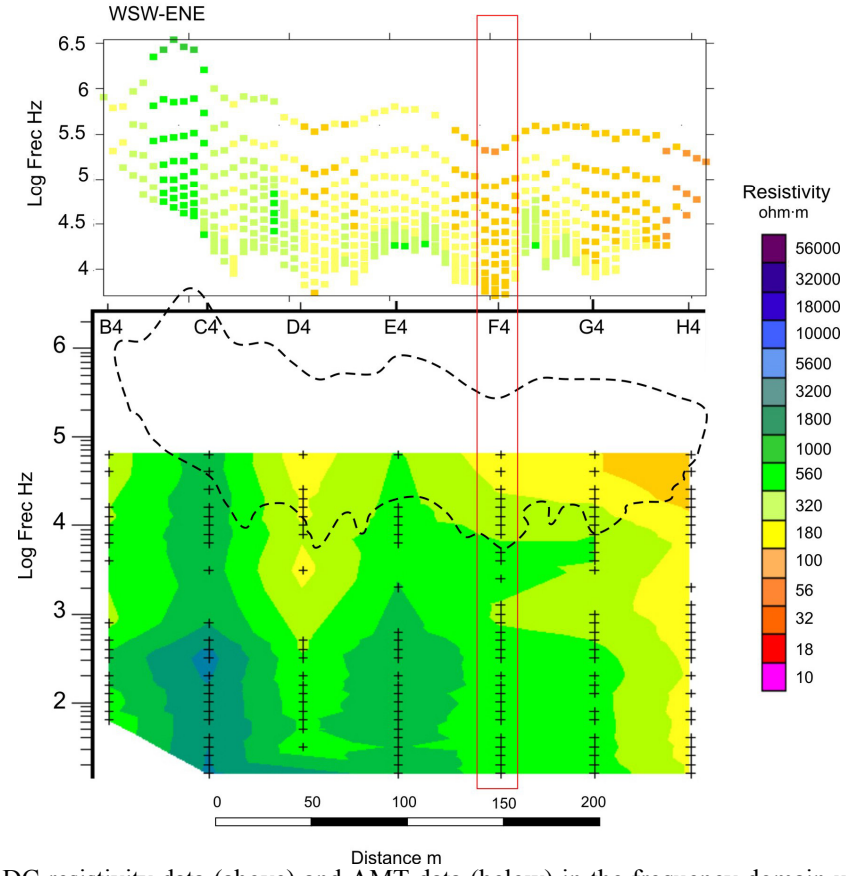

Figure 5.10: DC resistivity data (above) and AMT data (below) in the frequency domain using the same resistivity scale. Overlapped dashed area on the AMT pseudosection corresponds to the DC data scope showing relationships between both data sets. Rectangle is located on F4 sounding analyzed in more detail in Figure 5.11.

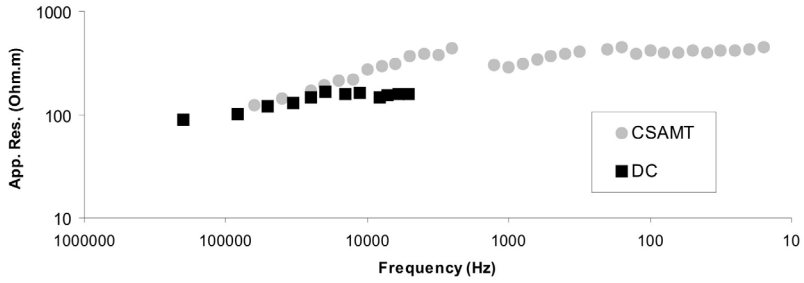

Figure 5.11: F4 DC resistivity data (black) in the frequency domain and AMT data (grey).

5.5.2. Model space comparison

Figure 5.12 presents L4 as a DC inverse model, the 2D AMT model and the coincident 3D forward model slice. The DC model was calculated by Behaegel *et al.* (2005) using the

Res2dinv code (Locke, 1999). The 2D AMT model was generated using the DetREBOCC code by inverting the impedance tensor determinant with an initial 100 ohm·m halfspace model and a 5 % error floor on the impedance components. 3D AMT model technical details have already been presented.

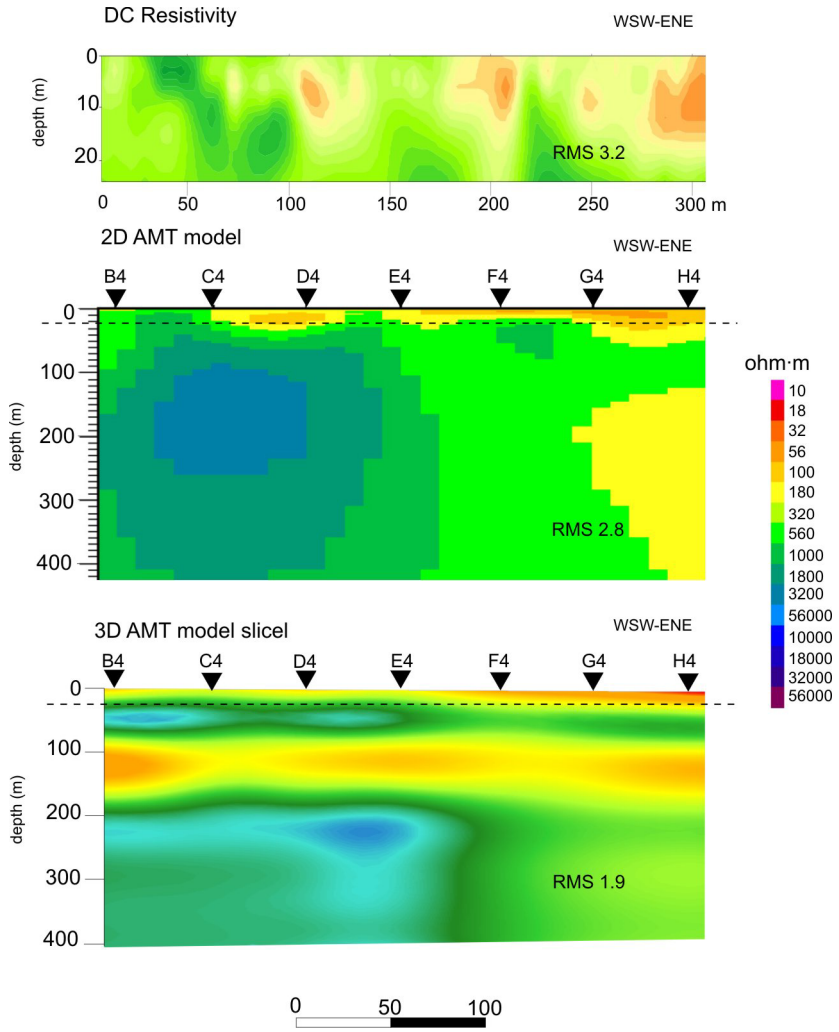

Figure 5.12: Line 4 2D DC resistivity inverse model (above), 2D AMT inverse model (middle) and 3D AMT model slice (below). 2D and 3D AMT models show the main discrepancies in zone 2 structure. Dashed line shows DC surface depth over the AMT models.

The principal similar surface geoelectrical tendencies could be retrieved from the three models, which are variations in the shallow low resistive zone related with water and clay in the weathered regolith. However, the DC model provides more detailed shallow geoelectrical targets.

Deeper structures must be regarded in the AMT models. Nonetheless, 2D and 3D AMT models present differences. 2D AMT and 3D AMT slices differ mainly in the low resistivity zone in depth present on the 3D model. 2D determinant models provide a smoother model integrating this geoelectrical structure into a high resistivity domain. As seen in section 5.4.5, the low resistivity zone is required to be included on the model to fit the data. Thus, the 3D model provides a better approach to imaging the deeper geoelectrical structures. In addition, the 3D slice improves the RMS of the 2D model, fitting the determinant of the impedance computed as the RMS average of each sounding of the profile.

Models derived from the combined use of both techniques, DC and AMT, may attain greater depth than those only using DC data. At the same time, resulting joint models may provide higher resolution in the shallow subsurface than the resolution obtained using only AMT data.

5.6. Conclusions

The main conclusions of the hydrogeophysical AMT experiment carried out on La Soutte are the following:

The AMT survey carried out on la Soutte was done over a 2D grid with 50 m of distance between soundings. Geology, frequency pseudosections, and dimensionality analysis coincide on the three-dimensionality behavior of the geoelectrical structures of the area. Therefore, data dimensionality induced the generation of a 3D AMT model.

The AMT 3D forward model obtained through a trial and error model-data fitting process shows 3 different geoelectrical structures that can be associated with different hydrogeological behaviors. The conductive top layer of the 3D model can be associated with a weathered soil developed on a fractured unit where fluids and clay materials are highly present. A more resistive zone corresponding to a less altered domain seals the near-surface top layer. Beneath, around 100 m deep, there is another conductive layer probably related to fractures or geologic discontinuities used as the fluid circulation path, sealed again for a more resistive and more homogeneous domain.

3D modeling has shown for be the correct appraisal to La Soutte geoelectrical structures. Although 3D and 2D determinant mode models retrieve similar structures, 2D models tend to be more regional and smoother. In particular, it is seen that the low resistivity zone 2 cannot be modeled in 2D. 3D sensitivity tests have proved the existence of this low resistive zone to correctly fit the data.

Work scale and resolution of the AMT soundings allows the study of aquifers from just several meters up to hundreds of meters depth, linking shallow dynamics with deeper parts of the fractured aquifer systems. DC profiles allow obtaining detailed images of the upper structures while the AMT shows coarser resolution but images deeper structures. Complementarities of DC and AMT methods have been proved on the DC frequency domain transformation. New perspectives to integrate both datasets to broaden either the resolution and/or work scale could be assessed by using joint inversion techniques.

Chapter 6: Hydrogeophysical application: Spring Valley, Nevada, USA.

This chapter presents the main results of a collaboration with the Geophysical Unit Menlo Park (GUMP research group) from the United States Geological Survey (USGS), where I spent three months as part of the international exchange program granted by the Spanish Education Ministry. The hydrogeophysical research carried out was in Spring Valley, in the Nevada desert, and was aimed at providing a structural framework for water resources exploration and hydrological modeling.

The area of study is a large watershed scale basin with a complex geological environment. AMT, gravity, and magnetic data were available to map the structure and sedimentary infill in a typical Basin and Range setting. Faults and stratigraphy are important targets as well as estimates of depth to basement for assessing ground water potential.

6.1. Introduction

The Basin and Range province is an arid, mountainous, sparsely populated region in the western USA. Desert regions in the western United States are experiencing increasing pressure on water resources to support urban growth (for example, Las Vegas). As the demand for reliable sources of water intensifies, desert groundwater basins are now under investigation for hydrologic potential. Spring Valley located in the central-eastern Nevada, is one of these valleys under investigation (Figure 6.1). This valley has had no significant groundwater pumping and as a result there is no hydrologic model available to predict groundwater withdrawal potential. In addition, there are few detailed geologic or geophysical studies that can be used to define the geologic structures important for a hydrogeological model of the valley due to the lack of surface expression of these targets. Consequently, geophysical data has been considered to provide the desired information in this exploration phase, funded by the Southern Nevada Water Authority (SNWA). Six AMT profiles were conducted on the western margin of Spring Valley (McPhee *et al*., 2006) that are complemented with gravity data and ground magnetic data

measured along the profiles. Here, we will focus on the AMT data and its comparison with gravity and magnetic results.

6.2. Hydrogeological setting

The study area is located in central-eastern Nevada in the Basin and Range geological region (B&R). B&R has a well documented geologic history from Precambrian throughout the Phanerozoic. A complete geologic summary, on which the following description is based, is found in Hose *et al.* (1976), Stewart (1980, 1987), Gans *et al.* (1985).

The geological record of the region has been affected by three main tectonic events: the Antler orogeny (late Devonian to Early Mississipian), the Sonoma orogeny (late Permian to Early Triassic) and the Sevier Orogeny (late Mesozoic) which, at about 17 My, changed into an extensional regime. Present day morpho-strucutre of B&R is the result of this late Cenozoic extension that consists of a complex horst and graven system due to active normal faults. Movement resulted in the relative uplift of the N-S linear segments to form the mountain ranges and the relative sinking of adjacent segments to form the valleys, and, consequently, continental sediments were trapped in fault related basins. The amount of valley fill ranges from few hundred of meters to more than 3000 m. The study area, Spring Valley, is one of those north-south trending valleys surrounded by high mountain ranges (Figure 6.1,Figure 6.2, and 6.3).

Groundwater in the Basin and Range province is organized into valley-regional systems where it can flow between adjacent topographic ranges and basins, along fractures and fault zones. Primary aquifers units include Paleozoic carbonate rocks, Cenozoic volcanic and sedimentary basin fill units (Plume, 1996; Mankinen *et al.*, 2006).

Spring Valley is a 180 kilometer long and ~20 km wide north-trending valley located between north-trending Schell Creek Range and the north-northwest-trending Fortification Ranges on the west, and the north-trending Antelope Range, Snake Range, and Linestone Hills on the east (Figure 6.1 and Figure 6.3 Gary Dixon unpublished data). Ranges lithologies and basin basement are composed from Precambrian quartzite rocks to a Paleozoic/Mesozoic thick sequence of deep marine sediments (Middle Cambrian to Lower Triassic), basically composed of limestone, dolomite and shales. During the Lower Triassic time continental margin shifted

westward and the sea retreated to shallow depths and began the continental deposition (Stewart, 1980). However only minor records of continental sediments exist due to posterior erosion.

Pre-Cenozoic basement in the study area also include intrusive igneous rocks exposed along the southern Snake Range. A major volcanic episode began during early Oligocene when voluminous ash-flow eruptions resulted in the formation of collapse caldera complexes (e.i Indian Peack Caldera Complex).

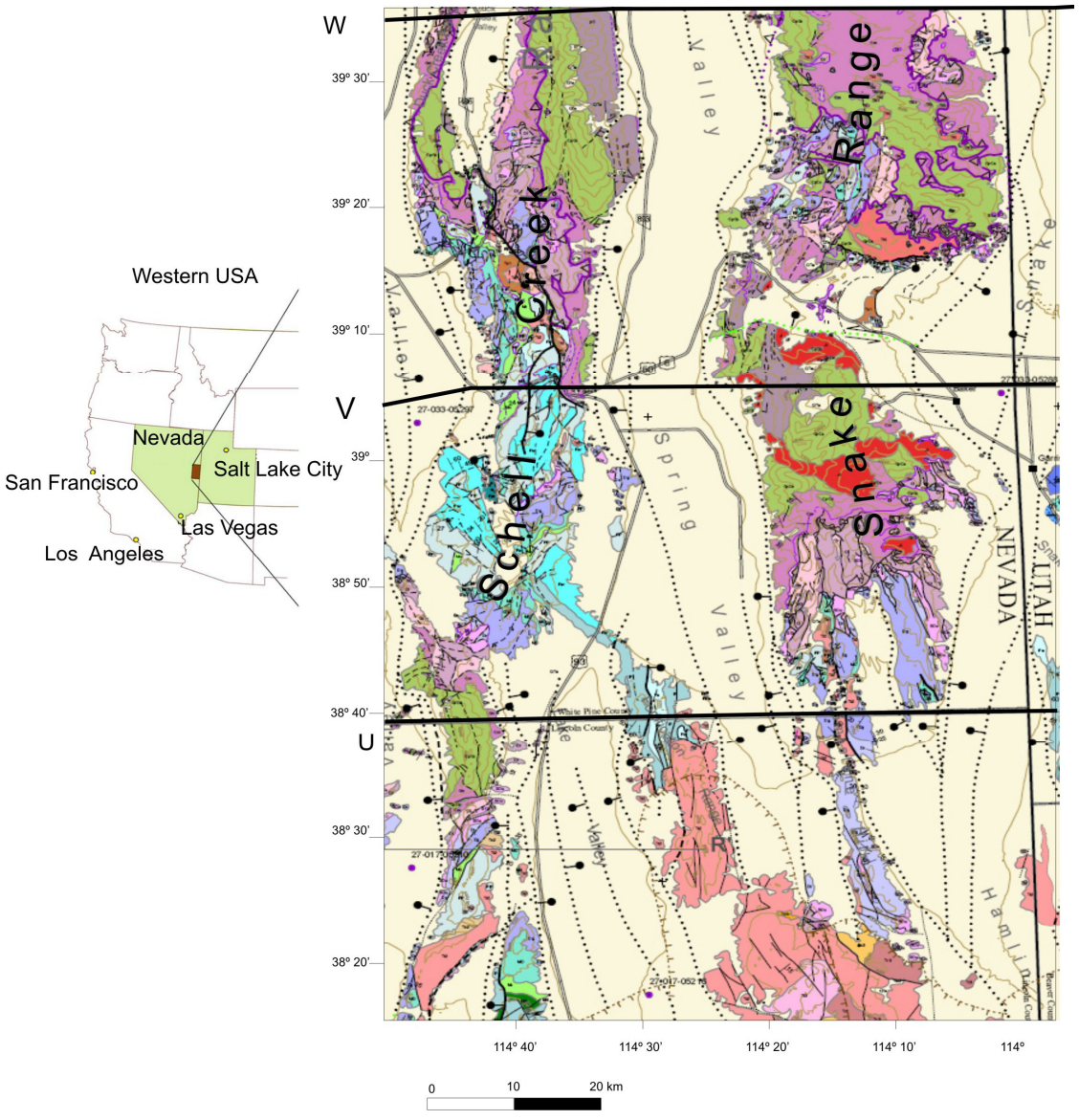

Figure 6.1: Geographical situation of the study area and its geological map, centered on Spring Valley and its surrounding Ranges, central eastern Nevada USA. U, V and W black lines correspond to geological cross sections (part of which are showed in figure 6.2) (Gary Dixon unpublished data).

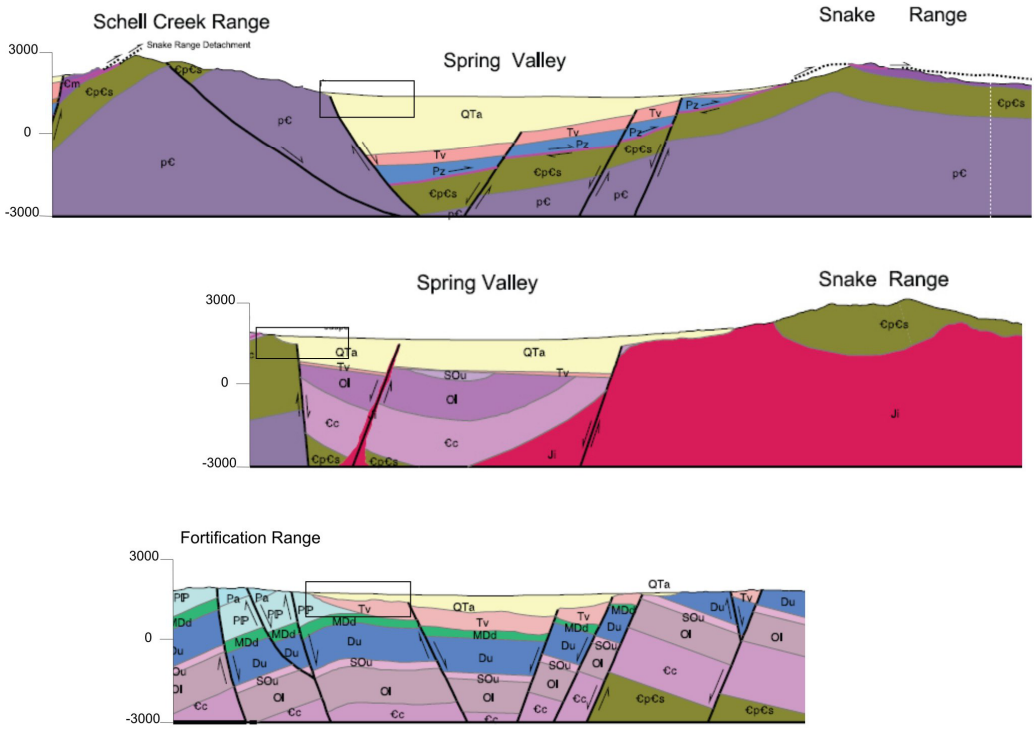

QTa	Quaternary and Tertiary basin-fill deposits
QTb	Quaternary and Tertiary thin basalt flows and cinder cones
Tv	Tertiary volcanic ash-flows, flows and ash-fall tuffs
Ts1	Tertiary fluvial and lacustrine sediments
Ti	Tertiary intrusive rocks
TKi	Tertiary-Cretaceous intrusive rocks
Ji	Jurassic intrusive rocks
Pp	Upper and Lower Permian Park City Group, undivided
Par	Permian Arcturus Formation and Rib Hill Sandstone
Pa	Permian Arcturus Formation
PIP	Permian and Pennsylanian Riepe Spring Limestone and Ely Limestone, undivided
IP	Pennsylvanian Ely Limestone
MDd	Upper Mississippian to Upper Devonian Diamond Peak Formation, Chainman Shale, Joana Limestone, and Pilot Shale, undivided
Md	Upper Mississippian Diamond Peak Formation
Mc	Upper Mississippian Chainman Shale
MD	Lower Mississippian to Upper Devonian Joana Limestone and Pilot Shale, undivided
Du	Devonian carbonate sedimentary rocks, undivided
Dg	Upper and Middle Devonian Guilmette Formation
Ds	Middle and Lower Devonian Simonson Formation
SO	Silurian and Ordovician sedimentary rocks, undivided
SOu	Silurian and Upper Ordovician dolomite, undivided
Ol	Middle and Lower Ordovician, mostly Eureka Quartzite and the Pogonip Goup
€c	Cambrian carbonate sedimentary rocks, undivided
€u	Lower Ordovician? And Upper Cambrian limestone and shale, undivided
€m	Upper and Middle Cambrian limestone and shale
€pCs	Middle Cambrian to Late Proterozoic sedimentary rocks
pC	Late to early Proterozoic metamorphosed and crystalline Precambrian basement rocks

Regional Faults

- Normal Fault
- Strike-slip Fault
- Thrust Fault
- Detachment Fault

Subsidiary Faults

- Normal Fault
- Strike-slip Fault
- Thrust Fault
- Detachment Fault

- Strike and Dip of Beds
- Caldera Boundary
- Elevation Contours - 1000Ft
- Oil Well Data Used in Cross Sections

SCALE 1:250,000

Figure 6.2: Geological cross sections W, V, and U from North to South and geological legend used as well on the Geological map in Figure 6.1. (Gary Dixon unpublished data) Western rectangles represent the ideal area that could be assessed on the AMT profiles.

Basin fill sediments deposited after B&R development consist of clastic materials derived from adjacent mountain ranges characterized by semi-consolidated to unconsolidated sands, gravels, silt and clay, where thickness varies from few meters to more than 4000 m (Gans *et al.*, 1985). Mean floor elevation of Spring Valley is about 2000 m, while Range elevations can exceed 3500 m.

Spring Valley has a closed surface drainage, resulting in two low spots or flats. In general, groundwater flows south. In the southern part of Spring Valley some groundwater flows southwest whereas the rest of it continues southeast to the low limestone Hills and then east through the Limestone Hills into Snake Valley and Utah.

6.3. Geophysical data

There are previous geophysical data, namely gravity data, and a 110 km long E-W MT transect that crosses Spring Valley (Johnston, J.M., 1992). The MT survey is a long period profile with a frequency range of 100 Hz to 0.001 Hz, where only 4 stations are located within the Spring Valley. This study provides only one frontal range basin morphology, since the main objective was to depict crustal targets, thus more detailed and shallower information along the basin were required for the hydrogeologic purposes.

During 2005-2006 several AMT surveys were carried out (McPhee *et al.*, 2006), and more future surveys will be carried out during 2007 (Figure 6.3). I was involved in the field work survey carried out in Spring 2006, and in posterior data analysis, modeling and interpretation. Two different modeling techniques have been applied. The first one (McPhee *et al.*, 2007) uses Winglink Software that uses the nonlinear conjugate gradient algorithm (Rodi and Mackie, 2001) and inverted the TM mode only. The second technique follows the working methodology used throughout this thesis, where the REBOCC and DetREBOCC code based on occam's algorthim (Siripunvaraporn and Egbert, 2000; Pedersen *et al.*, 2005) has been used: The latter methodology results are presented in the following sections.

Profiles carried out are 2-3 km long and are located on the western edge of the topographic basin, where stations were 200-400 m apart. Distances between profiles are from 5 km to 80 km which suggests that geology and basin morphology may change completely from one profile to the other (from the Schell creek Range towards the Fortification Range and the

Indian Peack Caldera complex). In addition, there is gravity and ground magnetic data collected along each profile to complement resistivity information.

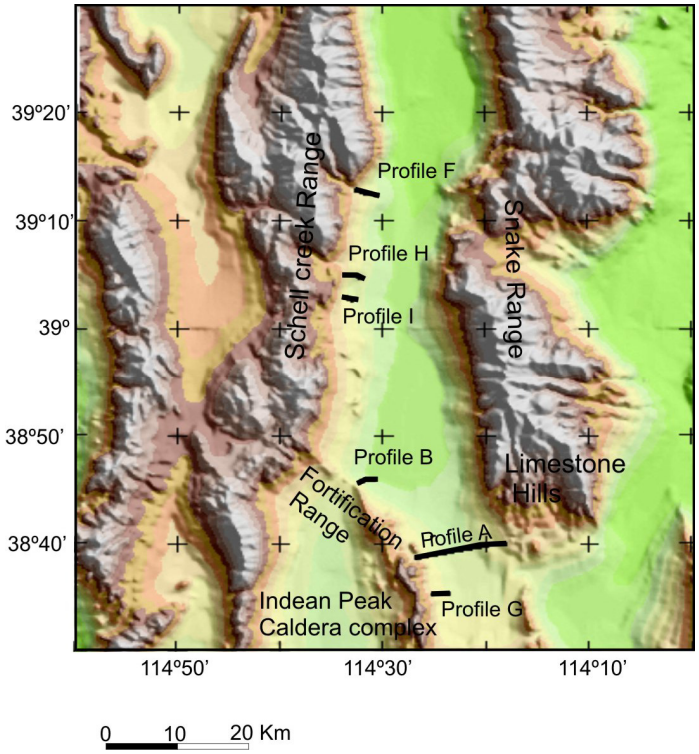

Figure 6.3: Digital elevation model centered on the Spring Valley and its surrounding ranges. Solid black lines correspond to the AMT lines acquired in the valley up to Spring 2006.

The USGS has been collecting gravity data in the region for over 20 years (Ponce, 1997; Mankinen *et al.*, 2006; Mankinen *et al.*, 2007 and references therein). More than 600 new gravity stations were collected during 2004, 2005 and 2006 within coverage gaps of the prior 5000 stations. Gravity data are located at roughly one mile spacing throughout Spring Valley and at 200 m spacing along AMT Profiles. Gravity data were obtained using LaCoste and Romberg gravity meters. The depth to basement inversion of Jachens and Moring (1990) has been used to convert the lower density contributions from the young deposits into a model of basin depth. The accuracy of thickness estimates is dependent on the initial density assigned to the basement rocks and basin fill. At several gravity stations, bedrock samples were collected to characterize density and magnetic susceptibility (Mankinen *et al.*, 2006).

Ground magnetic data were acquired along the AMT profiles using a portable truck-towed magnetometer. Magnetic data were collected using a cesium vapor magnetometer attached to an aluminum carriage, connected to the vehicle by aluminum tubing and towed

about 9 m behind the vehicle (Tilden *et al.*, 2006). Magnetometer and Geographic Positioning System (GPS) data were collected simultaneously at one-second intervals, which at an average speed of 30 mph, corresponds to approximately one measurement every 13.4 m. A centrally located portable proton-precession base station magnetometer was used to record diurnal variation of the Earth's magnetic field during the truck-towed magnetometer surveys.

6.4. AMT data and modelling

6.4.1 Data

5 AMT profiles (lines F, H ,I, B, and G in Figure 6.3) are presented in this chapter that were recorded with StrataGem EH4 equipment (frequency recording range 92000 Hz to 10 Hz). The AMT arrangement utilized north-south, west-east oriented induction coils and dipole electrodes, spaced 40 m.

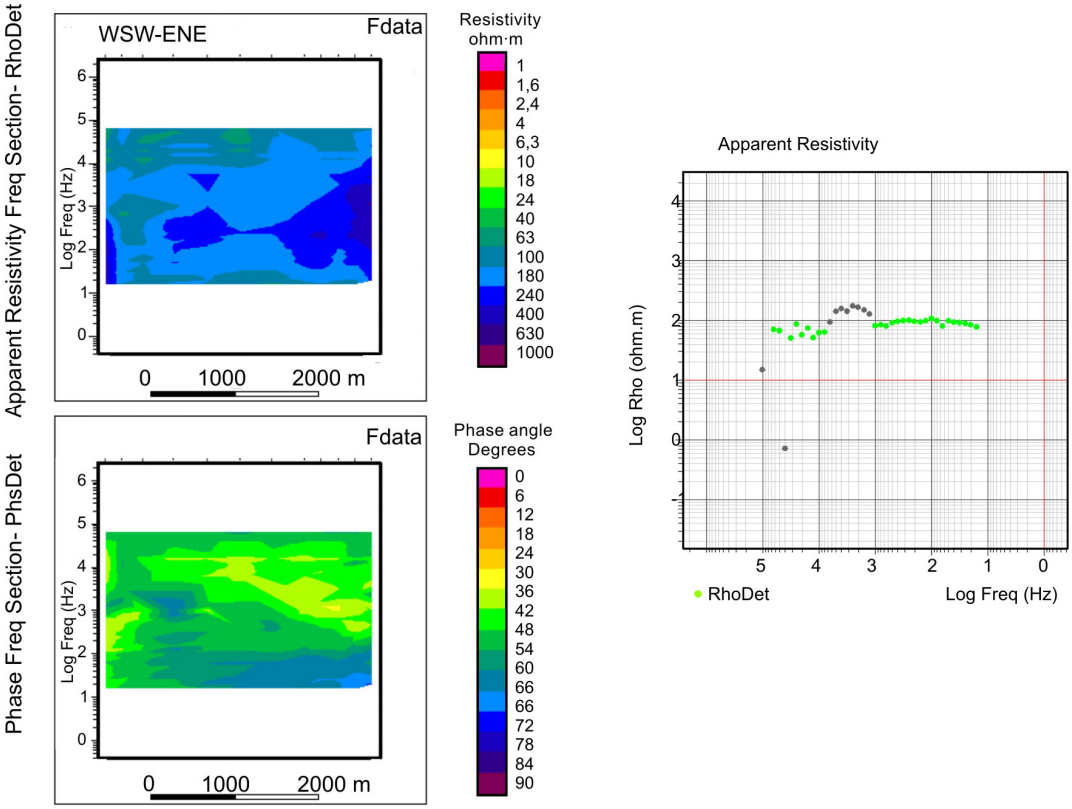

Figure 6.4: Line F apparent resistivity and phase pseudosections, where data show a non smooth shape, indicating the presence of noise. On the right, a selected apparent resistivity curve on line F is shown. Grey dots are those frequency signals removed and not used in the inversion process.

The use of the controlled source was compulsory since high frequency natural EM signal was weak in this zone. After several tests, the optimal transmitter receiver distance was between 200 and 300 m. In spite of using a controlled source in the high frequency band, cultural noise was present at specific frequencies (Figure 6.4). Affected frequencies have been removed creating frequency gaps in the apparent resistivity and phase curves in some cases. Models should represent large targets and less detailed structures in order to prevent overfitting the data and generating fake structures.

6.4.2. Dimensionality

The Basin and Range province shows a North-South valley trend as can be seen on the geologic map (Figure 6.1 and 6.3.) Expected strike direction was N-S, and surveys were conducted along lines that follow roughly W-E direction or slightly WNW-ESE depending on available space. Equipment array geometry follows a NS-EW orientation making it easy to rotate the data if a clear strike direction can be retrieved after dimensionality analysis. However dimensional analysis shows totally different results from the a priori assumption of a N-S strike direction.

Dimensional analysis of AMT data has been done using the WALDIM application (Martí, 2006; Martí *et al.,* 2004). Figure 6.7 presents dimensionality analysis of profiles F, H, I, B and G showing the mean dimension of all the data within each frequency decade. Arrows show the 2D direction of the geoelectrical structure retrieved in degrees. Arrow size is scaled inversely proportionally to the estimated angle error.

Although all profiles show mainly three dimensional geoelectrical structure, there are several 1D targets principally in the higher frequency decades (F, G and B lines) and several sites where a 2D strike could be retrieved in some frequency decades. 2D trends mostly point toward NE-SW or its perpendicular direction. A plausible explanation for the retrieved strike differing from the N-S range-front fault direction is the detailed scale of the measurement. Evidence is found on line B where the Fortification Range has an NW-SE direction shown by geomorphology, and many sites show 2D behaviour. To perform ideal MT modelling, data should be rotated before starting inversion of TE and TM modes together.

6.4.3. Modeling

Data along line B have been inverted using the TE+TM modes and using the determinant mode computing REBOCC and DetREBOCC codes. Before inverting TE and TM modes, data were rotated 30º anticlockwise according to dimensionality analysis and geologic strike direction. As seen in Figure 6.5, the TE+TM model and determinant model show mainly similar geoelectrical features. TE+TM model presents a rms of 4.7, higher than the determinant model (rms 3.07) however the difference is not relevant (Figure 6.5). The main differences are related to resistivity values and differences of depths on the order of tens of meters. For example, the basin morphology (low resistivity area), is slightly different (Figure 6.5). This comparison supports the applicability of the determinant mode as a good inversion tool given when data is not truly 2D, being is less affected by lateral inhomogeneities and finite structures, yet it reveals more regional geoelectrical structures.

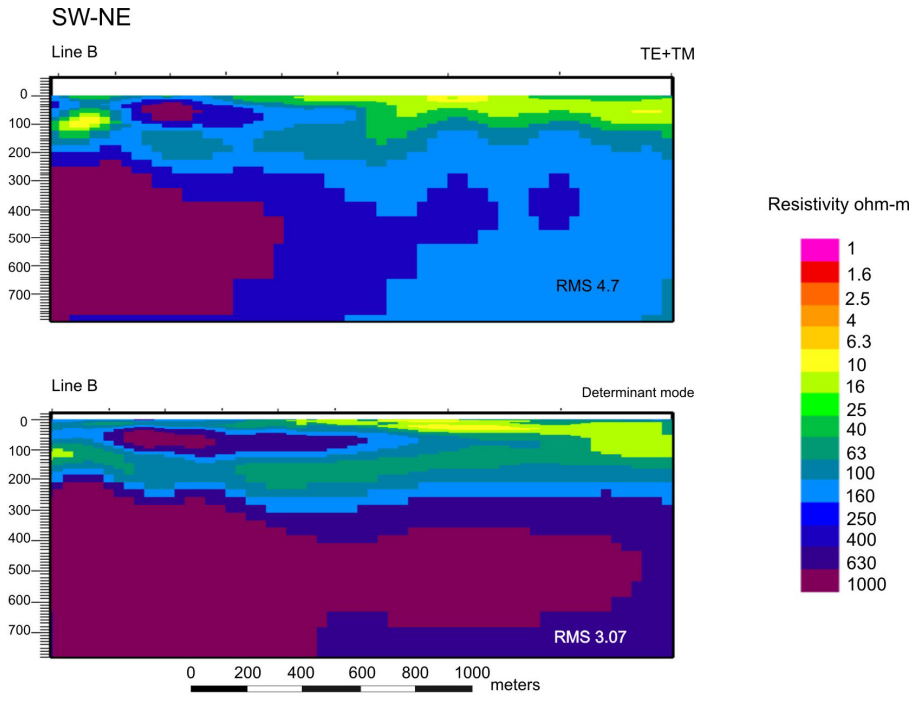

Figure 6.5: Line B models computed with TE and TM modes (above) and with the determinant mode (below).

Three-dimensional behavior dominates on all profiles except B, however given that surveys were conducted along profiles and that they are more than 5 km one to the other, cannot be computed a three-dimensional model, and thus five 2D models have been created. Inverse modeling has been done using the DetREBOCC code on all the profiles to keep coherency

among models for a better comparison. In addition, given that general structures of bounding graben faults may not be exactly N-S, the determinant mode may minimize the possibility of inclusion of 3D lateral effects, inducing artifacts. Initial models were 100 ohm.m halfspaces with an error floor of 5% of the impedance component. Reasonably good RMS values were obtained on all profiles ranging from 2.6 to 4, Table 6.1.

Model	DetREBOCC
F	3.56
H	3.94
I	3.05
B	3.07
G	2.57

Table 6.1: RMS misfit of all five profiles classed from north to south.

6.4.4. Sensitivity test

Model sensitivity of certain structures has been analyzed to ensure the presence of main geoelectrical targets imaged in the models. Sensitivity analysis has been performed similarly to that performed in the previous hydrogeophysical application chapters. Sensitivity tests increase the reliability of the models and also increase the accuracy of them with a trial and error process computing the forward problem (in this case using Wanamaker *et al.*, 1987 code) and performing data and response of the model comparison.

In all the models, the following features have been tested: 1) depth resolution, 2) basin-basement boundaries and depth where important low resistivity materials are present, and 3) the lateral and vertical variation of main resistivity changes. As an example of the procedure Figure 6.6 illustrates the sensitivity test done in model H.

6.5. Interpretation

AMT, gravity, and magnetic data are used to provide additional subsurface information for the construction of regional geologic cross-sections of structural range-front morphologies, and to detect tectono-sedimentary relationships and hydrologic connectivity in the valley. The

following differences can be recognized amongst the models: 1) different geological setting and basin morphologies, since profiles are widely separated along the long north-south trending valley, 2) different relative position above basin edge and 3) different extent of each profile over the basin.

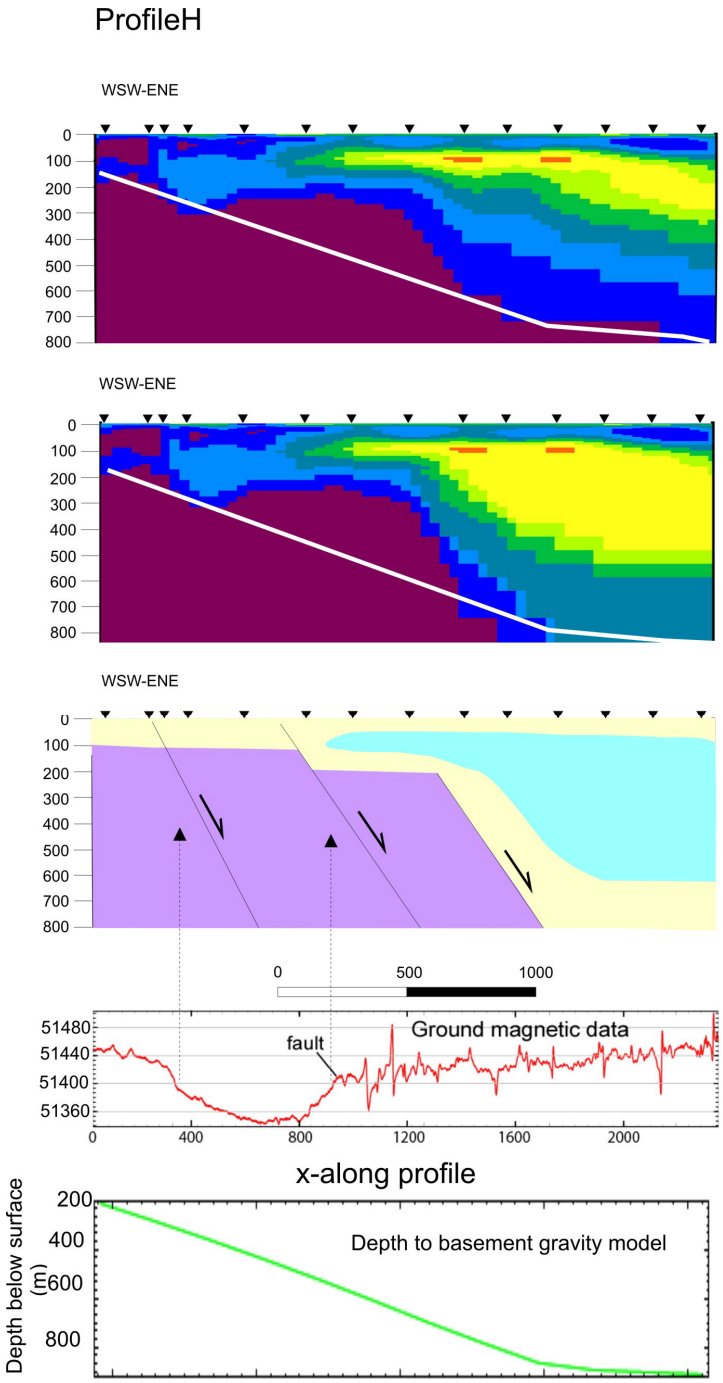

Figure 6.6: Profile H geophysical models and interpretation. Images from top to bottom show AMT determinant model, AMT selected model after performing sensitivity model, hydrogeological interpretation, ground magnetic data and depth to basement gravity model. Depth to gravity models are overlaid on the AMT models (white line).

It is worthy to mention that interpretation of AMT models has been inspired by the geological cross-sections. Despite that none of them coincide with the location of the AMT profiles, they provide valuable a priori information. Also, magnetic data and depth to basement gravity models has been considered (Figure 6.6).

Figure 6.7 presents all five profiles for a better comparison among them. For each profile the dimensionality analysis, AMT model, data and response of the model, magnetic data and depth to basement gravity model are plotted.

6.5.1 Basement and Range front fault

Models F, H, and I are located over the Schell Creek Range where the range front fault could be well defined on the AMT models. The lateral transition of relative high resistivity values to less resistive values may indicate the basement boundary. The ground magnetic data help to delineate faults. In particular, there is a distinct magnetic signature west of the range front fault that correlates with the AMT defined structure (see same magnetic signature on H and I profiles, Figure 6.6 and Figure 6.7). Basin edge morphology as one main bounding graben fault can be observed, where the main differences among graben bounding faults in the models are their positions over the range. For instance, basin morphology of line B, located over north Fortification range, shows a more gradual deepening, however this morphology is due to its position over the range and shallow basin depth.

Line G show a totally different resistivity scheme when looking for a range front fault and a relative high resistivity basement on the western side of the profile. Western end stations are located in the Indean Peack Caldera complex where a massive low resistive area related with the ash-flow volcanic sediments that extends to depth is recognized. Quaternary basin fill is clearly differentiated from the volcanic ash-flows due to resistivity changes.

Gravity models provide an estimate of depth to Pre-Cenozoic basement rocks. Although basin morphology interpreted from AMT and gravity defines similar overall shape, it presents depth discrepancies (Figure 6.6 and 6.7). Gravimetry basin depth in comparison to AMT basement is both shallower and deeper, thus a general dependence rule cannot be extracted here. Line F presents basement depth much shallower than AMT basement, conversely on lines H, I and B, gravity basement depth is located deeper. In these latter cases, the most critical discrepancies are observed where AMT basin presents lower thicknesses (see, for instance, Figure 6.6 where line H AMT basement estimate is shallower). In addition gravity and AMT

models disagree on detailed basin shape; gravity models show a constant deep basin whereas AMT presents a main fault describing the basin morphology. In a totally different context, AMT basement depth is not attained on line G, and the gravity model shows basement depths of more than 800 m.

Gravity models produce depth to basement estimates that are more sensitive to general shape than depth. In addition gravity models may provide little accuracy given that volcanic materials cannot be distinguished by gravity data alone considering density may be comparable to basin fill sediments.

6.5.2. Basin fill- aquifer considerations

Basin infill resistivity varies from 10 to 1000 ohm·m, however basement and sediments can be clearly differentiated. Anomalously high resistivity (>400 ohm·m) areas are interpreted as calcrete zones located in general in the shallow surface. Considering 100-200 ohm·m as mean basin fill resistivity value, lower resistivity values around 40 ohm·m can be interpreted as saturated zones. Resistivity values of 10-20 ohm·m could be explained by clay content of the detritic materials.

Interpreted saturated aquifer zones show elongated morphology along the basin edge increasing in thickness towards the valley center in models along lines H, I, and B. Potential thickness of the aquifer zone ranges from 100 m to 500 m, with top edge depths of 25 m to more than 200 m, depending on the model (F, H, I, and G). For instance, model B shows shallower values, conversely model F shows two low resistivity zones, around 100 m depth and at 500 m depth, which can also been interpreted as volcanic materials or/and a deep aquifer zone(Figure 6.7).

Connectivity through fractured and fault zones within the valley ranges is another key parameter of the exploratory phase of potential water resources. Giving that no lithological calibration with the AMT signal has been done on lithology or water content in the basement, it is difficult to recognize these specific targets on AMT images. A special characteristic in the basement is recognized on the line B geoelectrical model. Near outcrops reveals alternating layers of limestone (high resistivity) and shale (lower resistivity) and thus could suggest that AMT interpretation of the relative low resistivity within the basement could be related to the shales, however water flow through a highly fractured zone could also be plausible, since fractured carbonates in the area are considered good aquifers.

Volcanics also have been suggested to be potential aquifer zones. Volcanic materials have been interpreted on line G, and show low resistivity values. However no information about its water content has been retrieved. In addition any meaningful resistivity change that could be used to infer saturated or unsaturated ground is unknown at this time.

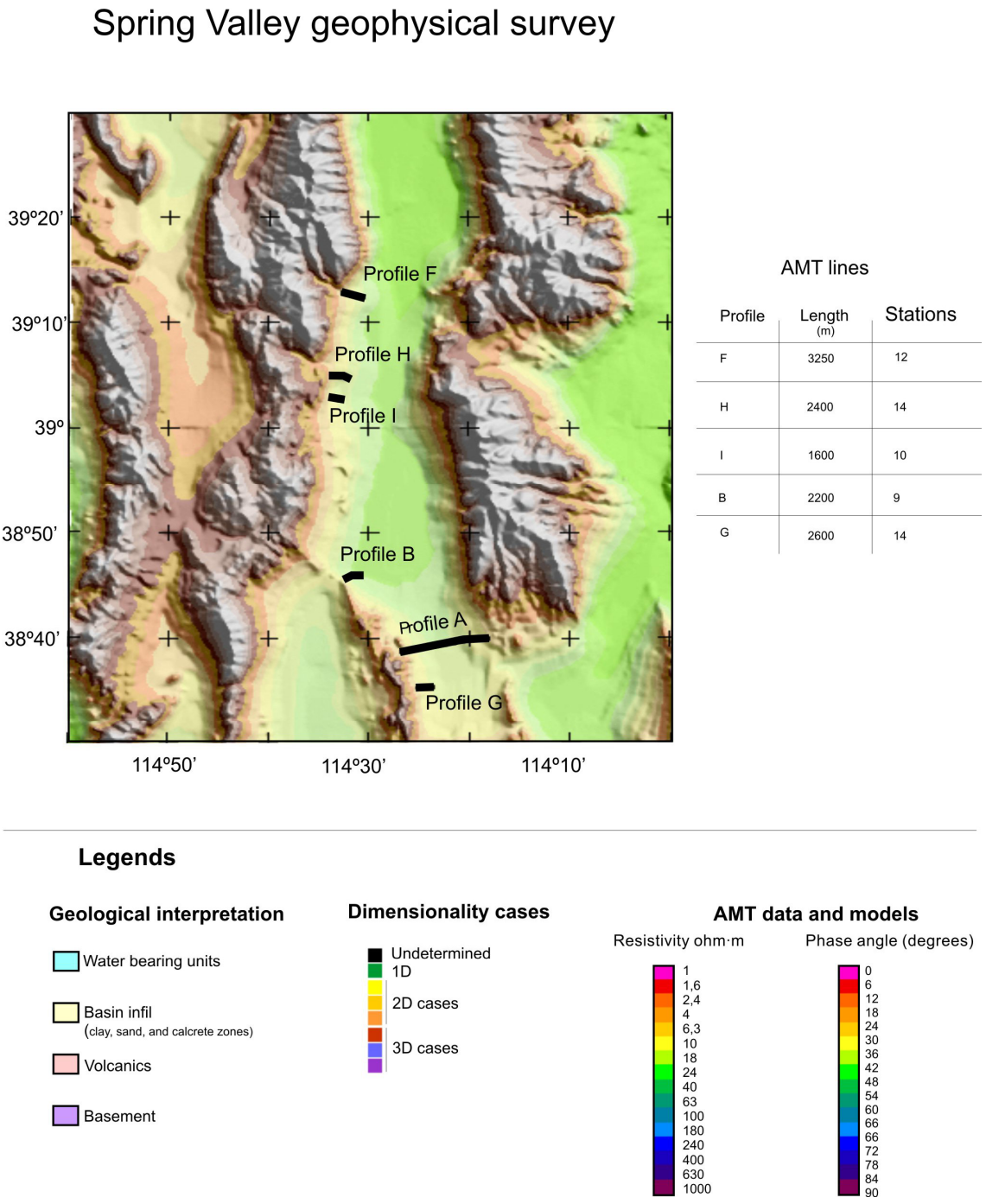

Figure 6.7: Spring valley geophysical survey; models and interpretation. On the left geophysical profiles location and the used legends for the right side of the figure. On the right F, H, I, B and G data and models are plotted. From bottom to top is shown AMT dimensionality analysis, AMT model response and AMT data (whose comparison show the goodness of the models), AMT model, depth to basement gravity model, ground magnetic data, and geological interpretation.

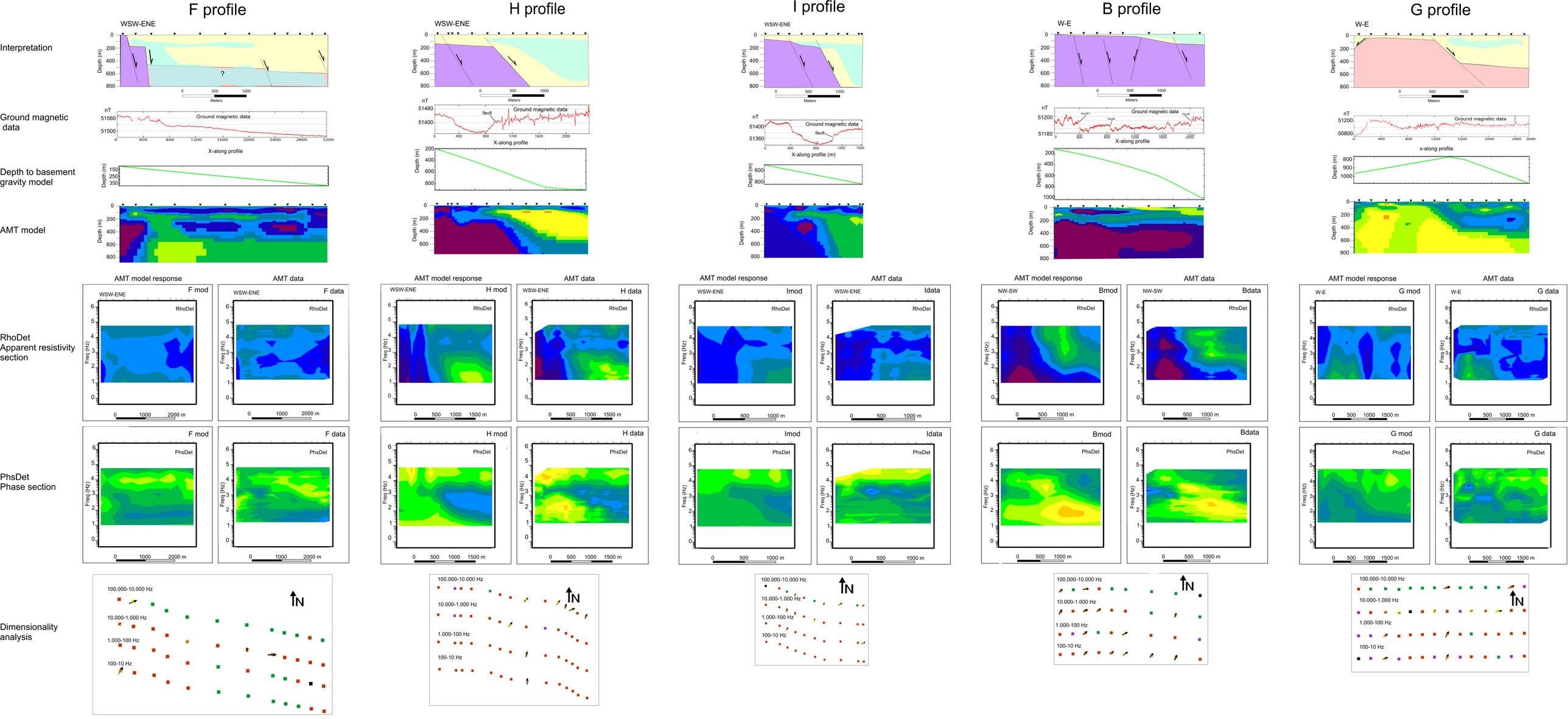
F profile
H profile
I profile
B profile
G profile
Interpretation
Ground magnetic data
Depth to basement gravity model
AMT model
RhoDet Apparent resistivity section
PhsDet Phase section
Dimensionality analysis
WSW-ENE
W-E
NW-SW
Depth (m)
Meters
nT
Ground magnetic data
fault
X-along profile
X-along profile (m)
x-along profile
AMT model response
AMT data
F mod
F data
H mod
H data
Imod
Idata
Bmod
Bdata
G mod
G data
RhoDet
PhsDet
Freq (Hz)
100.000-10.000 Hz
10.000-1.000 Hz
1.000-100 Hz
100-10 Hz
N

6.5.3. Summary of material resistivities

Basin fill sediments may comprise the overall grain sizes (gravel, sand, silt and clay) where saturated and unsaturated materials are distinguished (Figure 6.7) due to resistivity changes. Basement rocks reflect higher resistivities in general, given that they are composed of quartzite, limestone, dolomite and shales (may be less resistive), which could transmit water throughout fault and fractures. Volcanic ash flow tuffs show resistivities of 10-20 ohm.m, however, it cannot be stated if they are saturated or unsaturated.

Lithology	**Resistivity ohm·m**	
	Saturated	Unsaturated
Basin fill sediments	10- 40	100-1000
Volcanic	?10-20	?10-20
Basement	~ 100 ?	> 600

Table 6.2: Summary chart of lithologies and interpreted resistivity

6.6. Conclusions

Spring Valley has been investigated for hydrogeological modeling of the bounding range-front faults and potential aquifer thickness using several different geophysical methods. This chapter has been focused on the data analysis and modeling of five AMT profiles acquired on the western edge of the Spring Valley basin. StrataGem EH4 equipment has been used because its frequency range was ideal for the accuracy and required investigation depth.

AMT data analysis reveals two implications on the posterior models created: 1) Dimensionality analysis shows mainly three dimensional behavior, and 2) There is cultural noise in the area. Noise effects on the data provide a less detailed geoelectrical model, however main regional targets could be efficiently retrieved.

Models have been created using the DetREBOCC code using the determinant mode and testing the sensitivity of the main geoelectrical targets as a forward process. Due to the modeling process and noise effects, more regional models have been obtained.

Interpretation of the AMT models has been based primarily on the geological information available, using the ground magnetic data and, to a lesser degree, the depth to basement gravity models. Main graben range-front faults are imaged through the AMT models, given that basement rocks present higher resistivities than basin infill sediments. In addition, basin aquifer zones are observed due to low resistivity values of the valley sediment infill.

The ongoing Spring Valley Project is currently focusing on surveying the eastern side of the Spring Valley basin. In addition SNWA is drilling exploration wells that can be used to calibrate the AMT models in the future.

Chapter 7. Conclusions

The present thesis has been divided in two parts. In the first one, the state of the art of the geophysical methods and methodologies used on solving hydrogeological problems has been widely reviewed. The second part comprises three multidisciplinary case studies, where AMT has played an important role on the hydrogeophysical appraisal of the aquifer systems. A summary of the main conclusions and contributions of both parts is presented in this chapter.

Hydrogeophysics as a multidisciplinary tool for aquifer appraisal

Hydrogeophysics is a novel discipline that combines hydrogeological and geophysical data to improve groundwater system's knowledge. From the hydrological perspective, diverse strategies on using geophysical methods could be performed. The choice of which particular techniques or acquisition approach to use for a particular investigation depend mainly on the objective of the investigation relative to the sensitivity of the geophysical method, the desired resolution, conditions at the site, time, funds, and computational resources available for the investigations, and availability of previous data.

Multidisciplinarity, to improve hydrogeological models, is one of the main important goals of hydrogeophysics. Hydrogeological data may be considered as the hard data that controls and calibrates geophysical data, and thus geophysical models have to be in accordance with the hydrogeological data as the best assurance of good, reliable models. Geophysical data can provide more spatial and temporal-continuous information to complete hydrogeological punctual data. Therefore, it is obvious that both disciplines have a meaningful potential to complement each other.

Among the diverse geophysical methods used on aquifer appraisals, electric and electromagnetic methods are the most commonly used to characterize hydrogeological parameters and processes. Electrical resistivity and dielectric permittivity are highly dependent on material, porous structure, water content and its quality. On the other hand seismic,

magnetometry and gravity data could assist in characterizing the geological structure that controls the flow defining boundaries and internal structure of the aquifer systems.

Audiomagnetotellurics

Sensitivity to groundwater properties and processes, with a wide range of study length scales, and being a true 3D geophysical technique, makes audiomagnetotellurics (AMT) ideal for aquifer investigations.

The controlled source. Cultural noise is one of the main concerns on AMT, specifically near populated areas where environmental problems are settled. In order to improve the signal-to-noise ratio, the employed AMT equipment uses two perpendicular horizontal magnetic dipoles as a controlled source. However, care has to be taken to avoid source effects being too close to the source to fulfill the plane wave assumption. EM near field effects have been recognisable on the experimental field test, where apparent resistivity curves present negative slopes (45º degrees) and the phase angle stands up to 90 degrees.

Survey design. Computing synthetic data either in 2D or 3D, is a crucial step before the survey can be started. Prior survey models should be queried for better survey planning. They will provide better understanding of structure resolution and investigation depth of each particular environment. They will also ensure that the study objectives can be achieved.

Dimensionality analysis. AMT data dimensionality analysis has to be performed before multidimensional modelling procedures. Case studies presented show three-dimensional environments. Nonetheless an acceptable 2D modelling approach using DetREBOCC code has been demonstrated. This mathematical strategy uses the impedance tensor determinant that gives its property of being invariant under rotation. Hence it is useful when AMT data is not truly 2D. Good confidence on the created 2D determinant models has been attained on all case studies; that is, proven by 1) lithological and hydrochemistry validation of the 2D models and 2) the similitude shown between 2D AMT models, and the corresponding 2D slices of the 3D AMT inverse model.

Structures resolution. Sensitivity analysis of main geoelectrical targets has to be checked before final acceptance of the models. Working by an iterative trial and error forward

process will provide a better geophysical data-model fit. At the same time adjusting hydrogeological or other geophysical data may constrain the equivalence problem. Sensitivity of the key geoelectrical structures of Tordera 2D and 3D AMT models, La Soutte 3D forward model, and Spring Valley 2D models has been analysed to improve reliability on the final models.

3D models. The correct approach to three-dimensional geoelectrical environments is to build up 3D models. Either 3D forward or 3D inverse models are valuable tools for more complete aquifer appraisals. A 3D model provides a global view of properties and dynamic processes developing on every specific environment, whereas 2D models only provide limited and partial information. Although 3D forward and inverse modelling is a time consuming process due to high number of computational parameters, an initial model using the interpolation of the 1D AMT models has proven to be time efficient. Initial models aid the mathematical algorithm in seeking a 3D model that fits the data. Finer meshes, more periods and more stations would improve the presented models, but computational time would have experienced a substantial increase.

AMT monitoring. AMT method has been proven to be sensitive enough to image dynamic changes of hydrochemical changes of an aquifer system. In particular, AMT has been capable of monitoring seawater-freshwater transition zone seasonal movements that are in accordance with the hydrologic state of the system.

Hydrogeophysical applications

The three case studies presented in the second part of the dissertation correspond to three different hydrogeophysical appraisals proving AMT as a valuable working tool that may be used on modelling, planning, management and control of groundwater resources and reservoirs.

Basin-local scale. The Tordera case study aimed to approach a fluvio-deltaic aquifer system where seawater encroachment is one of the main concerns of actual groundwater management of the zone. The 3D hydrogeological model built with the collected lithological record is too coarse to be compared with the more continuous geophysical data, and therefore geophysical validation should be performed with collocated hydrogeological data points. A

multidisciplinary approach using hydrogeological, seismic and 2D and 3D inverse AMT models has provided improved geoelectrical images of the aquifer system that could be linked with different hydrofacies. Both 3D and 2D models clearly show seawater encroachment distribution and controls. Seawater intrusion over the deltaic space is induced through out an ancient paleochannel and constrained by basement morphology. In addition, an AMT time lapse experiment has shown seawater wedge seasonal dynamics along the main seawater path.

Catchment scale. The La Soutte case study aimed to study a small catchment zone on a natural hydrogeophysics laboratory located over a fractured media. The 3D forward model has shown different geoelectrical zones. At the surface, a low resistive zone associated with shallow upper perched aquifer zones on weathered and fractured areas has been interpreted. At depth, another low resistive zone is observed that may suggest the existence of a fractured zone used as a water flux transmission zone toward the deep regional aquifer. Analysis of AMT and DC surface resistivity data shows the resolution and investigation depth of each technique. Modelling using both datasets, may improve models attaining relative deep investigation depths while retrieving highly detailed shallow targets. Joint inversion of different datasets is one of the challenges of the hydrogeophysical discipline.

Basin-regional scale. And finally, the Spring Valley case study is a basin scale hydrogeophysical approach. AMT, gravity and magnetometry has been used on determination of the range frontal fault structure for groundwater exploration purposes. This chapter has been focused on the data analysis and modeling of five AMT profiles acquired on the western edge of the Spring Valley basin .Interpretation of the AMT models has been based primarily on the geological information available, using the ground magnetic data and, to a lesser degree, the depth to basement gravity models. Models show the main changes on bounding graven morphology as wells as basin infill characteristics along the valley. Main graben range-front faults are imaged through the AMT models, given that basement rocks present higher resistivities than basin infill sediments. In addition, basin aquifer zones are observed due to low resistivity values of the valley sediment infill.

Future perspectives

Similar to seismic methods a few years ago, AMT has gone through an acceptance process by the geoscientific community. It has been accepted as a good tool for imaging geologic, hydrogeologic, environmental and civil engineering targets. For this reason geoscientist have to work together to learn how to read all information that could be extracted from AMT data and models. Acquiring sensitivity on accuracy and resolution of the geoelectrical targets may complement the punctual lithological, hydrochemical information and classical seismic structural information to create improved models.

The real world needs to create 3D models that should include structures where dynamic processes can occur. Audiomagnetotellurics is a true 3D geophysical technique. Taking advantages of this multidimensional capability, 3D models are going to increase its usage. The 3D AMT inverse modelling process is still on a testing stage where many improvements have still to be done to ensure good results with faster computing times. Bigger models, that is, finer meshes, more periods and more soundings on both the Tordera and la Soutte 3D models should provide better results.

Petrophysics is one of the paramount perspectives and the ultimate goal that hydrogeophysics has to envisage. In each application study presented, hydrogeological quantification of the geophysical models has not been presented given that no general relationship exists. In general, site-specific relationships are generated using a big amount of collocated geophysical and hydrogeological data or using simple laws assuming standard parameters of ideal environments. These petrophysical relationships have not been derived from the presented case studies due to 1) the few collocated geophysical hydrogeological data available and 2) The usage of standard parameters has been considered a rough simplification of the heterogeneity of the environments. Therefore, further work is required to complete the Todera,, La Soutte aquifer and Spring Valley appraisals.

References

- ACA, 2002. Control de Recursos hídrics al tram baix de la Tordera. Període d'estudi: 15/07/2001-30/09/2003, On line at: http://mediambient.gencat.net/aca/ca//medi/aigues_subterranies. Salinity net control. On line at: http://mediambient.gencat.newt/aca/ca//medi/aigues_subterranies/.
- Annan, A. P., 2005. GPR Methods for Hydrogeological Studies, in Hydrogeophysics (Y. Rubin and S. Hubbard Eds.), Water Science and Technology Library, Springer, 185-215.
- Arango, C., 2005. Estudio Magnetotelúrico de la zona de Lluchmajor (Mallorca): Avances en el proceso de datos y modelo 3D, PhD Thesis, Dep. de Geodinàmica i Geofísica, Universitat de Barcelona.
- Archie, G.E., 1942. The electrical resistivity log as an aid in determining some reservoir characteristics, Trans. Amer. Inst. Mining Metallurgical and Petroleum Engineers, 146, 54-62.
- Arranz, D., M. Himi, A. Casas, J.M. Carmona, M. Viladevall, X. Font, R. Lazaro, J.C.Tapias, V. Pinto and L. Rivero, 2004. Evolución de la intrusión salina en el delta de la Tordera utilizando FDEM, Congreso Nacional de Geología, Zaragoza, España, Geo-Temas 6 (4).
- Auken, E., A.V. Christiansen and K. Sørensen, 2006 a. Structural mapping of large aquifer structures, 19th SAGEEP, Seattle, USA.
- Auken, E., L. Pellerin, A.V. Christiansen and K. Sørensen, 2006 b. A survey of current trends in near-surface electrical and electromagnetic methods, Geophysics, 71, 5, G249-G260.
- Avdeev, B. D., 2005. Three-Dimensional Electromagnetic Modelling and Inversion from Theory to Application, Surveys in Geophysics, 26 (6), 767-799.
- Bahr, K., 1988. Interpretation of the magnetotelluric impedance tensor:regional induction and local telluric distortion, Journal of Geophysics, 62, 119-127.
- Bastani, M., 2001. EnviroMT- a new Controlled Source /Radio Magnetotelluric System, PhD thesis, Upsala University.
- Bedrosian, P.A., 2006. MT+, Integrating Magnetotellurics to Determine Earth Structure, Composition and Processes. Invited review paper in 18th EMIW, El Vendrell, Spain.

- Behaegel, M., 2006. "Hydrogéophysique à l'échelle du petit bassin versant de La Soutte". PhD thesis, Université Louis Pasteur, Strasbour-I.
- Beheagel, M., P Sailhac, G. Marquís, E. Falgàs and J. Ledo, 2005. On the Usage of SP and ERT to Data to Build a Simple Model of Near Surface Flow,11th EAGE Near Surface, Palermo, Italy
- Benjumea, B., T. Teixidó, P. Martínez, and P.Valls, 2006. Sísmica de alta resolución en sedimentos no consolidados: ejemplos en áreas de depósitos de origen fluvio-deltaico en Catalunya, *5ª Asamblea Hispano-Portuguesa de Geodesia y Geofísica, Sevilla.*
- Berdichevsky, M.N. and Dimitriev V.I., 1976. Basic principles of interpretation of magnetotelluric curves, in Geoelectric and Geothermal Studies, (Á. Ádam Ed.), *KAPG* Geophysical Monograph, Akademiai Kaido, Budapest, 165-221.
- Binley, 2003. ProfileR ver. 2.5, User's guide, Lancaster University.
- Binley, A., and A. Kemma, 2005. DC resistivity and Induced Polarization Methods, in Hydrogeophysics (Y. Rubin and S. Hubbard Eds.), Water Science and Technology Library, Springer, 129-155.
- Binley, A., L. Slater, M. Fukes and G. Cassiani, 2005. The relationship between frequency dependent electrical conductivity and hydraulic properties of saturated and unsaturated sandstone, Water Resources Research, 41, W12417.
- Blakely, R. J., 1995. Potential Theory in Gravity and Magnetic Applications, Cambridge University Press, 441 p.
- Boerner, D. E., 1992. Controlled source electromagnetic deep sounding: theory, results and correlation with natural source results, Surveys in Geophysics, 13, 435-488.
- Buttler, D.K. 2006, Near-Surface Geophysics, Investigations in Geophysics, nº13, Society of Exploration Geophysicists, 732 p.
- Cagniard, L., 1953. Basics theory of the magnetotelluric method of geophysical prospecting, Geophysics, 18, 605-635.
- Caldwell, T.G., H.M. Bibby, and C. Brown, 2004. The Magnetotelluric Phase Tensor, Geophysical Journal International, 158, 457-469.
- Casas, E. and M. Rahola, 2003. Actualització hidrogeològica del aqüífer del Baix Tordera, XXXVII CIHS, FCIHS, Univeristat Politecnica de Catalunya.
- Chouteau, M., S. Krivochieva, R. Rodriguez., M. Gonzalez, and V.Jouanne , 1994. Study of the Santa Catarina aquifers system (Mexico Basin) using magnetotelluric soundings, Journal of Applied Geophysics, 31, 85-106.
- Choudhury, K., and D. K. Saha 2004. Integrated Geophysical and Chemical Study of Saline Water intrusion, Ground Water, 42 (5), 671-677.

- Constable, S. C., A.S. Orange, G.M. Hoversten, and C.G. Constable, 1987. Occam's inversion: A practical algorithm for generating smooth models from EM sounding data, Geophysics, 63, 816-825.
- CUAHSI, 2005. Consortium of Universities for the Advancement of Hydrologic Science
- Custodio, E. and M.R.Llamas, 1982 (2ond Edition). Hidrología Subterránea, 2 vols., Omega, Barcelona, 2350pp.
- Custodio, E. and C. Herrera, 2000. Utilización de la relación Cl/Br como trazador hidroquímico del agua subterránea. Boletín Geológico y Minero de España, 11, 49-67.
- Darnet, M., 2003. Caractérisation et suivi de circulations de fluides la mesure de Potentiels Spontanés (PS). PhD thesis, Université Louis Pasteur – Strasbourg I.
- Darnet, M. and G. Marquis, 2003. Modelling streaming potential (SP) signals induced movement in the vadose zone, Journal of Hydrology, 285 (2004),114–124.
- Dèzes, P., S.M Schmid, and P.A. Ziegler, 2004. Evolution of the European Cenozoic Rift System: interaction of the Alpine and Pyrenean orogens with their foreland lithosphere, Tectonophysics, 389, 1-33.
- Deutsch, C.V., and A.G. Journel, 1998. GSLIB, Geostadistical Software Library and User's Guide, Oxford University Press, New York.
- Edwards, L.S., 1977. A modified pseudosection for resistivity and IP. Geophysics, 42 (5), 1020-1036.
- Enrique, P., 1985. La associación plutónica tardi-herciniana del macizo del Montnegre, Catalanides septentrionals (Barcelona). Ph.D Thesis, Universitat de Barcelona, Spain.
- Everett, M.E. and M. Meju, 2005. Near SurfaceControlled-Source-Electromagnetic Induction: Background and Recent Advances, in Hydrogeophysics, (Y. Rubin and S. Hubbard Eds.), Water Science and Technology Library, Springer, 157-185.
- Falgàs, E., M. Beheagel, P. Sailhac, J. Ledo and G. Marquis, 2004. AMT characterization of a fractured aquifer, 17th EMIW, Hyderabad, India.
- Falgàs, E., J. Ledo, T. Teixidó, A. Gabàs, F. Ribera, C. Arango, P. Queralt, J.L. Plata, F.M. Rubio, J.A. Peña, A. Martí, and A. Marcuello, 2005. Geophysical Characterization of a Mediterranean coastal aqüífer: the baixa Tordera fluvio-deltaic aqüífer unit (Barcelona, NE Spain), in Groundwater and Saline Intrusion, IGME (L. Araguás, E. Custodio and M. Manzano Eds.), 395-404.
- FCIHS, 2002, Desenvolupament d'un model matemàtic per a la gestió dels aqüífers al·luvials i fluviodeltaics de la Tordera.

- Ferré, T.P.A., A. Binley, J. Geller, E. Hill, and T. Illangasekare, 2005. Hydrogeophysical Methods at the Laboratory Scale, in Hydrogeophysics (Y. Rubin and S. Hubbard Eds.), Water Science and Technology Library, Springer, 441-463.
- Fitterman, D.V., and M.T. Stewart, 1986. Transient Electromagnetic sounding for groundwater, Geophysics, 51 (4), 995-1005.
- Gabàs, A., 2003. Nous aspects metodològics en l'exploració elèctrica i electromagnètica, PhD thesis, Dpt. Geodinàmica i Geofísica, Universitat de Barcelona.
- Gallardo, L.A., and M. A. Meju, 2003. Characterization of heterogeneous near-surface materials by joint 2D inversion of dc resistivity and seismic data, Geophysical research letters, 30, 1658-1661.
- Galofré, A., A. Luque, and N. Vilarmau, 1998. Estudio hidrogeológico del funcionamiento del delta del Tordera, margen derecho (recopilación). Memoria master del Curso Internacional de Hidrología Subterránea. Fundación Hidrología Subterránea-Junta d'Aigües de Catalunya, p. 87.
- Gans, P.B., E.L. Miller, J. McCarthy, and M.L. Ouldcott, 1985. Tertiary extensional faulting and evolving ductile-brittle transition zones in the northern Snake Range and vicinity: New insights from seismic data. Geology, 13, 189-193.
- Gebrande, H. and Miller, H. 1985. Refraktionsseismik (in German). Angewandte Geowissenschaften II. Ferdinand Enke, F. Bender, Stuttgart, 226-260. ISBN 3-432-91021- 5.
- Gehman, C., D. Harry, and W. Sanford, 2006. Measuring Groundwater Storage Change in an Unconfined Alluvial Aquifer Using Temporal Gravity Surveys, 19th SAGEEP, Seattle, USA.
- Geonics, 1999. Selected Papers and examples, Groundwater Exploration Applications.
- Geometrics. http://www.geometrics.com/
- Geometrics, 2000. Operation Manual for Stratagem systems running IMAGEM. Ver.2.16
- Geoservei, 2001. Actualització i cartografia hidrogeològica del sistema fluvio-deltaic del curs mitjà i baix del riu Tordera,ACA, Barcelona. (Internal).
- Goldstain, M.A., and D.W., Strangway, 1975. Audio-frequency magnetotellurics with a grounded electric dipole source, Geophysics, 40, 669-683.
- Goldman, M., U. Kafri and Y. Yechieli, 2003. Application of the Time Domain Elecrtromagnetic (TDEM) Method for Studying Groundwater Salinity in Different Coastal Aquifers of Israel, in Coastal Aquifers Intrusion Technology: Mediterranean countries, (A. Lopez-Jeta, J. de Dios, J.A. de la Orden, G. Ramos and L. Rodriguez

Eds.)Publicaciones del Instututo Geologico y Minero de Espanya Serie: Hidrogeología y aguas subterranias nº8, tomo II, 45-56.

- Goldman, M., and U. Kafri, 2004. The use of time domain electromagnetic TDEM method to evaluate porosity of saline water saturated aquifers, in Groundwater and Saline intrusion, IGME (L. Araguás, E. Custodio and M. Manzano Eds.), 327-339.
- Gómez-Hernández, J., 2005. Geostadistics, in Hydrogeophysics (Y. Rubin and S. Hubbard Eds.), Water Science and Technology Library, Springer, 59-83.
- Grauch, V.J.S., M.R. Hudson, and S.A. Minor, 2001. Aeromagnetic expression of hydrogeologically important faults, Albuquerque basin, New Mexico SAGEEP, Denver Co., USA.
- Groom, R.W., and R.C Bailey, 1989. Decomposition of magnetotelluric impedance tensor in the presence of local three-dimensional galvanic distortion, Journal of Geophysical Research, 94 (B2), 1913-1925.
- Guérin, R., M. Descloitres, A. Coudrain, A. Talbi and R. Gallaire, 2001. Geophysical surveys for identifying saline groundwater in the semi-arid region of the central Altiplano, Bolivia, Hydrological Processes, 15, 3287-3301.
- Guérin, R., 2005. Borehole and surface-based hydrogeophysics, Hydrogeology Journal, 13, 251-254.
- Guimerà, J., S. Jordana, E. Ruiz, M. Iglesias, and G. Borràs, 2003. Un modelo 3D de densidad variable para simular el sistema acuífero multicapa del Delta Del Río Tordera (Barcelona, Cataluña, España), in Tecnología de la intrusión de agua de mar en acuíferos costeros: países mediterráneos, (López-Geta, de la Orden, de Dios Gomes, Ramos, Mejías and Rodríguez Eds.) IGME, Isbn.84-7840-470-8.
- Haber, E., U. M. Ascher, D. W. Oldenburg, 2004. Inversion of 3D Electromagnetic Data in Frequency and Time Domain Using an Inexact All-at-Once Approach, Geophysics, 69, 1216-1228.
- Haber, E., 2005. Quasi–Newton Methods for Large-Scale Electromagnetic Inverse Problems, Inverse. Problems. 21, 305-323.
- Hashin, Z. and S.Strickman, 1962. A variational approach to the theory of effective magnetic permeability of multiphase materials, Journal of Applied Physics, 33, 3125-3131.
- Himi, M., J.V. Navarro, J.A. Sabadía, and A. Casas, 2000. Delimitación de la intrusión salina en el delta del río Tordera por métodos electromagnéticos. Technical report, Actualidad de las Técnicas Geofísicas Aplicadas en Hidrogeología, IGME.

- Hirlemann, G. 1974. Le dispositif structural du champ de fractures de Rieauvillé (Haut-Rhin, France). Un exemple de fragmentation tectonique (block-faulting) en bordure occidentale du Fossé rhénan, in Approaches to Taphrogenesis, (J.Illes and K.Fuchs ed.), 172-176.
- Hose, R.K., and Blake, 1976. Geology Pt.I in Geology and mineral resources of White Pine Country, Nevada, Nevada Bureou, Mines and Geology Bulletin, 85, 1-32.
- Hohmann G.H., 1984. The Magnetotelluric Method, class notes, Geology and Geophysics Department, University of Utha.
- Hunter, J.A., S.E. Pullan, R.A. Burns, R.M. Gagne, and R.S. Good 1984. Shallow seismic reflection mapping of the overburden-bedrock interface with the engineering seismographsome simple techniques, Geophysics, 49, 1381-1385.
- Illes, J.H., 1974. Thaphrogenesis and Plate Tectonics, in Approaches to Taphrogenesis, (J.Illes and K. Fuchs Ed.), 33-460.
- Illes, J.H and K. Fuchs, 1974. Approaches to Taphrogenesis, Proceedings of and International Rift Symposioum, Karlsruhe, 1972, 460.
- Illes, J.H., 1977. Ancient and Recent Rifting in the Rhinegraben, in Fault Tectonics in N.W. Europe. Geol. Mijnbouw, 56 (4), 329-350.
- Jachens, R.C., and B.C. Moring, 1990. Maps of thickness of Cenozoic deposits and the isostatic residual gravity over basement for Nevada, USGS Open-File Report, 90-404, 15p.
- Jarvis, K. D., and R.J. Knight, 2002. Aquifer heterogeneity from SH-wave seismic impedance inversion, Geophysics, 67 (5), 1548–1557. doi:10.1190/1.1512800.
- Johnston, J.M., 1992. Magnetotelluric Transect of The Sevier Overthust Belt in South-western Utah and Eastern Nevada, Master Thesis, Dpt. Geology and Geophysics, University of Utah.
- Kaminsky, 2007. http://kaminae.boom.ru/Zond.htm, ZondRes2D.
- Kaufman, A.A. and G.V. Keller, 1981. The Magnetotelluric Sounding Method, Methods in Geochemistry and Geophysics, 15, Amsterdam.
- Keating, K. and R. Knight, 2007. A laboratory study to determine the effect ofiron oxides on proton NMR measurements, Geophysics , 72 (1) E27–E32.
- Keller, G.V., 1988. Rock and mineral properties, in Electromagnetic methods in applied Geophysics, (M. N. Nabighian Ed.), Society of Exploration Geophysicists.
- Knight, R., and A. Nur, 1987. The dielectric constant of sandstones, 60 kHz to 4 MHz, Geophysics, 52, 664-654.

- Knight, R., 2001. Ground penetrating radar for environmental applications, Annual Review of Earth and Planetary Sciences, 29, 229-255.
- Knight, R., and A. Endres, 2006. An introduction to rock physics principles for near-surface geophysics, in Near-Surface Geophysics, (D.K. Buttler Ed.), Investigation in Geophysics, 13, Society of Exploration Geophysicists.
- Korb, M., S. Mares and F. Paillet, 2005, Geophysical Well Logging: Borehole Geophysics for Hydrogeological Studies: Principles and Applications, in Hydrogeophysics, (Y. Rubin and S.S. Hubbard Eds.) Water Science and Technology Library, Springer, 291-333.
- Krivochieva, S., and M. Chouteau 2003. Integrating TDEM and MT methods for characterization and delineation of the Santa Catarina aquifer (Chalco Sub-Basin, Mexico), Journal of Applied Geophysics, 52 (1), 23-43.
- Lesmes D. P., and S.P. Friedman, 2005. Relationships between the Electrical and Hydrogeological Properties of Rocks and Soils, in Hydrogeophysics, Y. Rubin and S.S. Hubbard Eds.) Water Science and Technology Library, Springer, 87-129.
- Ledo, J., P. Queralt, A. Martí, and A.G Jones, 2002 a. Two-dimensional interpretation of three-dimensional magnetotelluric data: an example of limitations and resolution, Geophysical Journal International, 150,127-139.
- Ledo, J., A. Gabàs and A Marcuello, 2002 b. Static shift levelling using geomagnetic transfer functions, Earth Planets Space, 54, 493-498.
- Ledo, J., 2006. 2-D versus 3-D magnetotelluric data interpretation, Surveys in Geophysics, 27, 111–148. Doi: 10.1007/s10712-006-0002-4.
- Legchenko, A.V. and O.V. Shushakov, 1998. Inversion of surface NMR data. Geophysics, 63, 75-84.
- Linde, N., and L. B. Pedersen, 2004 a. Evidence of electrical anisotropy in limestone formations using the RMT technique, Geophysics, 69, 909-916, doi:10.1190/1.1778234.
- Linde, N., and L. B. Pedersen, 2004 b. Characterization of a fractured granite using radiomagnetotelluric (RMT) data, Geophysics, 69, 1155-1165, doi:10.1190/ 1.1801933.
- Linde, N., 2005. Characterization of Hydrogeological Media Using Electromagnetic Geophysics, PhD thesis, Uppsala Universitet, Sweden
- Linde, N., A. Binley, A. Tryggvason, L.B. Pedersen, and A. Revil, 2007. Improved hydrogeophysical characterization using joint inversion of crosshole electrical resistance and ground penetrating radar traveltime data, Water Resources Research, 42, W12404, doi:10.1029/2006ER005131.

- Loeffler, O., 2005. Módelisation géoradar de la proche surface estimation de la teneur en eau et influence d'un pulluant. PhD thesis, Université Louis Pasteur, Strasbour-I.
- Locke, M.H., 1999. Electrical imaging surveys for environmental and engineering studies. A practical guide to 2-D and 3-D surveys.
- Lubczynsky, M., and J. Roy, 2003. Hydrogeological interpretation and potential of the new magnetic resonance sounding (MRS) method, Journal of Hydrology, 283, 19-40.
- Mackie, R.L., T.R. Madden, 1993. Three-dimensional magnetotelluric modelling using difference equations- Theory and comparisons to integral equations solutions, Geophysics, 58, 215-226.
- Mackie, R., S. Rieven, and W. Rodi, 1997. User manual and software documentation for two-dimensional inversion of magnetotelluric data. GSY-USA Inc. San Francisco (USA).
- Mankinen, E. A., R.W. Carter, E.H. McKee, B.A. Cunchel and B.C. Moring, 2006. Geophysical Data from The Spring and Snake Valleys Area, Nevada and Utha, USGS Open file Report 2006-1160, 36p.
- Mankinen, E.A., C. W. Roberts, E. H. McKee, B. A. Chuchel and R. L. Morin, 2007. Geophysical data from Spring Valley to Delamar Valley, East-central Nevada: U.S. Geological Survey Open-File Report 2007-1190, 42 p. (http://pubs.usgs.gov/of/2007/1190/).
- Manzella A., G. Volpi, A. Zaja and M. Meju, 2004. Combined TEM-MT investigation of shallow-depth resistivity structure of Mt Somma-Vesuvius. Journal of Volcanology and Geothermal Research, 131, 1-2, 19-32.
- Marcuello, A., and J. Plata, 2005. Tomografia geoelectrical: Desarrollo para la caracterización de acuíferos, UB-IGME, Final Report REN2002-04538-C02-01/02, Ministerio de Educación y Ciencia, Dirección General de Investigación.
- Martí, A., P. Queralt, and E. Roca, 2004. Geoelectric dimensionality in complex geological areas: application to the Spanish Betic Chain, Geophysical Journal International, 157, 961-974.
- Martí, A., 2006. A Magnetotelluric Investigation of Geoelectrical Dimensionality and Study of the Central Betic Crustal Structure, PhD thesis, Dpt. Geodinàmica i Geofísica, Universitat de Barcelona.
- Maurer, H., and D.E. Boerner, 1998. Optimized design of geophysical experiments, The Leading Edge, August 1998, 8, 1119.
- Mazác, O., M. Císlerová, W. E. Kelly, I. Landa, and D. Venhodová, 1990. Determination of Hydraulic Conductivities by Surface Geoelectrical Methods, in

Geotechnical and Environmental Geophysics (2), (S.H. Ward Ed.), Environmental and Groundwater, Society of Exploration Geophysicists.

- McNiece, G., and A.G. Jones, 2001. Multisite, multifrequency tensor decomposition of magnetotelluric data, Geophysics, 66, 158-173.
- McPhee, D.K., B. A. Chunchel, and L. Pellerin, 2006, Audiomagnetotelluric data from Spring, Cave, and Coyote Spring Valleys, Nevada, USGS Open-File Report 2006-1164, 41p.
- McPhee, D. K., B. A Chuchel., and L. Pellerin, 2007. Audiomagnetotelluric data and two-dimensional models from Spring, Snake, and Three Lakes Valleys, Nevada: U.S. Geological Survey Open-File Report 2007-1181, 47 p. (http://pubs.usgs.gov/of/ 2007/1181/).
- Meju, M.A., 1996, Joint inversion of TEM and distorted MT soundings, Some effective practical considerations, Geophysics, 61, 56–65.
- Meju, M.A., 2000. Environmental Geophysics: tasks ahead, Journal of Applied Geophysics, 44, 63-65.
- Meju, M. A., L. Gallardo, and A. K. Mohamed (2003), Evidence for correlation of electrical resistivity and seismic velocity in heterogeneous near-surface materials, Geophysical Research Letters, *30*, 7, 1373, doi:10.1029/ 2002GL016048.
- Meju, M.A., 2004. Simple relative space time scaling of electrical and electromagnetic depth sounding arrays: implications for electrical static shift removal and joint DC-TEM data inversion with the most-squares criterion, Geophysical Prospecting, 53, 463-479.
- Mota, R., F.A. Monteiro Santos, A. Mateus, F.O. Marques, M.A. Gonçalves, J. Figueiras, and H. Amaral, 2004. Granite fracturing and incipient pollution beneath a recent landfill facility as detected by geoelectrical survey, Journal of Applied Geophysics, 57, 11-22.
- Nobes, D.C., 1996. Troubled waters: Environmental applications of electrical and electromagnetic methods, Surveys in Geophysics, 17, 393-454.
- Park, S.K., 1997. Monitoring resistivity change in Parkfield, California: 1988-1995, Journal of Geophysical Research, 102 (B11), 24.545-24.559.
- Palacky, G.C., 1988. Characteristics of Geologic Targets, in Electromagnetic Methods in Applied Geophysics (M. N. Nabighian Ed.), Society of Exploration Geophysicists.
- Pek, J. and T, Verner, 1997. Finite-difference modelling of magnetotelluric field in two-dimensional anisotropic media, Geophisical Journal International, 128, 505-521.

- Pedersen, L.B., M. Bastani, and L. Dynesius 2005. Groundwater exploration using combined controlled-source and radiomagnetotelluric techniques, Geophysics, 70, G8-G15, doi:10.1190/1.1852774.
- Pedersen, L.B. and M. Engels, 2005. Routine 2D inversion of magnetotelluric data using the determinant of the impedance tensor, Geophysics, 70, G33-G41.
- Pfaffhuber, A., 2001. Development and test of a controlled source MT method in the frequency range 1 to 50 kHz, Diploma Thesis, Technical University Berlin.
- Pellerin, L., and G.W. Hohmann, 1990, Transient electromagnetic inversion, A remedy for magnetotelluric static shifts: Geophysics, 55, 1242–1250.
- Pellerin, L., and D.L. Alumbaugh, 1997. Tools for electromagnetic investigation of the shallow subsurface, The Leading Edge, 16, 1631-1638.
- Pellerin, L., 2002. Applications of electrical and electromagnetic methods for environmental and geotechnical investigations, Surveys in Geophysics, 23, 101-132.
- Pellerin, L., and P.E. Wannamaker, 2005. Multi-dimensional electromagnetic modelling and inversion with application to near-surface earth investigations, Computers and electronics in agriculture, 46, 71-102.
- PHPO, 1985. E.E.-2 Estudio complementario sobre agues subterráneas. Zona 4 Tordera-Costa Brava Sur y alto Maresme. Aluvial del Tordera. Tomo-6.
- Pelton, J.R., 2006. Near-surface Seismology: Surface-Based Methods, in Near-Surface Geophysics (D.K. Butler Ed.), Investigation in Geophysics nº13, Society of Exploration Geophysicists, 219-136.
- Plata, J., and F. Rubio, 2002. MRS experiments in a noisy area of a detrital aquifer in the south of Spain, Journal of Applied Geophysisics, 50,83–94.
- Plume, R.W., 1996. Hydrogeologic framework of the Great basin Region of Nevada, Utah and adjacent states, USGS Professional Paper 1409-B, 64 p.
- Ponce, 1997. Gravity data of Nevada: U.S. Geological Survey Digital Data Series, DDS-42, 27p.
- Post, V. E. A., 2005. Fresh and saline groundwater interaction in coastal aquifers: Is our technologyready for the problems ahead?, Hydrogeology Journal, 13, 120-130.
- Purvance, D. T., and R. Andricevic, 2000. On the electrical-hydraulic conductivity correlation in aquifers, Water Resources Research, 36, 2905-2913.
- Queralt, P., A.G. Jones and J. Ledo, 2007. Electromagnetic imaging of a complex ore body: 3D forward modeling,sensitivity tests, and down-mine measurements, Geophysics, 72 (2), f85–f95,10.1190/1.2437105.

- Revil, A., and P.A. Pezard, 1999. Streaming potential in porous media 1. Theory of the zeta potential. Journal of Geophysical Research. 104,20033–20048.
- REPO, 1971. Estudio de los recursos hidráulicos totales del pirineo oriental. Zona Norte DGOH: CAPO y SGOP.
- Roca E., 1996. La evolución geodinámica de la Cuenca Catalano–Balear y áreas adyacentes desde el Mesozoico hasta la actualidad, Acta Geológica. Hispànica, 29 (1994), 3–25.
- Rodi, W. and R. Mackie, 2001. Nonlinear conjugate gradients algorithm for 2-D magnetotelluric inversion, Geophysics, 66 (1), 174-187.
- Rovira, A., R.J. Batalla, and M. Sala, 2005. Fluvial sediment budget of a Mediterranean river: the lower Tordera (Catalan Costal Ranges, NE Spain), CATENA, 60, 19-42.
- Roy, A., and A. Apparo, 1971. Depth of investigation in direct current methods, Geophysics, 36 (5), 943-959.
- Rubin, Y., G. Mavko, and J. Harris, 1992. Mapping permeability in heterogeneous aquifers using hydrologic and seismic data, Water Resources. Research, 28, 1809-1816.
- Rubin, Y., and S. Hubbard, 2005. Stochastic forward and inverse modeling: the hydrogeophysical challenge, in Hydrogeophysics (Y. Rubin and S.S. Hubbard Eds.) Water Science and Technology Library, Springer, 487-511.
- Sala, M., 1979. La cuenca del Tordera. Estudio geomorfológico. PhD thesis, University of Barcelona, Barcelona.
- Sailhac, P.and G. Marquis, 2001. Analytic potentials for the forward and inverse modeling of SP anomalies caused by subsurface fluid flow, Geophysical Research Letters, 28, 1643-1646.
- Sandberg, S.K., and G.W. Hohmann, 1982. Controlled-source audiomagnetotellurics in geothermal exploration, Geophysics, 47, 100-116.
- Sánchez-Vila, X., A. Guadagnini and J. Carrera, 2006. Representative Hydraulic Conductivities in Saturated Groundwater Flow, Reviews of Geophysics, 44, RG3002.
- Santamarina, J.C., V.A. Rinaldi, D. Fratta, K.A. Klein, Y. Wang, G.Ch. Cho, and G. Cascante, 2006. A Survey of Elastic and Electromagnetic Properties of Near-Surface Soils, in Near-surface Geophysics (D.K. Butler Ed.), Investigations in Geophysics nº13, Society of Exploration Geophysicists, 71-77.
- Scheirer, D.S., 2005. Gravity studies of Cave, Dry Lake, and Delemar Valleys, east-central Nevada, USGS Open-File Report 2005-1339, 27p.
- Schuster, G. T. and A. Quintus-Bosz, 1999, Wavepath eikonal traveltime inversion: Theory, Geophysics, *58*, 1314-1323 .

- Schwinn, W., and B. Tezkan , 1997. 1D joint inversion of radiomagnetotelluric (RMT) and transient electromagnetic (TEM) data; an application for groundwater prospection in Denmark, presented paper at 3rd EEGS, Århus, Denmark, 221–224.
- Sasaki, Y., 2001. Full 3-D Inversion of Electromagnetic Data on PC, Journal of. Applied Geophysics, 46, 45-54.
- Serra, J. and X. Valois, 2007. Evolución de la costa del delta del río Tordera durante el último ascenso eustático (holoceno), IV Jornadas de geomorfología litoral, Palma de Mallorca, Mayo, 2007.
- Shevnin, V., O.r Delgado, A. Mousatov and A. Ryjov, 2006, Estimation of Soil Hydraulic Conductivity on Clay Content, Determined from Resistivity Data, 19th SAGEEP, Seattle, USA.
- Simpson, F. and K. Bahr, 2005. Practical Magnetotellurics, Cambridge Univesity Press.
- Singha, K., and S.M. Gorelick, 2005. Saline tracer visualized with three-dimensional electrical resistivity tomography: Field-scale spatial moment analysis, Water Resources Research, 41, W05023, doi:10.1029/2004WR003460.
- Siripunvaraporn, W. and G. Egbert, 2000. An efficient data-subspace inversion method for 2-D magnetotelluric data, Geophysics, 65, 3, 791-803.
- Siripunvaraporn, W., M. Uyeshima, and G. Egbert, 2004. Three-Dimensional Inversion for Network-Magnetotelluric Data, Earth Planets Space, 56: 893-902.
- Siripunvaraporn, W., G. Egbert, Y. Lenbury, and M. Uyeshima, 2005 a. Three-dimensional magnetotelluric inversion: data-space method, Physics of the Earth and Planetary Interiors, 150, 3-14.
- Siripunvaraporn, W., G. Egbert and M. Uyeshima, 2005 b. Interpretation of 2-D Magnetotelluric Profile Data with 3-D Inversion: Synthetic Examples, Geophysical Journal International, 160, 804-814.
- Siripunvaraporn, W., 2006. http://www.gfz-potsdam.de/pb2/pb23/MT/ projects/3dinv/ where, How to use WSINV3DMT, .pdf.
- Slater, L.D, A. Binley and D. Brown, 1997. Electrical Imaging of Fractures Using Ground-Water Salinity Change, Ground Water, 35, 436-442.
- Slater, L., and D. Lesmes, 2002. IP interpretation in environmental investigations, Geophysics, 67, 77-88.
- Slater, L., A. Binley, R. Versteeg, G. Cassiani, R. Birken, and S. Sandberg, 2002. A 3D ERT study of solute transport in a large experimental tank, Journal of Applied Geophysics, 49, 211-229.

- Slater, L., R. Knight, K. Shinga, A. Binley, and E. Atekwana, 2006. About AGU, Near-Surface Geophysics: A New Focus Group, EOS, 87, 25.
- Slater, L., 2006. Near surface electromagnetic characterization of hydraulic conductivity: from petrophysical properties to aquifer geometries, review paper on 18th EMIW, September 2006, El Vendrell, Spain.
- Smith, J.T. and Booker, J., 1991. Rapid inversion of two- and three-dimensional magnetotelluric data, Journal of Geophysical. Research, 96, 3905-3922.
- Soler, A., A. Galofré, N. Otero, R.M. Corp, P. Masqué, J. Mas-Pla, and E. Garcia-Solsona, 2006. Cuantificación del aporte de aguas continentales a la planta desalinizadora de Blanes a partir de trazadores isotópicos, in De la toma de datos y la realización de modelos de agua subterránea a la gestión integrada. From de gathering and groundwater modelling to integrated management, Instituto Geológico y Minero de España, serie: Hidrogeología y Aguas Subterráneas, 21, 597-604.
- Sørensen, K, 1996. Pulled array continuous electrical profiling, First Break, 14, 85-90.
- Sørensen, K. and E. Auken, 2004. SkyTEM- a new high resolution helicopter transient electromagnetic system. Exploration Geophysics, 35, 191-199.
- Spichak, V., and I. Popova, 2000. Artificial Neural Network Inversion of Magnetotelluric Data in Terms of Three-Dimensional Earth Macroparameters, Geophysical Journal International 142, 15-26.
- Spies, B.R. and F.C. Frischknecht,1991. Electromagnetic sounding, in Electromagnetic Methods in Applied Geophysics, Vol. 2 (M.N. Nabighian Ed.), Society of. Exploration. Geophysicists, 285-425.
- Steeples, D.W., and W.E Miller, 1990. Seismic-reflection methods applied to engineering, environmental, and ground-water problems, in Geotechnical and Environmental Geophysics vol.1, (S. Ward Ed.), Society of. Exploration. Geophysicists, 1-30.
- Steeples, D.W., 2005. Shallow Seismic Methods, in Hydrogeophysics, (Y. Rubin and S.S. Hubbard Eds.) Water Science and Technology Library, Springer,215-253.
- Steuer, A., 2006. Airborne Electromagnteics at Buried Valleys: Frequency or Time Domain, 18th EMIW, El Vendrell, Spain.
- Stewart, J.H., 1978. Basin-range structure in western North America: A review, in Cenozoic tectonics and regional geophysics of the western Cordillera, R.B. (Smith and G.P. Eaton Eds.), Geological Society of America 152, 1-31.
- Stewart, J.H., 1980. Geology of Nevada: A Discussion to Accompany the Geologic Map of Nevada, Nevada Bureau of Mines and Geology, Special Publication, 4. 123 p.

- Szarka, L. and M. Menvielle, 1997. Analysis of rotational invariants of the magnetotelluric impedance tensor, Geophysical Journal International, 129, 133-142.
- Tarantola, A., 1987. Inverse problem theory, Elsevier, Amsterdam, 613.
- Teixidó, T., 2000. Caracterització del subsòl mitjançant sísmica de reflexió d'alta resolució. PhD thesis, Universitat de Barcelona.
- Tezkan, B., 1999. A review of environmental applications of quasi-stationary electromagnetic techniques, Surveys in Geophysics, 20, 279-308.
- Tezkan, B., P. Georgescu and U. Fauzi, 2005. A radomagnetotelluric survey on an oil-contaminated area near the Brazi Refinery, Romania, Geophysical Prospecting, 53, 311-323.
- Tikhonov, A.N., 1950. Determination of the electrical characteristics of deep strata of the Earth's curst, Dolkl. Akad. Nauk., SSSR, 73, 295-297.
- Tilden, J.E., D.A Ponce, J.A.G Glen, B.A. Chunchel, K. Tushman, A. Duval, 2006. Gravity, Magnetic and Physical Property data in the Smoke Creek Desert area, Northwest Nevada, Open-File Report 2006-1197, 35p.
- Topp, G.C., J.L. Davis, and A.P. Annan, 1980. Electromagnetic determination of soil water content: Measurements in coaxial transmission lines, Water Resources Research, 16 (3), 574-582.
- Trad, D.O., and J.M. Travassos, 2000. Wavelet filtering of magnetotelluric data. Geophysics, 65 (2), 482-491.
- Tullen, P., O. Turberg, and A. Parriaux, 2006. Radiomangetotelluric mapping, groundwater numerical modelling and 18-Oxygen isotopic data as combined tools to determine the hydrogeological system of a landslide prone area, Engineering Geology, 87, 195-204.
- Unsworth, M.J., X. Lu, M.D. Watts, 2000. AMT exploration at Sellafield: Characterization of a potential radioactive waste disposal site, Geophysics, 65, 1070-1079.
- Vozoff, K., 1972. The magnetotelluric method in the exploration of sedimentary basins, Geophysics, 37, 98-141.
- Vozoff, K., 1991. The magnetotelluric method, in: Electromagnetic Methods in Applied Geophysics, Vol 2. (M.N. Nabighian Ed.), Society of. Exploration. Geophysicists.
- Wannamaker, P.E., J.A. Stodt and L. Rijo, 1987. A stable finite element solution for two-dimensional magnetotelluric modelling, Geophysics, 49, 1517-1533.

- Ward, S. H. and G. W. Hohmann 1988. Electromagnetic theory for geophysical applications, in Electromagnetic methods in applied geophysics, (M.N. Nabighian Ed), Society of Exploration Geophysicists, 131-311.
- Waxman, M.H., and L.J.M. Smits, 1968. Electrical conductivities in oil-bearing shaly sands, Society of Petroleum Engineers Journal, 8, 107-122.
- Weaver, J.T., A.K. Agarwal, and F.E.M. Lilley 2000. Characterisation of the magnetotelluric tensor in terms of its invariants, Geophysical Journal International, 141, 321-336.
- Wempe, W.L., 2000. Predicting Flow Properties Using Geophysical Data: Improving Aquifer Characterization, PhD Thesis, Stanford University, CA ,USA.
- Wilson, S.R., M. Ingham, J.A. McConchie, 2006. The applicability of earth resistivity methods for saline interface definition, Journal of Hydrogeology, 316, 301-312.
- Wharton, R.P., G.A. Hazen, R.N. Rau, and D.L. Best, 1980. Electromagnetic propagation logging: Advances in technique and interpretation, Soc. Pet. Eng., 9267
- Yaramanci. U., G. Lange and K. Knödel, 1999. Surface NMR within a geophysical study of an aquifer at Haldensleben (Germany), Geophysical prospecting, 47, 923-943.
- Yaramanci, U., A. Kemna, and H. Vereeckens, 2005. Emerging technologies in Hydrogeophysics, in Hydrogeophysics (Y. Rubin and S. Hubbard Eds.), Water Science Technology and Library, Springer, 467-486.
- Zhang, Y. and K.V. Paulson, 1997, Enhancement of signal to noise ratio in natural source transient magnetotelluric data with wavelet transform, Pure and Applied Geophysics, 149, 405-419.
- Ziegler, P.A., M.E Schumacher, P. Dèzes, J.-D.vanWees, and S. Cloetingh, 2004. Post-Variscan evolution of the lithospherein the Rhine Graben area: constraints from subsidence modelling. In Permo–Carboniferous Magmatism and Rifting (Wilson, M., Neumann, E.-R., Davies, G.R., Timmerman, M.J., Heeremans, M., Larsen, B.T., Eds.), European Geological Society of London, Special Publications., vol. 223, pp. 289– 317.
- Zonge, K.L., and L.J. Hughes, 1988. Controlled Source Audio-Frequency Magnetotellurics, in Electromagnetic Methods in Applied Geophysics, vol. 2, (M. N. Nabighian Ed). Society of Exploration Geophysicists.
- Zonge, K.L., J. Wynn and S. Urquhat, 2006. Resistivity induced polarization and complez resistivity, in Near-surface Geophysics, (D.K. Butler Ed.), Investigations in Geophysics, Society of Exploration Geophysicists, 13, 265-300.

- Zyserman, F. I., and J. E. Santos, 2000. Parallel Finite Element Algorithm with Domain Decomposition for Three-Dimensional Magnetotelluric Modeling, Journal of Applied Geophysics, 44, 337-351.